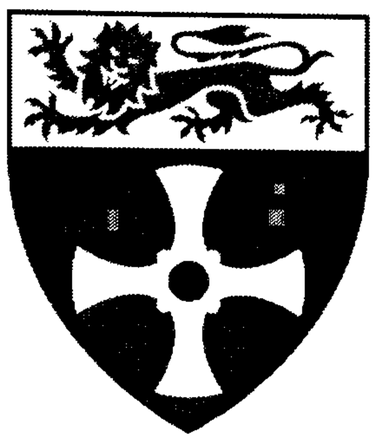

Newcastle University

The Recovery of Metals from Waste Solutions by Electrochemical Methods

A Thesis submitted by

Rachel Buckle

For the Degree of Doctor of Philosophy

School of Chemical Engineering and Advanced Materials

University of Newcastle upon Tyne

April 2007

ABSTRACT

Electronics is an important industry in the UK, as there are many home-grown manufacturing companies in the areas of optics, electronics and micro-systems. As a consequence of the growth in this industry, there has been an increase in the discharges from manufacturing. A process that could reclaim the metals contained in these wastes is desirable because of the increasing costs of raw materials and environmental compliance.

The aim of this project was to develop a systematic method to determine the feasibility of metal recovery from aqueous solutions. Waste tin stripping solution was chosen as a case study. This waste arises from a stage in the manufacture of printed circuit boards when a protective tin layer is stripped from the copper pattern. The solution is mainly nitric acid, but also contains suspension agents, ferric salts and inhibitors. After use it also contains suspended tin oxide and dissolved copper. It has been suggested that the tin and copper could be recovered from this waste by electrodeposition.

Initially the thermodynamics of the system were studied, followed by experiments to verify the theoretical work. Pourbaix diagrams were constructed to determine when the metals would be in the solid or liquid phase depending on the concentration of metal and anion, pH and system potential. This information was then compared to separation processes to determine or confirm the recovery route. This study showed that the dissolved copper and suspended tin oxide could be separated by filtration if the pH was maintained between -0.4 and 2.4. The dissolved copper could then be removed by electrodeposition.

After the metal recovery route has been established, the individual stages are studied in more detail. In this project the feasibility of copper recovery from the stripping waste was examined. Copper deposition occurs concurrently with nitrate, ferric and hydrogen reductions. Using a parallel plate electrochemical reactor, the copper concentration was reduced by approximately 30%, at a current efficiency of 70%.

ACKNOWLEDGEMENTS

The author would like to express her gratitude to the following people:

- Professor Sudipta Roy, for her invaluable support, encouragement and guidance throughout this project.
- Dr Charles Kerr, for introducing me to the subject and useful advice.
- Rob Dixon, Paul Sterling, Vince Scott, Stuart Latimer, Simon, Jimmy, Brian and Ian for their patience, advice and assistance.
- Dave Dunbar at the Chemical Analysis Unit, for ICP measurements.
- The Resource Efficiency Network for supporting the work through an industrial CASE award. The EPSRC and Tin Technology for funding this project.

CONTENTS

LIST OF FIGURES

1 INTRODUCTION

2 FUNDAMENTAL ASPECTS

3 EXPERIMENTAL

4 THERMODYNAMIC ANALYSIS

5 PRECIPITATION EXPERIMENTS

6 ELECTROCHEMICAL CHARACTERISATION

LIST OF TABLES

1 INTRODUCTION

2 FUNDAMENTAL ASPECTS

3 EXPERIMENTAL

4 THERMODYNAMIC ANALYSIS

5 PRECIPITATION EXPERIMENTS

6 ELECTROCHEMICAL CHARACTERISATION

7 METAL RECOVERY

NOMENCLATURE

a	activity	
A	area	m^2
c	concentration	M
C	cost	£
D	diffusion coefficient	$m^2\ s^{-1}$
d_e	equivalent diameter	m
$E / E_e / E^0 / E_{1/2}$	potential / equilibrium / standard / half wave	V
F	Faraday's constant	96485 C/mol
G / G^0	Gibbs Free energy / standard	$J\ mol^{-1}$
I / I_L	current / limiting	A
I_c	ionic strength	M
j / j_0	current density / exchange	$A\ m^{-2}$
K	reaction equilibrium constant	
k_m	mass transfer coefficient	$m\ s^{-1}$
L	length	m
m	number of moles	
n	number of electrons transferred	
Q	charge	C
Q_v	volumetric flow rate	$m^3\ s^{-1}$
R	universal gas constant	$8.314\ J\ mol^{-1}\ K^{-1}$
R_{cell} / R_s	cell / solution resistance	Ω
Re	Reynolds number	
Sc	Schmidt number	
Sh	Sherwood number	
t	time	s
T	temperature	K
u	velocity	$m\ s^{-1}$
V / V_T	volume of reactor / tank	m^3
W	energy	J
x	stoichiometric coefficient	

z	valency	
α_A / α_C	transfer coefficients for anode/cathode	
δ	Nernst diffusion layer thickness	m
Φ	current efficiency	%
γ	activity coefficient	
η	overpotential	V
κ	conductivity	S m^{-1}
λ	ionic conductance	S cm^2 / mol
Λ	conductance of a salt	S cm^2 / mol
μ	viscosity	kg m^{-1} s^{-1}
ν_+/ν_-	number of positive/negative ions in the salt	
ρ	density	kg m^{-3}
τ / τ_T	residence time in reactor / tank	s

ABBREVIATIONS

[X]	concentration of X
CSTR	continuously stirred tank reactor
US EPA	United States Environmental Protection Agency
ICP	inductively coupled plasma
IPPC	Integrated Pollution Prevention and Control
ISE	Ion selective electrodes
MSDS	material safety data sheet
PCB	printed circuit board
PFR	plug flow reactor
RDE	rotating disc electrode
SCE	saturated calomel electrode
SHE	standard hydrogen electrode
UV	ultra violet

1 INTRODUCTION

1.1 Background

Electronics is an important industry for the UK, as there are many home grown manufacturing companies in the areas of optics, electronics and micro-systems. In 2004, the electronic component market within the EU grew by 7% to a value of €47.7bn, with the UK & Ireland market growing by €1bn [1.1]. However, the consequence of this growth is a rise in the amount of computer, electronic and communication hardware in the environment and an increase in the discharges from manufacturing.

The waste hardware will either be from components at end-of-life, or rejects from manufacture. The waste is composed of polymers, silicon and a range of metals, and is usually sent to landfill. If the metals are leached away from the substrate and into the groundwater, damage to the environment may result. This can happen through a complex mixture of bacterial action, changing pH due to weather conditions, and the other constituents of the landfill.

The liquid discharges from manufacturing are usually aqueous solutions, for example rinse waters in which the concentrations of metal ions are quite low. They can also contain organic additives, cyanides, nitrates and phosphates which pose a threat to the environment.

A systematic method to determine the feasibility of recovering the metals contained in these aqueous waste streams for reuse will be developed during this project. This presents several challenges:

- The liquid discharges can have very low concentrations of metal ions, so may require concentration.
- The metals should be recovered in their purest forms or as useful alloys.

- The organic additives could affect the recovery processes.
- Ideally, the process should be a closed loop, therefore not generate any effluent.

It is proposed that electrowinning will be used to recover metals from the waste solutions. This process runs at low temperature and pressure so the capital and operating costs are relatively low. It does not require any additional reagents, does not produce pollutants and can produce metals of high purity. Studies have also shown that it can be used to recover a wide variety of metals [1.2, 1.3, 1.4].

The systematic approach will be developed by using waste from one source as a case study. The chosen waste is tin stripping solution; an aqueous solution that arises from the manufacture of printed circuit boards. The solution is nitric acid based and contains dissolved copper and iron, and suspended tin oxide.

1.2 PCB Manufacturing

The tin stripping process is part of the outer layer circuit formation of a multilayer printed circuit board (PCB) [1.5]. The manufacture of the outer layer of the circuit board starts with a rigid stack. This is created by pressing the inner layers, whose circuits are already defined, between sheets of laminate, with a layer of copper foil on the outside surfaces. Holes are then drilled through the panels to join the individual layers together (Figure 1-1). The holes are cleaned, made conductive and then plated with copper to form a complete circuit.

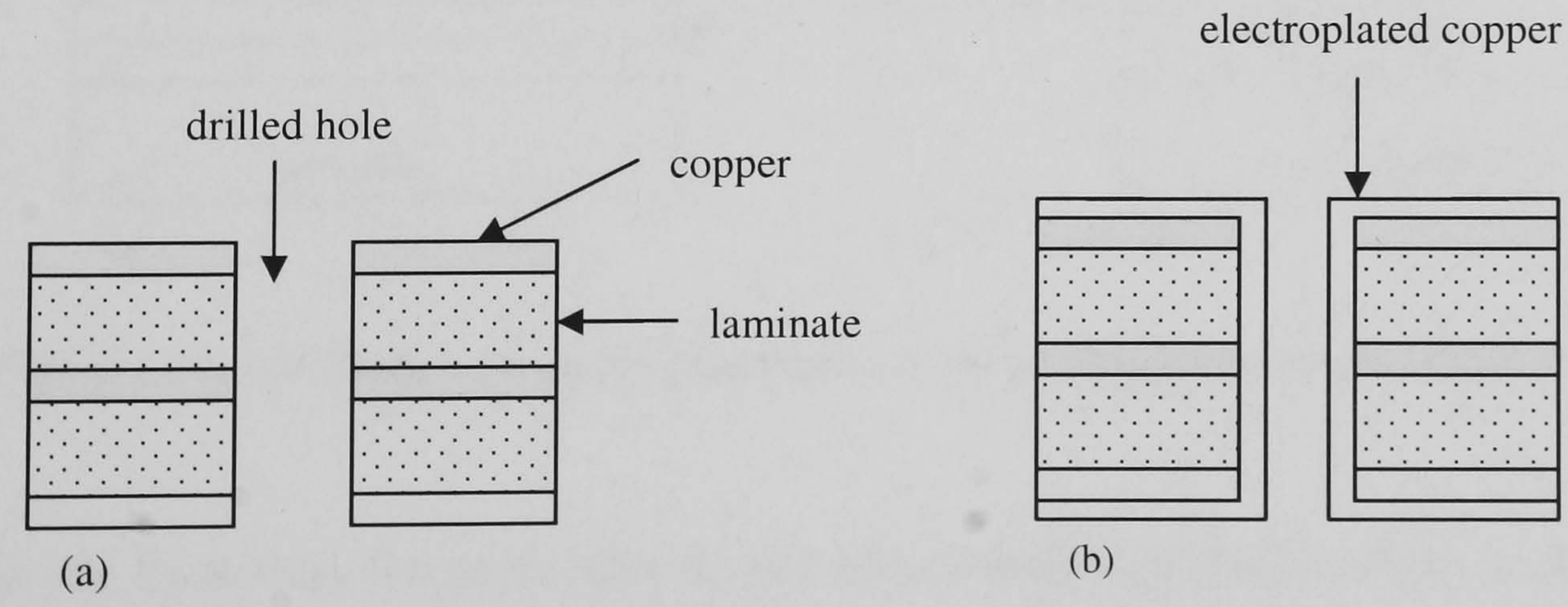

Figure 1-1 (a) Drilling of pressed stack (b) Copper plated holes

The design on the outer surface of the board is formed by pattern plating. A photoresist is applied and selectively exposed to UV light, creating a negative of the desired circuit traces. The unexposed resist is then removed, revealing the pattern of the circuit in copper foil. Additional copper is then electroplated onto the surface to build up the thickness of the design. These steps are illustrated in Figure 1-2, which only shows the top layer of the stack.

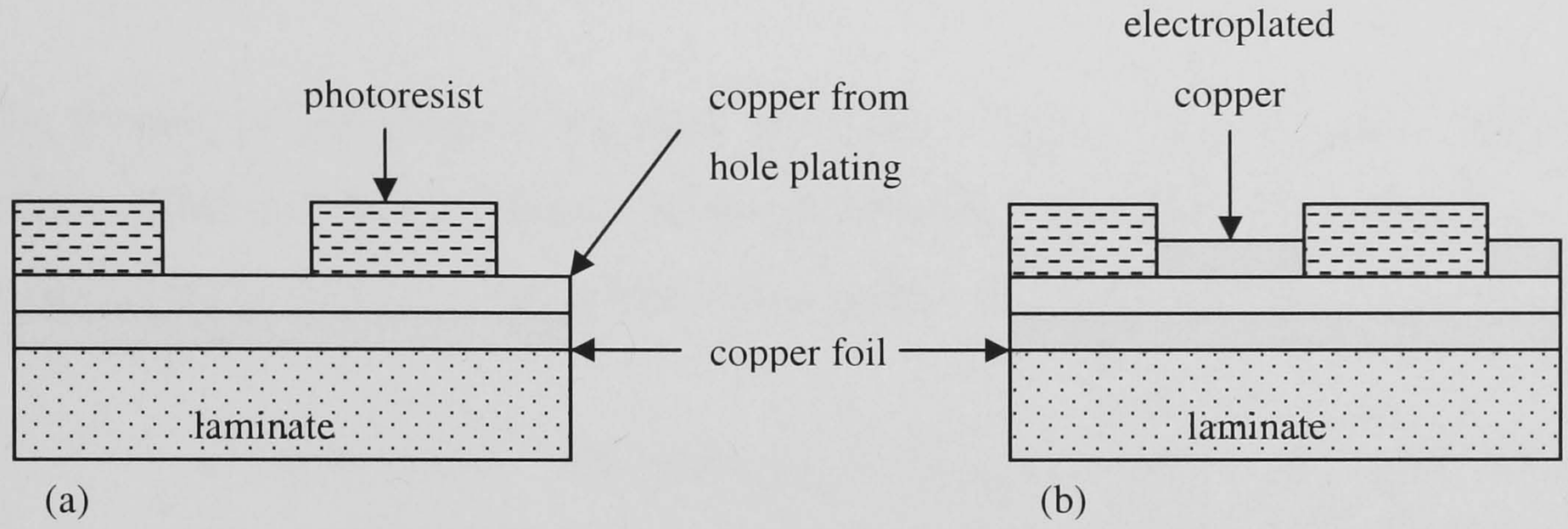

Figure 1-2 (a) Application of photoresist; (b) Additional copper plating

The next stage of the process involves electroplating tin on top of the copper. This protects the design when the photoresist and excess copper are removed to form the final pattern. Figure 1-3 shows the top layer of the circuit board after these processing steps.

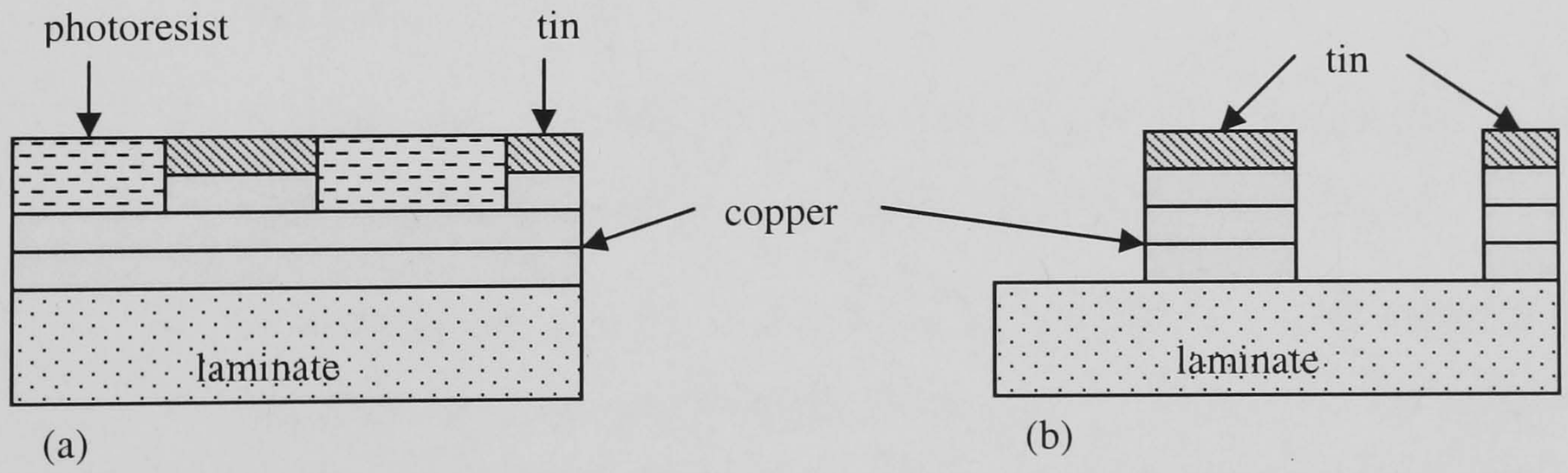

Figure 1-3 (a) PCB after tin electrodeposition; (b) After photoresist removal and copper etching

In the final step, the protective tin (or occasionally tin/lead) coating is stripped from the circuit board to leave the copper design.

1.3 Tin Stripping Process

Tin was plated onto the copper surface of the PCB to act as an etch resist, whilst the excess copper was dissolved to leave the final pattern. Dissimilar metals in close contact will often diffuse into each other to form intermetallic compounds. Copper and tin form two intermetallics: Cu_6Sn_5 and Cu_3Sn_1 [1.6]. Thus, in addition to the tin surface layer, the intermetallic layer which contains copper must be removed during the stripping stage.

The process of stripping the tin from the copper circuit board is usually carried out with a nitric acid based solution, although methane sulphonic acid is also used. The solutions are proprietary, but tend to contain the following components [1.7, 1.8]:

- Nitric acid. The removal of tin and copper by the acid are redox reactions; the tin and copper are oxidised, whilst the nitrate is reduced.

$$2Sn_{(s)} + 2HNO_3 \rightarrow 2SnO_2 + N_2O + H_2O$$

$$Cu + 4HNO_3 \rightarrow Cu(NO_3)_{2(aq)} + 2NO_{2(g)} + 2H_2O \quad \text{(Conc. Acid)}$$

$$3Cu + 8HNO_3 \rightarrow 3Cu(NO_3)_{2(aq)} + 2NO_{(g)} + 4H_2O \quad \text{(Dilute acid)}$$

- An inhibitor. Ideally the stripping process will preferentially remove tin over copper. However, as copper is more readily oxidised than tin, inhibitors are added to the solution to control the removal of copper and prevent tarnish.
- A ferric salt. In order to remove the tin/copper intermetallic a ferric salt is added increase the oxidising capability of the solution.
- A suspension agent. Tin forms an insoluble oxide (SnO_2) when oxidised, so is in suspension in the waste solution. The additive is used to ensure the oxide does not separate and adhere to the surface of the circuit board.

The tin stripping is carried out by spraying or submersing the circuit board in the stripping solution followed by rinse stages. The process can be operated as a batch process, or bleed and feed [1.9]. The batch process is operated until the metal

loading and pH go beyond a set range; the solution is then sent to disposal. With the bleed and feed method, the composition of the bath is kept constant by continually bleeding off a set volume and replacing it with fresh stripping solution. The metal concentration in the waste is typically 2-40g/l Cu and 150g/l SnO_2 [1.9].

Our industrial partner, from whom we have received used tin stripping solutions, operates a two stage stripping process. In the first stage, the majority of the tin is removed from the circuit board using a solution of Tinsolv 1000 (Atotech). The solution in the second stage (Tinsolv 2000) has a greater oxidising power than that of the first, due to the addition of Fe^{3+} ions; this removes the remainder of the tin and the tin/copper intermetallic. Thus the used Tinsolv 1000 contains tin and a small amount of copper, and the Tinsolv 2000 contains tin, copper and iron. The maximum amount of copper and iron in the waste Tinsolv 2000 is known from the process control limits (Table 1-1) and the dissolved tin concentration can be estimated from thermodynamic data [1.10].

Metal Ion	Tinsolv 1000	Tinsolv 2000
copper	0-2g/l (0-0.03M)	2-20g/l (0.03-0.3M)
tin	10^{-6}M	10^{-6}M
iron	n/a	4-14g/l (0.07-0.25M)

Table 1-1 Dissolved metal concentrations in waste stripping solution [1.11]

Waste tin stripping solution was chosen for this initial work because there are currently no schemes to recover the metals. At present the metals are precipitated and sent to landfill [1.7].

1.4 Reasons for Metal Recovery

It is common to recover metals from plating or etching processes, for example by electrowinning [1.12, 1.13]. However, there are currently no industrially used methods for recovering the metals from tin stripping solutions [1.7]. One of the reasons for this is that the tin exists as a very fine suspension of SnO_2 in the waste. This causes problems for many of the common recovery methods e.g. electrowinning

or ion exchange, which require the metal to be in solution. Filtration can also be difficult as the particle size of the SnO_2 is very small. There are further problems with the solution, other than the tin suspension: the additives, being complexing agents, have been reported to modify the electrochemistry making the deposition potential more negative and adversely affecting the current efficiency [1.14]. The acidity of the solution is also a factor, as a low pH will increase the hydrogen evolution, decreasing the current efficiency.

There are, however, economic drivers towards the recovery of metals in the solution. In a survey for the US Environmental Protection Agency [1.15], it is stated that on average, the volume of tin stripping solution to be disposed of is 17 gallons per 1000 board ft^2 of 4 layer boards (with approximately 0.5kg of tin per litre). If it is considered that this solution is often sent offsite for disposal, with costs of approximately $3.30/gallon, and the price of the metals is $6.05/kg for copper and $13.45/kg for tin [1.16], it can be seen that a method to treat the solution and recover the metals could be viable. In fact, the economics for the recovery are likely to improve due to the rising price of copper, which almost doubled in 2006 [1.17]. This rising price is thought to be linked to rapid industrialisation in China, where copper is used in the energy distribution network to bring power to new factories [1.18].

There are also environmental drivers for the recovery of metals from the solution. The cost of compliance with new legislation can be high, and much of this focuses on minimising waste. The directives that will have the most impact on the disposal of the tin stripping solution are the Integrated Pollution Prevention and Control Directive (IPPC), the Landfill Directive and Landfill Tax [1.19]. The IPPC directive is being introduced across Europe and will be fully implemented by October 2007. It covers emissions to air, land and water, which are considered together in order to attain the best environmental protection. One of the ways through which this is realised is the concept of Best Available Techniques. This concept balances the cost of implementation against the environmental protection acquired, taking into account consumption of raw materials, energy efficiency and waste minimisation. According to the guidance notes produced by Defra [1.20], "IPPC aims to prevent emissions and

waste production and where that is not practicable, reduce them to acceptable levels".

The Landfill Directive is implemented in the UK through the Landfill Regulations 2002. The regulations aim to reduce the effects of landfill sites by: reclassifying the sites into 3 categories (hazardous, non-hazardous and inert); reducing the amount of biodegradable material sent to the sites; prohibiting certain hazardous wastes, including liquids; and requiring pre-treatment of wastes. Hazardous waste (which includes tin stripping solutions) must be treated to [1.21]:

- reduce the quantity, or
- make it less hazardous, or
- make it easier to handle, or
- enhance recovery.

Landfill Tax was introduced in 1996 to discourage the use of landfill by charging per tonne of material disposed of. The rates are set at [1.22]:

- £2 per tonne for inert waste.
- £21 per tonne for all other waste, rising by at least £3 per year on the way to a medium to long term rate of £35 per tonne.

1.5 Proposed Recovery Methods for Tin and Copper

The separation of metals from the tin stripping solution has been studied previously, but a process that can work in industry has yet to be conceived. In general the separation schemes involve filtration to remove the SnO_2, followed by the electrodeposition of copper [1.7, 1.14, 1.23].

Proposed Method 1

Scott et al [1.14] suggest two alternative schemes for the recovery of metals from tin stripping solution, which in this case contained lead. In the first of these, the solution was aerated to ensure the tin was in the form of a hydrated precipitate, which was

then removed by filtration. The SnO_2 was then washed and dissolved in HCl and the tin recovered by electrowinning. The remaining stripping solution, after the filtration, went to electrowinning stages where first the Cu and then the Pb were removed. The process is illustrated in Figure 1-4:

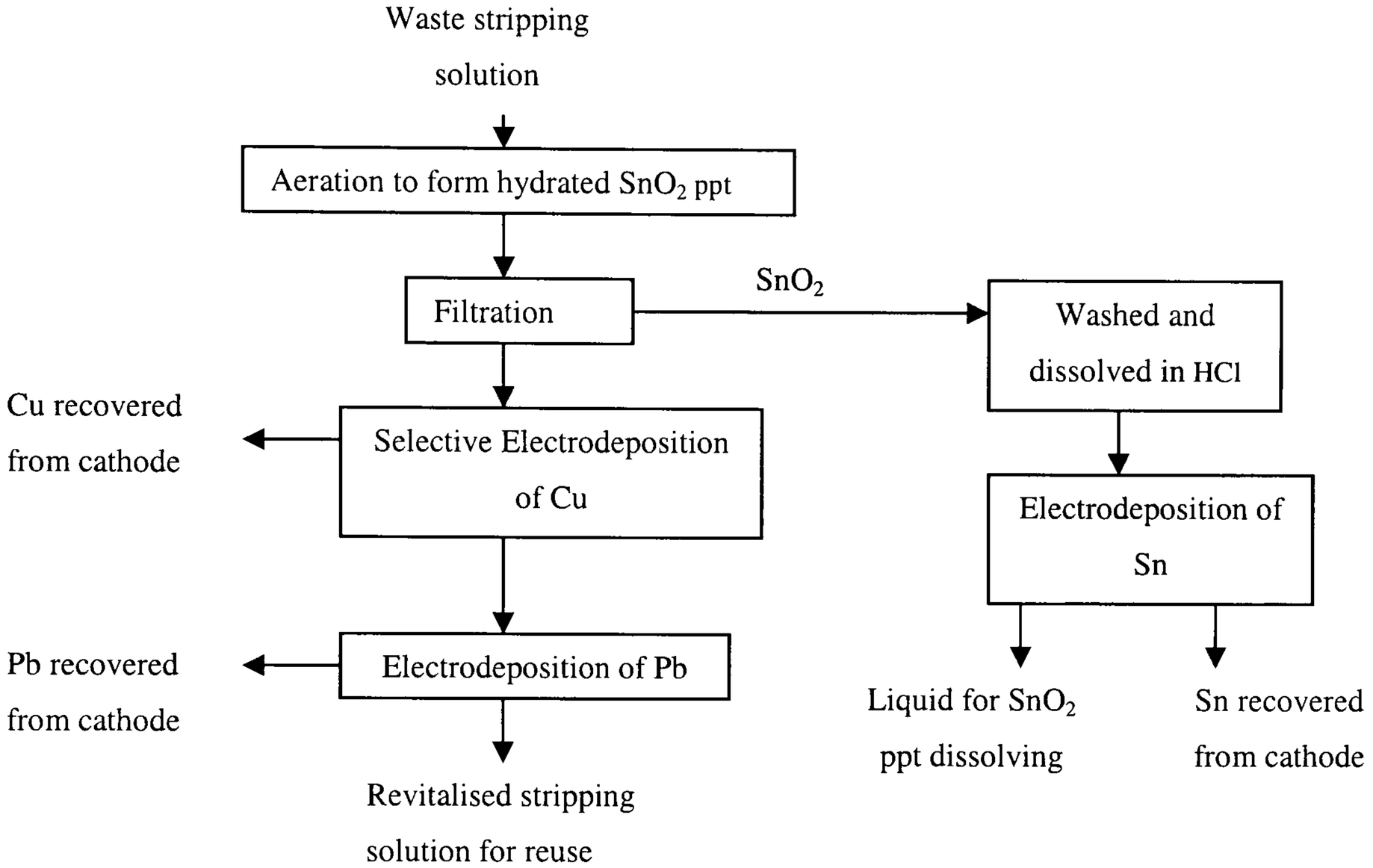

Figure 1-4 Method of *Scott et al* [1.14]

In the second scheme both the tin and the lead were removed by precipitation and filtration. As before, the solution was aerated to enhance the tin recovery and then sulphuric acid was added to precipitate the lead. The precipitates could then be sent to furnace refineries for further processing. The copper was electrowon from the filtrate.

Scott et al highlighted some limitations of the proposed recovery processes when used on waste commercial stripping solutions. The first of these is that tin was deposited with both the copper and the lead, so that separation was impossible. Also, the additives in the solution formed complexes with the metals, lowering their deposition potential and resulting in high energy consumption. These lower deposition potentials combined with the high HNO_3 (5M) content of commercial stripping solutions meant that the current efficiency was found to be low due to

hydrogen evolution. The proposed solution to these problems was to use a less concentrated solution of HNO_3 (1.4 - 2.1M) with no additives as the stripping fluid. Although this solution was shown to remove the tin-lead resist with little attack on the copper, and the tin and copper could be later recovered, this stripping solution is not used industrially.

Proposed Method 2

Lee et al [1.23] started their process by the extraction of nitric acid from the spent stripping solution using a solution of tributylphosphate in kerosene. The copper was then electrowon from the remaining solution, followed by the tin ions being precipitated as $Sn(OH)_2$ by increasing the pH with $Pb(OH)_2$. The lead was then removed by cementation with iron powder.

The method outlined above was based on experiments using synthetic solutions, so no account had been taken of the effect of the additives in a commercial solution. The paper also makes no mention of the fact that tin is in suspension in the spent stripping solution. Codeposition of tin with the copper was also found by this group, although they presumably had a higher concentration of tin in the deposition electrolyte, as no tin removal stages had been carried out.

Proposed Method 3

The suggested method for the selective recovery of copper and tin by *Kerr* [1.7] is shown in Figure 1-5. This separation scheme was the outcome of a scoping study which identified suitable separation technologies and assessed their possible combinations.

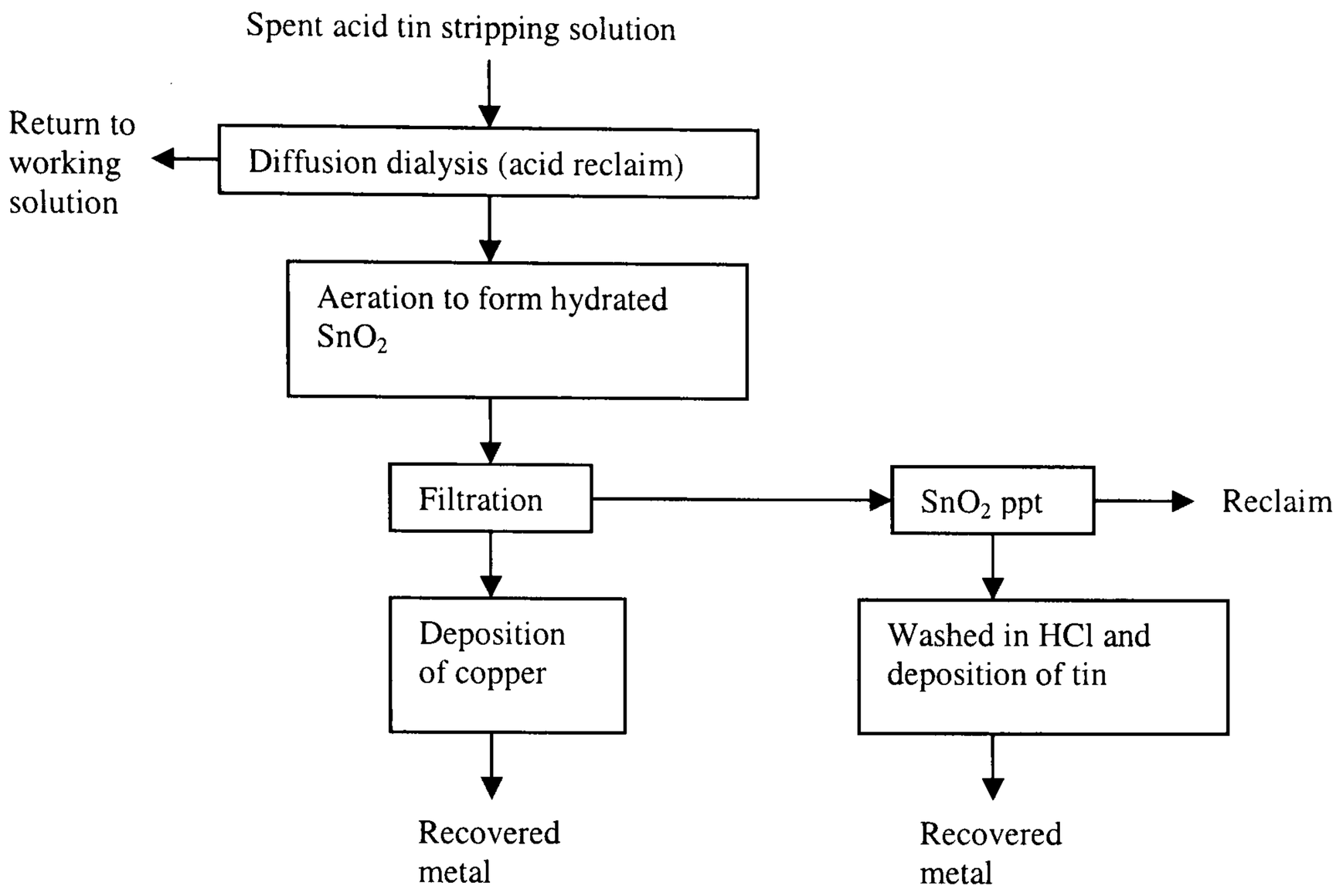

Figure 1-5 Method of *Kerr* [1.7]

The method combines the advantages of Methods 1 and 2. It can be seen that the recovery scheme is similar to that of *Scott et al* [1.14], except that there is an initial acid recovery stage (as in Method 2), which will remove hydrogen ions. This acid recovery step will therefore reduce the problem of low current efficiency, caused by hydrogen evolution. After the acid removal, the solution would be aerated, to precipitate any remaining tin, and passed onto a filtration stage to remove the SnO_2 precipitate. The SnO_2 could then be dissolved in hydrochloric acid and the tin electrowon, or sold as the oxide depending on the market. The filtrate would pass to another electrowinning stage where copper would be recovered. After the deposition of copper, the solution would be passed through ion exchange resins to remove iron and any other trace metals. It may then be possible to recycle the water back into a stage in the PCB manufacturing process. No experimental work has been carried out to validate this method.

Proposed Method 4

The approach of *McKeeson et al* [1.8, 1.24] is different from those outlined above; instead of removing the SnO_2 as a precipitate, they propose adding sodium hydroxide to ensure the tin is in solution. All the metals could then be electrowon. A problem

of this method is that when the hydroxide is added to the spent stripping solution, other metals came out of solution; complexing agents were therefore added. Thus, the consumption of additional chemicals is quite high. Also, the method involves plating out all the metals together, which could make subsequent recovery for reuse difficult.

Evaluation of Recovery Methods

The recovery method proposed by *Kerr* [1.7], is thought to be the most feasible. This process has the benefit that the only supplementary chemical required is HCl: this minimises operating costs. Also, because H^+ ions are removed, the current efficiency may be sufficiently high that the scheme can cope with a lower deposition potential caused by the additives. The proposed method also selectively recovers the metals.

Although the main stages of the process have been determined, there are still significant challenges to overcome to ensure the process is feasible.

- Metals need to be recovered in a usable form, either pure or as alloys. In the case of tin it is possible that the tin oxide will have a resale value without the need to process it further.
- The effect of the additives in the spent stripping solution need to be quantified. These may need removal prior to electrowinning.
- The process should be, as far as is possible, a closed loop and minimise the use of additional chemicals.

1.6 Electrodeposition

The method of *Kerr* [1.7], could involve two electrowinning stages: copper from nitrate solutions and possibly tin from a chloride solution. Literature has been reviewed so that any potential problems with the metal depositions were revealed, and also to gain knowledge of the experimental conditions required for the deposition.

1.6.1 Copper electrodeposition

The deposition of copper from nitrate solutions has been reported during electrorefining [1.25], for the recovery of copper from pickling liquors [1.26], as well as for copper recovery from stripping solutions as previously described (Section 1.5). Table 1-2 shows the conditions at which copper deposition from nitrate electrolytes has been successfully effected, and the resulting current efficiency for the deposition.

Ref.	[Cu]	$[HNO_3]$	j / mA cm^{-2}	t / hr	Φ
Lee et al [1.23]	0.22 – 0.005M	0.2M	20-220	20	22% after 5hrs
Choi et al [1.25]	initial 0.69M $Cu(NO_3)_2$; deposit 18.6g	pH kept at 1.5-1.7	20	72	61.5%
Scott et al [1.14]	0.109-0.068M	2M	14	?	92%
Mecucci et al [1.27]	initial 0.01M $Cu(NO_3)_2$	0.5M	20	2	43%

Table 1-2 Deposition conditions for copper from nitrate electrolytes

From the table it can be seen that the current densities used for the deposition are all similar at ~20mA cm^{-2}. However, the efficiencies of the copper deposition vary widely. The efficiency would be expected to decrease as the copper concentration decreases; this trend is not seen. For example, *Choi et al* [1.25] deposited copper from a nitrate solution at an efficiency of 61.5% after 72 hours. As they were electrorefining, the copper content was constant at 0.69M. This can be compared to the result of *Scott et al* [1.14] who achieved a current efficiency of 92% when the copper content was lower, in the range 0.109-0.068M. However, the time period over which this deposition was carried out was not stated. The efficiency will also depend on other factors, such as the pH, nitrate concentration and electrode material. The deposition conditions and efficiencies in Table 1-2 do, however, show that copper can be electrowon from nitrate solutions with reasonable efficiency.

Several problems have been reported with the deposition of copper from nitrate solutions; these include chemical dissolution of the deposited copper by nitric acid,

non-adherent copper deposits and concurrent reduction of nitrate with the copper. All these problems will lead to lower current efficiency for the deposition.

Antropov et al [1.28] investigated the corrosion of copper in nitrate copper plating electrolytes. They found that the deposited copper could be chemically dissolved by the nitric acid. The rate of the copper dissolution increased as the concentration of nitrate ions and the pH increased. However, if the HNO_3 concentration was maintained below 0.5M, and additives included in the electrolyte, the deposition rate exceeded the corrosion rate by several orders of magnitude. The main cause of the decrease in copper plating current efficiency was found to be the reduction of nitrates; this reduction was found to be catalysed by copper ions.

The dissolution of copper was also used by *Mecucci et al* [1.27] to explain why the efficiency of their copper deposition fell as the current density decreased and the HNO_3 concentration increased. They also found that adherent copper deposits were only obtained from electrolytes containing less than 2M HNO_3. At higher acid concentrations the deposit was rough, which was linked to substantial hydrogen evolution.

As ferric ions are a constituent of the tin stripping solution, it is possible that they will be in the copper deposition electrolyte. *Dew and Phillips* [1.29, 1.30] investigated the effect of Fe(II) and Fe(III) on the efficiency of copper electrowinning from sulphate solutions. They found that Cu(II) and Fe(III) reduction occur simultaneously at the cathode, decreasing the current efficiency for the copper deposition. They also looked at the anodic reoxidation of Fe(II) back to Fe(III) and found that this reaction can be suppressed by using a lead-antimony anode [1.29]. Fe(II) concentration was found not to affect the copper deposition efficiency [1.30].

The adverse effect of Fe(III) on copper deposition was also observed by *Das and Gopala Krishna* [1.31]. They found that for copper deposition from sulphate electrolytes, the current efficiency dropped if the Fe(III) concentration was greater than 1.0g/l.

1.6.2 Electrochemical reduction of nitrate

As the reduction of nitrate is reported to occur alongside copper deposition, decreasing the deposition efficiency, it is pertinent to review the literature on nitrate reduction to attempt to minimise its effect.

The reduction of nitrate ions has been studied for many reasons: the analysis of nitrate in drinking water [1.32], the production of chemicals [1.33], the cleaning of waste solutions [1.34] and the decontamination of ground waters [1.35]. The products from the reduction are varied, as there is strong dependence on the electrode material and preparation, the electrolyte and electrode potential [1.33]. The electrochemical reduction reactions of nitrate that can occur in acidic media, and their characteristic potentials, are shown in Table 1-3.

$2NO_3^- + 4H^+ + 2e^- \rightarrow N_2O_4(g) + 2H_2O$	$E^0 = 0.803$
$NO_3^- + 2H^+ + e^- \rightarrow NO_2(g) + H_2O$	$E^0 = 0.775$
$NO_3^- + 3H^+ + 2e^- \rightarrow HNO_2 + H_2O$	$E^0 = 0.98$
$NO_3^- + 2H^+ + 2e^- \rightarrow NO_2^- + H_2O$	$E^0 = 0.835$
$NO_3^- + 4H^+ + 3e^- \rightarrow NO(g) + 2H_2O$	$E^0 = 0.960$
$2NO_3^- + 10H^+ + 8e^- \rightarrow N_2O(g) + 5H_2O$	$E^0 = 1.116$
$2NO_3^- + 12H^+ + 10e^- \rightarrow N_2(g) + 6H_2O$	$E^0 = 1.246$
$NO_3^- + 10H^+ + 8e^- \rightarrow NH_4^+ + 3H_2O$	$E^0 = 0.875$

Table 1-3 Standard potentials (vs SHE) for nitrate reduction [1.10]

The nitrate reduction reactions have been found to proceed at more negative potentials than the standard values quoted in Table 1-3 [1.33]. *Pletcher and Poorabedi* [1.36] reported a value of $E_{1/2}$ = -0.06V vs SHE for 5mM NO_3^- in 1M perchloric acid, and *Carpenter and Pletcher* [1.32] observed a well formed reduction wave at $E_{1/2}$ = -0.38V vs SHE for 1mM NO_3^-. Both these values are for nitrate reduction on copper electrodes.

It is generally agreed that provided there are sufficient protons in the solution, the product of nitrate reduction in acidic media on a copper electrode is ammonia [1.36], following the reaction shown below. If the hydrogen ion concentration is limited, the end product is dependent on the ratio of nitrate to hydrogen ions [1.32].

$$NO_3^- + 8e^- + 9H^+ \rightarrow 3H_2O + NH_3$$

The rate determining step in the nitrate reduction has been found by *Dima et al* [1.33] to be the first electron transfer during the reduction of nitrate to nitrite. The NO_2^- is then further oxidised to NO and then finally to NH_3 [1.37] on bulk copper (the intermediate reactions are shown below). However, NO was oxidised to N_2O on a layer of underpotentially deposited copper on palladium.

$$NO_3^- + 2H^+ + 2e^- \rightarrow NO_2^- + H_2O$$

$$NO_2^- + 2H^+ + e^- \rightarrow NO + H_2O$$

Chloride (and other halide) ions have been found to suppress the nitrate reduction. *Pletcher and Poorabedi* [1.36] discovered that halide ions cause the nitrate reduction peak to shift to more negative potentials where it is masked by hydrogen reduction. *De Vooys et al* [1.37] suggested that chloride ions block nitrate reduction sites on the copper, causing a decrease in the current.

1.6.3 Tin electrodeposition

Carano [1.38] describes four basic choices when it comes to baths for electroplating tin; alkaline stannate, acid sulphate, acid fluoroborate and acid sulphonate.

- The alkaline stannate process is based on potassium or sodium stannate, with potassium being preferred as the salts are more soluble. The process does not require any organic additives, but does operate at elevated temperature (70-90°C).

- The acid sulphate bath requires additives to achieve an adherent deposit, but gives good efficiencies (~100%) and runs at ambient temperature.
- The fluoroborate bath is very corrosive, but has the advantages that it can be run at high current densities, has an efficiency of ~100% and runs at ambient temperature.
- The acid sulphonate bath contains methane sulphonic acid and is becoming more widely used because the wastes require simple treatment, and it can hold a high concentration of tin in solution. The disadvantage is that the chemical make up costs are higher than for the other processes.

The electrolytes described above have been designed for plating, rather than for the recovery of tin from wastes. According to the proposed recovery scheme, SnO_2 should be dissolved, so that tin could be electrowon from the resulting solution. If these baths are examined in the light of the proposed recovery process, problems with their use arise.

Scott et al [1.14] attempted to dissolve SnO_2 from waste tin stripping solution using sulphuric acid. The precipitate was found not to dissolve. H_2SO_4 was also trialled by *Stefanowicz et al* [1.4] to dissolve a tin containing sludge from the fluoroborate plating process. They found that after 30 minutes of stirring the sludge in 10-25wt% H_2SO_4, only 5wt% of the sludge had dissolved. Sulphuric acid would therefore be an unsuitable electrolyte for the dissolution and subsequent deposition of tin.

The alkaline bath was also thought to be unsuitable. *Stefanowicz et al* [1.4] attempted to dissolve the plating sludge in NaOH. The dissolution occurred slowly, with two thirds of the sludge having dissolved in 15% NaOH after a week. Tin was deposited from this electrolyte at a current efficiency of only 7%.

The fluoroborate process was discounted on the basis that it would introduce noxious chemicals into a stream that is being cleaned. This left the acid sulphonate process, along with the proposed chloride bath.

Both *Stefanowicz et al* [1.4] and *Scott et al* [1.14] tested the dissolution of tin sludge and SnO_2, respectively, in hydrochloric acid. They found that it was possible to dissolve the tin in 10% HCl solutions, if heated. Chloride solutions were also used by *Pilone and Kelsall* [1.39] to leach metals, including tin, from shredded waste electronic equipment, before deposition. It has been shown that it is possible to recover tin at reasonable current efficiencies after dissolution [1.4], even from very dilute solutions [1.40]. The reported conditions required for tin recovery from chloride electrolytes, and the resulting current efficiency are shown in Table 1-4.

Ref	initial [Sn]	[HCl]	j / mA cm^{-2}	t / hr	Φ
Chaudhary et al [1.40]	0.002M	0.4M	$25x10^{-4}$	8	5.4%
Stefanowicz et al [1.4]	0.45M	conc., diluted 1:1	0.05	3.17	93%
Scott et al [1.14]	0.354M	~1M	70	?	85%
Mecucci et al [1.27]	0.01M	1.5M	7.5	2	95.3%

Table 1-4 Deposition parameters for tin from chloride electrolytes

As a general trend, it can be seen that the current efficiency of the deposition decreases as the tin concentration decreases, the exception to this are the results from *Mecucci et al* [1.27]. Thus, for the most energy efficient deposition the tin concentration will need to be as high as possible. The concentration will, however, be limited by the solubility of SnO_2 in hydrochloric acid. To maintain the highest possible concentration, *Scott et al* [1.14] suggest performing the deposition with some tin in suspension, dissolving as the tin is plated. The current efficiency of the tin deposition is also affected by the current density. *Chaudary et al* [1.40] found that increasing the current density decreases the recovery time, but also the current efficiency. Therefore these factors need to be balanced to minimise the energy per unit mass deposited. A possible problem with the deposition from chlorides is that chlorine was reported to be evolved at the anode [1.4]; this could be solved by having a split cell [1.14].

1.7 Electrochemical Reactors for Metal Recovery

Industrially, the electrochemical recovery of metals would be carried out using a reactor. Electrochemical reactors have been utilised for many years to deposit metals from aqueous wastes for reuse. Examples include the recovery of silver from spent photographic fixer solution [1.41] and nickel from the rinse waters of plating baths [1.12]. Metal recovery via electrochemical reactors has the advantages that: additional chemicals are not required; the metals can be recovered in their metallic form; electrolytic processes generally have low operating costs; and the processes tend to operate at low temperature and pressure.

Electrochemical reactors are often individually designed for a specific application, in order to maximise metal recovery and minimise running costs. Factors that affect these include: cell voltage, cell current, electrode area, flow, ohmic drops in the cell and associated connections, and the required form of the deposited metal (e.g. powder or sheet).

1.7.1 Typical Reactor Designs

Although many reactors are individually designed, there are several commonly used reactor types. These designs are described below, along with their advantages and disadvantages. Typical uses, and possible concentration reductions for metal recovery, are also reviewed.

Tank Reactors

Tank reactors are of simple design, commonly consisting of vertical electrodes suspended in a rectangular tank containing the electrolyte. The mass transport characteristics of the reactor can be improved by agitating the electrolyte. The agitation is commonly via gas sparging or pumping the electrolyte through the cell [1.42]. Table 1-5 shows some advantages and disadvantages of this type of reactor.

Advantages	Disadvantages
Simple construction – low capital costs	Poorly controlled fluid flow and thus mass transport
Easy to remove the electrodes to recover metal (often as foil)	Limited space-time yield (i.e. mass of product per unit time that can be obtained per unit volume of reactor)
Easy to scale up/down	

Table 1-5 Advantages and disadvantages of tank reactors

Tank reactors are often used for electroplating, when the object to be plated and a soluble anode are placed into the tank, aluminium extraction, and water electrolysis [1.43]. For metal recovery, tank reactors would only be used if the metal concentration in the solution was high. For example, *Campbell et al* [1.44] recovered nickel from a solution of 20g/l down to 3g/l (20,000 – 3,000ppm) using a tank cell. They found that the current efficiency of the deposition decreased rapidly below concentrations of 7g/l.

Parallel Plate Reactors

Parallel plate reactors consist of many closely spaced electrodes, alternating cathode and anode. They are often constructed as a filterpress, where the electrodes, frames (which form the flow channels) and membranes are sealed into a module; these modules are then stacked together to form the reactor, known as a plate-and-frame reactor. Some advantages and disadvantages of parallel plate reactors are shown in Table 1-6.

Advantages	Disadvantages
Simple construction	Low space-time yield
Easy to scale up, as extra cells can be added onto the stack	Small interelectrode gaps are difficult to maintain for large area electrodes
	Difficult to extract solid products from plate and frame configurations

Table 1-6 Advantages and disadvantages of parallel plate reactors

Plate-and-frame reactors with 2-dimensional electrodes are not often used for metal recovery, but are employed for electrosynthesis [1.45] and in the chlor-alkali industry [1.42]. However, simple parallel plate reactors, with just one pair of electrodes and the fluid flowing normal to the current, have been used for metal recovery. *Scott and Paton* [1.46] used this type of reactor, with a non-conducting fluidised bed in the cathode compartment, to study the effect of iron on cadmium deposition. They managed to recover cadmium from a 200ppm solution down to a limit of 20ppm.

Rotating Electrode Reactors

In this type of reactor the electrode rotates in order to enhance the mass transfer of the metal ions from the bulk solution to the electrode. The most common type is the rotating cylinder electrode reactor. The cylinder can be either horizontal as in the case of metal foil production, or vertical as for metal ion removal. In the majority of cases metal removal is effected by removing the electrode and manual scraping, although blades to continuously scrape powder or foil from the cathode are in use [1.42]. Table 1-7 shows some advantages and disadvantages of this type of reactor.

Advantages	Disadvantages
Can obtain high rates of mass transport	Complex design as rotating seals, contacts etc are required
Relatively compact	
Control of shear forces can be used to obtain different sizes of metal powder/flake	

Table 1-7 Advantages and disadvantages of rotating electrode reactors

These reactors can be used to recover metals in relatively high concentration in solution, for example *Ragauskas et al* [1.41] used a horizontal cylinder in a tank to recover silver from spent photographic fixer from 20g/l down to 1.3g/l (20,000 – 1,300ppm). Rotating cylinder electrodes can also be used as a cascade of cells to reduce metal concentrations down to 1-2ppm [1.43].

Static Porous 3D Electrode Reactors

These reactors utilise 3-dimensional electrodes to increase the surface area available per unit reactor volume. There are many types of materials that have been used as electrodes: woven fabrics and felts, meshes, packed beds, and expanded metal or carbon foams. These electrodes can be incorporated into many of the reactors previously described. The advantages and disadvantages of 3D electrodes are shown in Table 1-8.

Advantages	**Disadvantages**
Porous electrode can act as a turbulence promoter, resulting in moderate mass transfer rates	Non-uniform current and potential distribution throughout the structure: - parts of the 'cathode' can become anodic so the metal redissolves - premature blocking of the matrix with deposited metal
High values of the space-time yield	Less range of materials than for 2D electrodes
	Performance is less predictable than for 2D electrode
	Can get high pressure drops as the electrolyte flows through the electrode
	Liable to plug with deposited metal

Table 1-8 Advantages and disadvantages of 3D electrodes

These 3D porous electrodes are often used to recover metals from dilute solutions. A graphite packed bed was used by *Campbell et al* [1.44] to recover nickel. The reactor was a modified plate and frame cell where the catholyte frame was packed with graphite granules. The concentration of nickel in the electrolyte was reduced from 60ppm down to 1ppm. The Porocell reactor was developed by EA Technology and consists of a porous carbon felt electrode, through which the electrolyte flows. It has been used to recover copper from rinse waters generated during printed circuit board production. The cell maintains the copper concentration in the rinse tank between 290ppm and 0.15ppm. The Porocell has also been used to recover silver from photographic fixers; in initial trials the concentration of silver was reduced from 3.6g/l (3,600ppm) to 1ppm in a single stage [1.47].

Moving 3D Electrode Reactors

These reactors utilise the high surface area 3-dimensional electrodes described above, with the electrode in motion. Examples of this type of reactor are the fluidised bed, rotating barrel reactor (a rotating cylinder filled with particles) and the spouted bed reactor (similar to a packed bed, but with a central fluidised section). Table 1-9 shows some advantages and disadvantages to incorporating the 3D electrodes into moving reactors.

Advantages	Disadvantages
Mass transport rates are higher than for the static 3D electrodes	Complex design, due to rotating parts or fluidised beds
Can continuously remove deposited metal by entraining particles in the outlet flow	Non-uniform flow distribution
Electrode movement can be used to control reaction rates	Non-uniform current/potential distribution

Table 1-9 Advantages and disadvantages of 3D electrodes in moving reactors

As is the case for the static 3D electrodes reactors, these moving 3D electrode reactors can recover metals from dilute solutions to meet discharge consent levels [1.43]. A spouted bed reactor was used by *Shirvanian and Calo* [1.48] to recover copper from an acidic solution. The metal concentration was reduced from approximately 1000ppm down to 80ppm. They noted that anodic points in the cathode can be minimised by keeping the voidage in the bed low and decreasing the bed height. A rotating barrel reactor was used by *Avci* [1.49] to recover copper from dilute (2400ppm) acidic copper solutions. The final copper concentration achieved was 1ppm, but the current efficiency of the deposition decreased sharply when the concentration reached ~400ppm.

1.7.2 Modes of Operation

The reactor designs described above can be used in different operating modes. There are three main modes of operation for electrochemical reactors: batch, continuously stirred tank (CSTR), and plug flow (PFR) [1.45]. In practice many electrochemical

reactors are hybrids of these extremes. Also, many reactors incorporate a recycle stream to increase the conversion or (in the case of the batch reactor) to allow for different volumes per batch.

In batch mode, all the solution to be processed (in this case for metal removal) is put into a single tank, which is usually agitated. The reaction will occur in this tank over a fixed time, after which the solution is discharged from the tank to make way for the next batch. During the batch time the concentration of the metal will decrease, although the concentration throughout the tank will be uniform at ay given moment. This operational mode is discontinuous and therefore often used when the solution for processing is generated sporadically.

The continuously stirred tank reactor is similar to the batch reactor in that it consists of a stirred tank in which the concentration of any species is uniform at any instant. However, this reactor mode has continuous inlet feed and outlet removal. With perfect mixing the concentration of species in the tank is the same as that in the outlet. This is achieved in practice by either stirring or electrode movement (as in the rotating cylinder electrode).

In the plug flow mode of operation, the solution flows continuously through a tubular reactor at constant rate. The species do not mix in the direction of flow, so the concentration of reactant changes along the length of the reactor.

1.8 Project Aims and Objectives

The increasing volume of liquid discharges from electronics manufacture poses an environmental threat, as these solutions can contain substances that are harmful, such as nitrates and phosphates. The wastes also contain dissolved metals which are sent to landfill sites for disposal, after precipitation from solution. The aim of this project was to develop a systematic methodology to determine the feasibility of recovering metals from such solutions.

The methodology involved investigating the recovery of metals from tin stripping solution; an aqueous waste stream from printed circuit board manufacture. Despite several studies into the recovery of copper and tin from this solution, none of the processes are used industrially. This project seeks to answer some of the remaining questions:

1. It is not known whether any of these proposed recovery processes are thermodynamically feasible, and how the recovery at each stage is constrained by pH, the constituent metal and anion concentrations, and potential.
2. There are no studies into how the concentration of the tin stripping components, such as NO_3^-, Cu(II) and Sn, affects the metal recovery.
3. Much of the previous work utilised simulated waste solutions, without the industrial additives such as ferric ions. How will the proposed recovery stages be affected if these are in solution?

The first step in the method that was used to determine the feasibility of recovering tin and copper from the waste tin stripping solution involved analysing the thermodynamics of the system. Once the theoretical conditions for metal separation were established, the processes (e.g. filtration, electrodeposition) that could be used were determined. Each separation stage could then be studied in more detail to verify that the theory was correct and to resolve any practical issues.

Therefore, to determine the feasibility of tin and copper recovery from waste tin stripping solution, the thermodynamic stability of copper, tin and iron in the presence of nitrate and chloride ions was investigated. The nitrate ions represent the waste; the chloride ions the tin dissolution stage. The objective of this theoretical analysis was to ascertain when the metals would be in the solid or liquid phase depending on the concentration of the metal and anions, pH and system potential. This information was then compared to the modus operandi of the separation processes proposed by *Kerr* [1.7]. The thermodynamic study was then verified empirically.

After the overall route to metal recovery was established, the project focussed on the copper electrodeposition stage. An electrochemical characterisation study was carried out to determine whether it is possible to deposit copper from a nitrate solution with reasonable efficiency, and to find the effect of the stripping additives and iron/tin on this efficiency.

Finally, copper recovery from stripping solution was carried out in a parallel plate reactor. The objective of this study was to determine the efficiency of the deposition as copper was recovered using an industrial reactor, and to estimate some of the costs involved.

1.9 References

1.1 European Electronic Component Manufacturers Association, *EECA Market Report*, EECA (2005)

1.2 P. Fornari and C. Abbruzzese, *Hydrometallurgy*, **52**(3): 209-222 (1999)

1.3 C. M. Juarez and A. J. B. Dutra, *Minerals Engineering*, **13**(10-11): 1083-1096 (2000)

1.4 T. Stefanowicz, T. Golik, S. Napieralskazagozda and M. Osinska, *Resources Conservation and Recycling*, **6**(1): 61-69 (1991)

1.5 Bay Area Air Quality Management District, *Bay Area Air Quality Management District Permit Handbook: Printed Circuit Board Manufacturing Operations*, http://www.baaqmd.gov/pmt/handbook/s07c01fr.htm, accessed on 25/06/06

1.6 Copper Development Association, http://www.copper.org/applications/industrial/DesignGuide/coppertin03.html, accessed on 06/03/2007

1.7 C. Kerr, *Transactions of the Institute of Metal Finishing*, **82**(B7-B12, Part1-2): (2004)

1.8 D. McKeeson, *Printed Circuit Fabrication*, **22**(7): 34-37 (1999)

1.9 C. Kerr and F. Coultard, *Sustainable Technologies for the Tin Stripping Process used in Printed Circuit Board Fabrication*, ITRI Ltd. & Intellect (2004)

1.10 A. J. Bard, R. Parsons and J. Jordan, ed. *Standard Potentials in Aqueous Solution*, Dekker, New York (1985)

1.11 R. Massey, Personal Communication, (2005) [e-mail, 27/04/05]

1.12 G. Orhan, C. Arslan, H. Bombach and M. Stelter, *Hydrometallurgy*, **65**(1): 1-8 (2002)

1.13 G. C. Cushnie, Jr, *Pollution Prevention and Control Technologies for Plating Operations*, http://www.nmfrc.org/bluebook/tocmain.htm, accessed on 14/02/05

1.14 K. Scott, X. Chen, J. W. Atkinson, M. Todd and R. D. Armstrong, *Resources Conservation and Recycling*, **20**(1): 43-55 (1997)

1.15 CAI Resources Inc, *Printed Wiring Board Pollution Prevention and Control Technology: Analysis of Updated Survey Results*, (1998)

1.16 London Metal Exchange, *Daily Stocks and Prices*, http://www.lme.co.uk/dataprices_daily_metal.asp, accessed on 05/03/07

1.17 A. Beattie, Fear and greed turn copper price red hot, in *Financial Times* (23/05/06)

1.18 G. Dyer, The Chinese building boom that is fuelling a mania for metals, in *Financial Times* (27/05/06)

1.19 Environment Agency, *Regulations / licences / guidance*, http://www.environment-agency.gov.uk/business/444304/444641/595811/?version=1&lang=_e, accessed on 15/02/05

1.20 Department for Environment Food and Rural Affairs, *Integrated pollution, prevention and control: a practical guide*, (2005)

1.21 Environment Agency, *Landfill Directive Summary Note 1: New Restrictions on Landfill of Special/Hazardous Waste*, http://www.environment-agency.gov.uk/business/444217/444663/landfill/475341/?version=1&lang=_e , accessed on 15/02/05

1.22 HM Customs and Excise, *Notice LFT1: A general guide to landfill tax*, http://www.hmce.gov.uk/channelsPortalWebApp/channelsPortalWebApp.portal?_nfpb=true&_pageLabel=pageHome_ShowContent&id=HMCE_CL_000509&propertyType=document, accessed on 15/02/05

1.23 M. S. Lee, J. G. Ahn and J. W. Ahn, *Hydrometallurgy*, **70**(1-3): 23-29 (2003)

1.24 D. McKeeson, Treatment of waste from printed circuit board production for recovery of tin and environmentally safe disposal. US Patent 6290835, to RD Chemical Company (2001)

1.25 J. Y. Choi and D. S. Kim, *Journal of Hazardous Materials*, **99**(2): 147-158 (2003)

1.26 Mockrin, Isadore, Hobin and A. Martin, Recovery of copper from waste nitrate liquors by electrolysis. US Patent 4003838, to Kawecki Berylco Industries, Inc (1977)

1.27 A. Mecucci and K. Scott, *Journal of Chemical Technology and Biotechnology*, **77**(4): 449-457 (2002)

1.28 L. I. Antropov, M. I. Donchenko and T. I. Motronyuk, *Protection of Metals*, **20**(1): 27-32 (1984)

1.29 D. W. Dew and C. V. Phillips, *Hydrometallurgy*, **14**: 331-349 (1985)

1.30 D. W. Dew and C. V. Phillips, *Hydrometallurgy*, **14**: 351-367 (1985)

1.31 S. C. Das and P. Gopala Krishna, *International Journal of Mineral Processing*, **46**: 91-105 (1996)

1.32 N. G. Carpenter and D. Pletcher, *Analytica Chimica Acta*, **317**: 287-293 (1995)

1.33 G. E. Dima, A. C. A. de Vooys and M. T. M. Koper, *Journal of Electroanalytical Chemistry*, **554-555**: 15-23 (2003)

1.34 M. Paidar, I. Rousar and K. Bouzek, *Journal of Applied Electrochemistry*, **29**: 611-617 (1999)

1.35 S. Kerkeni, E. Lamy-Pitara and J. Barbier, *Catalysis Today*, **75**: 35-42 (2002)

1.36 D. Pletcher and Z. Poorabedi, *Electrochimica Acta*, **24**: 1253-1256 (1979)

1.37 A. C. A. de Vooys, R. A. van Santen and J. A. R. van Veen, *Journal of Molecular Catalysis A: Chemical*, **154**: 203-215 (2000)

1.38 M. Carrano, *Plating and Surface Finishing*, **91**(8): 35, 37 (2004)

1.39 D. Pilone and G. H. Kelsall, *Electrochimica Acta*, **51**(18): 3802-3808 (2006)

1.40 A. J. Chaudhary, S. O. V. Dando and S. M. Grimes, *Journal of Chemical Technology and Biotechnology*, **76**(1): 47-52 (2001)

1.41 R. Ragauskas, J. Matulionyte, T. Vengris and A. Padarauskas, *Journal of Chemical Technology and Biotechnology*, **79**: 1003-1008 (2004)

1.42 F. C. Walsh, *A First Course in Electrochemical Engineering*, The Electrochemical Consultancy, (1993)

1.43 D. Pletcher and F. C. Walsh, *Industrial Electrochemistry*, Chapman and Hall, (1990)

1.44 D. A. Campbell, I. M. Dalrymple, J. G. Sunderland and D. Tilston, *Resources Conservation and Recycling*, **10**: 25-33 (1994)

1.45 K. Scott, *Electrochemical Processes for Clean Technology*, The Royal Society of Chemistry, (1995)

1.46 K. Scott and E. M. Paton, *Electrochimica Acta*, **38**(15): 2191-2197 (1993)

1.47 J. Bancroft and I. M. Dalrymple, *Porocell: A Dramatic Improvement in the Extraction of Metals from Waste Solutions*, EA Technology (1996)

1.48 P. A. Shirvanian and J. M. Calo, *Journal of Applied Electrochemistry*, **35**(1): 101-111 (2005)

1.49 E. Avci, *Journal of Applied Electrochemistry*, **18**: 288-291 (1988)

2 FUNDAMENTAL ASPECTS

The aim of this project was to develop a systematic method to determine the feasibility of metal recovery from aqueous waste streams. The first stage in this method was to examine the thermodynamics of the system, in order to determine when the metals would be in the solid or liquid phase. This depends on the metal and anion concentration, pH and the system potential. The classical approach of using Pourbaix diagrams was chosen for this study, and the technique for their construction is described in this chapter.

Once the Pourbaix diagrams were established, the processes that could be used to separate the metals could be determined. The fundamental aspects of metal separation by electrodeposition are described, along with the electrochemical parameters used to asses the feasibility of the separation. As the recovery would be carried out in a reactor, the theoretical metal depletion equations are also described.

2.1 Thermodynamic Theory of Metals in Solution

To determine the feasibility of the recovery process, the first stage in the systematic method was to study the system thermodynamics. This analysis will enable the phase of the metal to be determined depending on the potential, pH and metal/anion concentrations in the system. The thermodynamic analysis describes the state of the system at equilibrium.

2.1.1 Equilibrium Potential

At equilibrium, the electrode potential is dependent on the species in solution and their concentrations. The equilibrium potential is measured with respect to a reference electrode e.g. standard hydrogen electrode (SHE), which has a well defined, reproducible potential. Standard electrode potentials versus SHE for half cell reactions are widely published in literature [2.1]. These potentials are quoted at standard conditions where the activity of all species and the fugacity of any gas is unity, and the temperature is 298K. If the activity of ions in solution, or the fugacity

of any gas is not equal to unity, the value of the standard potential E^0 can be corrected using the Nernst Equation (Eq. 2.1).

$$pP + qQ + ne^- \rightarrow xX + yY$$

$$E_e = E^O + \frac{RT}{nF} \ln \frac{(a_P)^p (a_Q)^q}{(a_X)^x (a_Y)^y} \qquad (2.1)$$

where E_e is the equilibrium potential, R the universal gas constant, T the system temperature, n the number of electrons transferred, F Faraday's constant and a the ion activity. At this equilibrium potential, the forward and backwards rates of the reversible reactions on the electrode are equal in magnitude. In this case no current flows through the cell and no net change occurs at the electrodes.

In a real system, the measured equilibrium potential may differ from the potential calculated using the Nernst equation. This difference is due to the electrode taking up a mixed potential. For example, in a Cu(II)/Cu system dissolved oxygen can be reduced, shifting the electrode potential towards the value for the O_2/H_2O couple.

2.1.2 Pourbaix Diagrams

Pourbaix diagrams represent how the thermodynamic stability of different species are affected by pH and electrode potential. They clearly show when a metal is in solution, or exists as a solid, and the species it exists as. The diagrams were developed for the study of corrosion by Marcel Pourbaix in 1945 [2.2]. They give information on what is thermodynamically possible; in practice these reactions may not occur due to kinetic limitations.

Chemical Reactions

Pourbaix [2.3] defines a chemical reaction as "a reaction in which only chemical bodies participate (neutral molecules or positively or negatively charged ions)". An example of this type of reaction is shown below:

$$Cu^{2+} + 2H_2O \rightarrow HCuO_2^- + 3H^+$$

In general, a chemical reaction can be expressed as:

$$pP + cH_2O \rightarrow qQ + mH^+$$

If the system is at constant temperature and pressure and the reaction at equilibrium, the Gibbs free energy ΔG of the reaction can be related to the equilibrium reaction constant K by Eq. (2.2).

$$\Delta G^O = -RT \ln K \tag{2.2}$$

with $$K = \prod_i a_i^{x_i} = \frac{(a_Q)^q (a_{H^+})^m}{(a_P)^p (a_{H_2O})^c}$$

and $$\Delta G^O = \sum_i x_i \mu_i^O = q(\mu_Q) + m(\mu_{H^+}) - p(\mu_P) - c(\mu_{H_2O})$$

where x is the stoichiometric constant and μ the chemical potential.

Electrochemical Reactions

An electrochemical reaction is defined by *Pourbaix* [2.3] as "a reaction in which both chemical species and free electric charges take part (e.g., negative electrons dissolved in a metallic electrode)". An example is the metal deposition reaction, shown below for copper.

$$Cu^{2+} + 2e^- \rightarrow Cu$$

In general, an electrochemical reaction can be written:

$$pP + cH_2O + ne^- \rightarrow qQ + mH^+$$

If the Nernst equation (Eq. 2.1) is applied to this general reaction, the equilibrium potential can be determined from the standard potential (calculated from ΔG^0 using Eq. 2.3), the pH ($pH = -\log a_{H^+}$) and the other reactant activities.

$$\Delta G^O = -nFE^O \tag{2.3}$$

The calculations were carried out using Mathcad [2.4] (a worksheet based calculation package) and the diagrams were plotted using Matlab [2.5]. The diagrams are constructed using the ion activity, rather than the concentration; these quantities will only be the same in solutions with low ionic strength i.e. dilute solutions. A sample calculation using the copper-water system is shown below.

Copper-Water System

In order cross-check that my development of the Pourbaix diagrams was correct, a copper-water Pourbaix plot was constructed. This provided verification of the technique as they are widely published [2.2]. The copper-water example is simple (due to the limited number of species involved) and will provide a basis for later copper diagrams that include anions such as NO_3^-.

The species that were considered, along with their Gibbs free energy of formation are shown in Table 2-1. The dissolved species are shown in italic and the solids in bold.

Aqueous		**Solid**	
	ΔG^O / kJ mol^{-1}		ΔG^O / kJ mol^{-1}
Cu^+	50.2	**Cu**	0.0
Cu^{2+}	65.021	**Cu_2O**	-146.45
$HCuO_2^-$	-257.15	**CuO**	-127.28
CuO_2^{2-}	-182.1	H_2O	-237.35

Table 2-1 Thermodynamic data for copper – water substances, data from *Pourbaix* [2.2]

To start the diagram, a plot was constructed to show the regions of relative predominance of the dissolved substances. The reactions that were considered are divided into chemical and electrochemical types in Table 2-2. Also included in this table are the reaction equilibrium conditions, which were calculated from the equations described above (Eqs. 2.1-3) and the thermodynamic data in Table 2-1.

Chemical	Equilibrium Condition
$Cu^{2+} + 2H_2O \rightarrow HCuO_2^- + 3H^+$	$\log\left(\frac{a_{HCuO_2^-}}{a_{Cu^{2+}}}\right) = -26.73 + 3pH$
$Cu^{2+} + 2H_2O \rightarrow CuO_2^{2-} + 4H^+$	$\log\left(\frac{a_{CuO_2^{2-}}}{a_{Cu^{2+}}}\right) = -39.88 + 4pH$
$HCuO_2^- \rightarrow CuO_2^{2-} + H^+$	$\log\left(\frac{a_{CuO_2^{2-}}}{a_{HCuO_2^-}}\right) = -13.15 + pH$
Electrochemical	
$Cu^+ \rightarrow Cu^{2+} + e^-$	$E = 0.153 + 0.0591 \cdot \log\left(\frac{a_{Cu^{2+}}}{a_{Cu^+}}\right)$ [2.6]
$Cu^+ + 2H_2O \rightarrow HCuO_2^- + 3H^+ + e^-$	$E = 1.773 - 0.1773pH + 0.0591 \cdot \log\left(\frac{a_{HCuO_2^-}}{a_{Cu^+}}\right)$ data from *Bard* [2.6]
$Cu^+ + 2H_2O \rightarrow CuO_2^{2-} + 4H^+ + e^-$	$E = 2.510 - 0.2365pH + 0.0591 \cdot \log\left(\frac{a_{CuO_2^{2-}}}{a_{Cu^+}}\right)$

Table 2-2 Reactions between dissolved substances for copper-water, all potentials vs SHE

The lines that divide the regions of predominance are calculated with equal activity of the two relevant ions. The plot that emerges is shown in Figure 2-1.

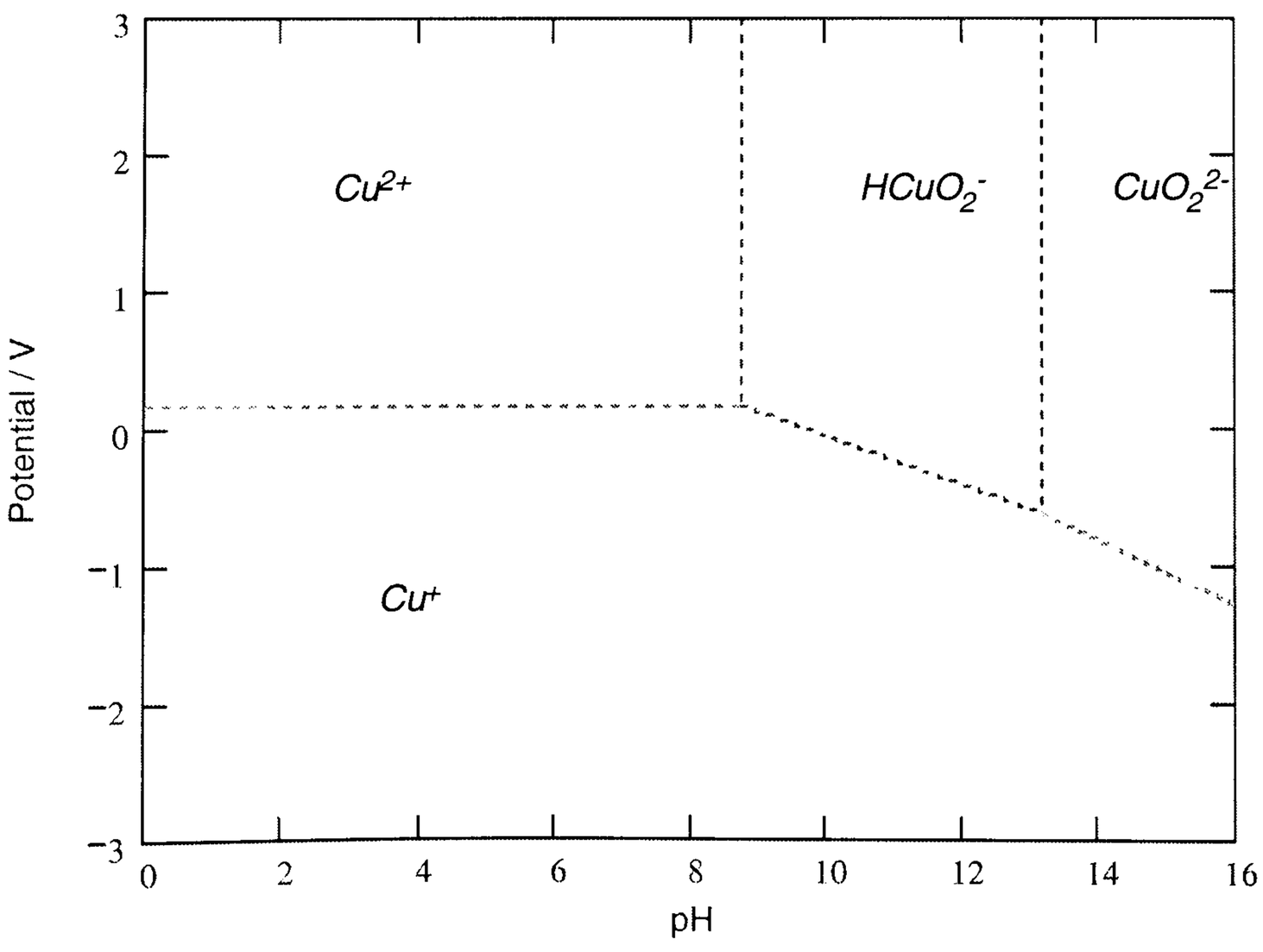

Figure 2-1 Predominance area diagram for copper-water

The next stage in the construction of the Pourbaix diagram is the calculation of the equilibrium conditions for the solid substances. These are then marked on the predominance area plot. The reactions that were considered and their equilibrium equations are shown in Table 2-3.

	Equilibrium Condition
$Cu_2O + H_2O \rightarrow 2CuO + 2H^+ + 2e^-$ ①	$E = 0.669 - 0.0591pH$
$2Cu + H_2O \rightarrow Cu_2O + 2H^+ + 2e^-$ ②	$E = 0.471 - 0.0591pH$ [2.6]
$Cu + H_2O \rightarrow CuO + 2H^+ + 2e^-$	$E = 0.570 - 0.0591pH$

Table 2-3 Reactions between solid substances for copper-water (E vs SHE)

The result of plotting these lines can be seen in Figure 2-2. The line for the equilibrium between Cu and CuO is not drawn because the Gibbs free energy change for the reaction Cu → CuO_2 is more negative, and thus more energetically favourable, than ΔG for Cu → CuO. As the potential is increased it is assumed that all the Cu will have been transformed into Cu_2O before the stability region for CuO is reached.

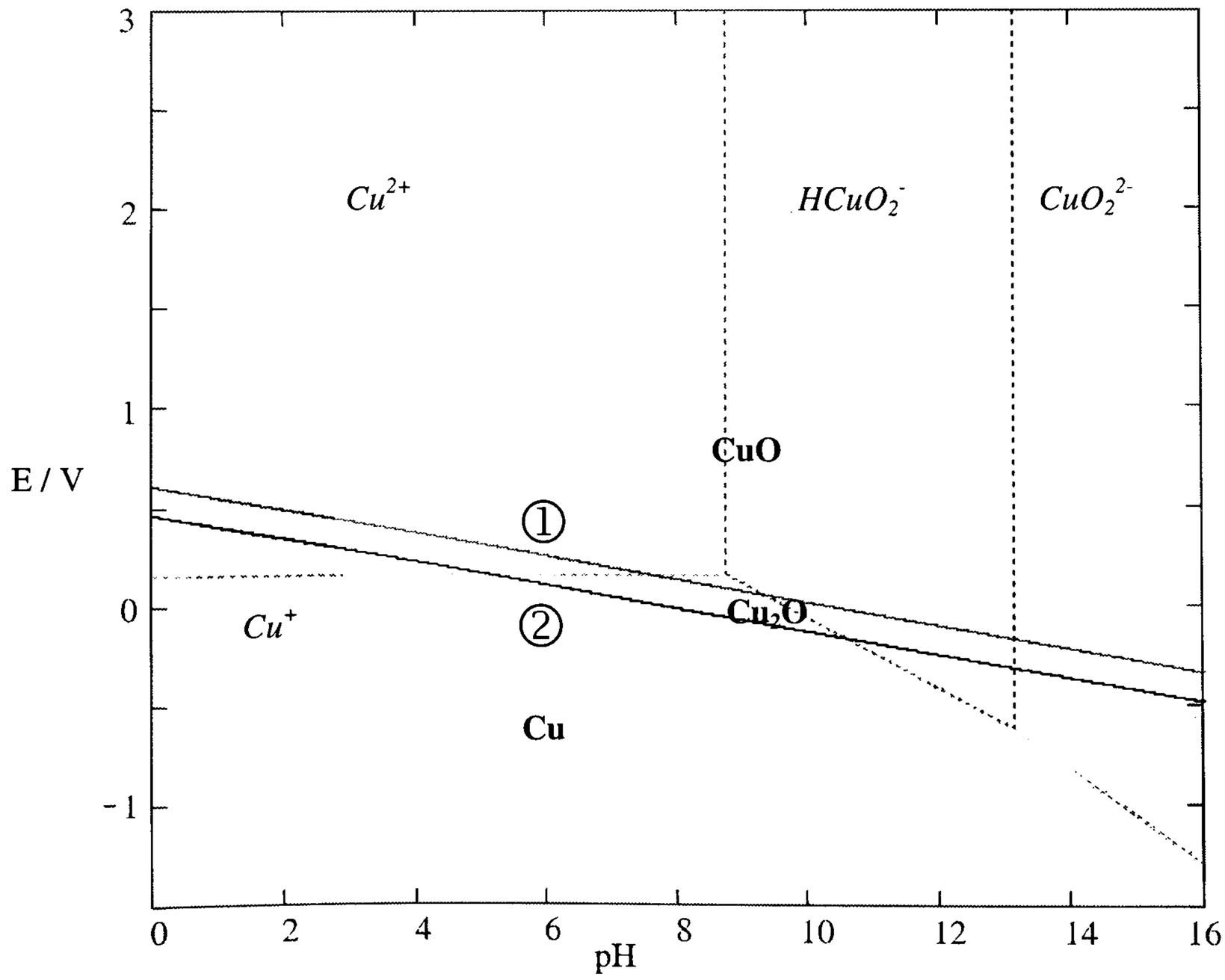

Figure 2-2 Plot showing regions of stability of the ions and the solid phases for copper-water

The final stage in the construction of the plot is to delineate between the stable regions for solids and dissolved species. The reactions and their equilibrium conditions are shown in Table 2-4. The lines between the solid and dissolved phases have been drawn for four values of metal ion activity: 10^{0}, 10^{-2}, 10^{-4} and 10^{-6}.

Chemical	**Equilibrium Condition**
$2Cu^{+} + H_2O \rightarrow Cu_2O + 2H^{+}$	$\log(a_{Cu^{+}}) = -1.66 - pH$
$Cu^{2+} + H_2O \rightarrow CuO + 2H^{+}$	$\log(a_{Cu^{2+}}) = 7.89 - 2pH$
$HCuO_2^{-} + H^{+} \rightarrow CuO + H_2O$	$\log(a_{HCuO_2^{-}}) = -18.83 + pH$
$CuO_2^{2-} + 2H^{+} \rightarrow CuO + H_2O$	$\log(a_{CuO_2^{2-}}) = -31.99 + 2pH$
Electrochemical	
$Cu \rightarrow Cu^{+} + e^{-}$	$E = 0.521 + 0.0591 \cdot \log(a_{Cu^{+}})$
$Cu \rightarrow Cu^{2+} + 2e^{-}$	$E = 0.337 + 0.02955 \cdot \log(a_{Cu^{2+}})$
$Cu + 2H_2O \rightarrow HCuO_2^{-} + 3H^{+} + 2e^{-}$	$E = 1.127 - 0.0887\,pH + 0.0296 \cdot \log(a_{HCuO_2^{-}})$
$Cu + 2H_2O \rightarrow CuO_2^{2-} + 4H^{+} + 2e^{-}$	$E = 1.515 - 0.118\,pH + 0.0295 \cdot \log(a_{CuO_2^{2-}})$
$Cu^{+} + H_2O \rightarrow CuO + 2H^{+} + e^{-}$	$E = 0.620 - 0.118\,pH - 0.0591 \cdot \log(a_{Cu^{+}})$
$Cu_2O + 2H^{+} \rightarrow 2Cu^{2+} + H_2O + 2e^{-}$	$E = 0.203 + 0.0591pH + 0.0591 \cdot \log(a_{Cu^{2+}})$
$Cu_2O + 3H_2O \rightarrow 2HCuO_2^{-} + 4H^{+} + 2e^{-}$	$E = 1.783 - 0.118\,pH + 0.0591 \cdot \log(a_{HCuO_2^{-}})$
$Cu_2O + 3H_2O \rightarrow 2CuO_2^{2-} + 6H^{+} + 2e^{-}$	$E = 2.560 - 0.177\,pH + 0.0591 \cdot \log(a_{CuO_2^{2-}})$

Table 2-4 Reactions between solid and dissolved substances for copper-water (E vs SHE)

Some of the reaction equilibrium conditions are not shown on the Pourbaix diagram, as the stability regions do not overlap. For example, lines denoting the equilibrium between Cu → Cu^{+} are not shown because the Gibbs free energy for the Cu → Cu^{2+} reaction is more negative, and therefore energetically favourable, than the dissolution to Cu^{+}. The omission of these equilibria on the Pourbaix plots does not mean the reactions do not happen, but that the species involved are not the most dominant at that particular value of pH and/or electrode potential. The fully constructed Pourbaix diagram for copper and water is shown in Figure 2-3. In this figure the bold lines represent the solid-solid boundaries, the thin lines the boundaries between solids and

dissolved ions, and the dotted lines the dissolved region boundaries. The numbers on the solid-dissolved boundaries represent the activity of the dissolved species. It is common practice to include the lines that represent water stability on the plots (marked A and B); if the metal deposition potential is below the lower line (hydrogen equilibrium) there is a possibility that hydrogen will be liberated during the deposition. The upper line represents oxygen stability.

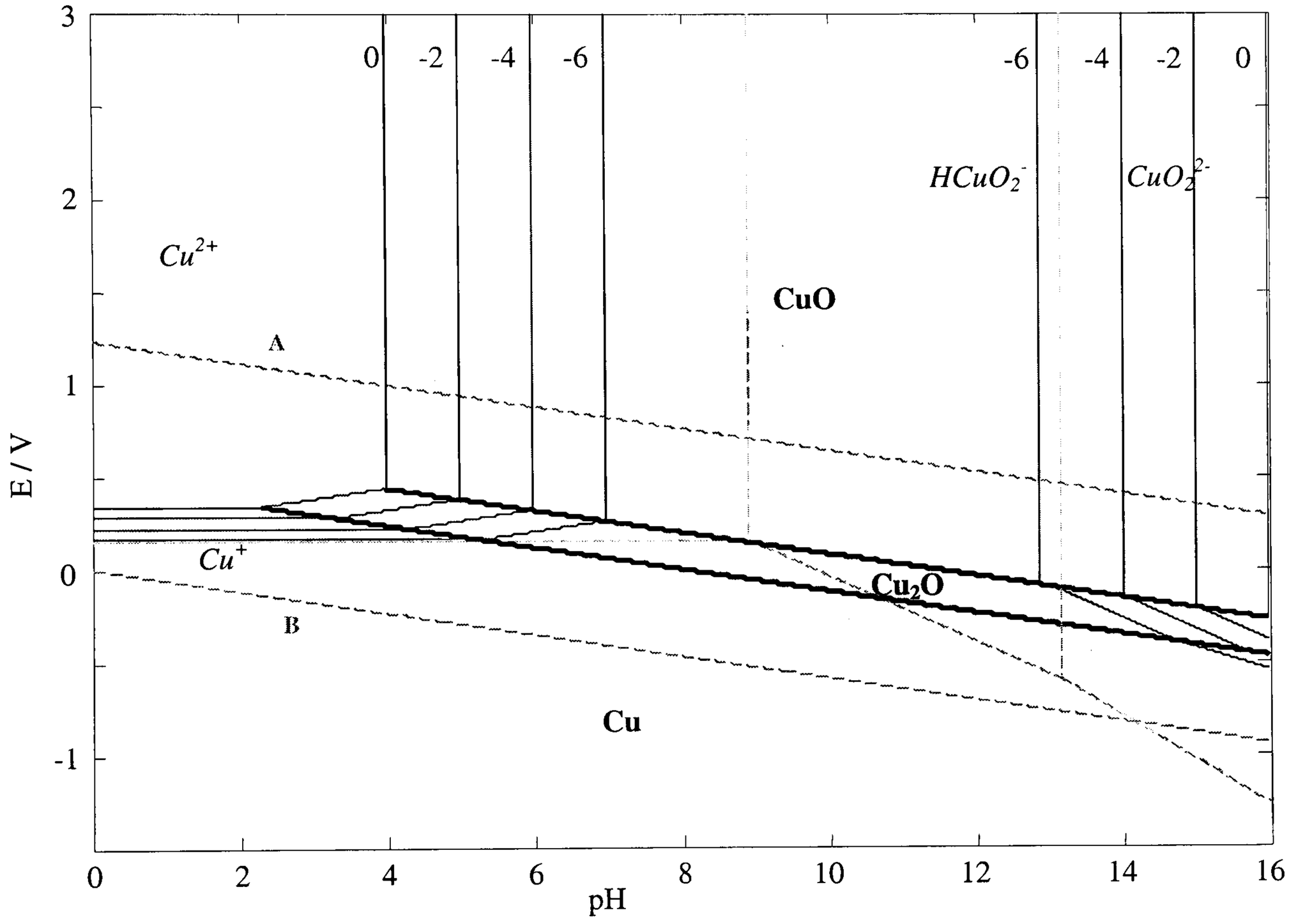

Figure 2-3 Pourbaix diagram for copper-water (298K)

It can be seen from the diagram that copper will exist in solution in the form of Cu^{2+} at low pH, and can be deposited without hydrogen evolution at potential of approximately 0V. This does not mean that no potential needs to be applied to the system to deposit the copper. When an electrode is placed in the copper solution, it will rest at a potential defined by the solution activity and the electrode material; for a solution of 1M Cu^{2+} in contact with copper, this would be 0.337V (Table 2-4). The potential of the electrode would then have to be brought back to 0V by applying an overpotential of -0.337V to the system. The copper-water Pourbaix diagram is valid

for systems that do not contain substances that can form complexes with copper, for example sulphates.

2.2 Metal Separation by Electrodeposition

To remove a metal from solution by electrodeposition, it must be reduced from its dissolved form (e.g. Cu^{2+}) to a solid, usually the metal (e.g. Cu^{0}). Electrodeposition can be used to remove a single metal from solution, or to separate several metals dissolved the same solution. Separation is possible if the metals have sufficiently different equilibrium potentials. In order to drive the reactions, the electrode potential must be shifted away from equilibrium, so that current flows. The amount the potential differs from the equilibrium value is known as the overpotential. During deposition metal ions are reduced, therefore the cathode is shifted to potentials more negative than the equilibrium value.

Figure 2-4 shows the half cell for the deposition of metal M^{+} from solution. The potential of the cathode is measured against a reference electrode and the current in the cell flows between the anode and cathode. Current is prevented from flowing between the reference electrode and cathode by a high impedance voltmeter as a current will alter the potential of the reference electrode.

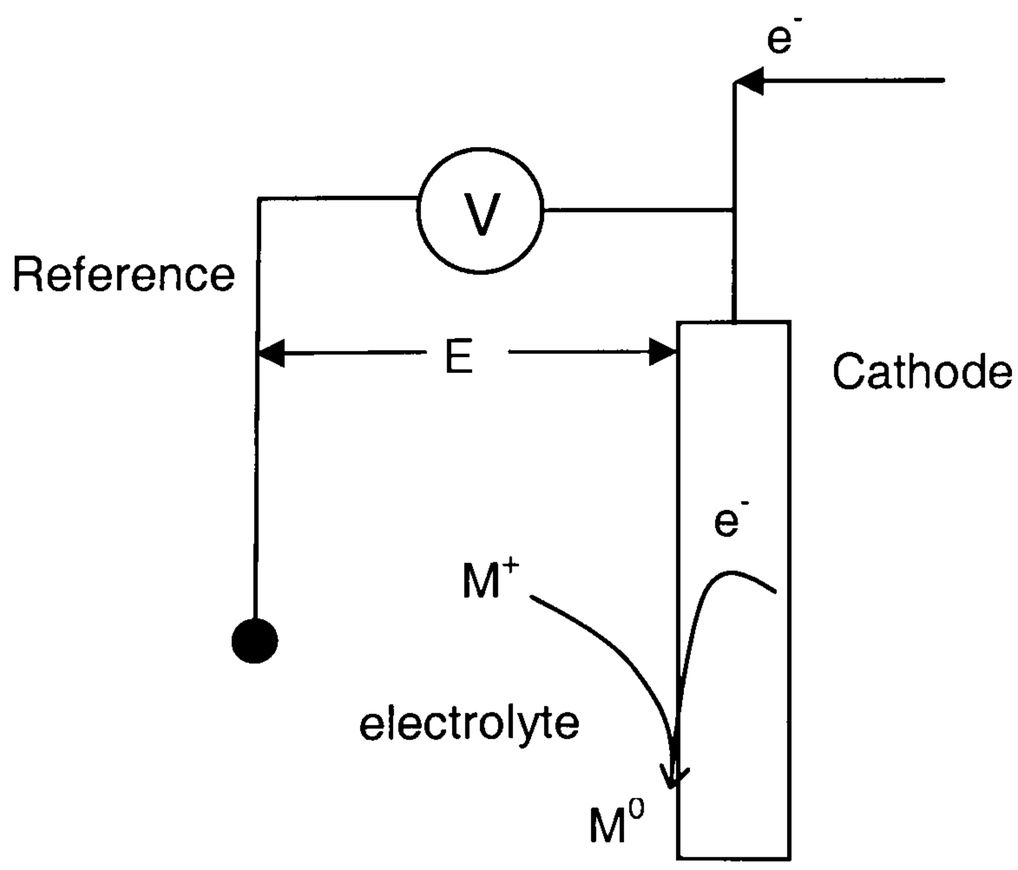

Figure 2-4 Half cell for reaction $M^{+} + e^{-} \rightarrow M^{0}$

2.2.1 Electrode Reactions

As the potential is shifted from equilibrium and current flows, the electrode reactions occur in several stages, with the overall rate governed by the slowest step. As a simple model these reaction stages can be considered to be:

- Mass transport of the reactant to the electrode.
- Charge transfer at the surface.
- Mass transport of the product away from the surface.

Charge Transfer

As the potential is shifted from equilibrium and current flows, the reaction is initially under charge transfer control. The Butler-Volmer equation (Eq. 2.4) describes the relationship between the overpotential η and the current density j at the electrode surface. It can be seen that the current increases in magnitude with the overpotential, which therefore increases the rate of deposition according to Faraday's law.

$$j = j_0\left[\exp\left(\frac{\alpha_A nF\eta}{RT}\right) - \exp\left(\frac{-\alpha_C nF\eta}{RT}\right)\right] \tag{2.4}$$

where j_0 is the exchange current density and α the transfer coefficient. The exchange current density is the partial current density occurring on the electrode at equilibrium. The value of j_0 changes with electrode surface; if j_0 is small, a given current density will only be achieved at large overpotentials.

Mass Transport

As the overpotential and therefore rate of reaction is increased, the concentration of the reactant at the electrode surface will be depleted (Figure 2-5). At some potential the concentration of reactant at the surface c_s reaches zero, and the rate is entirely controlled by the transport of reactant from the bulk solution. This is known as the mass transfer limiting current.

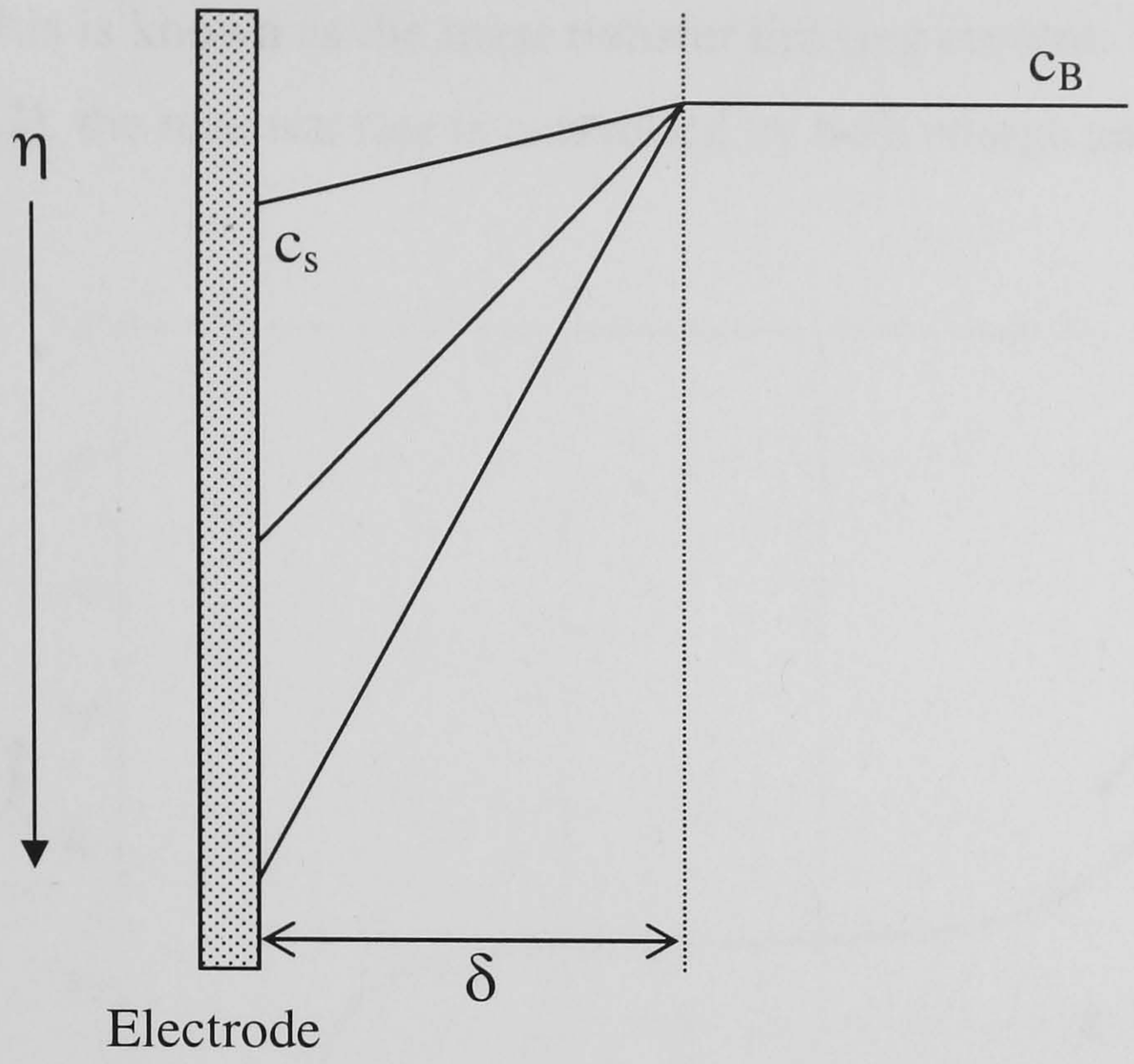

Figure 2-5 Diagram showing concentration profiles according to the Nernst diffusion layer model

The rate of mass transport can be modelled using the Nernst diffusion layer model, which assumes the solution can be divided into two zones. Close to the electrode there is a stagnant layer of thickness δ through which material can only be transported by diffusion. Further from the electrode the bulk solution is assumed to be well mixed. The mass transfer limiting current I_L is given by Eq. (2.5), and can be seen to be a function of the diffusion coefficient D, the diffusion layer thickness δ, electrode area A and the bulk reactant concentration c_B.

$$I_L = \frac{AnFDc_B}{\delta} \tag{2.5}$$

Regions of Rate Control

The regions of rate control can be observed on typical polarisation data, such as Figure 2-6. In region (1) the rate of reaction is limited by charge transfer; the current increases with increasing polarisation. However, the current does not continue to increase. By region (3) the reaction rate is entirely controlled by the transfer of reactants to the electrode surface, and the current is independent of the overpotential;

this is known as the mass transfer limiting current. Between these extremes in region (2), the reaction rate is controlled by both charge and material transfer.

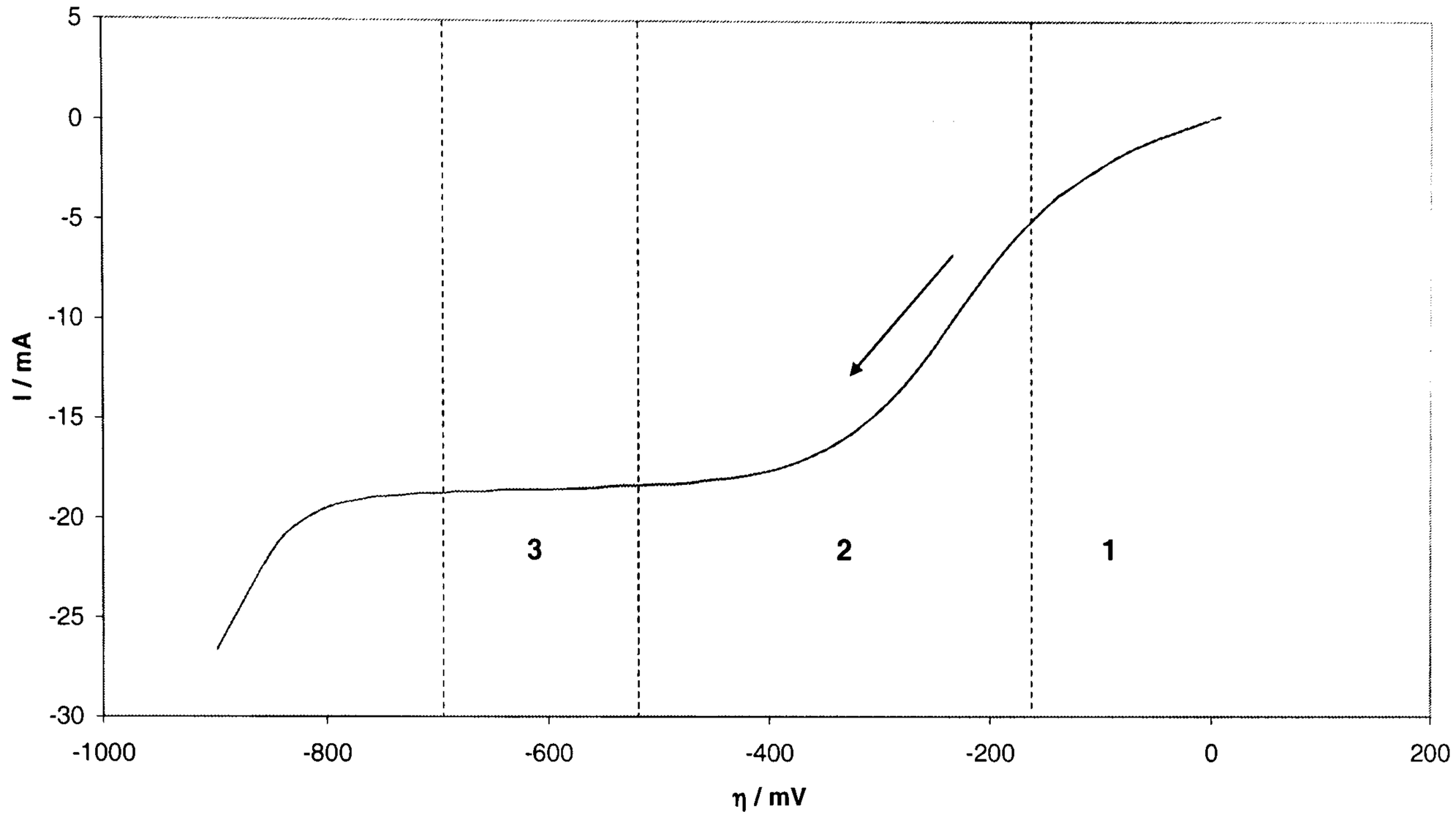

Figure 2-6 Linear voltammogram showing regions of rate control (1) charge transfer (2) mixed control (3) mass transfer

2.2.2 Mixed Potential Systems

In reality, the electrochemical system is often more complicated than a single species in solution. Multiple reactions can occur simultaneously. A classic example of this type of system is corrosion; for example the dissolution of copper from the PCB by the action of ferric ions. Figure 2-7 demonstrates the current response for the Cu^{2+}/Cu and Fe^{3+}/Fe^{2+} systems. If a solution of ferric ions was in contact with copper, the potential of each couple would contribute to the system potential, illustrated on the diagram as E_1. The copper would therefore dissolve, and the ferric ions be reduced at current I_1.

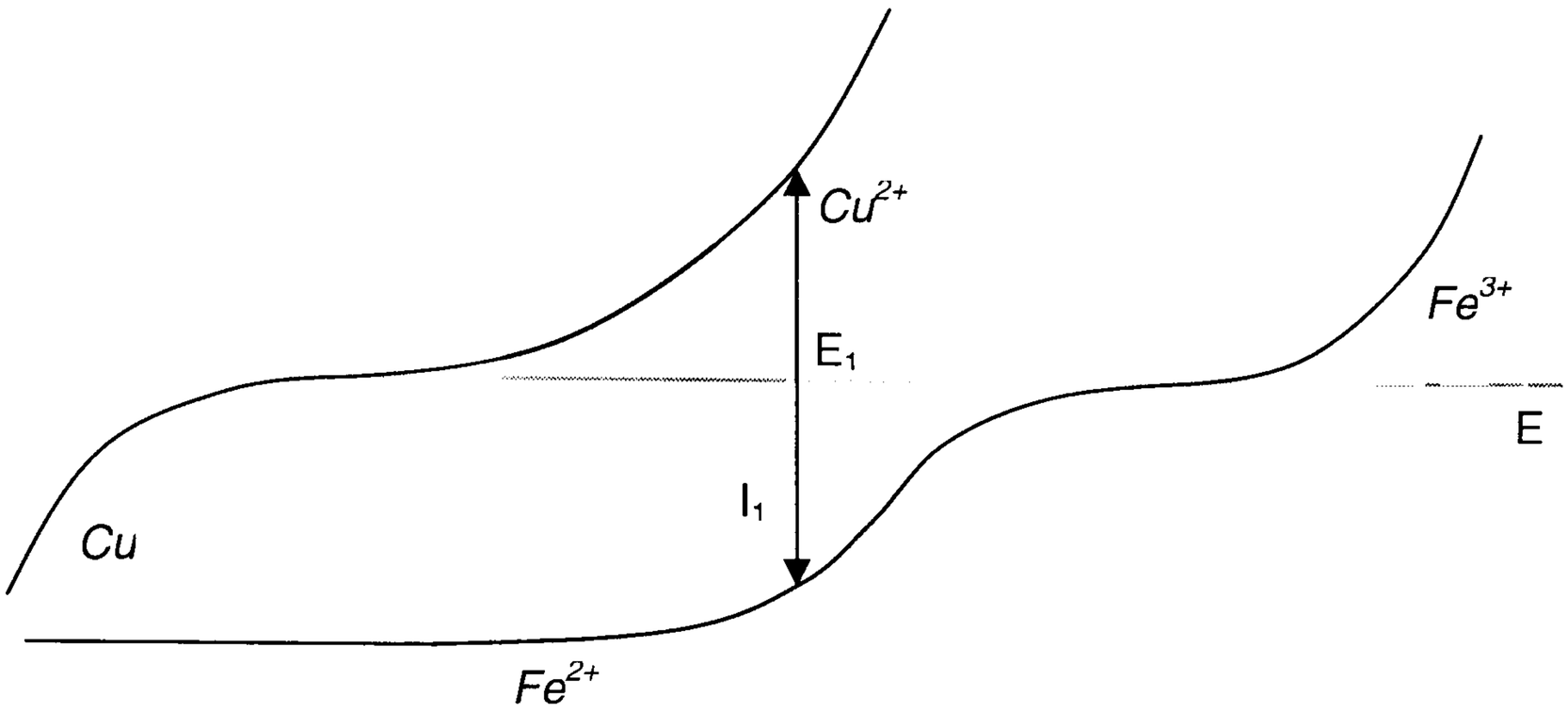

Figure 2-7 Diagram showing mixed potential system

The charge and mass transfer equations for the estimation of reaction rate or mass transfer properties are only valid if the current due to a single reaction can be measured, or calculated from the i-E data. If more than one reaction occurs at a given potential, the measured response contains contributions from all the reactions. This is illustrated in Figure 2-8; at potential E_1 the measured current has elements from Cu(II) and H^+ reductions. The current due to unwanted reactions can completely mask the limiting current plateau and charge transfer region for the reaction of interest. It is possible to subtract the current, in this case for H_2 evolution, by recording polarisations in a solution that contains the same concentration of H^+, but no Cu(II). However, this method of subtraction is only valid if the reactions are all independent.

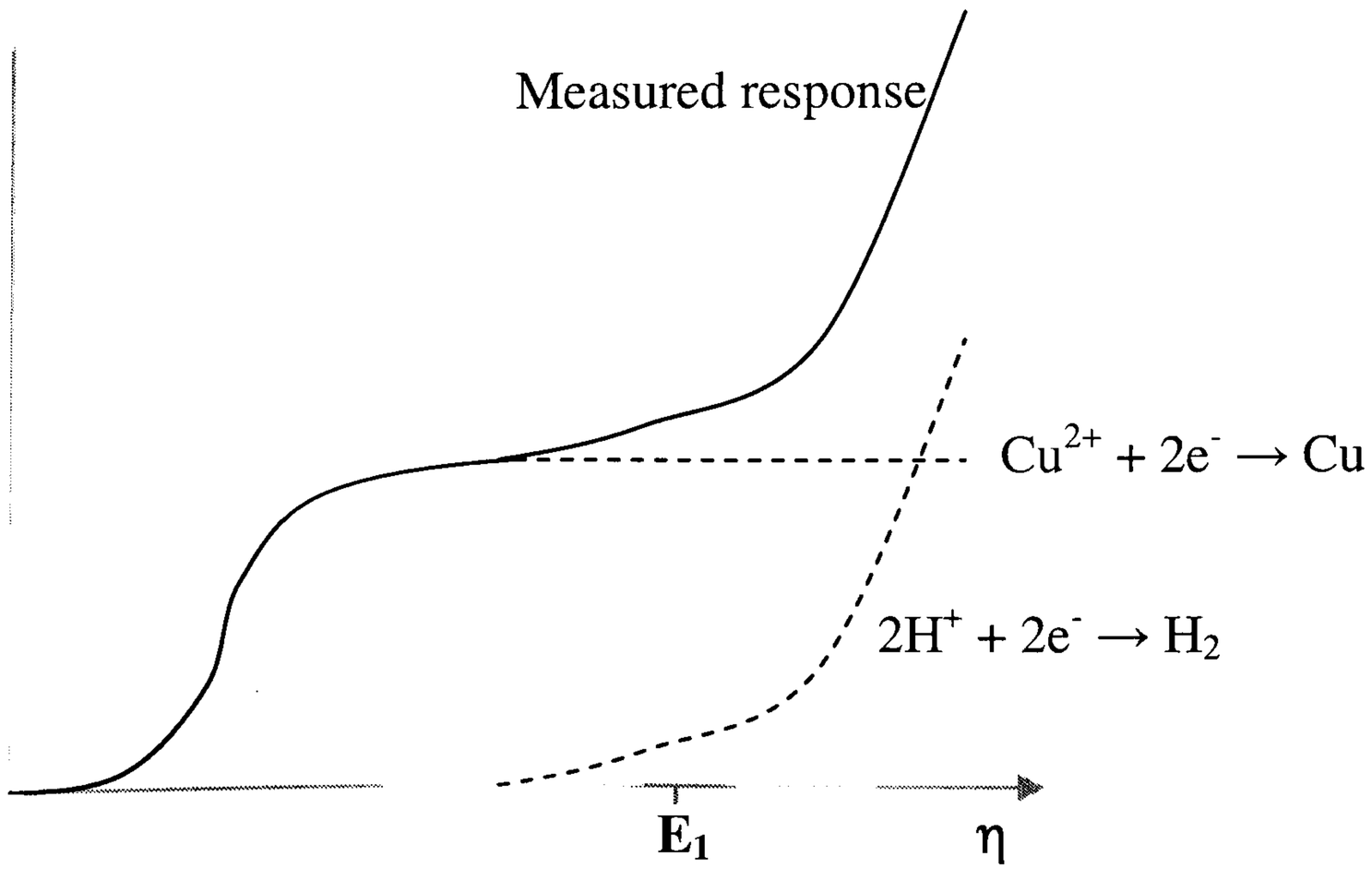

Figure 2-8 Diagram showing current response from multiple reactions

2.3 Electrochemical Parameters

The reduction of metal ions in solution will take place in an electrochemical cell. A typical cell (Figure 2-9) contains an anode, a cathode, an electrolyte (to maintain contact between the two electrodes) and a power supply to drive the reaction. Reductions occur at the cathode, oxidations at the anode.

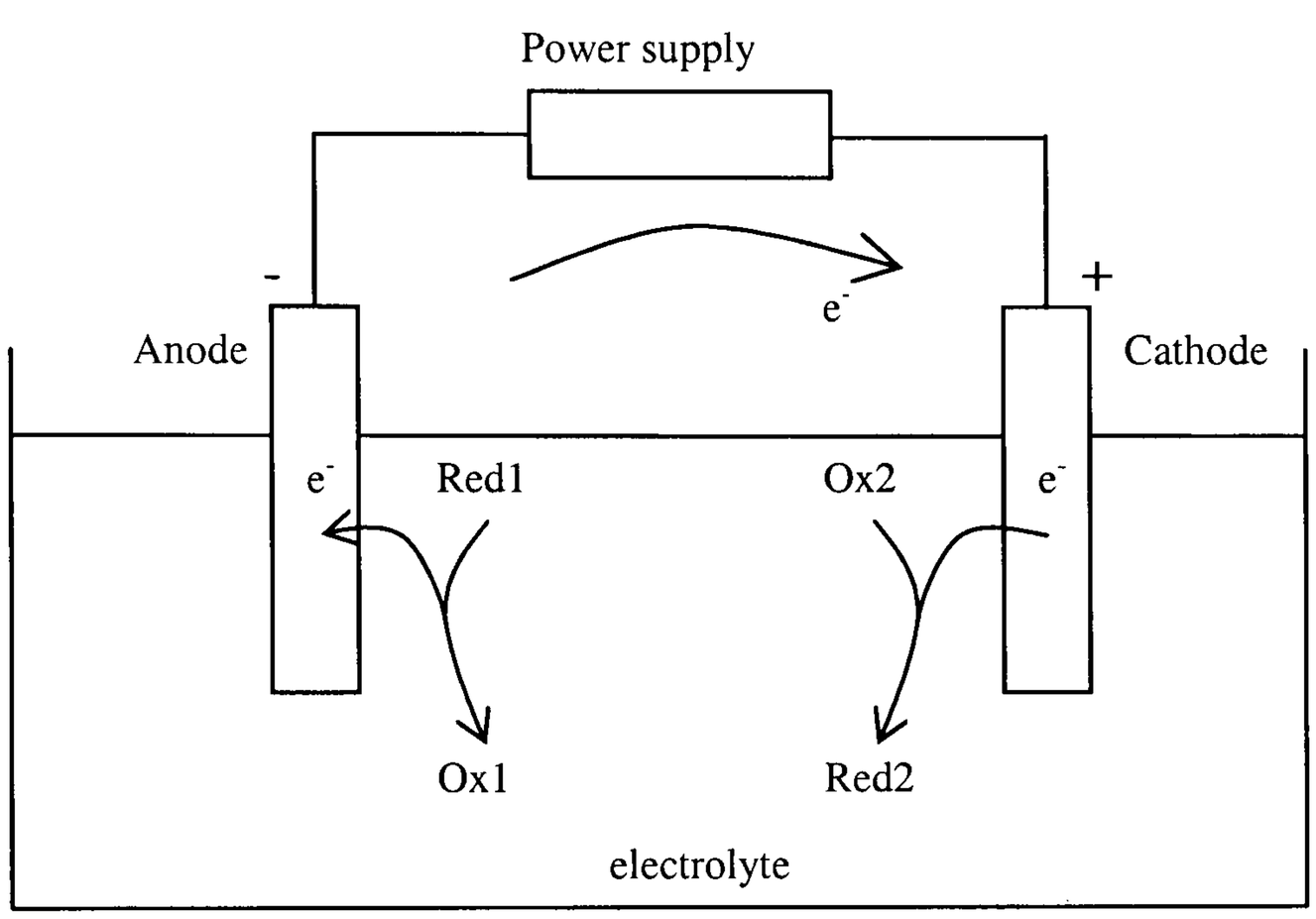

Figure 2-9 An electrochemical cell

To effect a separation, the potential of the cathode is shifted away from the equilibrium potential. The current flowing through the cell can then be measured. These values of current and potential can be used to gain an estimate of the feasibility of the metal recovery by calculating the rate of the metal deposition, the current efficiency and the electrolytic energy requirement per mass of metal.

2.3.1 Overall Deposition Rate

The overall rate of an electrochemical reaction can be calculated as a function of the cell current I using Faraday's law (Eq. 2.6).

$$m = \frac{Q}{nF} \tag{2.6}$$

At constant current the charge Q can be expressed as: $Q = \int I \cdot dt = I \cdot t$. If this is substituted into Eq. (2.6), and the amount of material reacted m differentiated with respect to time t, then the rate of the electrochemical reaction can be expressed as:

$$\frac{dm}{dt} = \frac{I}{nF} \tag{2.7}$$

2.3.2 Current Efficiency

In a system where multiple reactions occur at the same potential, the measured current is not all consumed by the reaction of interest. In the example shown in Figure 2-8, if copper was deposited at potential E_1 a portion of the current would be taken by hydrogen evolution. The charge that is consumed by unwanted side reactions is therefore a source of inefficiency. The percentage of the total charge that is used for the desired reaction is known as the current efficiency Φ. The efficiency can change considerably with the electrolyte composition, applied current/potential and reactant concentration. It is defined as the charge necessary for the reaction of interest Q_r, divided by the total electrical charge used Q_{TOT} (Eq. 2.8).

$$\Phi = \frac{Q_r}{Q_{TOT}} \times 100 \tag{2.8}$$

2.3.3 Energy Considerations

The energy W required to deposit a fixed mass of metal will depend upon the current and the potential drop across the cell, as shown by Eq. (2.9)

$$W = Q \cdot E_{cell} \qquad \text{where } Q = \int I \cdot dt \tag{2.9}$$

The potential drop in the system is dependent on the reactions occurring at the electrodes, the chosen overpotentials and the ohmic drop through the cell. This is shown in Eq. (2.10), where R_{cell} is the resistance across the electrochemical cell.

$$E_{cell} = E_e - |\eta_A| - |\eta_C| - IR_{cell} \tag{2.10}$$

For metal deposition the equilibrium potential of the cathode will be fixed, however the anodic reaction can significantly alter the energy requirements. For example, copper is usually deposited from an acidic solution with oxygen evolution occurring at the anode. If ferrous ion oxidation is substituted as the anodic reaction, the cell potential would be 0.46V lower than for oxygen evolution [2.7]. The electrode overpotentials are dependent on the required rate of reaction which can affect surface finish, and the electrode material. The ohmic drop through the cell is dependent on the solution conductivity, electrode gap and the presence of separators. Therefore, in the above example although the cell potential could be reduced by the substitution of ferrous oxidation, a separator would be required between the anolyte and catholyte increasing the ohmic drop.

In an industrial situation, the cell current, rather than the potential, is usually fixed because a galvanostatic power supply is cheaper than a potentiostatic supply. The applied current will again be dependent on the reactions and overpotentials, as the current is a function of the potential. The applied cell current will also be affected by the current efficiency.

The form of the metal in solution also influences the energy requirement. For example, copper is usually deposited from acid electrolytes where it exists as Cu(II). If copper could be deposited from a solution containing Cu(I) ions, the charge, and therefore energy requirement, would be halved (assuming 100% current efficiency).

$$Cu^{2+} + 2e^{-} \rightarrow Cu$$

$$Cu^{+} + e^{-} \rightarrow Cu$$

2.4 Electrochemical Reactors

To deposit metals on an industrial scale, an electrochemical reactor is used. There are various types of reactors e.g. parallel plate, rotating electrode, which can be operated in a batch or continuous mode; these were discussed in Section 1.8. The reactor that was used in this study was a parallel plate reactor operating in batch recycle mode. The reactor system is illustrated in Figure 2-10.

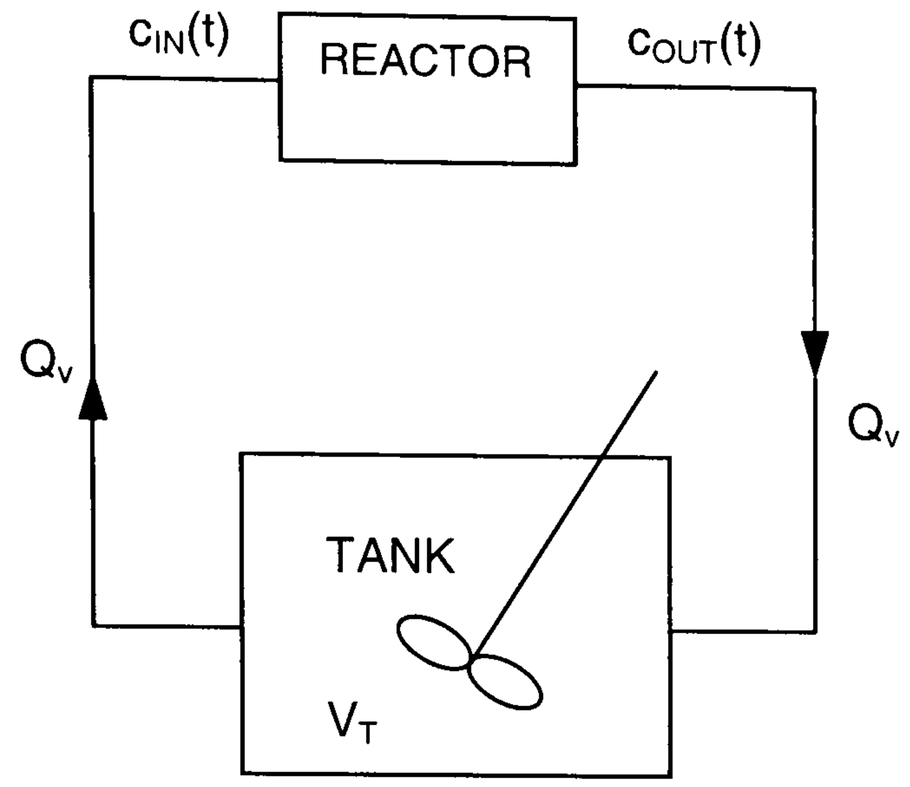

Figure 2-10 Batch recycle reactor

In order to model the concentration change in the system, it is assumed the reactor operates as a plug flow reactor. Initially the equations relating to steady state operation in a plug flow reactor are derived from a material balance across the reactor (Eq. 2.11)

$$Q_v c_{OUT} - Q_v c_{IN} = -\frac{I}{nF} \tag{2.11}$$

where Q_v is the volumetric flowrate and c_{IN} and c_{OUT} the concentrations at the inlet and outlet of the reactor respectively. If the reactor is of total length L with current density j_x across the electrode, then for an element of length δx and concentration change δc_x, the mass balance can be expressed as:

$$Q_v \cdot dc_x = \frac{j_x A}{nFL} dx \tag{2.12}$$

The residence time τ through the reactor element δx is defined as $\tau = V_x/Q_v$, where the element volume $V_x = xA$. Therefore $dx = d\tau . Q_v/A$. Also, if the reaction is mass transfer limited across the whole surface of the electrode, then $j_x = nFk_m c_x$. If these relationships are used to substitute dx and j_x in Eq. (2.12), Eq. (2.13) is obtained.

$$\int_{c_{IN}}^{c_{OUT}} \frac{dc_x}{c_x} = -\frac{k_m A}{V} \int_0^{\tau} d\tau \tag{2.13}$$

where V is the reactor volume. This equation is integrated between the limits to obtain:

$$c_{OUT} = c_{IN} \cdot \exp\left(-\frac{k_m A \tau}{V}\right) \tag{2.14}$$

This expression is valid for steady state operation, however in a batch recycle reactor the reactor inlet concentration c_{IN} changes with time t. A mass balance is therefore carried out across the tank (volume V_T) to give:

$$Q_v c_{OUT} = Q_v c_{IN} + V_T \cdot \frac{dc_{IN}}{dt} \tag{2.15}$$

The expression for c_{OUT} from Eq. (2.14) is then substituted into Eq. (2.15) to obtain an equation describing the concentration change in the system:

$$Q_v c_{IN} \cdot \exp\left(-\frac{k_m A \tau}{V}\right) = Q_v c_{IN} + V_T \cdot \frac{dc_{IN}}{dt} \tag{2.16}$$

Eq. (2.16) can be rearranged, the tank residence time $\tau_T = V_T/Q_v$ substituted, and the expression integrated to obtain:

$$c_{IN}(t) = c_{IN}(0) \cdot \exp\left[-\frac{t}{\tau_T}\left(1 - \exp\left\{-\frac{k_m A \tau}{V}\right\}\right)\right] \tag{2.17}$$

This expression can be simplified if the reactor volume is a lot smaller then the tank volume, which also implies that $\tau << \tau_T$. As τ is small, $exp(-k_m A \tau / V)$ can be approximated to $1 - k_m A \tau / V$. Eq. (2.17) therefore becomes:

$$c_{IN}(t) = c_{IN}(0) \cdot \exp\left(-\frac{t}{\tau_T} \cdot \frac{k_m A \tau}{V}\right) \tag{2.18}$$

Eq. (2.18) is then further simplified using the definition for residence time ($\tau = V/Q_v$) to give the final expression:

$$c_{IN}(t) = c_{IN}(0) \cdot \exp\left(-\frac{k_m A}{V_T} t\right) \tag{2.19}$$

This equation has the same form as that for conversion in a batch reactor, except that the reactor volume has been replaced by the tank volume [2.8]. The relationship is only valid if the reaction occurs under mass transfer control across the whole surface of the electrode at 100% current efficiency. When the current efficiency is lower, deviations from Eq. (2.19) will be observed.

2.5 References

2.1 A. J. Bard, R. Parsons and J. Jordan, ed. *Standard Potentials in Aqueous Solution*, Dekker, New York (1985)

2.2 M. Pourbaix, *Atlas of Electrochemical Equilibria in Aqueous Solutions*, National Association of Corrosion Engineers, Houston, Texas (1974)

2.3 M. Pourbaix, *Lectures on Electrochemical Corrosion*, Plenum Press, New York (1973)

2.4 Mathcad, Version 11, Mathsoft Engineering and Education, Inc (2002)

2.5 Matlab, Version 6.5, The MathWorks Inc (2002)

2.6 A. J. Bard, ed. *Encyclopedia of electrochemistry of the elements*, Dekker, New York (1973)

2.7 L. Cifuentes, R. Glasner and J. M. Casas, *Chemical Engineering Science*, **59**: 1087-1101 (2004)

2.8 F. Goodridge and K. Scott, *Electrochemical Process Engineering: a guide to the design of electrolytic plant*, Plenum Press, New York (1995)

3 EXPERIMENTAL

This chapter describes the experimental equipment and methods used during the project. The feasibility of the recovery process proposed by *Kerr* [3.1] was established by constructing theoretical Pourbaix diagrams, which were then verified by precipitation experiments. After the feasibility of the recovery process had been ascertained, the project focussed on the copper electrodeposition stage. A characterisation study was carried out to find the effect of the iron/tin and the stripping additives on the current efficiency and deposition potential of the copper. Thereafter, the recovery of copper was performed using an electrochemical reactor. The feasibility and efficiency of the copper recovery from waste tin stripping solution was found using a parallel plate reactor. As part of these characterisation and reactor experiments, the concentration of copper ions in solution had to be determined.

3.1 Precipitation Experiments

Precipitation experiments are carried out by studying a characteristic property of the system (e.g. precipitation pH, particle size), as a function of initial composition and reaction conditions [3.2]. Previously, this type of investigation has been used to find how the filtration properties of a slurry alter with pH and temperature [3.3], the mechanism of copper precipitation to assist with wastewater treatment design [3.4], and the verification of Pourbaix diagrams to understand the formation of cerium coatings [3.5].

To establish the feasibility of the recovery process, Pourbaix diagrams were constructed to determine if the metals would be in the solid or liquid phase depending on the metal and anion concentration, pH and system potential; the details of which are presented in Chapter 2. The aim of these precipitation experiments was to verify the theoretical predictions from the Pourbaix diagrams. The experiments were carried out using a titration technique, where the dissolved salt of the metal of interest was titrated against an alkaline solution [3.6].

The objective of these experiments was to measure the pH at which the dissolved metal precipitates in acidic conditions. The alkaline region was not validated because the recovery process that operated in the alkaline region had previously been deemed unfeasible (Section 1.5). The systems Cu / NO_3^- / H_2O, Fe / NO_3^- / H_2O, and Sn / Cl^- / H_2O were tested, as they represented the metals in the recovery stages proposed by *Kerr* [3.1], and represented the constituent anions in the process solutions.

3.1.1 Solution Concentrations

The Pourbaix plots that were constructed during the theoretical analysis are applicable for metals in contact with a large volume of bulk solution. The reaction products therefore do not appreciably change the concentration of anions. In order to replicate this restriction in these experiments, the metal ion concentration was kept low in comparison to that of the anion. The experiments were therefore carried out with two concentrations of metal ions, 0.1M and 0.01M, to determine the effect on the pH when the metal ion concentration changes over one order of magnitude, whilst the anion concentration was kept at 1M. For the copper and iron experiments, the nitrate concentration was then set at 0.5M, 1M and 2M with the metal concentration fixed at 0.01M, as the final nitrate concentration in the stripping waste was expected to vary in this range.

The solutions were prepared using AnalaR reagents and de-ionised water. The salts were weighed to an accuracy of ±0.05g or ±0.0005g depending on the quantity required for the experiment. The volume of the acids was measured with a measuring cylinder to an accuracy ±0.5ml in 100ml.

3.1.2 Equipment and Method

The pH was measured using a CE711/DJ/KNO_3 pH probe from ThermoElectron Corp. and a Radiometer PHM200 pH meter. The pH probe is accurate to ±0.02 for pH>2 and ±0.05 for pH<2. The pH measuring equipment was calibrated using an automatic two point calibration procedure against buffer solutions of pH 4 and pH 7.

Two methods to find the precipitation pH were used during these experiments. The first method was derived from a paper by *Hayes et al* [3.5], who were examining the precipitation of cerium oxide films from aqueous solutions. For each experiment a 100ml sample of the metal salt in solution, acidified so the nitrate/chloride concentration corresponded to the Pourbaix plot, was prepared. Concentrated KOH was added in 1ml increments and the pH was recorded after each addition. The pH probe was allowed to equilibrate for 10mins before each reading was taken. After the first experiment, the addition volume and the concentration of KOH were reduced, because the initial result was a wide pH range in which precipitation had occurred. This method was revised because the technique did not allow for slow kinetics in the precipitation reaction.

In the second method, four 50ml samples were prepared. KOH was added until the sample pH spanned the theoretical value, preferably with at least one sample precipitated. For example, if theory predicted that precipitation would occur at pH 4.5, then the samples could have been at pH 4.00, 4.25, 4.50 and 4.75. The samples were then left for at least a week to allow for the equilibration of slow reactions. The pH of all samples was then remeasured. This revised method had additional advantages; it was quicker, as only four pH readings must be accurate, and if too much KOH was added and the precipitation point missed, the sample still provided a useful data point. The majority of the experiments in this report were carried out using this second method, apart from runs A-E for the copper/nitrate system.

3.2 Electrochemical Characterisation

The aim of the electrochemical characterisation experiments was to determine whether it is possible to deposit copper from a nitrate solution with reasonable efficiency, and to find the effect of the stripping additives and iron/tin on this efficiency. The deposition of copper from nitrate solutions has been accomplished by other researchers [3.7, 3.8]. However, problems with low current efficiency have been reported [3.9] which are thought to be caused by the concurrent reduction of nitrate with copper deposition [3.10] and the redissolution of copper into the acid

[3.8]. The deposition of copper from waste tin stripping solution has also been found to be less efficient than that from nitric acid [3.11].

The electrochemical characterisation experiments were initially carried out with only copper and nitrate in solution. This indicated the ability to recover copper from the additive free solution. Thereafter, experiments with iron/tin and the stripping additives were carried out and compared against the results from the copper/nitrate solutions to evaluate the effect of the additives on the deposition. Experiments were carried out to determine:

a. The deposition potential and mass transport limiting current for copper deposition from nitrate solutions, and how the copper and nitrate concentrations affect these.
b. The efficiency of copper deposition across a range of currents, and how the copper and nitrate concentrations affect this.
c. The effect of the addition of Fe(III) and Sn(IV) to the copper/nitrate solution on points (a) and (b) above.
d. The difference in points (a) and (b) when repeated with waste stripping solution.
e. The copper recovery that could be obtained. Could the discharge limit of 1.5ppm (2.4×10^{-5}M) be reached via electroreduction?

3.2.1 Electrolytes

The maximum Cu(II) concentration that can exist in the waste stream is 0.3M (as per the process control information supplied by our industrial partners, cf. Table 1-1). The concentration could be less than this if, for example, rinse water is mixed with the stripping waste, or the bath is changed prematurely before a new batch. Experiments were therefore carried out for Cu(II) concentrations of 0.3M, 0.03M and 0.003M. The lower concentrations also show how the electrochemical behaviour of the solution changes as copper is recovered from the process solution.

The NO_3^- concentration at the deposition stage will be dependent on the amount of acid recovered during the diffusion dialysis. The maximum NO_3^- concentration in

the waste is 1M; therefore the chosen concentrations for these experiments were 1M, 0.1M and 0.01M. 0.1M NO_3^- will remain in the waste if 90% of the acid were recovered, and 0.01M NO_3^- if 99% of the acid were recovered. Concentrations lower than these were not investigated as it is unlikely that more than 99% of the acid would be recovered or the waste would be sufficiently diluted.

After the characterisation of the copper/nitrate solutions, subsequent experiments were carried out with the addition of iron/tin. The Fe(III) concentration that was added to the copper/nitrate solutions was 0.25M. According to the process control information (Table 1-1), this is the maximum concentration of Fe(III) in the stripping solution during processing, which enables the efficiency to be determined for the worst case. As tin exists as a suspension of SnO_2 in the waste stripping solution, SnO_2 was added to the iron/tin solutions to form a saturated solution.

Based on the above reasoning, Table 3-1 shows the full matrix of simulated solutions that were studied. These electrochemical characterisation experiments were also carried out using real waste tin stripping solutions.

Solution no.	[Cu] / M	[NO_3^-] / M	Sn / Fe added?	Solution no.	[Cu] / M	[NO_3^-] / M	Sn / Fe added?
1	0.3	1	N	10	0.3	1	Y
2	0.3	0.1	N	11	0.3	0.1	Y
3	0.3	0.01	N	12	0.3	0.01	Y
4	0.03	1	N	13	0.03	1	Y
5	0.03	0.1	N	14	0.03	0.1	Y
6	0.03	0.01	N	15	0.03	0.01	Y
7	0.003	1	N	16	0.003	1	Y
8	0.003	0.1	N	17	0.003	0.1	Y
9	0.003	0.01	N	18	0.003	0.01	Y

Table 3-1 Solution concentrations used for electrochemical characterisation

The solutions were prepared using high purity water (14MΩ) and AnalaR grade $Cu(NO_3)_2.3H_2O$, $Fe(NO_3)_3.9H_2O$ and SnO_2 (BDH), with additional nitrate added as

HNO_3 (BDH, 65%). In the real solution, H^+ ions are consumed faster than NO_3^- ions when copper and tin are dissolved from the circuit board (Section 1.3). It is therefore reasonable to have a higher concentration of NO_3^- ions than H^+ ions in these simulated solutions.

Solutions 2, 3, 6, 11, 12 and 15 from the matrix were impossible to make without the addition of other ionic species (e.g. sulphate). These solutions contain more copper ions than nitrate and therefore cannot be made from $Cu(NO_3)_2$, or by dissolving Cu powder in nitric acid, as the copper needs sufficient nitrate in the solution with which to react and thus dissolve. The reaction equations for the dissolution of copper in dilute and strong acids are shown in Section 1.3. For example, Solution 2 was to contain 0.3M Cu^{2+} and 0.1M NO_3^- ions, which is impossible. The maximum amount of copper that could be dissolved in 1 litre of 0.1M HNO_3 would be 0.0375mol, considerably less than the 0.3mol required.

3.2.2 Equipment

These electrochemical characterisation experiments were performed using a Sycopel Scientific rotating disc electrode (RDE). A gold disc with a diameter of 7mm was the working electrode. A platinised titanium sheet of area 20 x 25mm was used as a counter electrode. Cyclic voltammetry and anodic stripping were carried out using an EG&G Instruments bi-potentiostat and the data was logged on a PC via a Sycopel PCI 100 data acquisition system (Figure 3-1). The potential was measured against a saturated calomel electrode (SCE) placed approximately 7mm from the RDE via a Luggin.

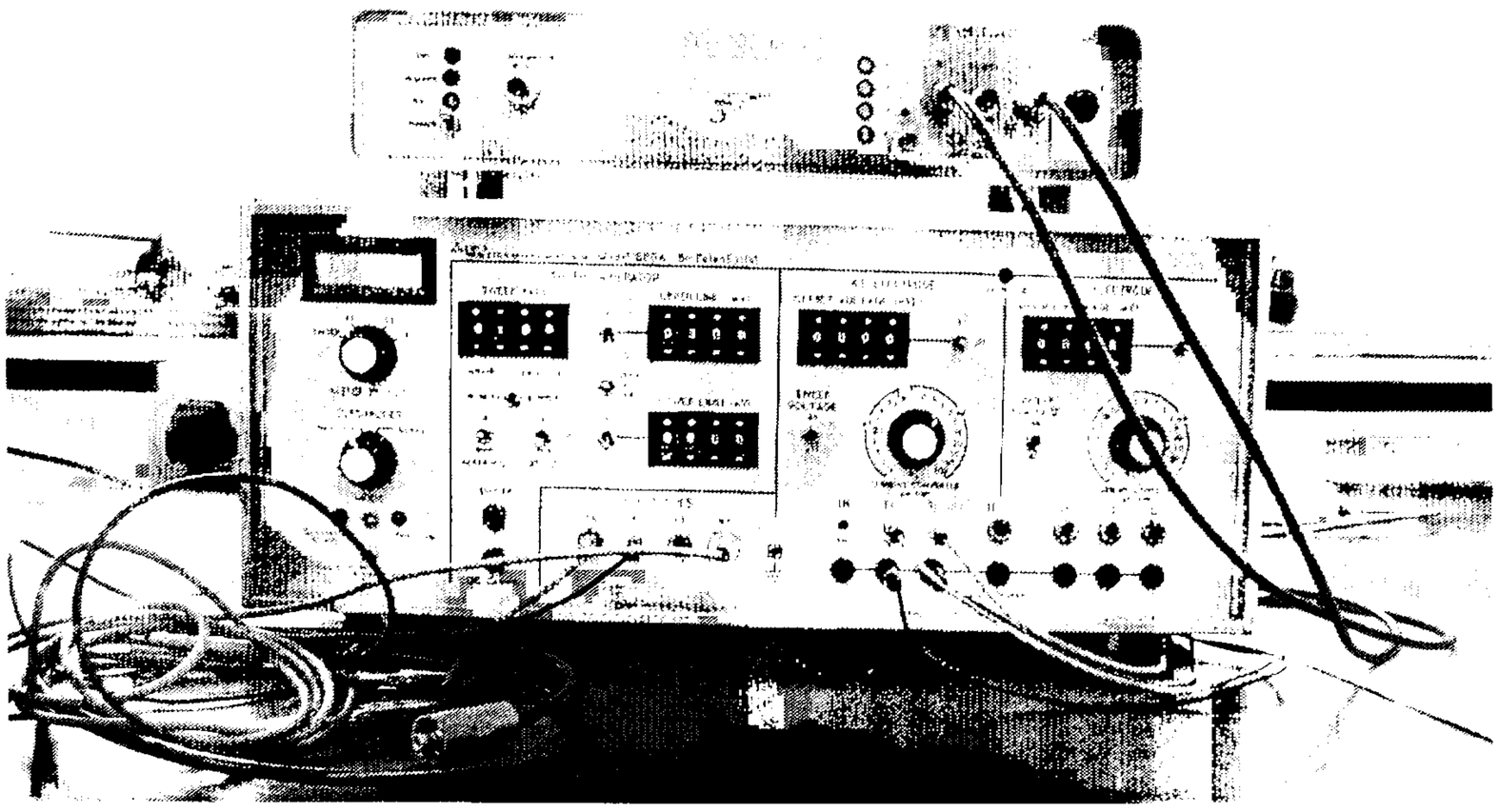

Figure 3-1 Bi-potentiostat and data acquisition system

The characterisation studies were carried out in an H-cell (Figure 3-2). The anolyte and catholyte sections were separated by a glass frit, and were each filled with 50ml of the solution under study. The SCE was connected to the cell via a Luggin capillary; this section was filled with HNO_3 for the voltammetry, or HCl during the anodic stripping.

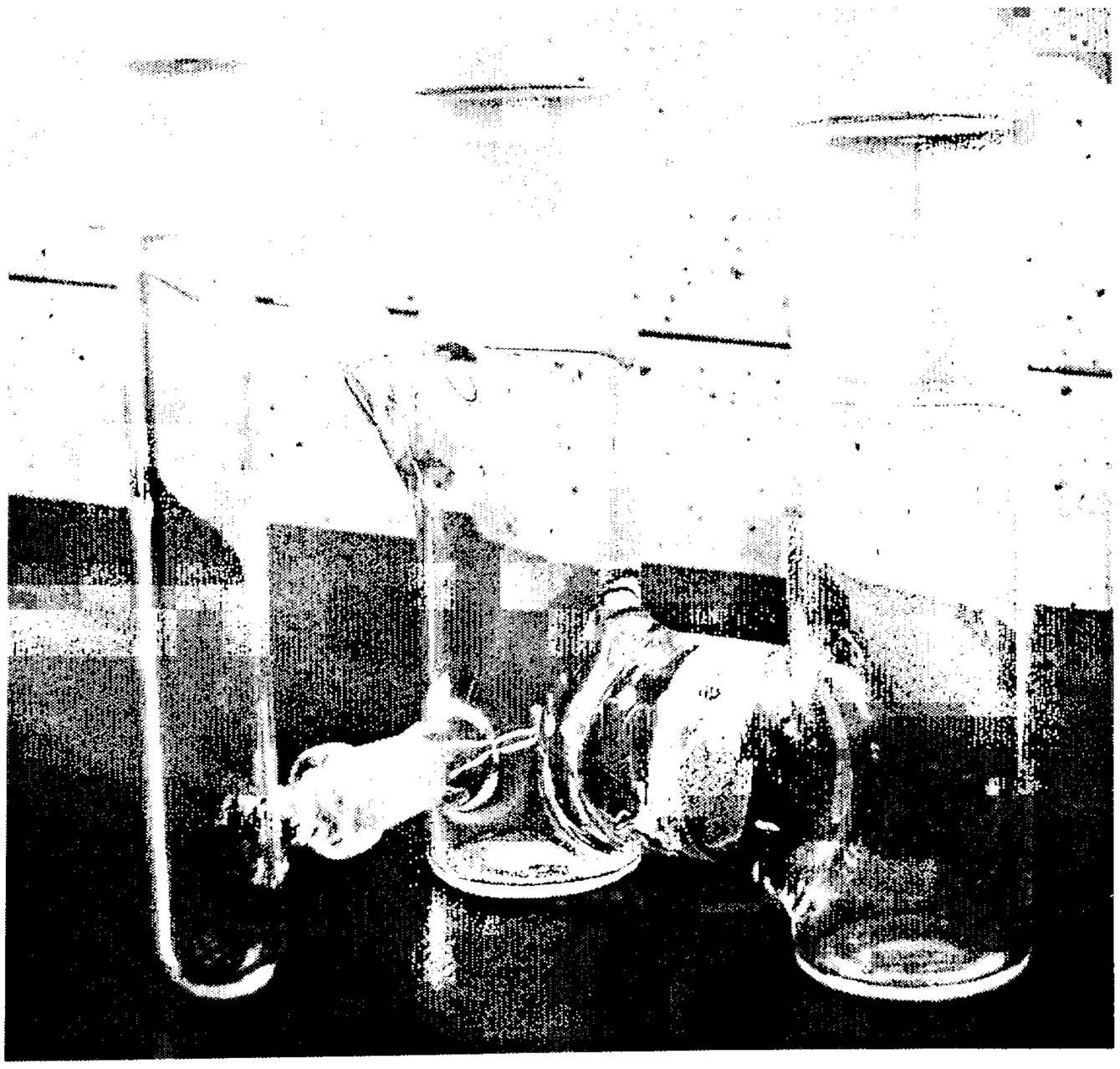

Figure 3-2 The H-cell

The measurement of the solution conductivity was performed using a Hanna Instruments HI 8633 conductivity meter. The conductivity range the meter could measure was 0-199.9mS.

3.2.3 Electrochemical Techniques

Cyclic Voltammetry

Cyclic voltammograms are often the first stage in experimentation to find deposition potentials and limiting currents for metal recovery processes [3.12, 3.13]. To record a cyclic voltammogram, the potential is swept continuously between two set limits at a particular rate. The potential-time waveform is shown in Figure 3-3.

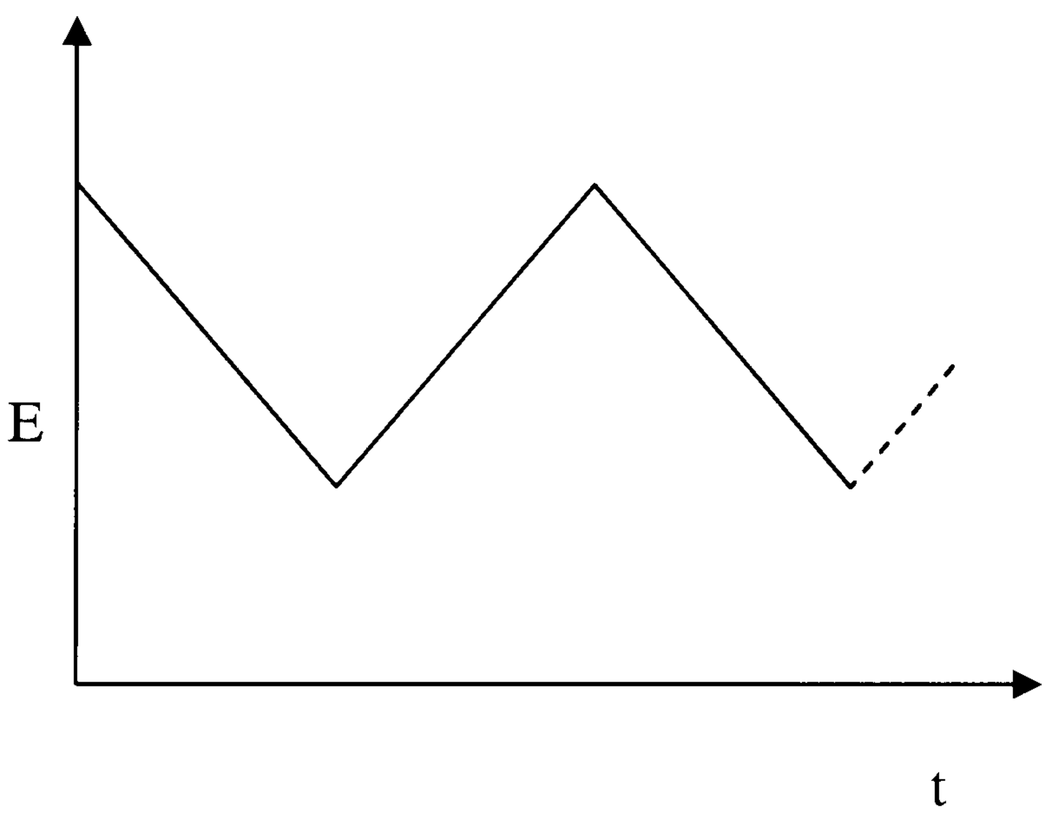

Figure 3-3 Potential-time waveform for cyclic voltammetry [3.14]

The current is recorded as a function of the applied potential; this provides information on the potentials at which any reductions or oxidations occur. These reactions are seen when the current is non-zero; for our experiments, the reactions include copper deposition and dissolution. An RDE is often used as the working electrode for this technique because the transport of species to the disc can be controlled reproducibly [3.14].

Stripping Techniques

Stripping techniques involve the initial deposition of a metal from a solution of interest onto an electrode, followed by the metal being stripped off under controlled conditions. The technique has been used to find the concentration of trace metals in solution, as the initial deposition concentrates the metal in the mercury electrode allowing a reasonable currents to be measured during stripping [3.15]; the current efficiency of deposition; and the composition of an alloy [3.16, 3.17].

To find the current efficiency of a deposition, the metal is first deposited onto the electrode from the chosen electrolyte, and the quantity of charge used recorded. The electrode is then transferred into a solution where the metal dissolves entirely into a single oxidation state, and no other reactions occur at the stripping conditions e.g. hydrogen evolution [3.17]. The charge measured during the dissolution can then be attributed entirely to the metal, and the theoretical metal deposition charge calculated. This is then divided by the total charge consumed during the actual deposition to find the efficiency of electroreduction.

3.2.4 Method

The characterisation experiments were conducted in two parts: firstly voltammetry to find the Cu(II) deposition potential, Cu(II) limiting current and an estimate for the efficiency of copper deposition from nitrate electrolytes. Anodic stripping experiments were then performed to find the efficiency for a variety of applied currents. Both parts of these experiments were carried out for copper in nitrate solution, copper and nitrate solutions with iron/tin, as well as real waste solutions.

Cyclic Voltammetry

Cyclic voltammograms were recorded for each solution detailed in Table 3-1. The voltammograms were recorded at several rotation speeds ranging between 200rpm and 1000rpm, at a scan rate of 10mV/s. The potential was scanned in the cathodic direction from 0mV to -600mV and then anodically until all the copper had been removed from the electrode (zero current).

It was expected that some of the nitrate in solution would be reduced during the copper deposition [3.10, 3.18]. Therefore cyclic voltammograms for the background electrolyte were recorded. If the reactions are uncoupled, which research has suggested [3.19], then the current due to the background electrolyte can be subtracted from the copper solution curve, allowing one to calculate the current due to the copper deposition only. This procedure can enable the true values for the Cu(II) deposition potential and Cu(II) limiting deposition current to be determined.

The deposition potential of the copper was taken to be the potential arising when the current flowing through the cell was -2mA. This definition was chosen because it was difficult to find the exact potential at which the current became non-zero, due to the resolution limitation of the instrument (background current). The value of -2mA was measurable on all the scans and when used consistently, showed clear differences in the deposition potential.

The efficiency of the copper deposition during the cyclic voltammetry, at rotation speeds of 800rpm, was determined from a graph of current against time, by integrating the area under the curve (Figure 3-4). The total charge during the deposition $Q_{cathodic}$, which included contributions from copper deposition and other competitive reactions, such as nitrate reduction and hydrogen evolution was the area denoted by 1.

$$Q_{cathodic} = \int_0^{t_1} I_{cathodic} \cdot dt \tag{3.1}$$

The charge from copper deposition alone was equal to that from copper stripping Q_{anodic} (area 2), as in these solutions no other reactions occur at these potentials. The potential was not positive enough for water to break down, and nitrate cannot be oxidised as nitrogen is already in its highest valence state of +5.

$$Q_{anodic} = \int_{t_1}^{t_2} I_{anodic} \cdot dt \tag{3.2}$$

The efficiency of the copper deposition was then calculated as shown in Eq. (3.3). This method cannot be used to estimate the efficiency for deposition at a single current.

$$\Phi = \frac{Q_{anodic}}{Q_{cathodic}} \times 100 \tag{3.3}$$

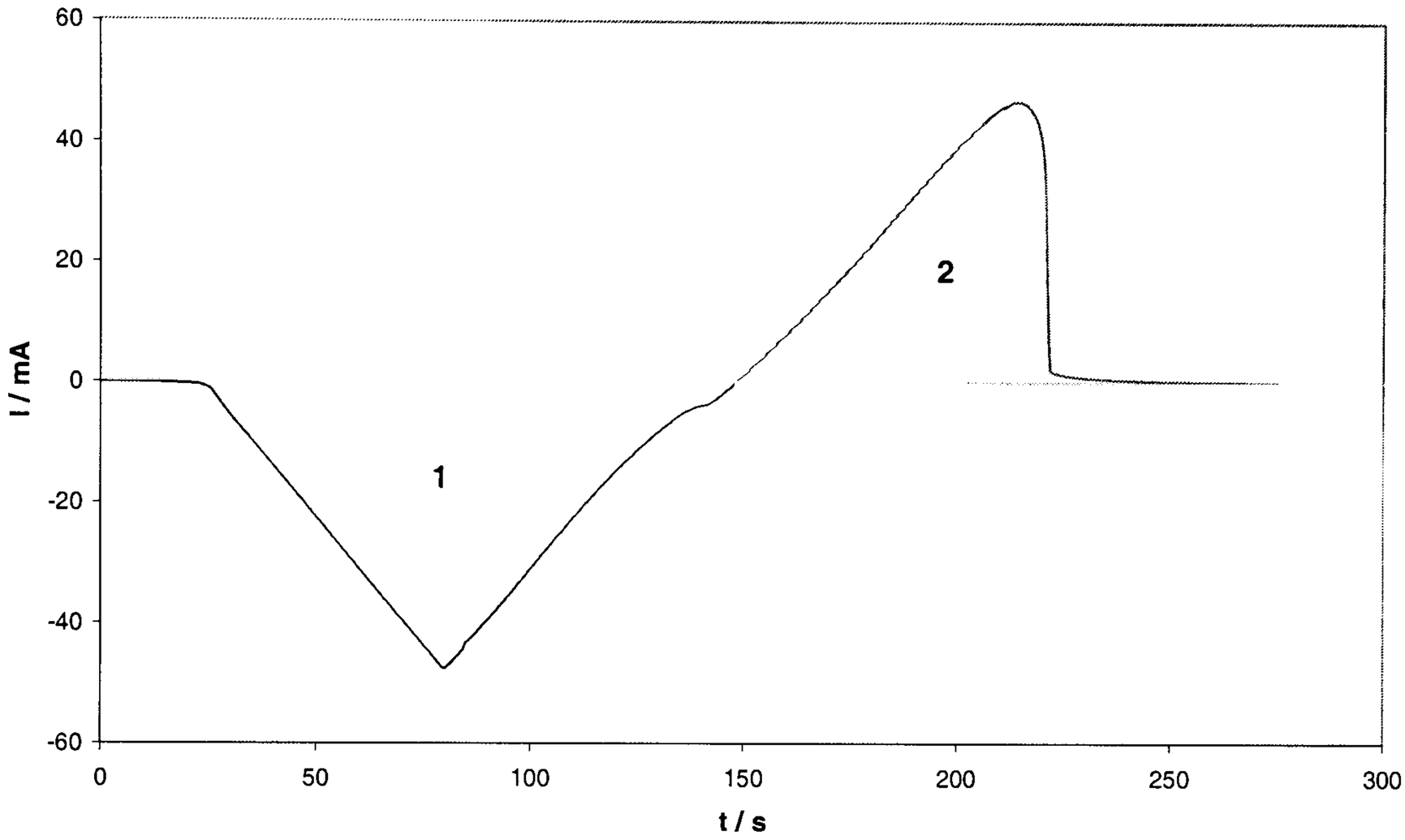

Figure 3-4 Cyclic voltammogram plotted as current against time, to show efficiency calculation

As the ionic concentration of some of the solutions detailed in Table 3-1 are fairly dilute, there may be uncompensated resistance between the working and reference electrodes. This resistance will cause errors in the i-E data. There are several methods used to measure this resistance: the simplest is to determine the solution conductivity and calculate the resistance assuming the solution is a conductor of area equal to the cell diameter; a more accurate value can be obtained by the current interrupt or impedance methods. In the interrupt technique the current through the cell is suddenly interrupted, and the potential recorded. The potential immediately falls by the product of the original cell current and the uncompensated resistance. After this initial drop the potential decays exponentially as the effective capacitor across the double layer discharges [3.14]. The AC impedance method involves measuring the impedance of the electrochemical cell as a function of frequency. The real part of the measured impedance is then plotted against the imaginary part. The

solution resistance is given by the intercept on the real axis as the frequency tends to infinity.

In order to estimate the solution resistance, and thus the errors in the i-E data, the simple conductivity method was chosen. The solution conductivity was calculated using Kohlrausch's law of independent migration of ions (Eq. 3.4). This relates the conductance of a salt Λ to the conductance of the individual ions λ; where ν is the number of positive or negative ions in the salt, and z the valency.

$$\Lambda = z_+\nu_+\lambda_+ + z_-\nu_-\lambda_- \tag{3.4}$$

The conductivity of the solution κ is then the sum of the product of the conductance and molarity of each component (Eq. 3.5)

$$\kappa = \sum \Lambda \cdot c \tag{3.5}$$

The values of ionic conductance used in the calculations are shown in Table 3-2.

	λ / S cm^2 per equivalent
Cu^{2+}	54
H^+	349.8
NO_3^-	71.4

Table 3-2 Values of ionic conductance at infinite dilution in water at 298K [3.20]

The resistance of the solution between the working and reference electrodes can then be calculated from the solution conductivity using Eq. (3.6), where L is the electrode separation, and A is the cross sectional area of the solution between the reference and working electrodes. These calculated solution resistances were checked using a conductivity meter, calibrated in dilute KCl.

$$R_S = \frac{L}{\kappa \cdot A} \tag{3.6}$$

This simple conductivity measurement is only strictly suitable for systems that have simple geometry, where the current lines flow normal to the electrode surface, and the reference electrode is between the anode and cathode. This is not the case in the H-cell. However, the solution resistance was subtracted from the i-E data to determine whether the shape of the voltammogram was altered, rather than to determine the potential at which peaks or other artefacts occur at. Therefore, quite large inaccuracies in the value of the solution resistance can be tolerated.

Anodic Stripping

In order to determine the Cu(II) deposition efficiency at a particular current, separate stripping experiments were performed. Copper was deposited from each solution at a range of currents because nitrate ions are thought to be reduced concurrently with Cu(II). Therefore, the proportion of the cell current used for the deposition will vary as the current changes. This is illustrated in Figure 3-5, where the deposition efficiency for Cu(II) at the current I_4 is seen to be less than at I_3.

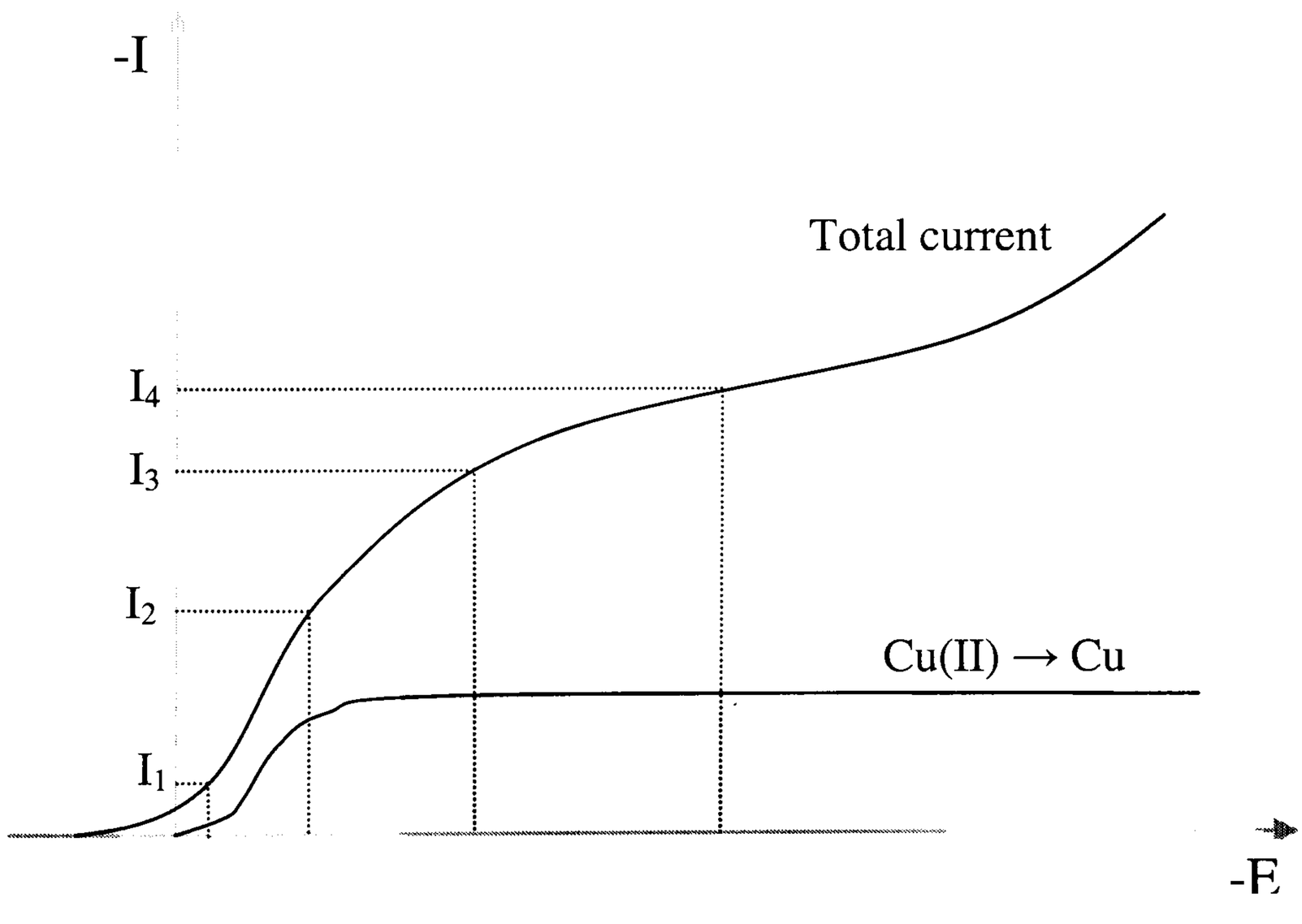

Figure 3-5 Diagram showing how the efficiency can change with cell current

Initially, copper was deposited from solution onto the gold electrode at 800rpm. The deposition was carried out for t_d seconds at a current I_1. The copper deposit was then washed with deionised water and transferred into 0.5M HCl. Copper was stripped

from the disc at constant potential and the current recorded. The disc speed was kept at 800rpm. This deposition/stripping cycle was carried out at four different deposition currents for each solution, to study the effect of applied current. The experiments were repeated at least three times for each current to gain an estimate of the reproducibility. The experimental uncertainty at 95% confidence interval could then be calculated.

Hydrochloric acid was chosen as the stripping electrolyte as it can dissolve copper into cuprous ions only, rather than a mixture of Cu(I) and Cu(II) [3.21]. The dissolution is thought to proceed via the mechanism shown below [3.22].

$$Cu + Cl^- \rightarrow CuCl + e^- \qquad\qquad CuCl + Cl^- \rightarrow CuCl_2^-$$

The potential at which copper could be removed as cuprous ions was determined by stripping the copper potentiodynamically, according to the method described by *Horkans et al* [3.16]. It can be seen from Figure 3-6 that as the potential was scanned anodically, copper was stripped from the electrode at potentials more positive than -200mV. It is important to ensure that the copper is dissolved entirely into the +1 oxidation state. The second peak is thought to be the result of a thick film of CuCl forming on the electrode surface, leading to dissolution into mixed oxidation states [3.16]. The stripping was therefore carried out in the potential range of the first peak; the chosen value being 0V vs SCE.

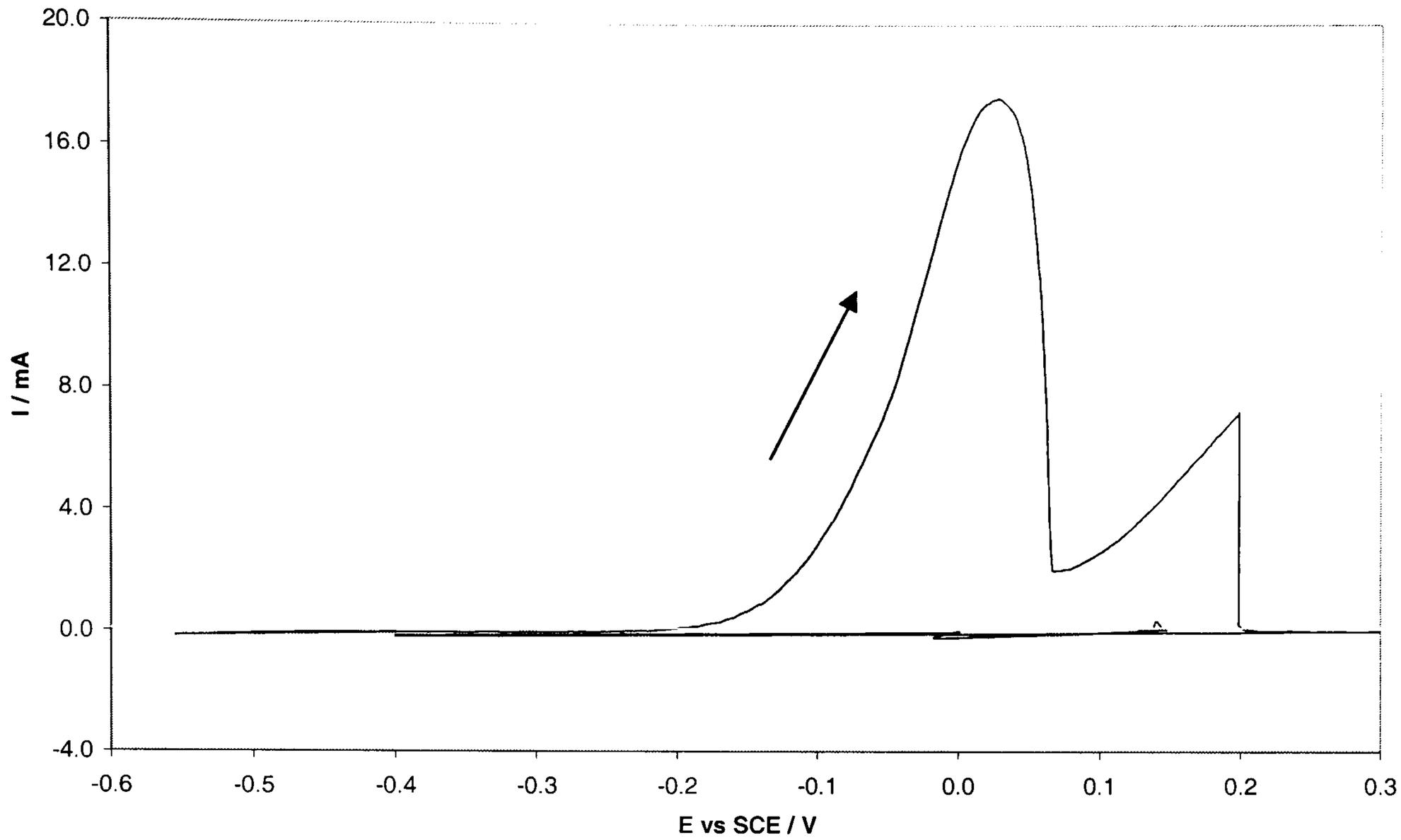

Figure 3-6 Current due to potentiodynamic stripping of copper into 0.5M HCl, 800rpm, scan rate 10mVs^{-1}

To ensure the dissolution was occurring entirely as Cu(I), copper was deposited onto the rotating disc from a 0.05M $CuSO_4$ + 2M H_2SO_4 solution, at -0.7V for 1min. This deposit was then stripped potentiostatically at 0V in 0.5M HCl. If the Cu is stripped entirely as Cu(I), the charge from the dissolution of m moles of copper Q_{strip} is:

$$Q_{strip} = mnF \quad , \; where\ n = 1 \tag{3.7}$$

The charge Q_{theor} that would have been used to deposit this mass will be twice Q_{strip}, as copper was deposited from a solution of Cu(II):

$$Q_{theor} = mnF = 2 \cdot Q_{strip} \quad , \; as\ n = 2\ in\ this\ case \tag{3.8}$$

The efficiency was therefore calculated as twice the stripping charge Q_{strip}, divided by the charge actually used during the deposition $Q_{deposit}$. If any copper was dissolved into the +2 state, the efficiency as calculated above will become >100%. Example deposition and stripping data are shown in Figure 3-7. The calculated efficiencies for three experiments were 94.1%, 95.9%, 95.5%. These efficiencies are

within 2% of each other and close to 100%, therefore this method was thought to be practicable.

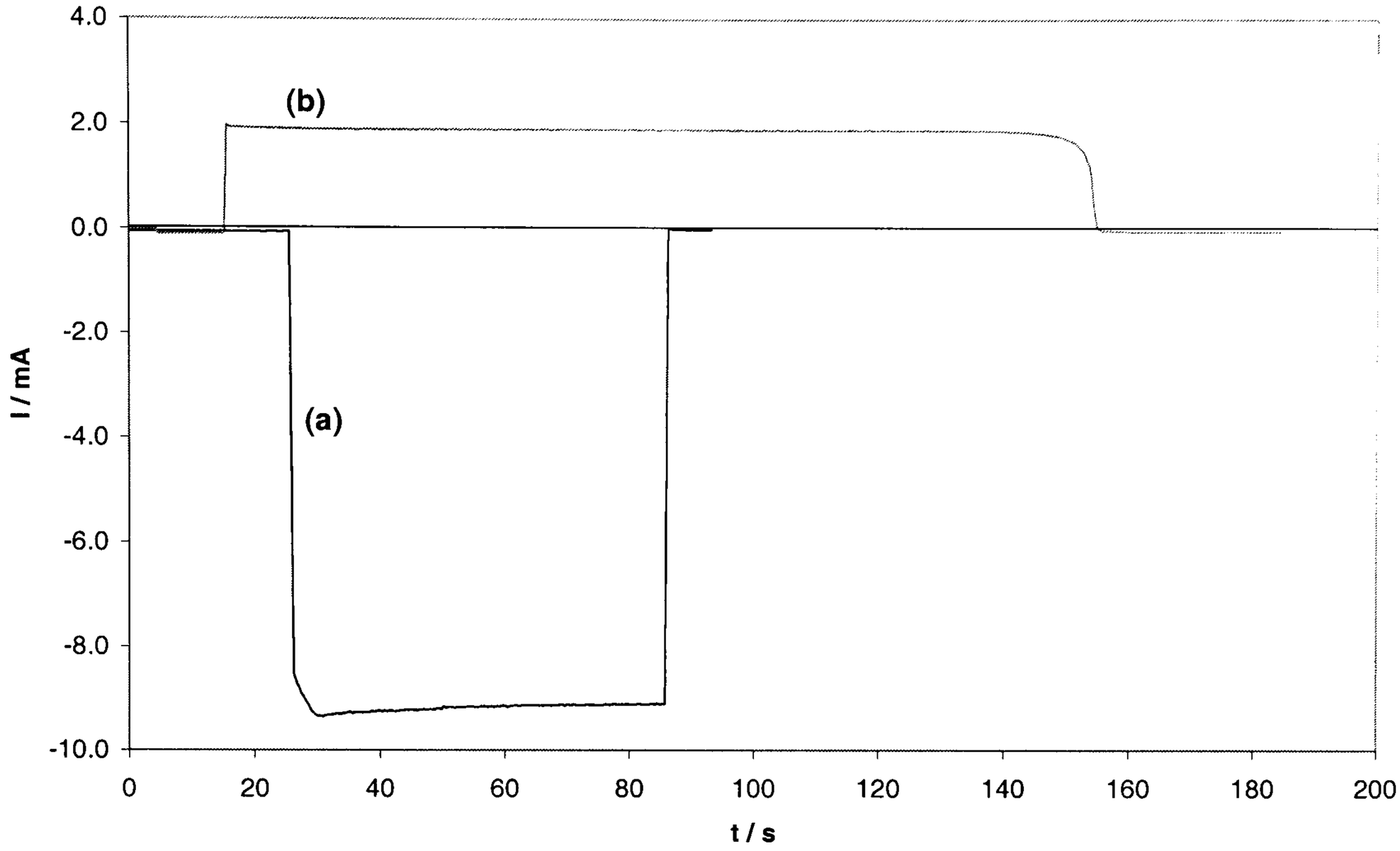

Figure 3-7 (a) Deposition of Cu from 0.05M CuSO4 + 0.2M H_2SO_4 (b) Copper stripping into 0.5M HCl. Scan rate 10mVs^{-1}, 800rpm

The method described above was not used to determine the efficiency of copper deposition from the real waste solution, because the deposited copper was powdery and could not be removed electrochemically. After deposition from the waste, these copper deposits were left overnight in a known volume of 0.5M HNO_3 (Suprapur, Merck). The copper deposits from several runs were dissolved in the same volume of HNO_3 to ensure there was a sufficiently high concentration for subsequent detection and analysis. The copper concentration, and thus the number of moles of copper that had been deposited, were then determined using an ion selective electrode (Radiometer). The theoretical charge to deposit this amount of copper was calculated using Faraday's law, and divided by the actual charge used to obtain the deposition efficiency.

3.3 Reactor Recovery

The ability to recover copper from nitrate containing solutions was validated by the electrochemical characterisation study. Industrially, an electrochemical reactor would be used for this recovery stage. Therefore the aim of these reactor experiments was to determine the feasibility and efficiency of copper recovery from waste tin stripping solution using a parallel plate reactor.

3.3.1 Electrolytes

These experiments were conducted in two stages: initially the mass transfer properties of Cu(II) reduction in the reactor were determined, and then copper was recovered from the simulated waste stripping solution. The mass transfer properties were determined using solutions of $CuSO_4$ in H_2SO_4. Sulphuric acid was used as a reference electrolyte because sulphates are not reduced concurrently with copper, unlike nitrates. To determine if the Cu(II) deposition was mass transport controlled, two Cu(II) concentrations were used. As the Cu(II) concentration in the stripping waste is 0.3M [3.23], the chosen concentrations were 0.3M and 0.03M. The initial solution of 0.3M $CuSO_4$ + 1M H_2SO_4 was diluted to produce 0.03M $CuSO_4$ + 0.1M H_2SO_4. All solutions were made using AnalaR reagents and high purity water (14MΩ).

Ideally, the copper recovery experiments would have been performed using waste tin stripping solution as the electrolyte. However, insufficient process waste solution was available to fill the $0.01m^3$ tank associated with the reactor. A simulated solution was therefore prepared. The composition of the fresh stripping solution was known from the Tinsolv 2000 material safety data sheet (MSDS) and is shown in Table 3-3. The waste stripping solution will also contain dissolved copper, and tin as a suspension of SnO_2.

HNO_3	<15%
$Fe(NO_3)_3.9H_2O$	<10%
NH_4NO_3	<5%
glycolic acid	<2%

Table 3-3 Composition of Tinsolv 2000 (Atotech UK) [3.24]

Tinsolv 2000 is the second stripping solution used in a two stage process; therefore the majority of the tin has already been removed. During this second stripping stage, ferric and nitrate ions are reduced as the copper-tin intermetallic is dissolved from the PCB. The pertinent reactions are shown below:

$$Cu^0 + 8HNO_3 \rightarrow Cu(NO_3)_2 + 2NO + 4H_2O$$

$$Cu^0 + 2Fe(III) \rightarrow Cu(II) + 2Fe(II)$$

To prepare a simulated waste solution, the proportion of ferric ions and nitric acid consumed during the dissolution need to be calculated or measured. The full details of these calculations are shown in Appendix A. The composition of the simulated stripping solution used for the reactor recovery experiments is shown in Table 3-4.

HNO_3	1M
$Cu(NO_3)_2$	0.3M
$FeSO_4$	0.2M
$Fe(NO_3)_3$	0.05M
NH_4NO_3	0.375M
glycolic acid	0.131M

Table 3-4 Composition of simulated waste stripping solution for reactor recovery experiment

3.3.2 Equipment

A parallel plate reactor was used to recover copper in this study (Figure 3-8). This reactor was originally designed for the recovery of gold from thiosulphate-sulphite electrolytes [3.25]. The reactor was composed of four Perspex blocks (0.28 x 0.10 x 0.025 m): the anode and cathode were recessed into the outer blocks, and the inner two formed a flow channel of 2.688×10^{-3} m^2. The cathode consisted of a flat copper

plate of area $6x10^{-3}$ m^2 and the anode was a platinised titanium mesh. The reference electrode was a copper wire inserted into the flow immediately above the cathode. The copper wire gave a measured potential of +51mV against the SCE in 0.3M $CuSO_4$ +1M H_2SO_4.

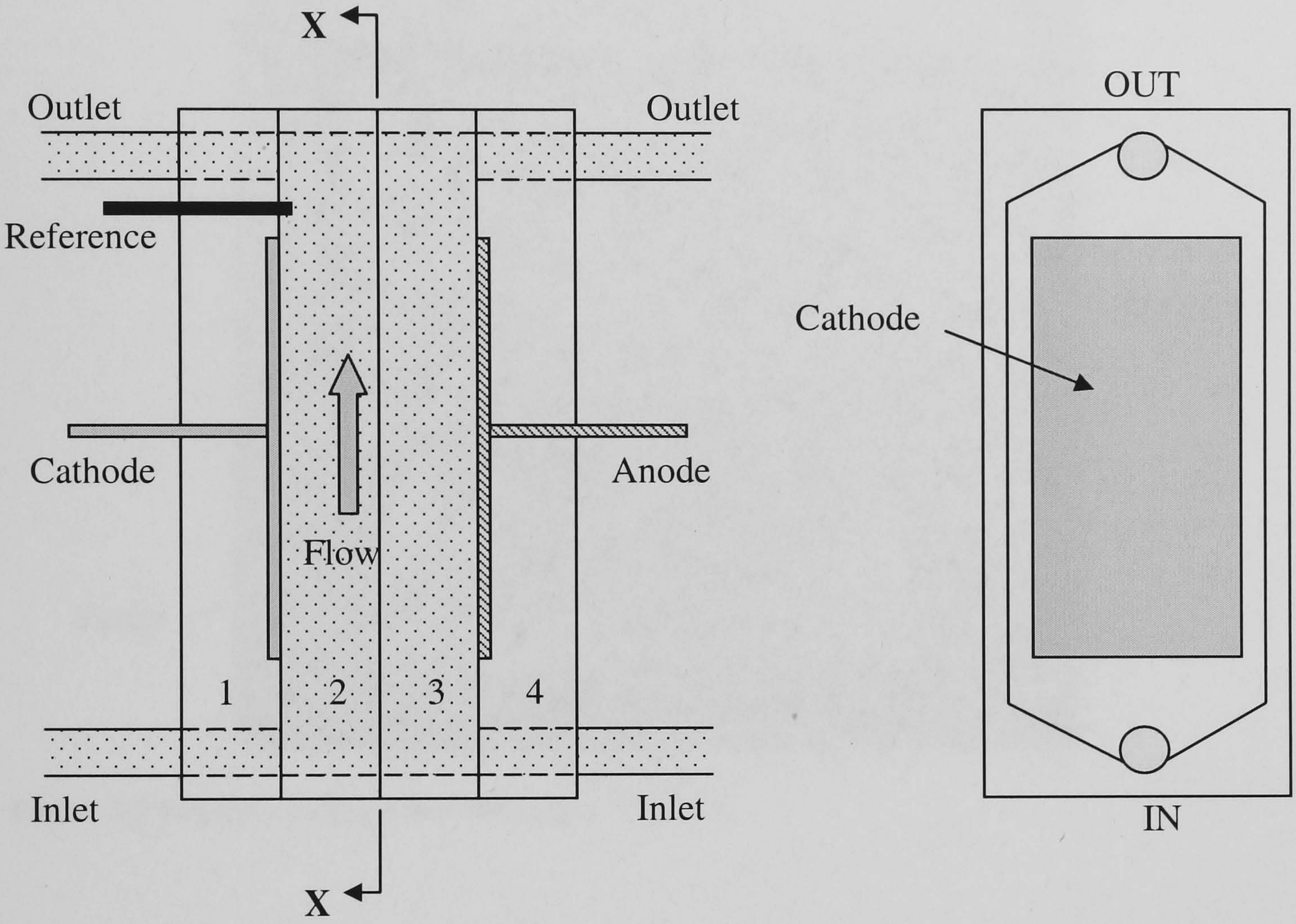

Figure 3-8 Parallel plate flow reactor used for recovery experiments

The reactor was configured as a batch recycle reactor (Figure 3-9). The electrolyte was stored in a $0.01m^3$ tank and pumped into the base of the reactor through two inlets. The flowrate was measured using rotameters on the inlet piping. The current to deposit the copper was supplied by a Digimess HY3010 10A power supply. The potential generated between the cathode and copper reference electrode was measured using a Thandar TM351 digital multi-meter.

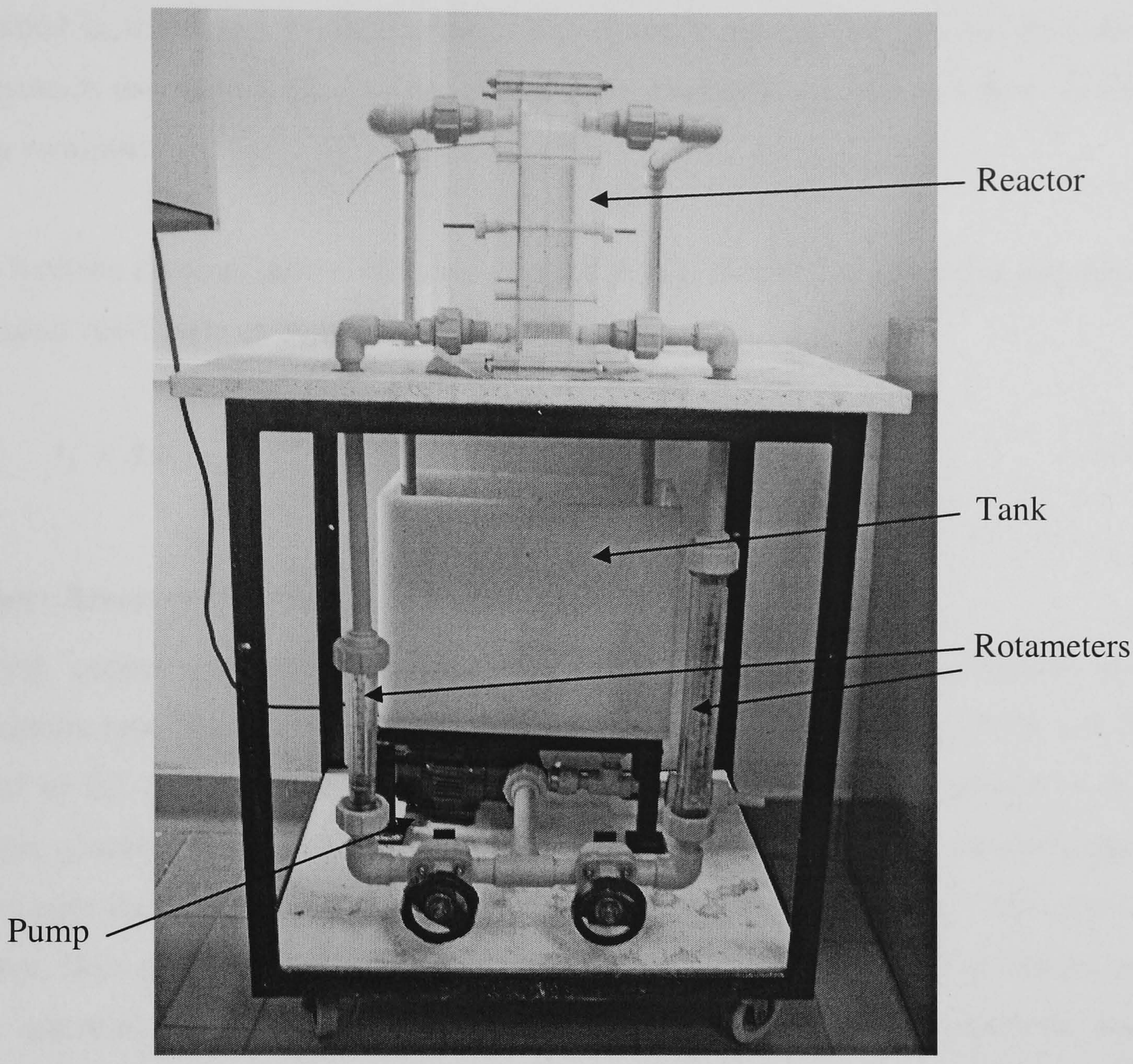

Figure 3-9 Reactor configuration for copper recovery

3.3.3 Method

The reactor experiments were carried out in two parts: initially the limiting current for copper deposition was determined from i-E data, which allowed the mass transfer coefficient for the copper to be estimated. The reactor was then used to deposit copper from the simulated waste stripping solution at the Cu(II) limiting current.

Mass Transfer of Copper in Reactor

To determine the maximum rate that copper could be deposited, the limiting current for copper in the reactor was found by recording linear voltammograms. These polarisations were taken by adjusting the current across the reactor and measuring the potential of the cathode with respect to the copper reference electrode. To determine if the copper deposition is mass transport controlled, voltammograms were

recorded in 0.3M and 0.03M $CuSO_4$. The flowrate through the reactor was also adjusted in the range 1.67 – 3.33 x 10^{-4} m^3s^{-1} to determine the effect of flow on the mass transport.

The limiting currents determined from the i-E data were used to determine the mass transport coefficient of copper in the reactor via Eq. (3.9).

$$I_L = Ank_m c_0 \tag{3.9}$$

Copper Recovery from Waste

During copper recovery from the simulated waste tin stripping solution, the maximum rate of copper deposition will occur when the current through the cell is equal to the copper limiting current. This limiting current is proportional to the copper concentration, as shown by Eq. (3.9). Therefore, as the copper concentration decreases, the limiting current for the deposition will also decrease. Any excess charge, from a cell current higher than the copper limiting current, will be wasted on side reactions e.g. NO_3^-, H^+ reduction. To minimise these parasitic reactions, and thus maximise the deposition efficiency, the cell current should be periodically reduced in line with the copper concentration, as described by *Sobri* [3.25].

To reduce the cell current in line with the copper concentration, the variation of Cu(II) concentration with time in the simulated waste needs to be estimated. A theoretical plot of the normalised Cu(II) concentration was therefore constructed using Eq. (3.10). This equation assumes that copper is reduced at its mass transfer limiting current.

$$c(t) = c(0) \cdot \exp\left(-\frac{k_m A}{V_T} t\right) \tag{3.10}$$

For Eq. (3.10) to model to recovery of copper from the nitrate based stripping solution, the value of k_m should be based on a nitrate electrolyte. However, the values calculated from the i-E data were from a sulphate electrolyte. The Nernst diffusion layer model was used to derive a relationship between the mass transfer

coefficients in sulphate and nitrate electrolytes. This relationship is given by Eq. (3.11), with the diffusion coefficients D shown in Table 3-5.

$$k_m(Cu, NO_3) = k_m(Cu, SO_4) \cdot \frac{D(Cu, NO_3)}{D(Cu, SO_4)} \tag{3.11}$$

	D x 10^{-6}/ cm^2 s^{-1}
Cu in NO_3^-	8.71
Cu in SO_4^{2-}	5.16

Table 3-5 Diffusion coefficients of 0.3M copper [3.26]

The theoretical plot of normalised copper concentration, with a representation of how the cell current is reduced, is shown in Figure 3-10. Initially the cell current is set to the limiting value for *[Cu]=c(0)*, after a set time the current is reduced to the limiting value for *[Cu]=c(t1)* where *c(t1)* is calculated from Eq. (3.10) and I_L from Eq. (3.9).

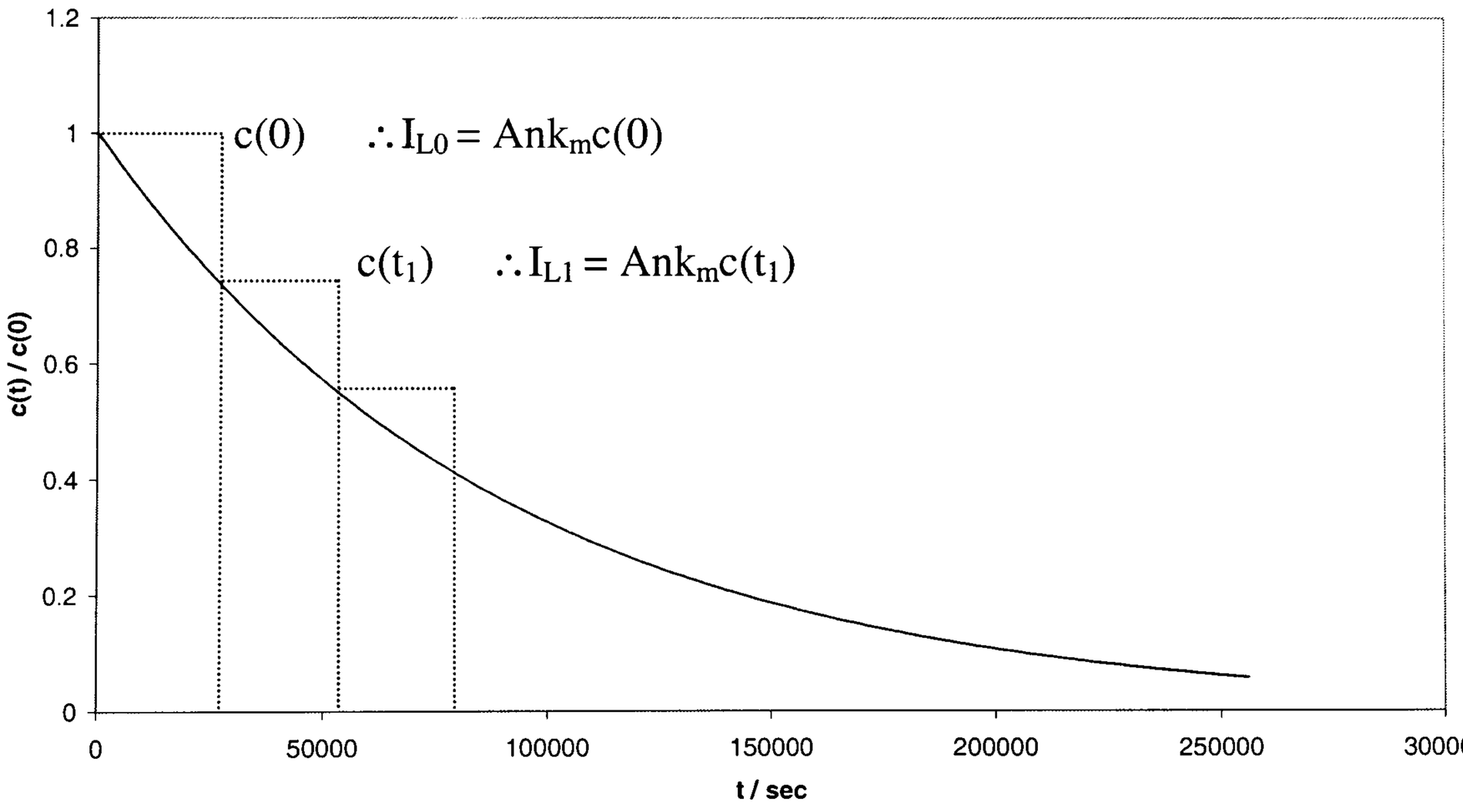

Figure 3-10 Theoretical copper reduction illustrating how the cell current is reduced with [Cu]

The reactor was run for 16 hours, and the cell current was reduced every hour to the value calculated for the theoretical copper concentration. The cell and cathodic potential were recorded every time the current was reduced. A 50ml sample of the

electrolyte was also removed every hour for later analysis by ICP. The flow through the reactor was set to the maximum value of $3.33x10^{-4}$ m^3s^{-1} in order to determine the highest copper recovery possible.

3.4 Metal Ion Analysis

The analysis of solutions to determine the Cu(II) concentration was required for two of the experimental stages in this project. During the electrochemical characterisation, the Cu(II) concentration in a known volume of HNO_3 was needed to determine the deposition efficiency of copper from the real waste solution. In subsequent experiments to establish the feasibility of copper recovery using an electrochemical reactor, the Cu(II) concentration was measured every hour to find the depletion and efficiency.

3.4.1 Review of Techniques

There are several families of techniques that could be used to analyse the concentration of copper ions in the nitrate solutions. These are spectrophotometry, chromatography and electrochemical methods.

In its simplest form, spectrophotometry involves relating the colour intensity of a solution to its concentration [3.27]. The measurement can be by visual standards or by a colorimeter, which measures the intensity of light of the complimentary colour to the solution, after it has passed through the sample. Atomic spectroscopy is a variation of this technique where the sample is vaporised, and electromagnetic radiation of characteristic wavelength, is passed through the sample [3.28]. The absorbance of this light is then measured; this is known as atomic absorption spectrometry (AAS). The disadvantage of this technique is that a source lamp is required for each element to be analysed [3.29]. Another variation of atomic spectroscopy is inductively coupled plasma (ICP) spectrometry. The sample is introduced into high temperature argon plasma which excites the atoms [3.29]. The radiation emitted is then recorded. The technique is widely used for the quantitative analysis of metals, especially at trace levels.

Chromatography separates substances by their differing migration rates through a stationary phase [3.29]. However, after they have been separated the concentrations of the components still have to be determined. In gas chromatography this is done by converting the substances into ions and measuring the current produced as they are attracted by charged plates. In high pressure liquid chromatography, which would be used for our metal ion determination, the concentration is found via the electrical conductivity of the solution at the exit of the ion exchange resin.

The electrochemical family of techniques involve measuring the potential or current generated between electrodes placed in the sample. The magnitude of the response is related to the concentration of the species in solution. There are a large variety of methods used, for example: voltammetry and ion selective electrodes [3.28]. The techniques are able to determine the concentration of several metals in a single sample, detect trace levels and require relatively inexpensive instrumentation [3.30]. In voltammetry a potential is applied across the sample and the current response measured. As electroactive species respond at characteristic potentials, and the magnitude of the current is proportional to the concentration of the ion in solution, the technique is both qualitative and quantitative [3.31]. Ion selective electrodes (ISE) are specific to a single ion, for example pH probes are specific to H^+. The potential is measured between two reference electrodes; one immersed in the solution of interest, the other in an internal reference solution, separated by a membrane [3.32]. This potential is proportional to the concentration of the specific ion in the solution.

A Cu ISE was chosen to measure the concentration of copper in HNO_3 as part of the anodic stripping experiments. The electrode could detect copper in the range required and the measurement could be made with minimal sample preparation. The concentration of copper also needed to be measured in the simulated stripping solution during the reactor recovery experiments. However, this solution contained Fe(III) which interferes with the Cu ISE [3.33]. Although reagents can be added to the stripping solution to overcome this problem, the concentrations were measured using an alternative analysis method. ICP was chosen as ferric ions do not interfere

with this method; however the samples had to be significantly diluted before the analysis.

3.4.2 Ion Selective Electrodes

An ion selective electrode system consists of two identical reference electrodes; one immersed in the solution to be analysed, the other in an internal reference solution. These two solutions are separated by a membrane. The cell for ion analysis is shown diagrammatically in Figure 3-11, in reality the membrane, internal reference solution and a reference electrode are all contained in a single probe.

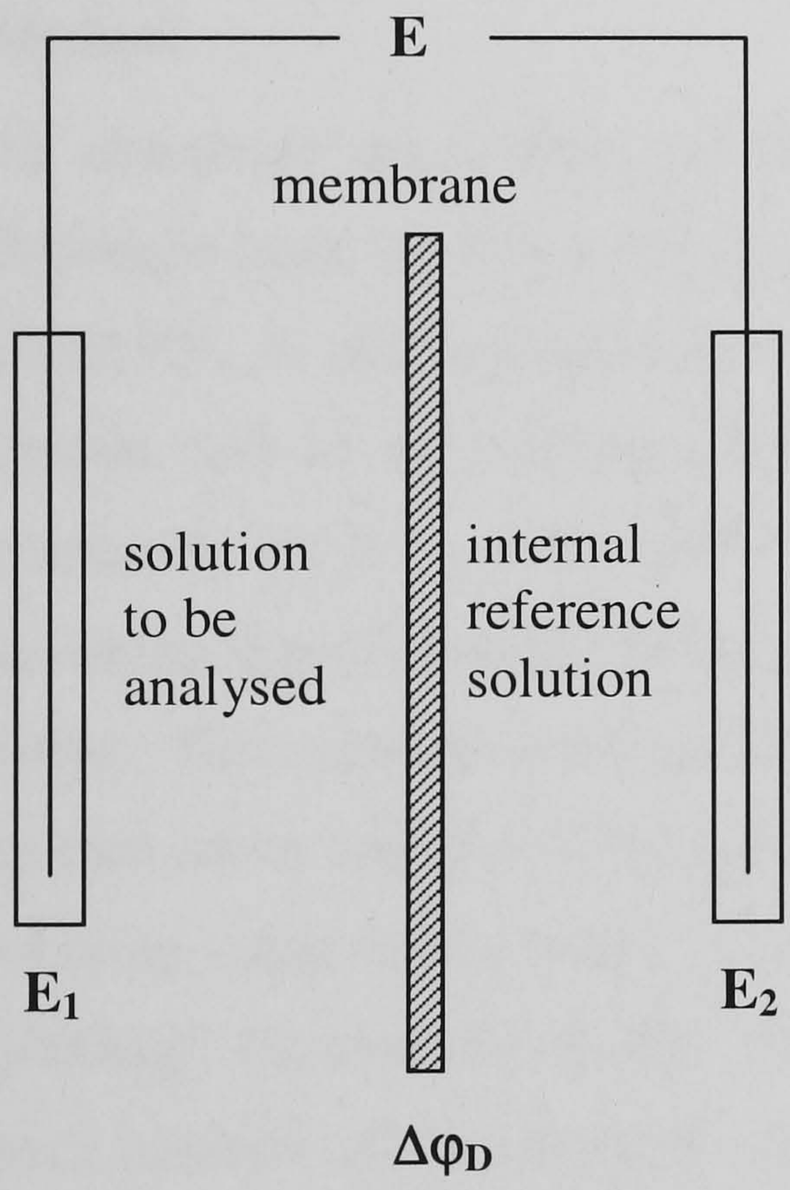

Figure 3-11 Diagram of an ISE

The membrane is only permeable to particular ions e.g. cations, therefore when the ISE is immersed in the solution of interest these ions selectively diffuse through the membrane due to the concentration gradient between the solutions. This diffusion causes a build up of charge on one side of the membrane, preventing further diffusion. The potential generated at this equilibrium is known as the Donnan potential $\Delta\varphi_D$ [3.34]. For the example illustrated above, the cell potential E can be expressed as:

$$E = E_2 + \Delta\varphi_D - E_1 \tag{3.12}$$

where E_1 and E_2 are the potentials of the reference electrodes. It can be assumed that the potential of these reference electrodes are constant and the Donnan potential can be expressed by the Nernst equation, with the internal reference concentration a constant. Therefore, for dilute solutions, the cell potential is a function of the concentration of the species of interest c [3.32], as shown in Eq. (3.13).

$$E = \text{constant} + \frac{RT}{nF}\ln(c) \tag{3.13}$$

Method

To determine the Cu(II) concentration in 0.5M HNO_3, after copper had been deposited from the real waste as part of the anodic stripping experiments, a Cu ISE (ISE25CU_9, Radiometer) was used in conjunction with an SCE. Initially, the system had to be calibrated using solutions of differing concentrations. The maximum Cu(II) concentration that could occur in the samples was calculated, assuming that the copper had been deposited at 100% current efficiency from the real waste. This calculation gave a calibration range of $10^{-4} - 10^{-5}$M. The calibration was carried out in 100ml of 0.5M HNO_3, neutralised with KOH so the pH was within the working range for the probe (3 to 7). Copper was then added incrementally from a 1000mg/l Cu standard (BDH). The potential of the system was then measured after each addition of Cu standard. A plot of *ln[Cu]* against the measured potential *E*, should produce a straight line. Figure 3-12 shows the calibration curve produced; the measured potentials closely approximate a straight line, so the calibration was thought to be acceptable.

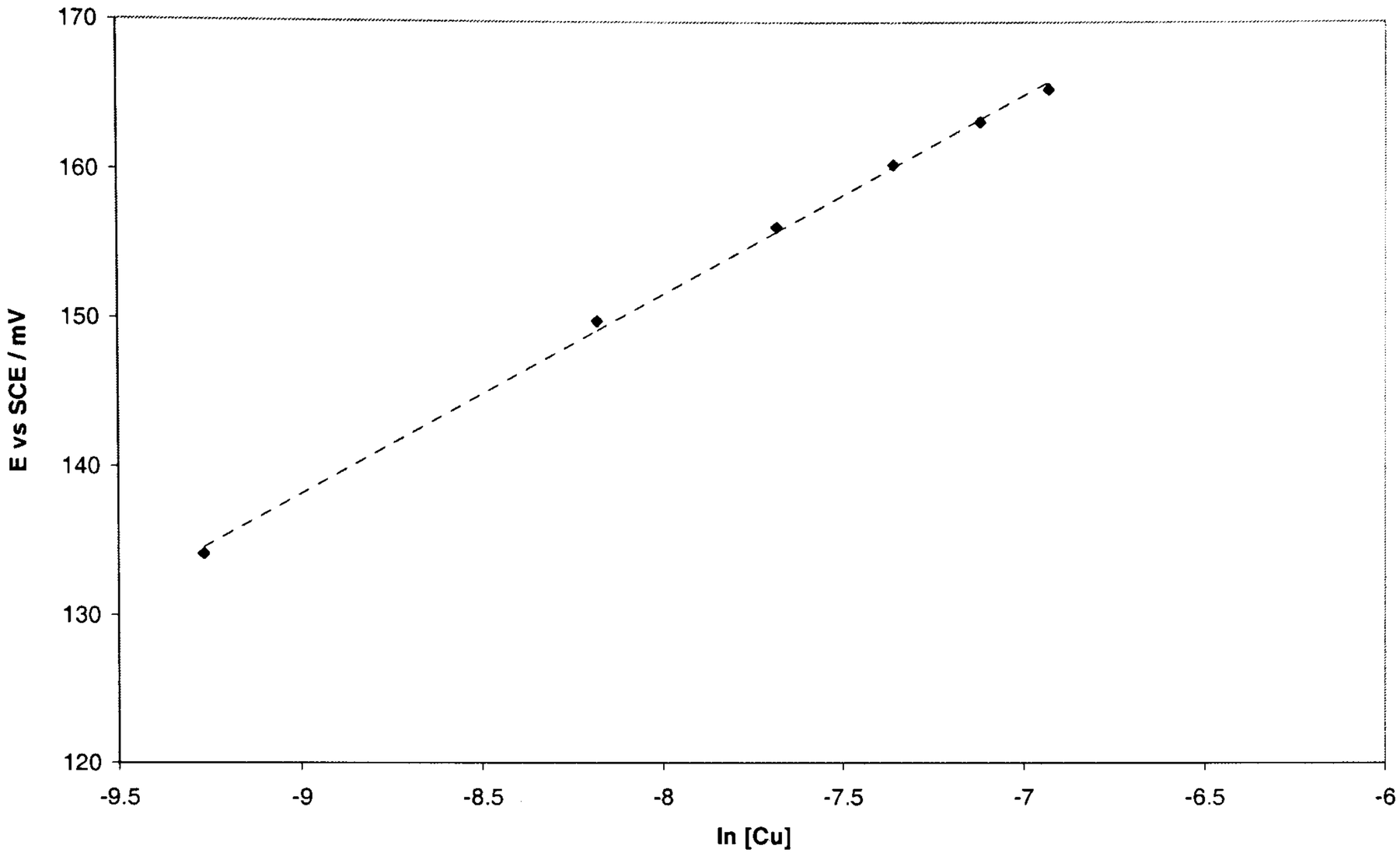

Figure 3-12 Calibration curve for Cu ISE in 0.5M HNO_3

The anodic stripping samples consisted of dissolved copper in 100ml of 0.5M HNO_3. To determine the copper concentration, only 50ml of this sample was used because the test is destructive. Initially KOH was added to adjust the pH to the optimum range for the Cu ISE. After about 10 minutes to allow for equilibration, the potential between the ISE and SCE was measured. The concentration of this test sample was then obtained from the calibration curve (Figure 3-12). This concentration was not the same as the original sample, because a volume of KOH had been added. However, the number of moles in the test solution, and therefore in the original sample, could be calculated.

3.4.3 ICP Spectrometry

Inductively coupled plasma – optical emission spectrometry is an analysis technique based on the emission of electromagnetic radiation by excited atoms [3.35]. The sample to be analysed is introduced into the ICP via a nebuliser to convert the liquid into an aerosol. This aerosol is then atomised, and the atoms excited by argon plasma at temperatures of up to 8000K. When excited, atoms emit electromagnetic radiation at characteristic wavelengths as they relax to their ground state. The radiation is separated (e.g. by diffraction gratings) and then detected. The radiation intensity is converted to a concentration by comparison with standards.

The copper concentration in the simulated waste samples from the reactor recovery experiments was measured by the Chemical Analysis Unit, Newcastle University, using a UNICAM 701 Series Emission Spectrometer. Three concentration measurements were made from each sample, which enabled the combined uncertainty, at 95% confidence interval, due to this measurement technique to be calculated. The maximum Cu(II) concentration that could be measured using ICP was 500ppm; 0.3M Cu(II) is equivalent to 18,900ppm. The samples were therefore diluted 100 times using 1M HNO_3 (Suprapur, Merck) made with deionised water (14MΩ).

3.5 References

3.1 C. Kerr, *Transactions of the Institute of Metal Finishing*, **82**(B7-B12, Part1-2): (2004)

3.2 O. Sohnel and J. Garside, *Precipitation: Basic Principles and Industrial Applications*, Butterworth Heinemann, (1992)

3.3 D. G. Stevenson, *Transactions of the Institute of Chemical Engineers*, **42**: T316 (1964)

3.4 J. W. Patterson, R. E. Bolce and D. Marani, *Environmental Science and Technology*, **25**(10): 1780-1787 (1991)

3.5 S. A. Hayes, P. Yu, T. J. O'Keefe, M. J. O'Keefe and J. O. Stoffer, *Journal of the Electrochemical Society*, **149**(12): C623-C630 (2002)

3.6 J. Dousma and P. L. De Bruyn, *Journal of Colloid and Interface Science*, **56**(3): 527-539 (1976)

3.7 J. Y. Choi and D. S. Kim, *Journal of Hazardous Materials*, **99**(2): 147-158 (2003)

3.8 A. Mecucci and K. Scott, *Journal of Chemical Technology and Biotechnology*, **77**(4): 449-457 (2002)

3.9 M. S. Lee, J. G. Ahn and J. W. Ahn, *Hydrometallurgy*, **70**(1-3): 23-29 (2003)

3.10 L. I. Antropov, M. I. Donchenko and T. I. Motronyuk, *Protection of Metals*, **20**(1): 27-32 (1984)

3.11 K. Scott, X. Chen, J. W. Atkinson, M. Todd and R. D. Armstrong, *Resources Conservation and Recycling*, **20**(1): 43-55 (1997)

3.12 R. D. Armstrong, M. Todd, J. W. Atkinson and K. Scott, *Journal of Applied Electrochemistry*, **27**(8): 965-969 (1997)

3.13 M. A. Diaz, G. H. Kelsall and N. J. Welham, *Journal of Electroanalytical Chemistry*, **361**: 25-38 (1993)

3.14 Southampton Electrochemistry Group, *Instrumental Methods in Electrochemistry*, Horwood Publishing, (2001)

3.15 T. Nedeltcheva, M. Atanassova, J. Dimitrov and L. Stanislavova, *Analytica Chimica Acta*, **528**: 143-146 (2005)

3.16 J. Horkans, H. C. I-Chia, P. C. Andriacacos and E. J. Podlaha, *Journal of the Electrochemical Society*, **138**(2): 411-416 (1991)

3.17 K. H. Wong and P. C. Andricacos, *Journal of the Electrochemical Society*, **137**(4): 1087-1090 (1990)

3.18 D. Pletcher and Z. Poorabedi, *Electrochimica Acta*, **24**: 1253-1256 (1979)

3.19 A. Mecucci, *Recycling of Waste Electronic Circuit Boards*, PhD Thesis, University of Newcastle upon Tyne (2006)

3.20 J. Newman and K. E. Thomas-Alyea, *Electrochemical Systems*, Wiley-Interscience, (2004)

3.21 R. S. Cooper and J. H. Bartlett, *Journal of the Electrochemical Society*, **105**(3): 109-116 (1958)

3.22 H. P. Lee and K. Nobe, *Journal of the Electrochemical Society*, **132**(5): 1031-1037 (1985)

3.23 R. Massey, Personal Communication, (2005) [e-mail, 27/04/05]

3.24 Atotech UK Ltd, Material Safety Data Sheet, *Tinsolv 2000* (1999)

3.25 S. Sobri, *Electrocrystallisation and recovery of gold from thiosulphate-sulphite aged electrolyte*, PhD Thesis, University of Newcastle upon Tyne (2006)

3.26 T. Rubcumintara and K. N. Han, *Metallurgical Transactions B*, **21B**: 429-438 (1990)

3.27 C. E. Housecroft and E. C. Constable, *Chemistry*, Pearson, (2006)

3.28 G. A. Ottewill, B. A. Plunkett and F. C. Walsh, *Transactions of the Institute of Metal Finishing*, **71**(4): 166-170 (1993)

3.29 F. W. Fifield and D. Kealey, *Principles and Practice of Analytical Chemistry*, Blackie Academic and Professional, (1995)

3.30 G. Sömer and U. Unal, *Talanta*, **62**: 323-328 (2004)

3.31 D. A. Skoog, F. J. Holler and T. A. Nieman, *Principles of Instrumental Analysis*, Harcourt Brace and Co., (1998)

3.32 D. Pletcher and F. C. Walsh, *Industrial Electrochemistry*, Chapman and Hall, (1990)

3.33 A. M. Bond, H. A. Hudson, P. A. van den Bosch, F. L. Walter and H. R. A. Exelby, *Analytical Chemistry*, **55**: 2071-2075 (1983)

3.34 J. Koryta, *Ion Selective Electrodes*, Cambridge University Press, (1975)

3.35 T. J. Manning and W. R. Grow, *The Chemical Educator*, **2**(1): (1997)

4 THERMODYNAMIC ANALYSIS

To ensure that the proposed recovery process (Section 1.5) is feasible, the preliminary stage in this work was to study the solution thermodynamics. Calculations have been performed to discover when the metals are in solution and what form they take at different values of pH and electrode potential. This information is then compared to the proposed unit operations. For example, if two metals are to be separated by filtration, one metal should be in solution, the other solid; these calculations tell us when/if this will occur. This theoretical analysis will be achieved by constructing Pourbaix diagrams [4.1], and utilising MINEQL+ [4.2] (chemical equilibrium modelling software) to produce speciation plots. The thermodynamic information can be used to determine:

- how much of the tin will exist as a precipitate after aeration; ideally no tin will remain in solution,
- whether the filtration can be used to separate tin and copper, and the conditions required,
- the distribution of the iron between the precipitated tin and dissolved copper,
- and the conditions for copper and tin electrowinning.

4.1 Pourbaix Diagrams

The spent tin stripping solution contains copper, tin and iron in nitric acid. The focus of the thermodynamic work is therefore on these three metals. For both copper and tin (the metals of interest), diagrams have been constructed for the metals in conjunction with water, aqueous chloride and aqueous nitrate solutions. The reason for the chloride solution being included is that the proposed recovery scheme (Section 1.5) involves the dissolution of tin in hydrochloric acid, and it is possible that some copper could be carried over into this stage. Diagrams have also been constructed for iron with water and in nitrate solutions; chlorides were not initially

included because there is a lower concentration of iron than copper, so significant amounts are unlikely to be carried into the tin stage.

There are several assumptions inherent in the construction of these diagrams:

- The temperature is 298K, which is within the operating range of 25-35°C for the stripping process and also standard room temperature, so the assumption is valid whether the waste is processed immediately or left.
- The most stable solids have been considered, whilst transient species ignored.
- Species for which there is no thermodynamic information have not been included.
- The chemical potential for a solid is constant. The actual value is dependent on the perfection of the crystal lattice [4.3].
- No metal/metal compounds are formed between copper, iron and tin.

4.1.1 Copper

Copper is etched from the surface of the circuit board along with the tin during the stripping process using a nitric acid solution. This was calculated to contain 1M HNO_3 (Appendix A). During the filtration stage, it is possible that some copper could be carried over into the tin electrodeposition stage where it would be dissolved into HCl.

The diagram for the copper-water system was used as a sample calculation and can be found in Section 2.1.2.

Copper-Nitrate-Water

The spent stripping solution is predominantly aqueous nitric acid, with a concentration of approximately 1M. Initially the tin would be removed from the waste by filtration, therefore copper must be dissolved or it will contaminate the tin precipitate. After the filtration stage it is proposed to electrowin copper directly from

the nitrate solution. It is therefore important to know how the nitrate ions change the copper speciation so that the conditions for filtration and electrowinning can be determined.

The substances considered, in addition to those in the copper-water plot, are show in Table 4-1 along with their thermodynamic information. Also contained in this table are more recent values for the Gibbs free energy for the copper species than were used by Pourbaix [4.4].

Aqueous		**Solid**	
	ΔG^O / kJ mol^{-1}		ΔG^O / kJ mol^{-1}
$CuNO_3^+$	-48.5 [4.5]	**$Cu(NO_3)_{2\,(s)}$**	-109
$Cu(NO_3)_{2\,(aq)}$	-154.6 [4.5]	**Cu_2O**	-148.1
NO_3^-	-111.3	**CuO**	-134
Cu^+	50.3	H_2O	-237.178
Cu^{2+}	65.7		
$HCuO_2^-$	-258.9		
CuO_2^{2-}	-183.9		

Table 4-1 Thermodynamic data for copper-nitrate substances (all data *Bard* [4.6], unless specified)

The diagram was constructed by the same method that was described in Chapter 2. The reactions that were found to be relevant are shown in Table 4-2.

Electrochemical	**Chemical**
Dissolved	
$Cu^+ + NO_3^- \rightarrow CuNO_3^+ + e^-$	$HCuO_2^- + NO_3^- + 3H^+ \rightarrow CuNO_3^+ + 2H_2O$
$Cu^+ + 2H_2O \rightarrow HCuO_2^- + 3H^+ + e^-$	$HCuO_2^- \rightarrow CuO_2^{2-} + H^+$
$Cu^+ + 2H_2O \rightarrow CuO_2^{2-} + 4H^+ + e^-$	
Solid	
$2Cu + H_2O \rightarrow Cu_2O + 2H^+ + 2e^-$	
$Cu_2O + H_2O \rightarrow 2CuO + 2H^+ + 2e^-$	

Solid / Dissolved	
$Cu_2O + 3H_2O \rightarrow 2CuO_2^{2-} + 6H^+ + 2e^-$	$CuO_2^{2-} + 2H^+ \rightarrow CuO + H_2O$
$Cu + 2H_2O \rightarrow CuO_2^{2-} + 4H^+ + 2e^-$	$CuO + NO_3^- + 2H^+ \rightarrow CuNO_3^+ + H_2O$
$Cu_2O + 2NO_3^- + 2H^+ \rightarrow 2CuNO_3^+ + H_2O + 2e^-$	
$Cu + NO_3^- \rightarrow CuNO_3^+ + 2e^-$	

Table 4-2 Reactions represented in the copper-nitrate-water Pourbaix plot

The completed Pourbaix diagram is shown in Figure 4-1, where it can be seen that the region that was occupied by the Cu^{2+} ion in the copper-water plot has been replaced by the $CuNO_3^+$ ion. The deposition potential does not change significantly compared to the non-complexing case; to remove copper to an activity of 10^{-6}, a potential of 0.15V, compared to 0.16V for copper-water, is required. However, the region of pH where copper is in solution is smaller, with the precipitation of a solution with copper activity 1 occurring at pH 3.54, compared to 3.95 without the nitrate.

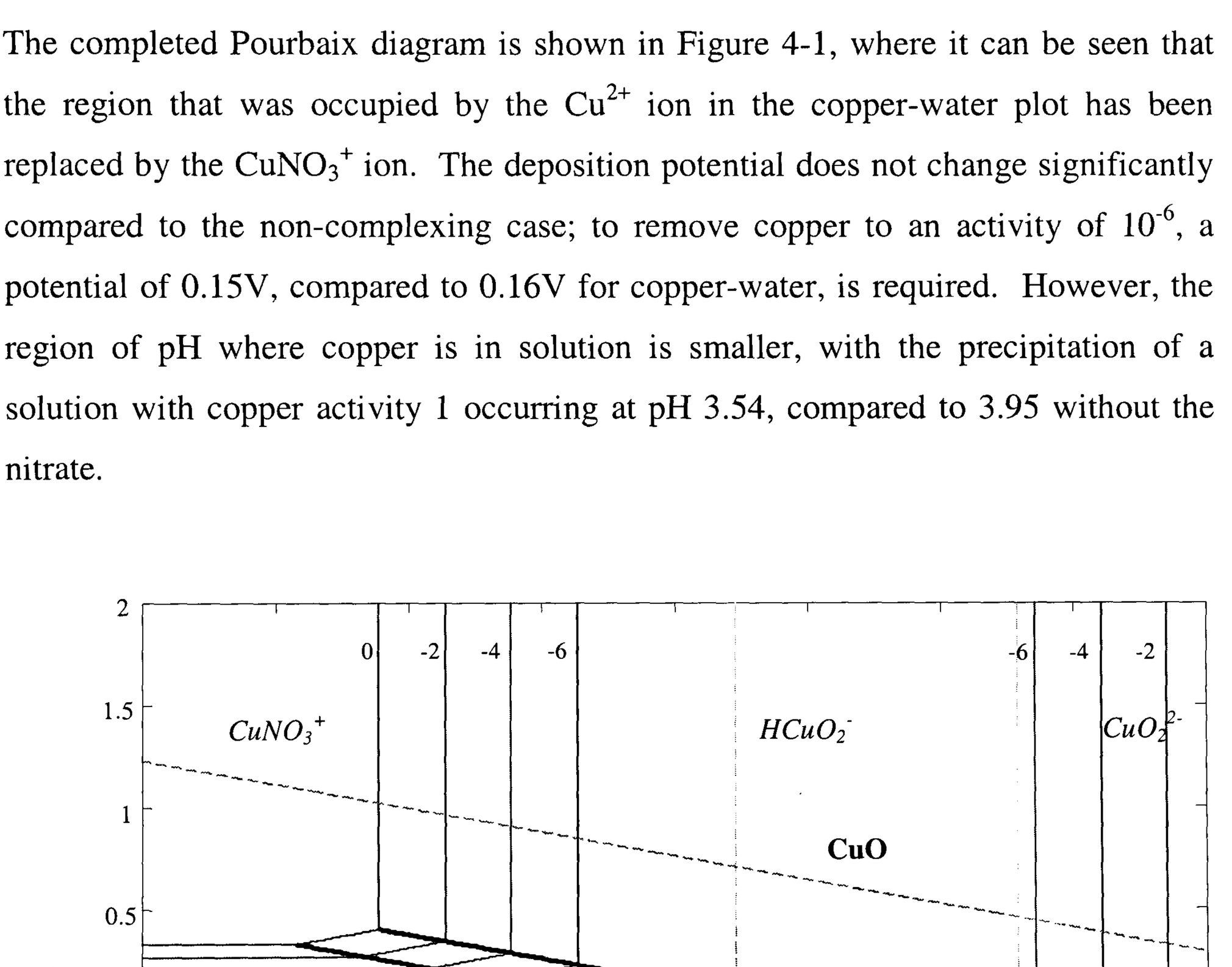

Figure 4-1 Pourbaix diagram for copper-nitrate-water system (298K, a_{NO3} =1)

The stripping solution contains 0.3M copper [4.7], if it is assumed that the concentration and activity are equivalent, it can be estimated from the $CuNO_3^+/CuO$ equilibrium that all the copper will be in solution if the pH is less than 3.8. To separate the copper and tin, the tin must exist as a solid in this region. The Pourbaix plot also shows that 0.3M Cu(II) will start to be deposited at +0.31V.

Copper–Chloride-Water

The recovery method proposed by *Kerr* [4.8], includes a stage where tin(IV) oxide is filtered from the stripping solution. This may then be dissolved in HCl to recover the tin by electrowinning. If any copper is carried over in the residue it will enter the tin electrowinning stage; it is therefore interesting to know the behaviour of copper in these solutions. The actual chloride concentration that would be required is unknown, so a value of 0.1M was chosen to gauge the effect.

The species that were considered, in addition to those from the copper-water plot are shown in Table 4-3, along with their Gibbs free energies.

Aqueous		**Solid**	
	ΔG^O / kJ mol^{-1}		ΔG^O / kJ mol^{-1}
Cl^-	-131.0563	**CuCl**	-119.8
$CuCl_2^-$	-240.5	**$CuCl_2$**	-173.9
$CuCl^+$	-68.2 [4.5]	**$Cu_2(OH)_3Cl$**	-669.83 [4.9]

Table 4-3 Thermodynamic data for copper-chloride substances (data from *Bard* [4.6], unless specified)

This plot was constructed by the method described for the copper-water diagram. The reactions that were used in the construction are shown in Table 4-4.

Electrochemical	Chemical
Dissolved	
$Cu^{2+} + 2Cl^- + e^- \rightarrow CuCl_2^-$	$Cu^{2+} + 2H_2O \rightarrow HCuO_2^- + 3H^+$
$HCuO_2^- + 2Cl^- + 3H^+ + e^- \rightarrow CuCl_2^- + 2H_2O$	$HCuO_2^- \rightarrow CuO_2^{2-} + H^+$
$CuO_2^{2-} + 2Cl^- + 4H^+ + e^- \rightarrow CuCl_2^- + 2H_2O$	
Solid	
$2Cu + H_2O \rightarrow Cu_2O + 2H^+ + 2e^-$	$2CuO + Cl^- + H_2O + H^+ \rightarrow Cu_2(OH)_3Cl$
$Cu_2O + H_2O \rightarrow 2CuO + 2H^+ + 2e^-$	
$Cu + Cl^- \rightarrow CuCl + e^-$	
$Cu_2O + 2Cl^- + 2H^+ \rightarrow 2CuCl + H_2O$	
$Cu_2O + Cl^- + 2H_2O \rightarrow Cu_2(OH)_3Cl + H^+ + 2e^-$	
$2CuCl + 3H_2O \rightarrow Cu_2(OH)_3Cl + Cl^- + 3H^+ + 2e^-$	
Solid / Dissolved	
$CuCl \rightarrow Cu^{2+} + Cl^- + e^-$	$Cu_2(OH)_3Cl + 3H^+ \rightarrow 2Cu^{2+} + Cl^- + 3H_2O$
$Cu_2O + 3H_2O \rightarrow 2HCuO_2^- + 4H^+ + 2e^-$	$HCuO_2^- + H^+ \rightarrow CuO + H_2O$
$Cu_2O + 3H_2O \rightarrow 2CuO_2^{2-} + 6H^+ + 2e^-$	$CuO_2^{2-} + 2H^+ \rightarrow CuO + H_2O$
$Cu + 2H_2O \rightarrow CuO_2^{2-} + 4H^+ + 2e^-$	$Cu_2O + 4Cl^- + 2H^+ \rightarrow 2CuCl_2^- + H_2O$
$Cu_2(OH)_3Cl + 3Cl^- + 3H^+ + 2e^- \rightarrow 2CuCl_2^- + 3H_2O$	
$CuO + 2Cl^- + 2H^+ + e^- \rightarrow CuCl_2^- + H_2O$	
$Cu + 2Cl^- \rightarrow CuCl_2^- + e^-$	

Table 4-4 Reactions represented in the copper-chloride-water Pourbaix diagram

The completed Pourbaix diagram is shown in Figure 4-2.

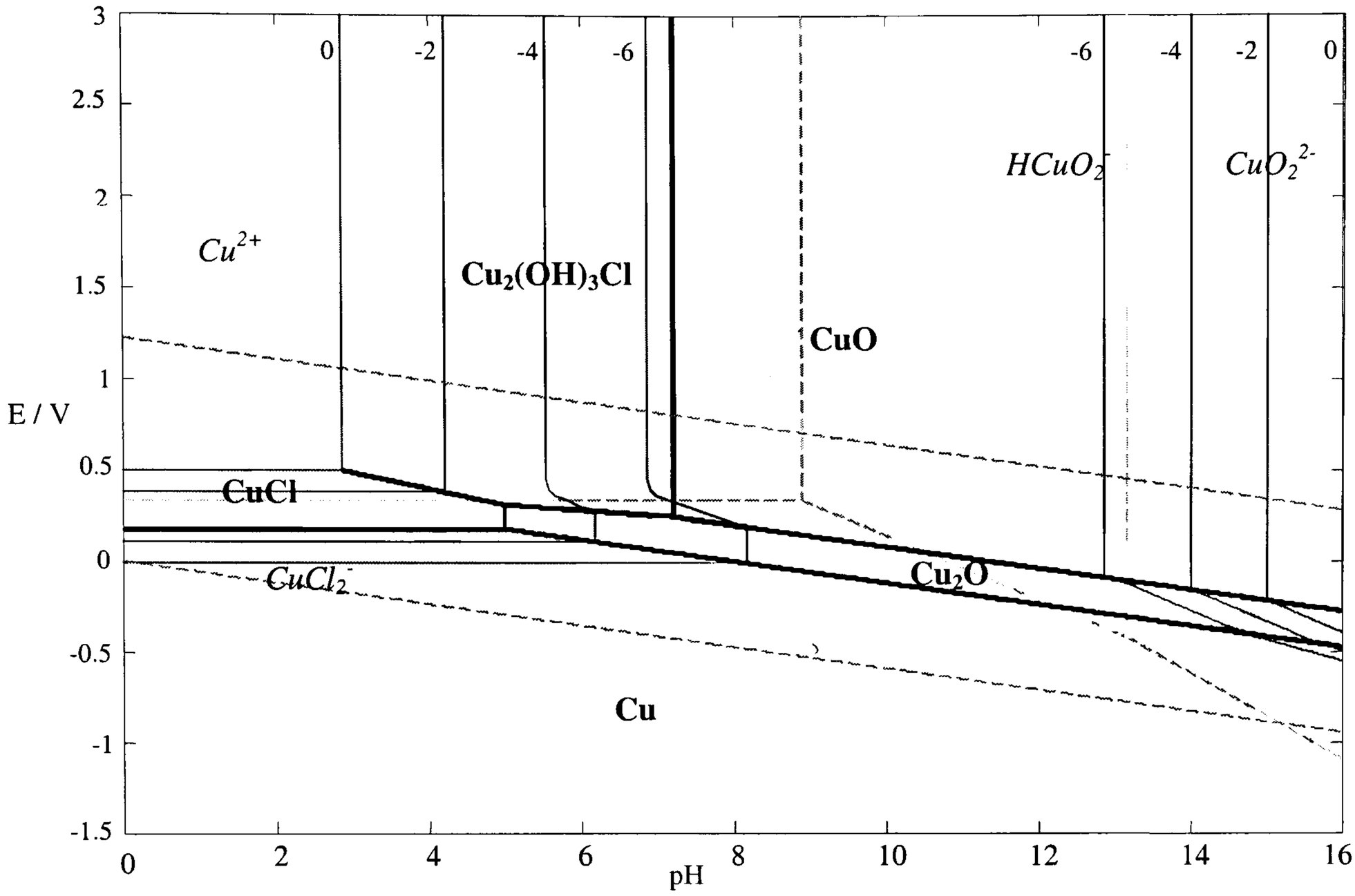

Figure 4-2 Pourbaix diagram for copper-chloride-water system (298K, a_{Cl}=0.1)

It is found that the addition of chloride ions affects the low pH region of the diagram. The main changes are that the $CuCl_2^-$ ion is more stable than the Cu^+ ion and replaces it in the plot, and there are extra solid substances. The implications of these changes are that the region where the copper is dissolved has been decreased, so precipitation will happen at lower values of pH than with non-complexants; for a_{Cu}=1 precipitation occurs at a pH of 2.86 for copper/chloride as opposed to 3.95 in the copper-water system. It could be inferred from the equilibrium condition of the Cu^{2+} / $Cu_2(OH)_3Cl$ reaction (Eq. 4.1) that the precipitation pH would continue to decrease as the chloride ion concentration is increased. However, by the time the chloride activity has reached 1, Cu^{2+} is no longer the predominant ion in that region, but is replaced by $CuCl^+$ and the effect is mitigated [4.1].

$$2 \cdot \log\left(a_{Cu^{2+}}\right) = 7.58 - \log\left(a_{Cl^-}\right) - 3pH \tag{4.1}$$

The change of predominant ion ($CuCl_2^-$) in the deposition region (i.e. dissolved ion/metal boundary) has the consequence that the potential required for deposition

will need to be decreased from the copper-water case. The copper-water Pourbaix diagram (Figure 2-3) shows that copper of activity 10^{-6} will be deposited at +0.16V, however looking at this potential on the copper-chloride diagram (Figure 4-2) the line that represents an activity of 10^{-6} $CuCl_2^-$ is more negative (-0.012V). Thus to remove all the copper from a chloride solution, a more negative potential is required than for the non-complexing case.

4.1.2 Tin

The spent stripping solution will contain tin as a precipitate of tin(IV) oxide. For effective separation from the copper containing solution, it is important to know the conditions that prevent tin existing in solution. Thermodynamic calculations will also be required to provide details of tin behaviour in chloride solutions; the media proposed for its deposition.

Tin-Water

The tin-water Pourbaix diagram will be constructed to provide a basis against which to compare the effect of the anions. The species that were considered and the relevant thermodynamic data are shown in Table 4-5.

Aqueous		**Solid**	
	ΔG^O / kJ mol^{-1}		ΔG^O / kJ mol^{-1}
Sn^{4+}	2.72	**Sn**	0
Sn^{2+}	-26.27	**SnO**	-258
SnO_3^{2-}	-575.4	**SnO_2**	-515.8
$HSnO_2^-$	-410		
Other			
H_2O	-237.35	$SnH_{4\,(g)}$	415

Table 4-5 Thermodynamic data for tin-water substances (data from *Pourbaix* [4.4])

The tin hydroxides were not considered, as they are less stable than the oxides [4.4]. The pertinent reactions are shown in Table 4-6.

Electrochemical	Chemical
Dissolved	
$Sn^{2+} \rightarrow Sn^{4+} + 2e^-$	$Sn^{4+} + 3H_2O \rightarrow SnO_3^{2-} + 6H^+$
$Sn^{2+} + 3H_2O \rightarrow SnO_3^{2-} + 6H^+ + 2e^-$	$Sn^{2+} + 2H_2O \rightarrow HSnO_2^- + 3H^+$
$HSnO_2^- + H_2O \rightarrow SnO_3^{2-} + 3H^+ + 2e^-$	
Solid	
$Sn + 2H_2O \rightarrow SnO_2 + 4H^+ + 4e^-$	
Solid / Dissolved	
$Sn \rightarrow Sn^{2+} + 2e^-$	$Sn^{4+} + 2H_2O \rightarrow SnO_2 + 4H^+$
$Sn + 2H_2O \rightarrow HSnO_2^- + 3H^+ + 2e^-$	$SnO_3^{2-} + 2H^+ \rightarrow SnO_2 + H_2O$
$Sn^{2+} + 2H_2O \rightarrow SnO_2 + 4H^+ + 2e^-$	
$HSnO_2^- \rightarrow SnO_2 + H^+ + 2e^-$	
Gas / Solid	
$SnH_4 \rightarrow Sn + 4H^+ + 4e^-$	

Table 4-6 Reactions represented in the tin-water Pourbaix diagram

The Pourbaix diagram for tin-water (Figure 4-3) shows that in the acidic region, tin only exists as a dissolved species across a small range of potentials at around 0V, or if the pH is less than -0.42. Tin also exists as a dissolved species in very alkaline conditions if pH is greater than 12.6. This diagram is valid for tin in the absence of substances with which it forms soluble complexes or insoluble compounds.

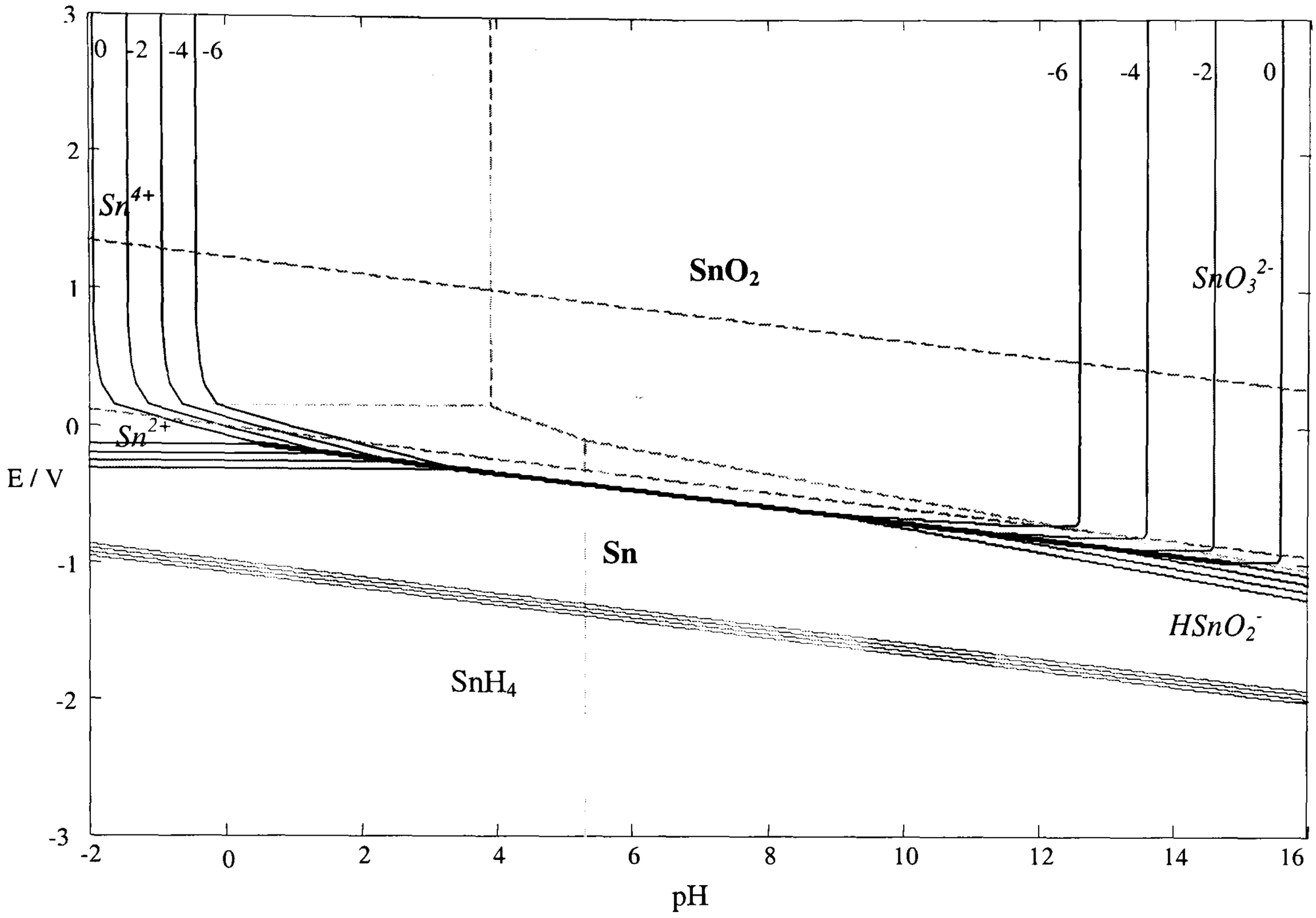

Figure 4-3 Pourbaix diagram for tin-water (298K)

Tin-Chloride-Water

It is proposed to dissolve tin in hydrochloric acid in order to recover it by electrowinning. Therefore the potential at which the deposition occurs and the regions where the tin is in solution need to be quantified. Initially the Pourbaix plot was constructed with a chloride concentration of 0.1M, as for the copper.

The species that were considered and their Gibbs free energies are shown in Table 4-7, which also contains more up to date values for the tin-water compounds (the tin-water diagram was not modified, as the effect was found to be insignificant).

Aqueous		Solid	
	ΔG^O / kJ mol^{-1}		ΔG^O / kJ mol^{-1}
Sn^{4+}	2.72	**SnO**	-257
Sn^{2+}	-27.24	**SnO_2**	-519.9
SnO_3^{2-}	-574.965	**$SnCl_2$**	-302.1
$HSnO_2^-$	-410.0	**$Sn(OH)Cl.H_2O$**	-648.35 [4.10]
$SnCl_6^{2-}$	-795.99 [4.11]	**Other**	
$SnCl_4^{2-}$	-560.89 [4.11]	H_2O	-237.178
$SnCl^+$	-167.9	Cl^-	-131.0563
$SnCl_3^-$	-431.82 [4.5]	$SnH_{4\,(g)}$	414

Table 4-7 Thermodynamic data for tin-chloride substances (all data *Bard* [4.6], unless specified)

The applicable reactions are summarised in Table 4-8.

Electrochemical	Chemical
Dissolved	
$SnCl^+ \rightarrow Sn^{4+} + Cl^- + 2e^-$	$SnCl^+ + 2H_2O \rightarrow HSnO_2^- + Cl^- + 3H^+$
$SnCl^+ + 3H_2O \rightarrow SnO_3^{2-} + Cl^- + 6H^+ + 2e^-$	$Sn^{4+} + 3H_2O \rightarrow SnO_3^{2-} + 6H^+$
$HSnO_2^- + H_2O \rightarrow SnO_3^{2-} + 3H^+ + 2e^-$	
Solid	
$Sn + 2H_2O \rightarrow SnO_2 + 4H^+ + 4e^-$	
Solid / Dissolved	
$SnCl^+ + 2H_2O \rightarrow SnO_2 + Cl^- + 4H^+ + 2e^-$	$Sn^{4+} + 2H_2O \rightarrow SnO_2 + 4H^+$
$Sn + Cl^- \rightarrow SnCl^+ + 2e^-$	$SnO_3^{2-} + 2H^+ \rightarrow SnO_2 + H_2O$
$Sn + 2H_2O \rightarrow HSnO_2^- + 3H^+ + 2e^-$	
$HSnO_2^- \rightarrow SnO_2 + H^+ + 2e^-$	
Gas / Solid	
$SnH_4 \rightarrow Sn + 4H^+ + 4e^-$	

Table 4-8 Reactions represented in the tin-chloride-water Pourbaix diagram

The tin-chloride-water Pourbaix diagram (Figure 4-4) shows that the addition of 0.1M chloride ions has little effect on the tin solubility. The $SnCl^+$ ion is more predominant than the Sn^{2+} ion, resulting in a change in the dissolved species region, but the effect this has on the deposition potential is marginal – the potential for a solution of $SnCl^+$ (activity equal to 10^{-6}) in equilibrium with tin is -0.339V, whereas with a solution of Sn^{2+} the potential is -0.314V. It should be noted that the deposition potential for the tin is below the hydrogen stability line (B), so hydrogen evolution is possible.

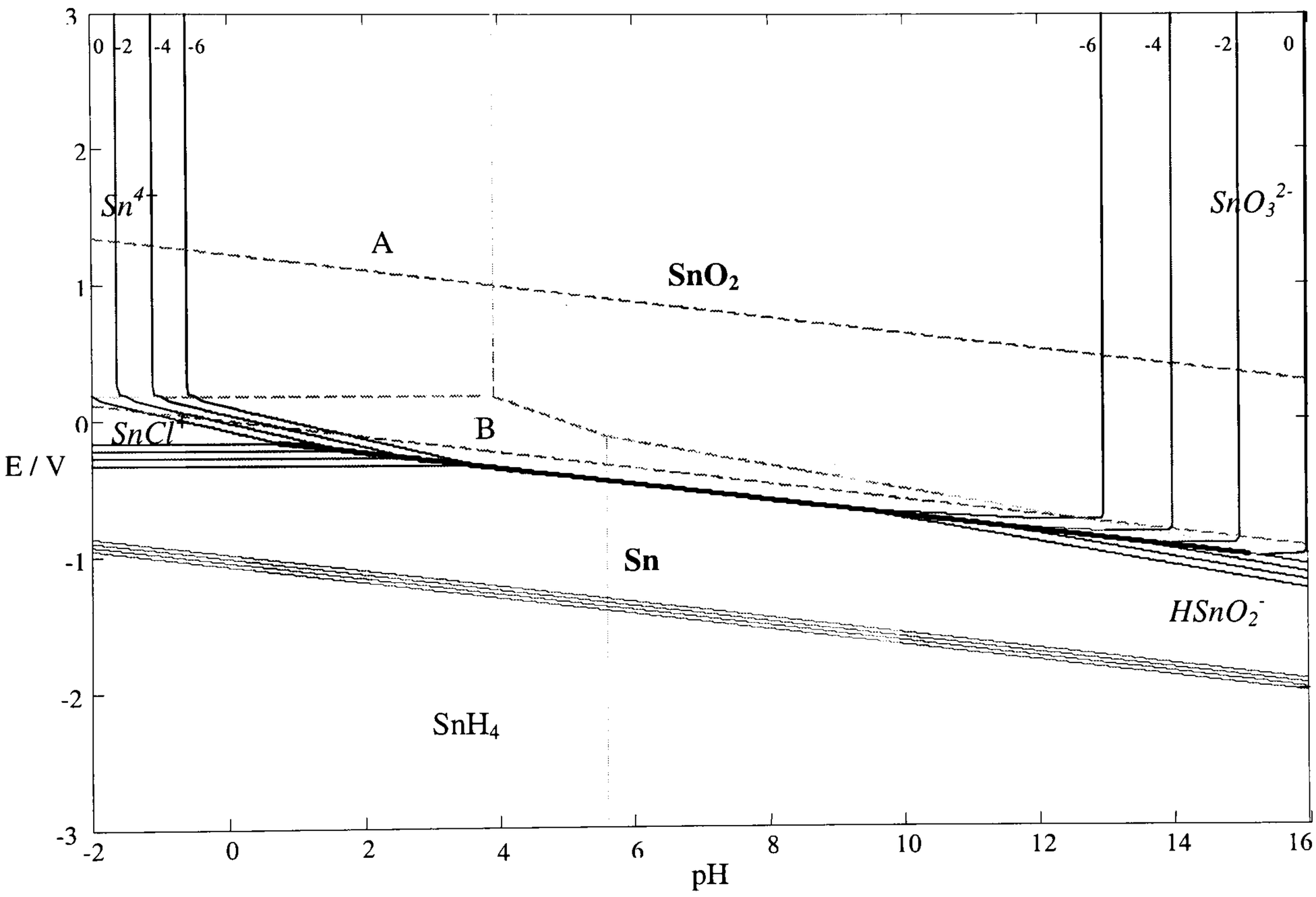

Figure 4-4 Pourbaix diagram for tin-chloride-water (298K, a_{Cl}=0.1)

It has been suggested in the literature that tin can be dissolved if the HCl is concentrated [4.12, 4.13] or the temperature is elevated [4.4.12, 14]. To verify this, another Pourbaix plot was constructed with the activity of chloride ions set equal to 5. The result can be seen in Figure 4-5.

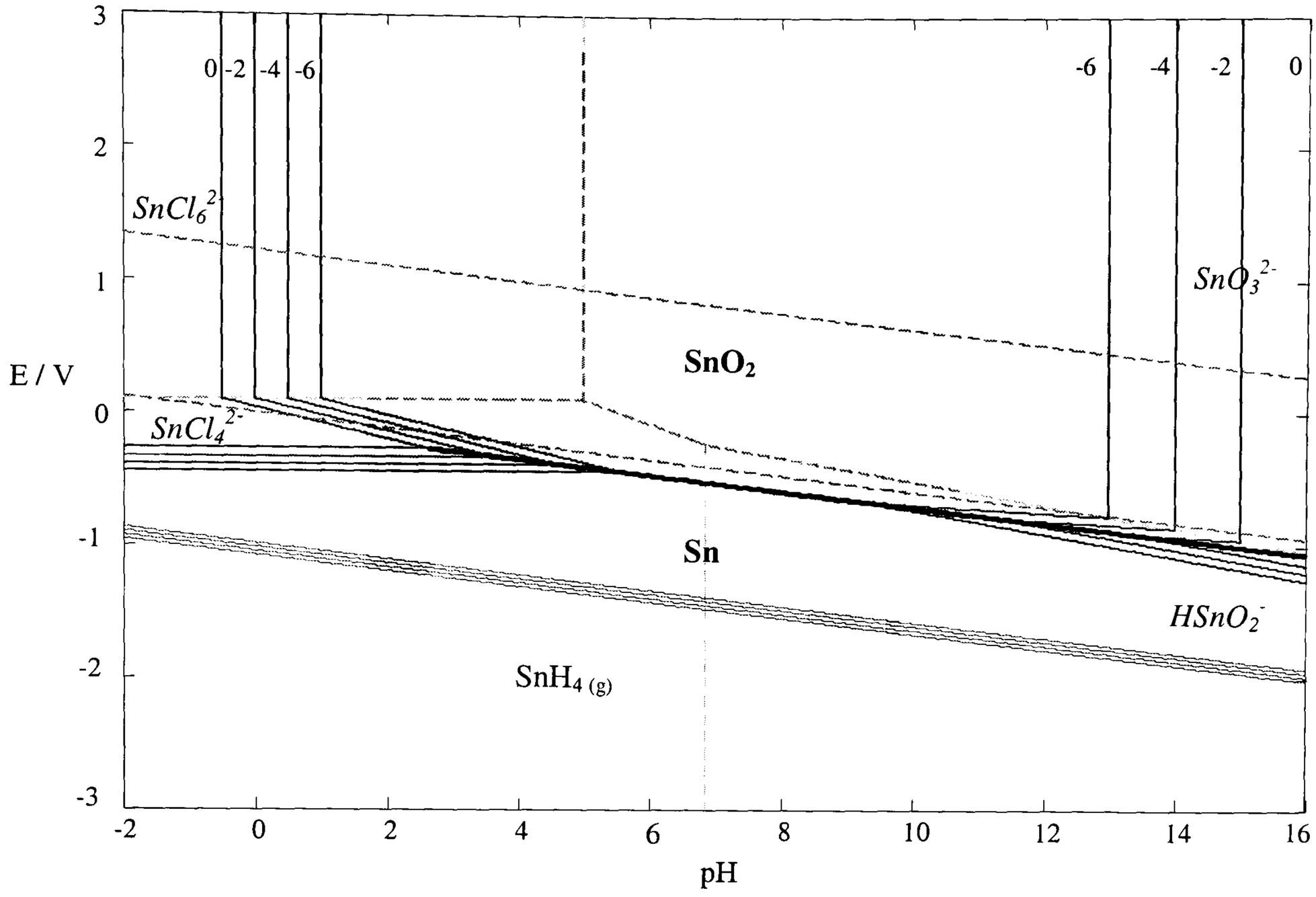

Figure 4-5 Pourbaix diagram for tin-chloride-water (298K, a_{Cl}=5)

The region where tin exists as a dissolved species has increased in size, with tin existing as a dissolved species at pH less than 0.98. The predominant ions have also altered again; Sn^{4+} ions have been replaced by $SnCl_6^{2-}$, and the $SnCl^+$ ions with $SnCl_4^{2-}$. The potential at which a solution of tin ions of activity 10^{-6} are in equilibrium with tin has decreased to -0.45V compared with -0.34V for a solution containing chloride ions with an activity of 0.1.

Tin-Nitrate-Water

In the proposed recovery scheme all the tin should be removed from the spent stripping solution via a filtration stage after acid recovery. For this to be effective, all the tin must exist as a precipitate or it may contaminate the copper electrowinning stage (or at least restrict the deposition potential). The tin-nitrate-water Pourbaix plot will show whether any of the tin is liable to be in solution and the conditions required to ensure there is not.

The species that was considered, in addition to those in the tin-water plot, was $SnNO_3^+$, which was calculated to have a Gibbs free energy of -103.74kJ/mol [4.2]. For $SnNO_3^+$ to affect the diagram, it must appear on the predominance area plot. The reactions of the dissolved species and their equilibrium conditions are shown in Table 4-9.

Dissolved Reaction	Equilibrium Condition
$SnNO_3^+ \rightarrow Sn^{2+} + NO_3^-$	No dependence on pH or electrode potential, so does not appear on diagram.
$SnNO_3^+ \rightarrow Sn^{4+} + NO_3^- + 2e^-$	$E = -0.0251 + 0.0296 \cdot \log a_{NO_3^-} + 0.0591 \cdot \log\left(\frac{a_{Sn^{4+}}}{a_{SnNO_3^+}}\right)$
$SnNO_3^+ + 3H_2O \rightarrow SnO_3^{2-} + NO_3^- + 6H^+ + 2e^-$	$E = 0.669 + 0.296\log a_{NO_3^-} - 0.1773pH + 0.0296\log\left(\frac{a_{SnO_3^{2-}}}{a_{SnNO_3^+}}\right)$
$SnNO_3^+ + 2H_2O \rightarrow HSnO_2^- + NO_3^- + 3H^+$	$\log\left(\frac{a_{SnNO_3^+}}{a_{HSnO_2^-}}\right) = 9.954 + \log a_{NO_3^-} - 3pH$
$Sn^{2+} \rightarrow Sn^{4+} + 2e^-$	$E = -0.155 + 0.0296 \log\left(\frac{a_{Sn^{4+}}}{a_{Sn^{2+}}}\right)$
$Sn^{2+} + 2H_2O \rightarrow HSnO_2^- + 3H^+$	$\log\left(\frac{a_{Sn^{2+}}}{a_{HSnO_2^-}}\right) = 10.80 - 3pH$

Table 4-9 Reactions between dissolved substances for tin-nitrate-water

Considering the data, for the $SnNO_3^+$ ion to change the diagram it would have to displace the Sn^{2+} ion. This would happen when the equilibrium potential between the $SnNO_3^+/Sn^{4+}$ couple is more positive than that between the Sn^{2+}/Sn^{4+} couple, which is calculated to occur at a nitrate activity of $\sim 10^6$. This is not feasible; therefore nitrate ions will not have an effect on the tin-water equilibrium.

4.1.3 Iron

Iron exists in the tin stripping solution to provide extra oxidising power to remove the copper/tin intermetallic from the circuit board. To minimise the number of separations required, all the iron should stay in solution and pass through the filtration step with the copper, or it should all precipitate and be removed with the

tin. A Pourbaix diagram of the iron-water-nitrate system was therefore constructed to find the distribution of the iron between these two streams.

Iron-Water

The basic iron-water Pourbaix diagram will be constructed to provide a basis against which to compare the effect of the nitrate ions. The substances considered and the required thermodynamic data are shown in Table 4-10.

Aqueous		**Solid**	
	ΔG^O / kJ mol^{-1}		ΔG^O / kJ mol^{-1}
Fe^{2+}	-78.87	**Fe**	0
Fe^{3+}	-4.6	**Fe_2O_3**	-742.2
$FeOH^{+}$	-277.4	**Fe_3O_4**	-1015.5
$FeOH^{2+}$	-229.41	**$Fe(OH)_{2\ (s)}$**	-486.6
$Fe(OH)_{2\ (aq)}$	-441.0	**$Fe(OH)_{3\ (s)}$**	-696.6
$Fe(OH)_2^{+}$	-438.1		
$Fe(OH)_{3\ (aq)}$	-659.4		
$Fe(OH)_3^{-}$	-615.0	**Other**	
$Fe(OH)_4^{-}$	-842.2	H_2O	-237.178
$Fe(OH)_4^{2-}$	-769.9		

Table 4-10 Thermodynamic data for iron-water substances (data from *Bard* [4.6])

The pertinent reactions are shown in Table 4-11.

Electrochemical	**Chemical**
Dissolved	
$Fe^{2+} \rightarrow Fe^{3+} + e^{-}$	$Fe^{2+} + H_2O \rightarrow FeOH^{+} + H^{+}$
$Fe^{2+} + H_2O \rightarrow FeOH^{2+} + H^{+} + e^{-}$	$Fe^{3+} + H_2O \rightarrow FeOH^{2+} + H^{+}$
$Fe^{2+} + 3H_2O \rightarrow Fe(OH)_{3(aq)} + 3H^{+} + e^{-}$	$FeOH^{2+} + 2H_2O \rightarrow Fe(OH)_{3(aq)} + 2H^{+}$
$FeOH^{+} + 2H_2O \rightarrow Fe(OH)_{3(aq)} + 2H^{+} + e^{-}$	$Fe(OH)_4^{-} + H^{+} \rightarrow Fe(OH)_{3(aq)} + H_2O$
$FeOH^{+} + 3H_2O \rightarrow Fe(OH)_4^{-} + 3H^{+} + e^{-}$	$FeOH^{+} + 2H_2O \rightarrow Fe(OH)_3^{-} + 2H^{+}$

$Fe(OH)_3^- + H_2O \rightarrow Fe(OH)_4^- + H^+ + e^-$	$Fe(OH)_3^- + H_2O \rightarrow Fe(OH)_4^{2-} + H^+$
$Fe(OH)_4^{2-} \rightarrow Fe(OH)_4^- + e^-$	
Solid	
$3Fe + 4H_2O \rightarrow Fe_3O_4 + 8H^+ + 8e^-$	
$2Fe_3O_4 + H_2O \rightarrow 3Fe_2O_3 + 2H^+ + 2e^-$	
Solid / Dissolved	
$2Fe^{2+} + 3H_2O \rightarrow Fe_2O_3 + 6H^+ + 2e^-$	$2Fe^{3+} + 3H_2O \rightarrow Fe_2O_3 + 6H^+$
$3Fe^{2+} + 4H_2O \rightarrow Fe_3O_4 + 8H^+ + 2e^-$	$2Fe(OH)_4^- + 2H^+ \rightarrow Fe_2O_3 + 5H_2O$
$3FeOH^+ + H_2O \rightarrow Fe_3O_4 + 5H^+ + 2e^-$	
$Fe + H_2O \rightarrow FeOH^+ + H^+ + 2e^-$	
$Fe \rightarrow Fe^{2+} + 2e^-$	
$Fe_3O_4 + 8H_2O \rightarrow 3Fe(OH)_4^- + 4H^+ + e^-$	
$3Fe(OH)_4^{2-} + 4H^+ \rightarrow Fe_3O_4 + 8H_2O + 2e^-$	
$3Fe(OH)_3^- + H^+ \rightarrow Fe_3O_4 + 5H_2O + 2e^-$	
$Fe + 3H_2O \rightarrow Fe(OH)_3^- + 3H^+ + 2e^-$	
$Fe + 4H_2O \rightarrow Fe(OH)_4^{2-} + 4H^+ + 2e^-$	

Table 4-11 Reactions represented in the iron-water Pourbaix diagram

The Pourbaix diagram (Figure 4-6) shows that iron exists as a dissolved species at low pH; this dissolved region extends to almost neutral conditions depending on the potential of the whole system.

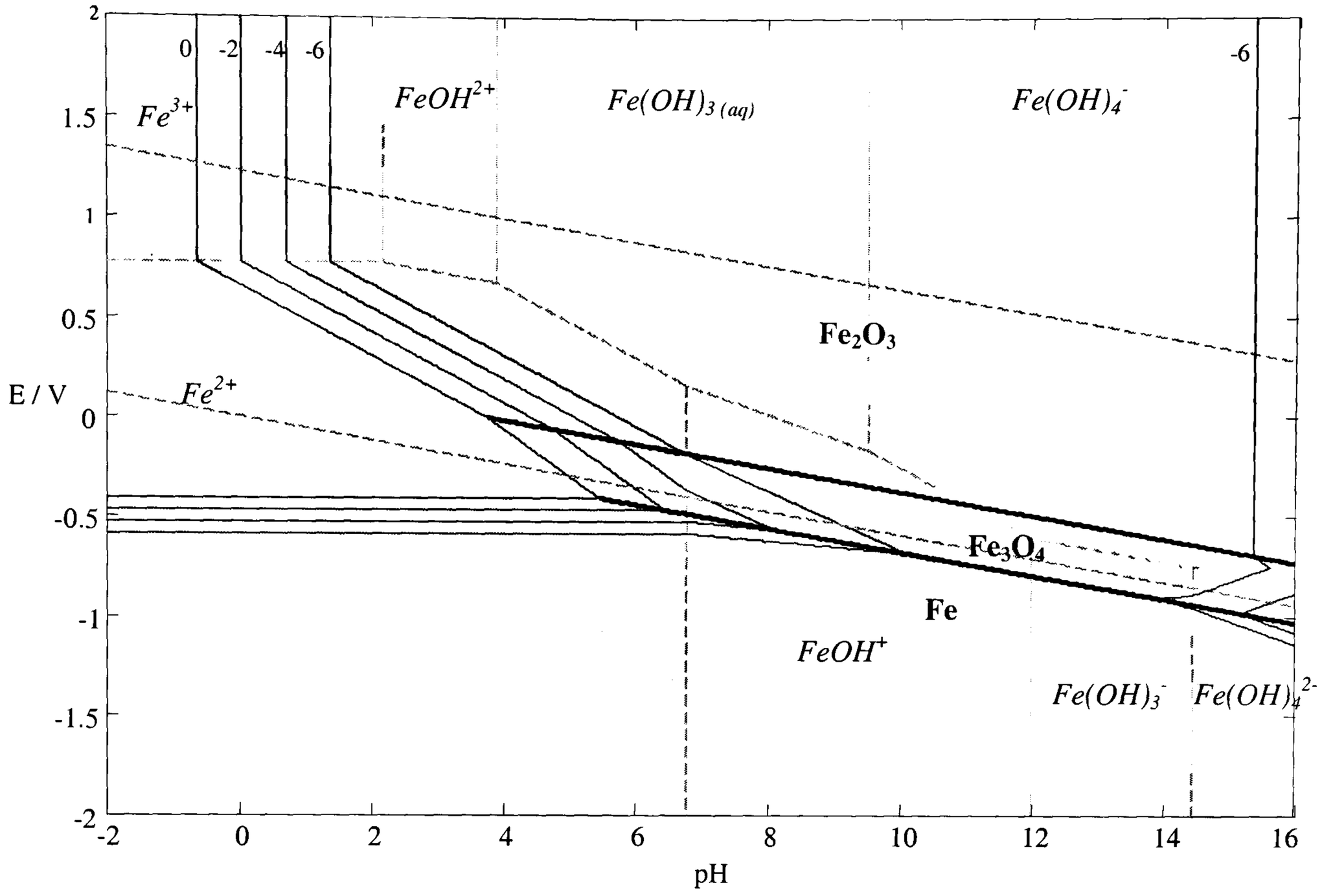

Figure 4-6 Pourbaix diagram for iron-water (298K)

Additional dissolved iron species were included in this diagram, compared to those in the original by Pourbaix [4.4]. However, this is in line with a more recent publication on iron Pourbaix diagrams [4.15]; the change of species with increasing pH corresponds to the description in this work.

Iron-Nitrate-Water

As the stripping waste is a predominantly nitric acid solution, the knowledge of how nitrates affect the iron solubility is important for finding its distribution at the stripping stage. The nitrate concentration was 1M, as for the copper and tin diagrams.

The species that were considered in addition those in the iron-water diagram are shown in Table 4-12 (no data about solid iron nitrate compounds could be found, although $Fe(NO_3)_3.9H_2O$ exists).

	ΔG^O / kJ mol^{-1}
$Fe(NO_3)^{2+}$	-121.8
$Fe(NO_3)_{3\,(aq)}$	-338.5

Table 4-12 Thermodynamic data for iron-nitrate species (data *Bard* [4.6])

Following the same argument used for the tin-nitrate system, nitrate ions were found to affect the Pourbaix plot, with $Fe(NO_3)^{2+}$ replacing the Fe^{3+} at low pH. The relevant reactions are shown in Table 4-13.

Electrochemical	Chemical
Dissolved	
$Fe^{2+} + NO_3^- \rightarrow Fe(NO_3)^{2+} + e^-$	$FeOH^{2+} + NO_3^- + H^+ \rightarrow Fe(NO_3)^{2+} + H_2O$
$Fe^{2+} + H_2O \rightarrow FeOH^{2+} + H^+ + e^-$	$Fe^{2+} + H_2O \rightarrow FeOH^+ + H^+$
$Fe^{2+} + 3H_2O \rightarrow Fe(OH)_{3(aq)} + 3H^+ + e^-$	$FeOH^{2+} + 2H_2O \rightarrow Fe(OH)_{3(aq)} + 2H^+$
$FeOH^+ + 2H_2O \rightarrow Fe(OH)_{3(aq)} + 2H^+ + e^-$	$Fe(OH)_4^- + H^+ \rightarrow Fe(OH)_{3(aq)} + H_2O$
$FeOH^+ + 3H_2O \rightarrow Fe(OH)_4^- + 3H^+ + e^-$	$FeOH^+ + 2H_2O \rightarrow Fe(OH)_3^- + 2H^+$
$Fe(OH)_3^- + H_2O \rightarrow Fe(OH)_4^- + H^+ + e^-$	$Fe(OH)_3^- + H_2O \rightarrow Fe(OH)_4^{2-} + H^+$
$Fe(OH)_4^{2-} \rightarrow Fe(OH)_4^- + e^-$	
Solid	
$3Fe + 4H_2O \rightarrow Fe_3O_4 + 8H^+ + 8e^-$	
$2Fe_3O_4 + H_2O \rightarrow 3Fe_2O_3 + 2H^+ + 2e^-$	
Solid / Dissolved	
$2Fe^{2+} + 3H_2O \rightarrow Fe_2O_3 + 6H^+ + 2e^-$	$2Fe(OH)_4^- + 2H^+ \rightarrow Fe_2O_3 + 5H_2O$
$3Fe^{2+} + 4H_2O \rightarrow Fe_3O_4 + 8H^+ + 2e^-$	$2Fe(NO_3)^{2+} + 3H_2O \rightarrow Fe_2O_3 + 2NO_3^- + 6H^+$
$3FeOH^+ + H_2O \rightarrow Fe_3O_4 + 5H^+ + 2e^-$	
$Fe + H_2O \rightarrow FeOH^+ + H^+ + 2e^-$	
$Fe \rightarrow Fe^{2+} + 2e^-$	
$Fe_3O_4 + 8H_2O \rightarrow 3Fe(OH)_4^- + 4H^+ + e^-$	
$3Fe(OH)_4^{2-} + 4H^+ \rightarrow Fe_3O_4 + 8H_2O + 2e^-$	

$3Fe(OH)_3^- + H^+ \rightarrow Fe_3O_4 + 5H_2O + 2e^-$	
$Fe + 3H_2O \rightarrow Fe(OH)_3^- + 3H^+ + 2e^-$	
$Fe + 4H_2O \rightarrow Fe(OH)_4^{2-} + 4H^+ + 2e^-$	

Table 4-13 Reactions represented in the iron-nitrate-water Pourbaix diagram

The resulting Pourbaix diagram (Figure 4-7) shows that although $Fe(NO_3)^{2+}$ has replaced the Fe^{3+} ion, the only effect this has is to slightly increase the area of solubility at positive potentials and low pH. A solution containing iron at an activity of 0.01 precipitates at pH 0.38 when nitrate (a_{NO3}=1) is in solution, but precipitates at pH 0.04 with only water.

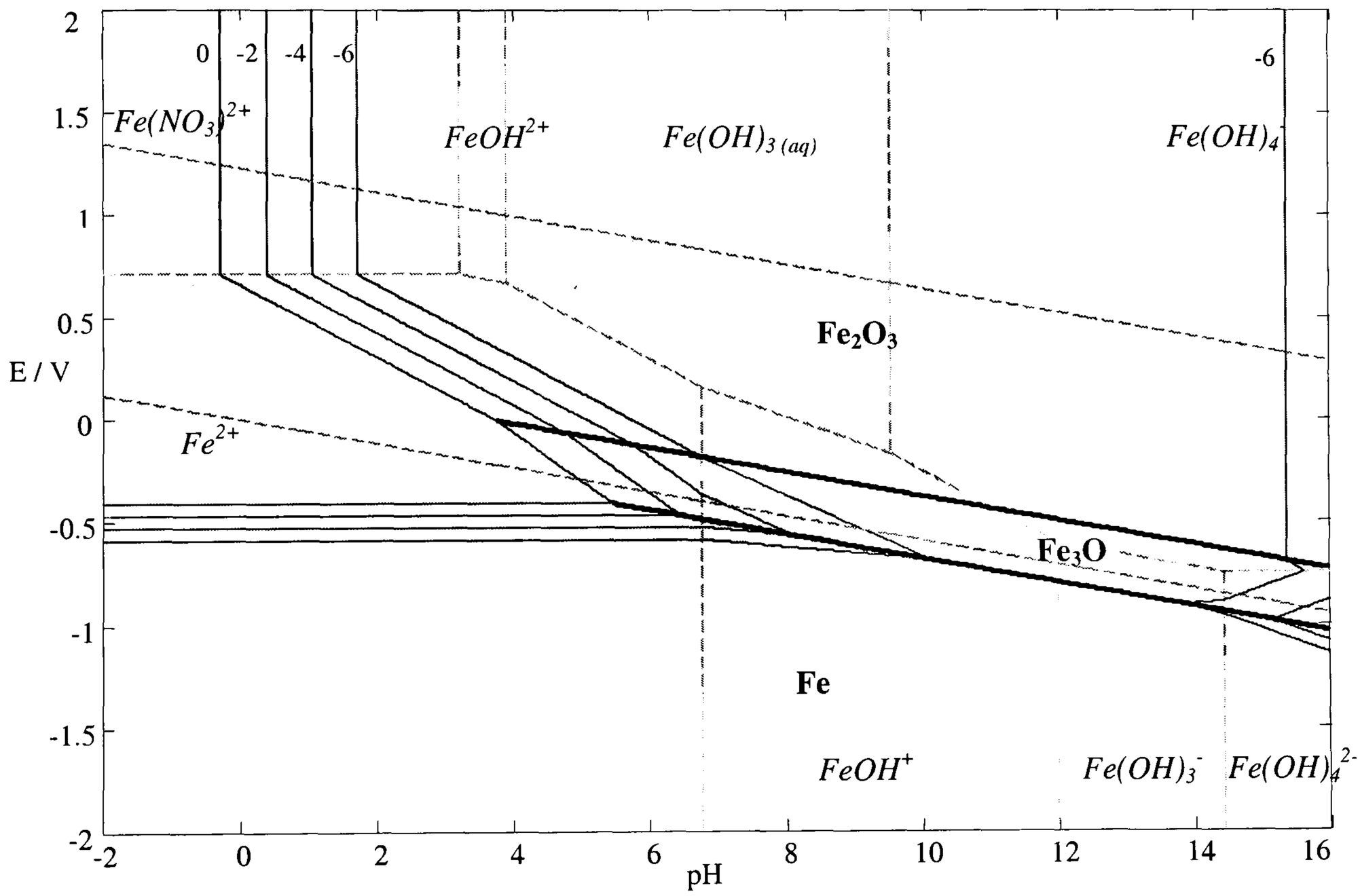

Figure 4-7 Pourbaix diagram for iron-nitrate-water (298K, a_{NO3}=1)

The stripping solution contains 0.25M iron [4.16], if it is assumed that the concentration and activity are equivalent, the iron will start to be deposited at a potential of -0.43V. However, the ability of the iron to remain in solution is also dependent on the potential of the system which is fixed by the species present in the waste.

4.2 MINEQL+

In addition to the Pourbaix analysis, a thermodynamic software package, MINEQL+, was used to:

- check the precipitation pH of copper, tin and iron found using the Pourbaix diagrams,
- carry out a sensitivity analysis on the effect of nitrate concentration on the precipitation pH,
- and to simulate the thermodynamic changes in the process solution during the removal of nitric acid with diffusion dialysis.

MINEQL+ [4.2] is a software package designed to model chemical equilibrium conditions. The user inputs components (e.g. Cu^{2+}, NO_3^-), their concentrations, pH and temperature. The software solves a set of non-linear equations (Eqs. 4.2, 4.3) based on the mass balance for an individual component [4.17]; these components are used to form species (e.g. $CuNO_3^+$) by chemical reaction.

$$C_i = K_i \prod_{j=1}^{n} X_j^{x_{i,j}} \quad \text{for i = 1,m} \tag{4.2}$$

$$Y_j = \sum_{i=1}^{m} x_{i,j} C_i - T_j \quad \text{for j = 1,n} \tag{4.3}$$

where C_i is the concentration of species i, K_i the equilibrium constant for species i, X_j the concentration of component j, $x_{i,j}$ the stoichiometric coefficient of component j in species i, T_j the total concentration of component j, m the number of species and n the number of components. The equations are solved for X_j to make Y_j equal to zero (the values of $x_{i,j}$ and K_i are found from an internal database).

The internal data used by MINEQL+ in the thermodynamic calculations are based on the 1999 revision of the US EPA MINTEQA2. The equilibrium constants are specified at zero ionic strength. MINEQL+ has the ability to correct the values of these equilibrium constants for higher ionic strengths through the Davis equation

(Eq. 4.4) [4.18], where γ is the activity coefficient of the species. This coefficient relates the activity and the concentration by $a = \gamma \cdot c$.

$$-\log(\gamma_i) = 0.51 \cdot z_i^2 \left(\frac{\sqrt{I_c}}{1+\sqrt{I_c}} - 0.30 I_c \right) \tag{4.4}$$

where $I_c = 0.5 \sum z_i^2 c_i$

These ionic corrections are only strictly valid for I_c<0.5M. As the nitrate concentration in the waste is 1M, the ionic strength of the tin stripping waste will be higher than this value. Therefore, the results from these analyses do not strictly model the stripping solution. However, the model is sufficient to check the Pourbaix plots and evaluate the feasibility of stages in the recovery process.

4.2.1 Copper

To calculate the speciation, it has been assumed that the dissolved copper is in the +2 oxidation state. This is supported by the Pourbaix diagram for copper-nitrate-water (Figure 4-1), which shows that at a pH of 0 (approximately equivalent to 1M HNO_3), copper is either in the form $CuNO_3^+$ or Cu^0(metal) depending on the potential.

The first run was carried out as a fixed pH titration, where a series of calculations are carried out at set pH values. The precipitation pH of the solution can be seen as the point where the solid species appear on the speciation. This method also shows the distribution of the copper between the dissolved species, unlike Pourbaix plots which only show the predominant ion. The inputs to MINEQL+ are shown in Table 4-14.

Species considered	Cu^{2+}, Cu^+, NO_3^-, H^+, H_2O
Cu^{2+} concentration	0.3M
NO_3^- concentration	1M
ionic strength corrections	on
pH varied	0→14, 29 steps

Table 4-14 MINEQL+ inputs for copper pH titration

It can be seen from Figure 4-8 that copper stays in solution until a pH of ~4, above which it rapidly precipitates as $Cu_2(OH)_3NO_3$. This precipitation pH agrees with the value of 3.8 found from the Pourbaix analysis; although a different solid, which was not included in the diagrams, is seen to precipitate before CuO.

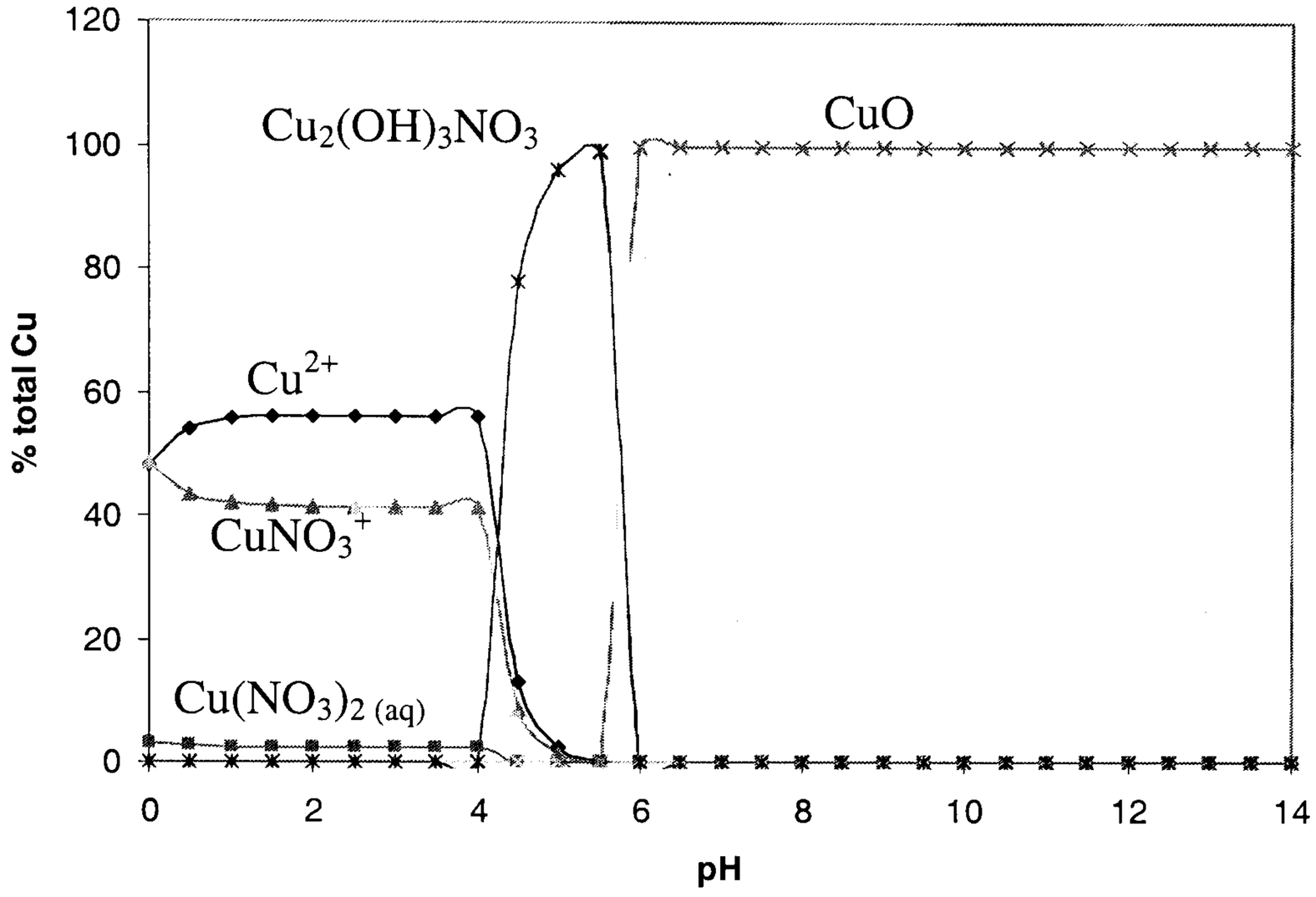

Figure 4-8 Copper speciation (0.3M Cu, 1M NO_3^-)

The sensitivity of the precipitation pH to nitrate concentration in the range 0.5-1.5M was investigated: there are likely to be variations in the tin stripping process (a batch operation) that lead to a range of nitrate concentration in the waste, also in the proposed acid recovery stage nitrate ions are removed, as well as hydrogen ions. These runs were carried out using the same inputs as in Table 4-14, except that the nitrate concentration was varied (0.5-1.5M in 5 steps), as well as the pH. It was determined that the nitrate concentration does not affect the precipitation pH in the range studied, although the distribution of dissolved copper species changed significantly. Comparing Figure 4-9 and Figure 4-10, a solution with a NO_3^- concentration of 0.5M will predominantly contain Cu^{2+} ions (70%), whereas if the NO_3^- concentration is increased to 1.5M, the $CuNO_3^+$ ions begin to predominate (52%) with the proportion of Cu^{2+} ions reduced to 40%.

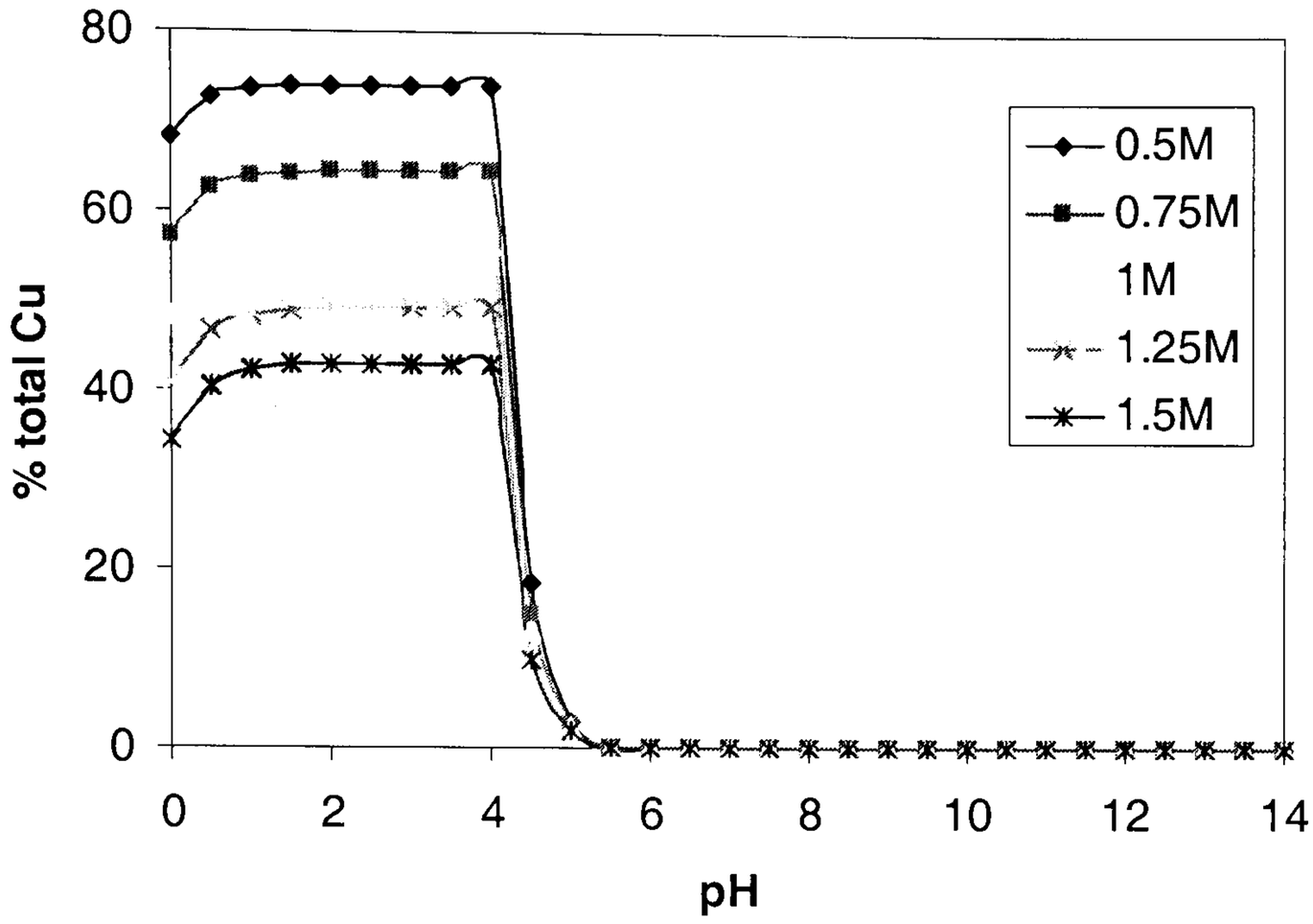

Figure 4-9 Effect of NO_3^- concentration on percentage of Cu^{2+}

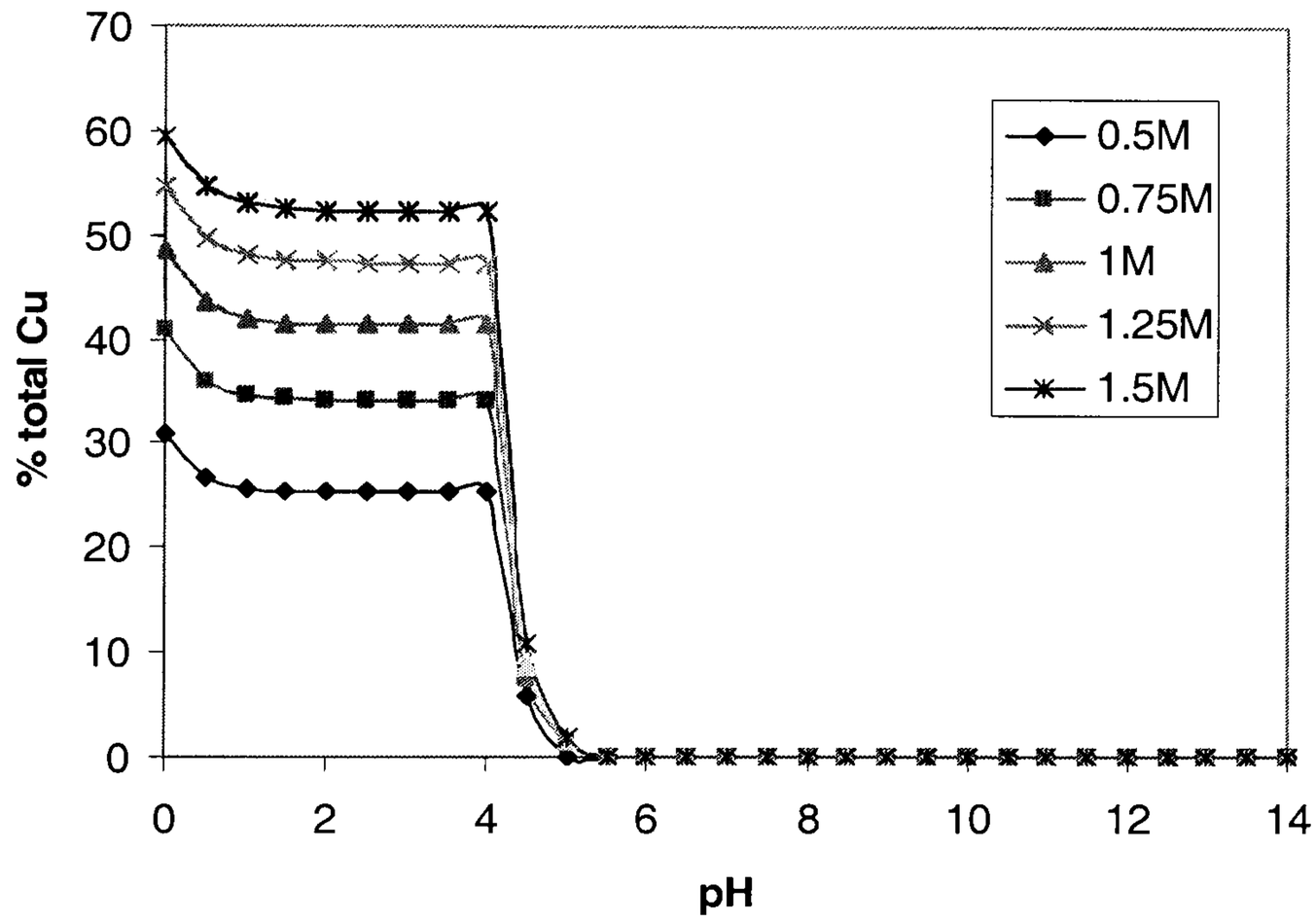

Figure 4-10 Effect of NO_3^- concentration on percentage of $CuNO_3^+$

A separate analysis was carried out to simulate the removal of HNO_3 during the acid recovery stage (Section 1.5). For these runs, the species considered and the concentration of copper, were as detailed in Table 4-14. However, the nitrate concentration was varied 1→0.01 (99% recovery). It was not necessary to vary the concentration of hydrogen ions because MINEQL+ was set to calculate the pH based on electroneutrality.

Figure 4-11 shows how the pH varies as nitric acid is removed – the pH gradually increases until the concentration of nitrate reaches 0.6M, when the pH sharply rises to around 4. At this point the solid $Cu_2(OH)_3NO_3$ starts to precipitate (Figure 4-12). At NO_3^- concentrations of less than 0.6M, the pH change is again gradual, with more copper precipitating as $Cu_2(OH)_3NO_3$ and finally as CuO.

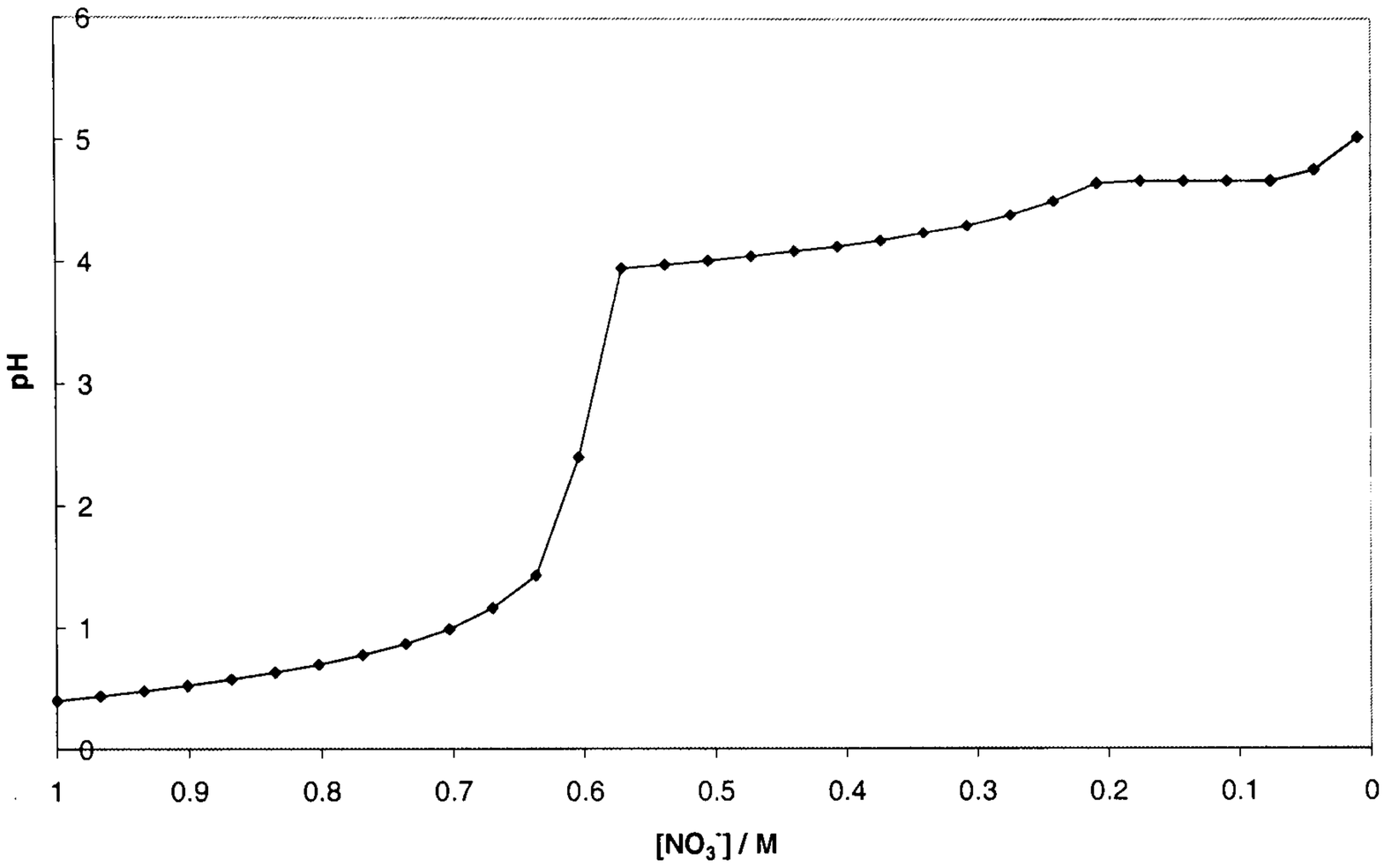

Figure 4-11 pH change as HNO_3 is removed from a 0.3M Cu solution

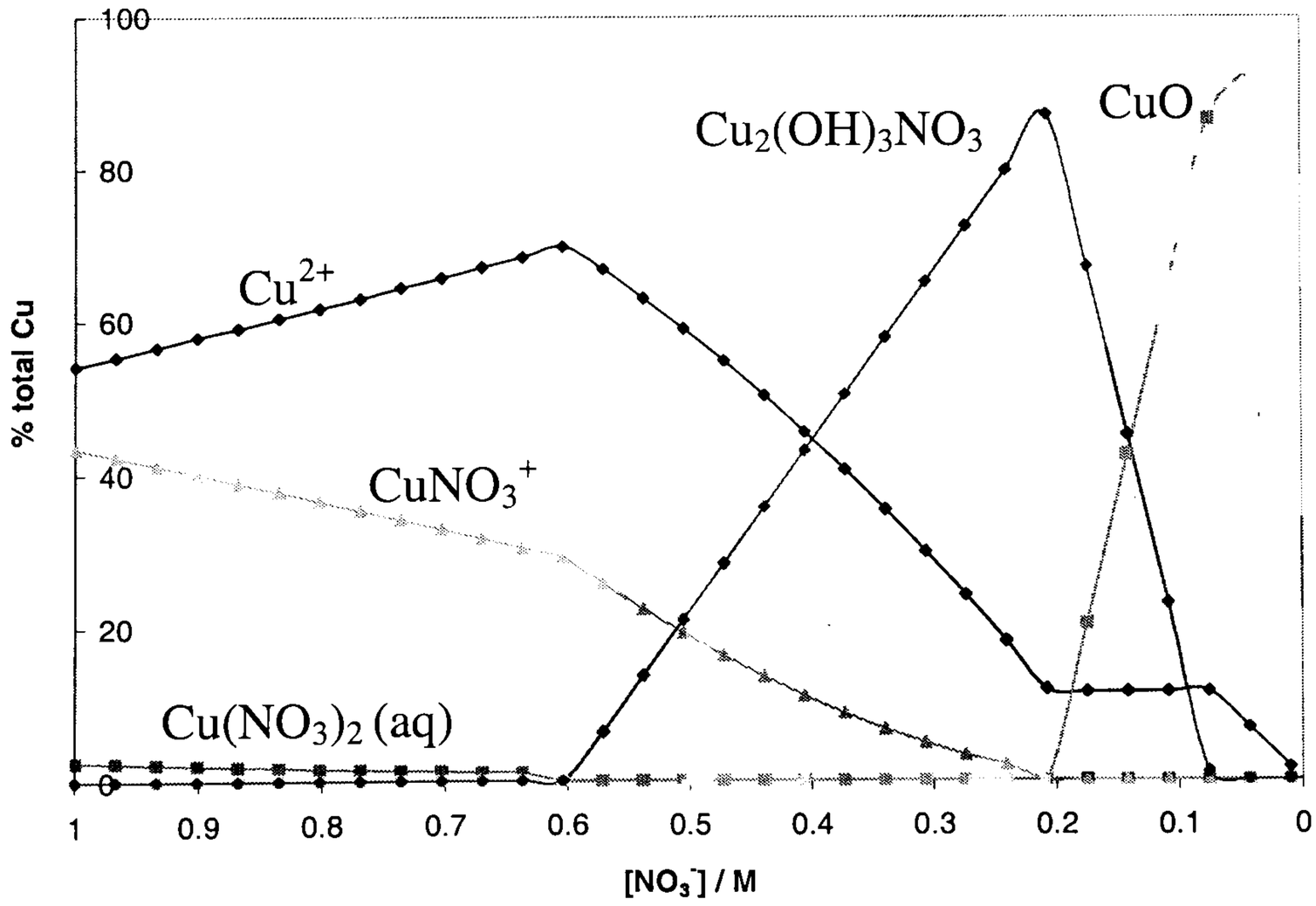

Figure 4-12 Copper speciation as HNO_3 is removed from a 0.3M Cu solution

At the acid recovery stage, copper must stay in solution so that it can be separated from the tin by filtration. This analysis shows that the recovery of acid is limited by

the precipitation of copper which occurs when the NO_3^- concentration falls below 0.6M; this corresponds to a pH of 2.4. This copper precipitation pH is lower than that previously found from the Pourbaix plots (pH 3.8) because only the change in hydrogen ions was taken into account in this previous analysis.

4.2.2 Tin

To calculate the speciation for tin in nitric acid, it was assumed that all the tin exists in the +4 oxidation state; corresponding to the expected solid SnO_2. The concentration of tin was taken to be 75g/l, a mid-range value from process control information [4.7]. A pH titration was carried out using the inputs to MINEQL+ shown in Table 4-15.

Species considered	Sn^{4+}, Sn^{2+}, NO_3^-, H_2O, H^+
Sn^{4+} concentration	0.63M (=75g/l)
NO_3^- concentration	1M
ionic strength corrections	on
pH varied	0→14, 29 steps

Table 4-15 MINEQL+ inputs for tin pH titration

The tin speciation (Figure 4-13) shows that tin will exist as a precipitate of SnO_2, unless conditions are very alkaline when it will exist as the dissolved species $Sn(OH)_6^{2-}$. This result was expected considering the Pourbaix diagram (Figure 4-3). It is not possible to reach these conditions by acid recovery, so theoretically tin will stay in suspension to be removed by the filtration stage.

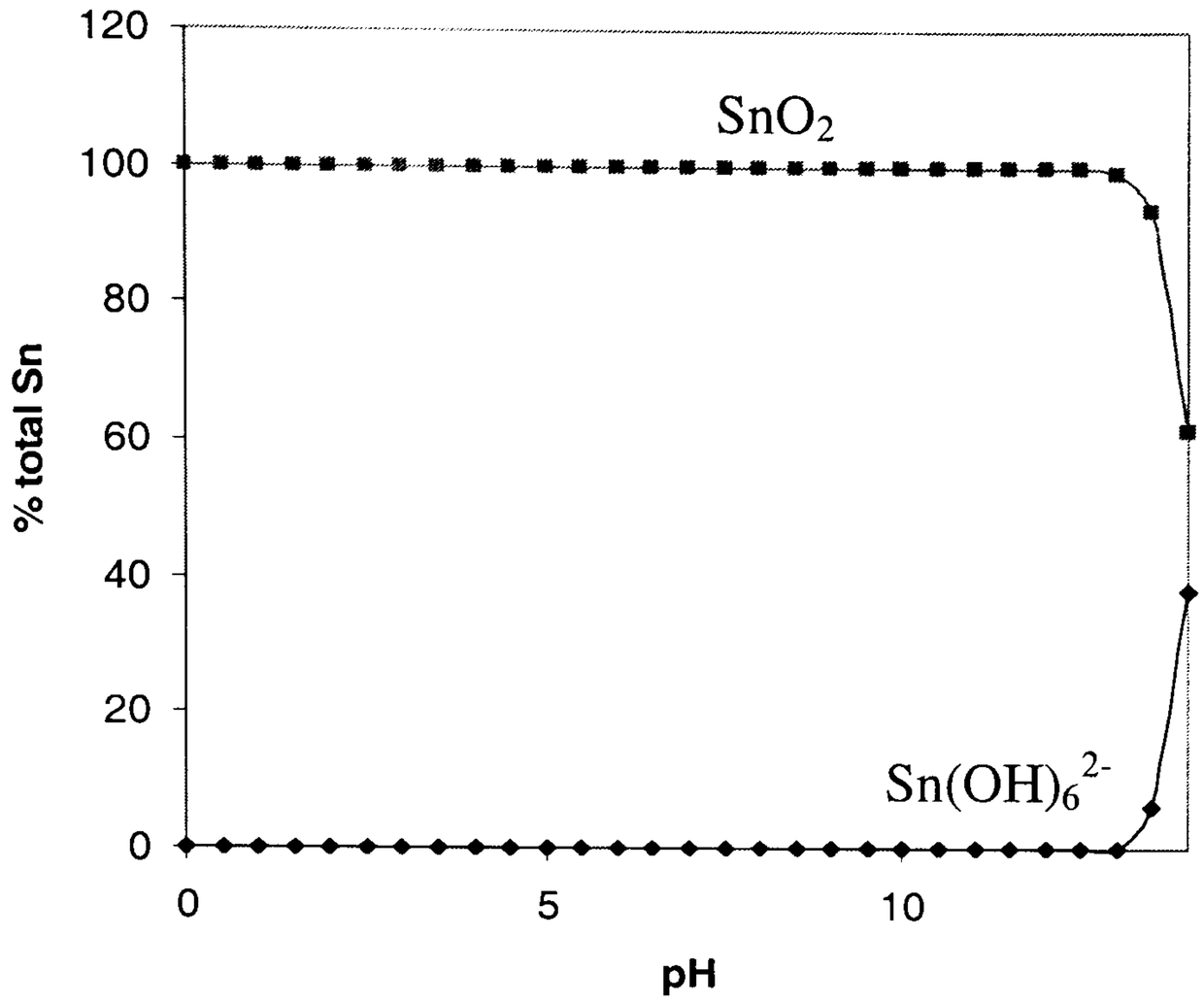

Figure 4-13 Tin speciation (0.63M Sn, 1M NO_3^-)

Analysis of the sensitivity of the speciation to nitrate concentration was also performed, but there were only slight differences seen at high pH. Therefore, any variations in the tin stripping process, that cause the nitrate concentration to change, will not affect the tin precipitation.

4.2.3 Iron

The speciation of iron was calculated with the assumption that all the iron in solution exists in the +3 oxidation state. In the waste stripping solution some of the iron will have been reduced to Fe(II) during the dissolution of the tin/copper intermetallic from the circuit board. Therefore these runs are only valid as a tool to check the precipitation pH calculated from the Pourbaix plots.

The concentration of iron in solution was taken to be 0.25M, as specified in the MSDS sheet for the fresh stripping solution (Tinsolv 2000) [4.16]. The MINEQL+ inputs are shown in Table 4-16, and the resulting speciation in Figure 4-14.

Species considered	Fe^{3+}, Fe^{2+}, NO_3^-, H_2O, H^+
Fe^{3+} concentration	0.25M
NO_3^- concentration	1M
ionic strength corrections	on
pH varied	0→14, 29 steps

Table 4-16 MINEQL+ inputs for iron speciation

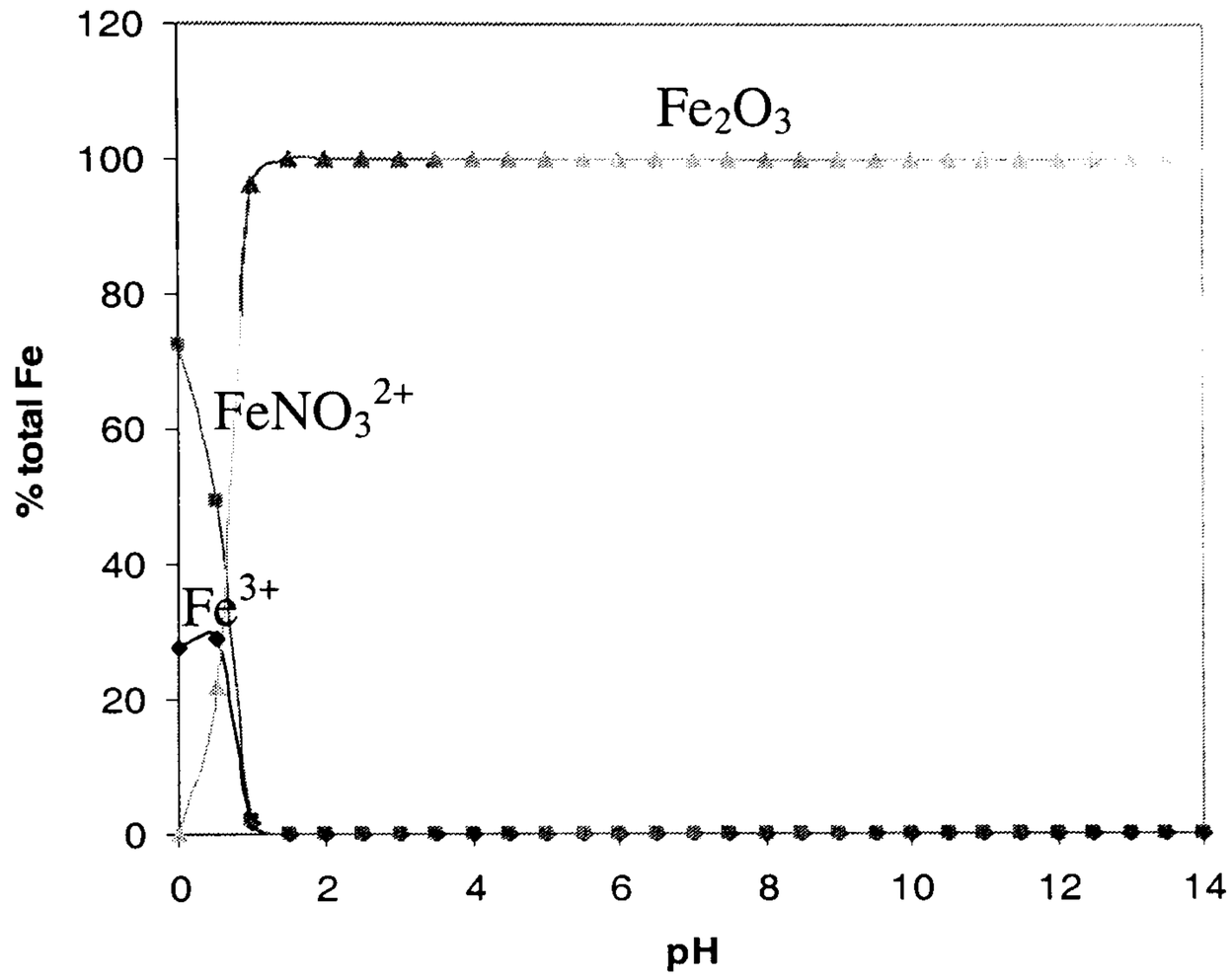

Figure 4-14 Iron speciation (0.25M Fe, 1M NO_3^-)

The iron starts precipitating as the solid Fe_2O_3 at all pH values greater than zero. The MINEQL+ speciation corresponds well to the Pourbaix analysis which assumes $FeNO_3^{2+}$ is the predominant dissolved ion and precipitates as Fe_2O_3 according to the equilibrium relationship shown below as Eq. 4.4.

$$\log\left(a_{FeNO_3^{2+}}\right) = -0.8470 + \log\left(a_{NO_3^-}\right) - 3pH \tag{4.4}$$

Using this relationship, a solution of 0.25M iron in 1M NO_3^- will precipitate at a pH of -0.082.

4.3 Discussion

The theoretical analysis has been carried out in order to determine whether the recovery process suggested by *Kerr* [4.8] is feasible. The initial stage in the process, shown in Figure 4-15, is to recover acid from the waste by diffusion dialysis. The removal of HNO_3 from the stripping solution was modelled using MINEQL+. It was determined that the acid recovery was limited by the precipitation of copper, which occurred at a pH of 2.4. This pH corresponded to a HNO_3 concentration of 0.6M, therefore the maximum acid recovery that can be achieved is 40%.

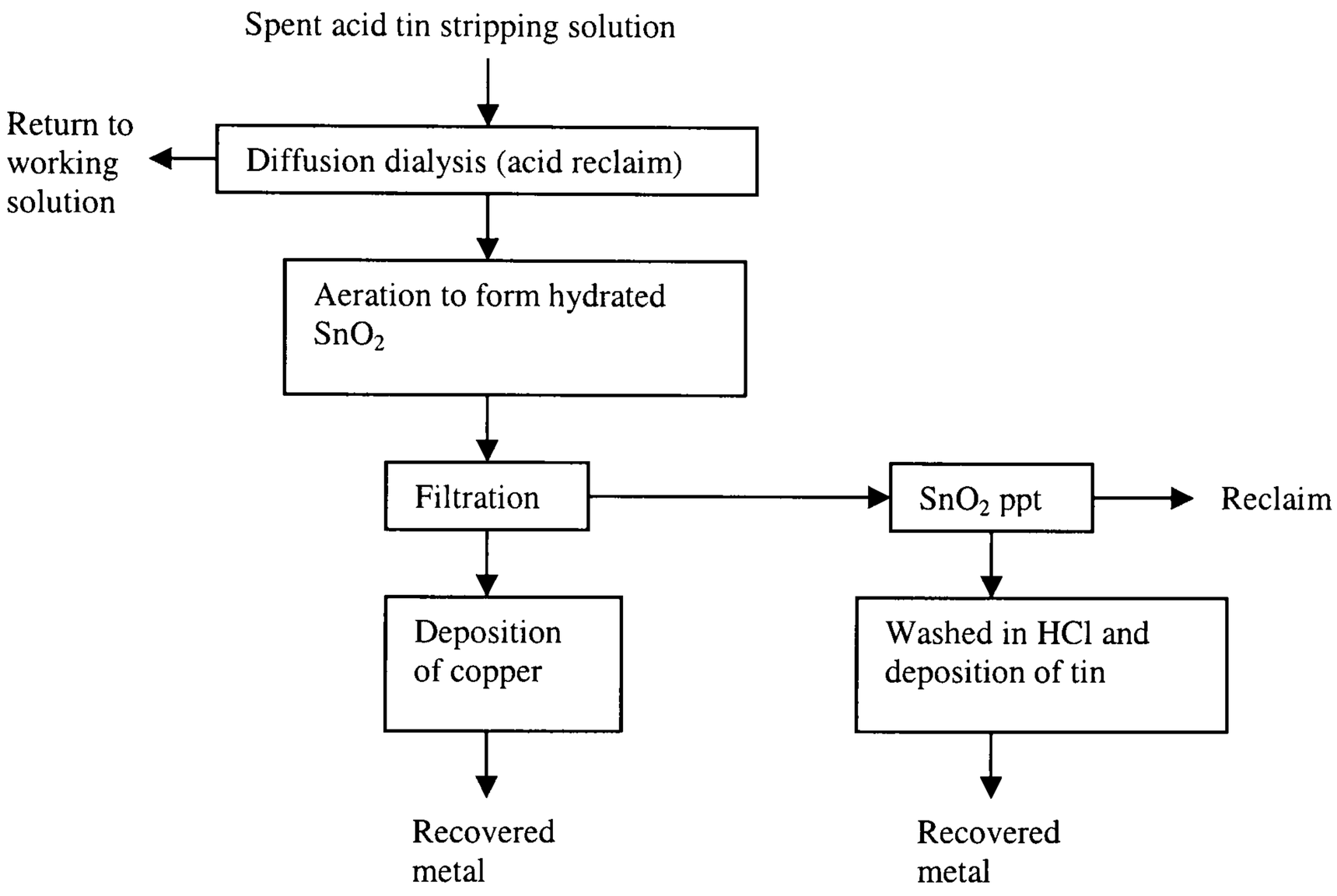

Figure 4-15 Recovery method for copper / tin from stripping solution, proposed by Kerr [4.8]

The next stage in the proposed recovery process is to aerate the waste stripping solution to ensure that all the tin exists as a precipitate. The tin-water Pourbaix diagram (Figure 4-3), which is also valid for tin in the presence of NO_3^-, shows that tin is exists in solution for a small range of pH if the system potential is approximately 0V. The aeration will increase the system potential, thus ensuring the tin exists as the solid SnO_2. The MINEQL+ simulations show that tin is in the form of SnO_2 for pH in the range $0 \rightarrow 13$, therefore it is possible that the aeration stage could be omitted.

After the acid recovery stage, it is proposed to separate the tin and copper by filtration. For this stage to be successful, one of the metals should be in solution, the other a solid. The tin is already a precipitate of SnO_2 in the stripping waste; therefore all the copper should be in solution. Comparing the diagrams for tin and copper in nitrate solutions (Figure 4-1, Figure 4-3), it can be seen that tin exists as a solid (i.e. activity in solution $<10^{-6}$) at pH>-0.4, and for the estimated Cu(II) concentration in the stripping waste of 0.3M, copper is in solution if pH<3.8. The separation of tin and copper at the filtration stage can therefore be effected if the pH is maintained between -0.4 and 3.8 by the acid recovery stage. As copper will precipitate during acid recovery if the pH is greater than 2.4, the filtration stage would operate in the pH range -0.4 to 2.4.

Ferric ions are added to the tin stripping solution in order to increase the oxidising power. To minimise the separations required, iron would ideally all stay in solution and pass through the filtration stage with the copper, or all precipitate and be removed with the tin. If the iron is in solution with the copper, it will pass to an electrowinning stage, where the copper can be separated from the iron as their deposition potentials are sufficiently different to make co-deposition unlikely (0.3M Cu(II) at 0.31V, 0.25M Fe(II) at -0.43V). If the iron was to be precipitated with the tin, information on the behaviour of iron in chloride systems would be required and an extra separation step may be needed. Comparing the Pourbaix plots for copper, tin and iron in nitrate solutions it can be seen that to precipitate iron with the tin(IV) oxide would require careful control of the pH to prevent co-precipitation of copper. However, the ability of the iron to stay in solution is strongly dependent on the system potential. This will be resolved by later experimentation. However, as it appears to be more practicable to have iron remain in solution, rather than to precipitate it, Pourbaix plots were not constructed for the iron-chloride-water system.

The final stages in the proposed recovery process are the electrodeposition of copper from the nitrate containing waste solution, and the dissolution of SnO_2 prior to the electrodeposition of tin from hydrochloric acid. From the copper-nitrate-water plot (Figure 4-1), it can be seen that copper starts to deposit at a potential of +0.31V, and can be removed to an activity of 10^{-6} if a potential of +0.15V is applied. Iron is

unlikely to be co-deposited as a 0.25M Fe(II) solution does not start to deposit until a potential of -0.43V is attained.

In the case of SnO_2, concentrated hydrochloric acid and/or elevated temperatures will be needed to dissolve it for electrodeposition; this may not be practicable for health and safety reasons. To obtain SnO_2 as a product, it should not be contaminated with copper. Comparing the chloride Pourbaix diagrams for copper and tin (Figure 4-2, Figure 4-4) it can be seen that if any copper is carried over into the tin stages it should be relatively easy to separate the two metals as copper is soluble at pH 2 whereas tin is not.

4.4 References

4.1 M. Pourbaix, *Lectures on Electrochemical Corrosion*, Plenum Press, New York (1973)

4.2 MINEQL+, Version 4.5 for Windows, Environmental Research Software, Hallowell, ME (2003)

4.3 U. Bertocci and D. R. Turner, in *Encyclopedia of the Electrochemistry of the Elements*, A. J. Bard, ed., Vol. 2, Chap. 6, Marcel Dekker, New York (1974).

4.4 M. Pourbaix, *Atlas of Electrochemical Equilibria in Aqueous Solutions*, National Association of Corrosion Engineers, Houston, Texas (1974)

4.5 A. E. Martell and R. M. Smith, *Critical Stability Constants*, Plenum Press, New York (1974)

4.6 A. J. Bard, R. Parsons and J. Jordan, ed. *Standard Potentials in Aqueous Solution*, Dekker, New York (1985)

4.7 R. Massey, Personal Communication, (2005) [e-mail, 27/04/05]

4.8 C. Kerr, *Transactions of the Institute of Metal Finishing*, **82**(B7-B12, Part1-2): (2004)

4.9 M. R. Schock, D. A. Lytle and J. Clement, *Effect of pH, DIC, Orthophosphate and Sulfate on Drinking Water Cuprosolvency*, US Environmental Protection Agency (1995)

4.10 T. P. Hoar, *Transactions of the Faraday Society*, **33**: 1152-1167 (1937)

4.11 J. A. Dean, ed. *Lange's Handbook of Chemistry*, McGraw-Hill, (1999)

4.12 T. Stefanowicz, T. Golik, S. Napieralskazagozda and M. Osinska, *Resources Conservation and Recycling*, **6**(1): 61-69 (1991)

4.13 C. I. House and G. H. Kelsall, *Electrochimica Acta*, **29**(10): 1459-1464 (1984)

4.14 K. Scott, X. Chen, J. W. Atkinson, M. Todd and R. D. Armstrong, *Resources Conservation and Recycling*, **20**(1): 43-55 (1997)

4.15 B. Beverskog and I. Puigdomenech, *Corrosion Science*, **38**(12): 2121-2135 (1996)

4.16 Atotech UK Ltd, Material Safety Data Sheet, *Tinsolv 2000* (1999)

4.17 W. D. Schecher and D. C. McAvoy, *MINEQL+: A Chemical Equilibrium Modeling System, Version 4.5 for Windows, User's Manual*, Environmental Research Software, Hallowell, Maine (2003)

4.18 C. W. Davies, *Electrochemistry*, Newnes, London (1967)

5 PRECIPITATION EXPERIMENTS

The feasibility of the proposed process to recover copper and tin from waste tin stripping solution [5.1] has been determined by the thermodynamic analysis in Chapter 4. The equilibria represented on the Pourbaix diagrams show what is thermodynamically possible, however if the kinetics of the reactions are very slow, some of the transformations may never occur. Therefore the aim of these precipitation experiments was to verify the theoretical predictions for the pH at which the metal ions precipitate.

The experiments were carried out using a titration technique, where the metal salt of interest was titrated against an alkaline solution. To represent the proposed recovery stages, and the constituent ions in the stripping solution, the systems $Cu/NO_3^-/H_2O$, $Fe/NO_3^-/H_2O$ and $Sn/Cl^-/H_2O$ were tested.

5.1 Copper

The nitrate concentration in the waste stripping solution was estimated to be 1M (cf. Appendix A). As the Pourbaix diagrams are applicable for metals in contact with a large volume of bulk solution, the metal ion concentration should be lower than 1M so that reaction products do not appreciably alter the anion concentration. Precipitation experiments for copper/nitrate were therefore carried out using 0.1M and 0.01M Cu(II) to determine the effect on the precipitation pH when the concentration changes over one order of magnitude. As the nitrate concentration in the waste stripping solution depends on the amount of metal dissolved during the stripping process, experiments to find the precipitation pH were also carried out using 0.5M, 1M and 2M NO_3^-, whilst keeping the Cu(II) concentration at 0.01M.

The results from the copper/nitrate precipitation studies are summarised in Table 5-1. The pH at which the salt precipitates is shown as a range, because it is impossible to say when the solution precipitated during an incremental addition of KOH; only the pH before the addition, and the pH after the precipitation are known. The theoretical

precipitation pH, calculated using two different methods, is also shown in this table. Firstly, in order to verify the prediction from the Pourbaix diagram, the pH was calculated using the appropriate equilibrium reaction, with the metal and anion concentrations assumed equal to their activities.

$$CuNO_3^+ + H_2O \rightarrow CuO + NO_3^- + 2H^+$$

$$\log[CuNO_3^+] = 7.076 + \log[NO_3^-] - 2\,pH \qquad (5.1)$$

A predicted value was also estimated using MINEQL+.

Exp. No.	[Cu] / M	[NO_3^-] / M	precipitation pH range	theoretical (Poubaix)	theoretical (MINEQL+)
A	0.1	1	1.3 - 4.7	4.0	4.3
B	0.1	1	2.2 - 4.7	4.0	4.3
C	0.1	1	3.5 - 4.1	4.0	4.3
D	0.01	1	2.9 - 4.8	4.5	5.0
E	0.01	1	5.0 - 5.3	4.5	5.0
F	0.01	1	4.9 - 5.4	4.5	5.0
G	0.01	0.5	5.4 - 5.6	4.4	5.0
H	0.01	2	4.8 - 5.2	4.7	5.0
I	0.01	0.5	<5.3	4.4	5.0
J	0.01	0.5	4.8 - 5.1	4.4	5.0

Table 5-1 Copper/nitrate precipitation pH results

Comparing experiments A-C (0.1M Cu) with experiments D-F (0.01M Cu) it can be seen that the precipitation pH increases as the Cu(II) concentration decreases. This trend is consistent with the equilibrium expression for the $CuNO_3^+$ precipitation (Eq. 5.1) plotted on the Pourbaix diagram. However, this expression also predicts that the nitrate concentration will affect the precipitation pH. The experimental results (D-J), also shown graphically in Figure 5-1, show no correlation between the nitrate concentration and the precipitation pH.

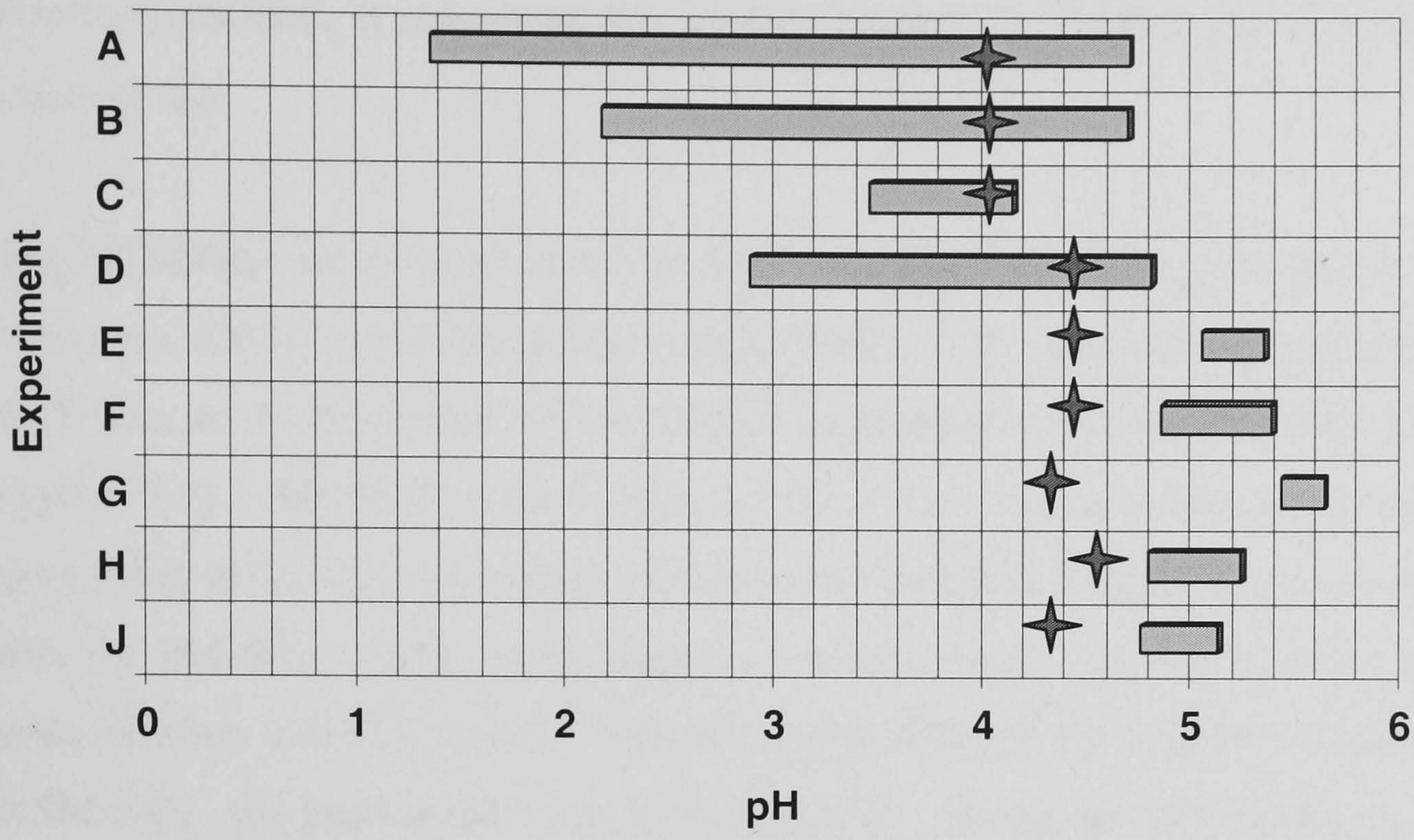

Figure 5-1 Graphical representation of copper/nitrate precipitation results (bars = experiments, stars = Pourbaix predictions)

The values of the precipitation pH for 0.01M Cu(II) (D-J) do not match the theoretical predictions as well as those for 0.1M Cu(II), especially with regards to the change in nitrate concentration. There are several reasons that could account for these discrepancies.

- Additional reactions occur concurrently with the precipitation of CuO from $CuNO_3^+$.
- The concentration of metal and/or anion is not equal to the activity.
- Experiment errors, such as non standard temperature, weighing errors, equilibrium not reached, and sample dilution due to the addition of KOH.
- The method of mixing the solutions has been found to affect the final properties of the system [5.2].

The estimation of the theoretical precipitation pH from the Pourbaix diagram was based on the precipitation of CuO from $CuNO_3^+$. However it is possible that other reactions could occur concurrently. This possibility was investigated by running MINEQL+ simulations. Although this program uses Gibbs free energy data like the

Pourbaix method, it calculates the species present by finding the minimum total value of ΔG.

The MINEQL+ simulations show that Cu^{2+} ions and $Cu(NO_3)_{2\,(aq)}$ are also in solution with the $CuNO_3^+$ ions in the acidic region (Figure 5-2). The relative concentration of each species is dependent on the nitrate concentration (illustrated for $CuNO_3^+$ in Figure 5-3). MINEQL+ shows that as the NO_3^- concentration is increased, the proportion of $CuNO_3^+$ ions (predominant in the Pourbaix diagrams) also increases, so that for 2M NO_3^- ~60% of the copper is in this form. However, when the NO_3^- concentration is 0.5M, $CuNO_3^+$ only represents 30% of the copper in solution. For 0.5M NO_3^-, the predominant ion is actually Cu^{2+}, taking up 60% of the copper; the remaining 10% of the copper is in the form $Cu(NO_3)_{2\,(aq)}$. These proportions are for a Cu(II) concentration of 0.01M, but the same trends are seen with concentrations of 0.1M and 1M Cu(II). MINEQL+ also predicts that the NO_3^- concentration does not influence the pH at which copper precipitates; a result that differs from the Pourbaix equilibria prediction.

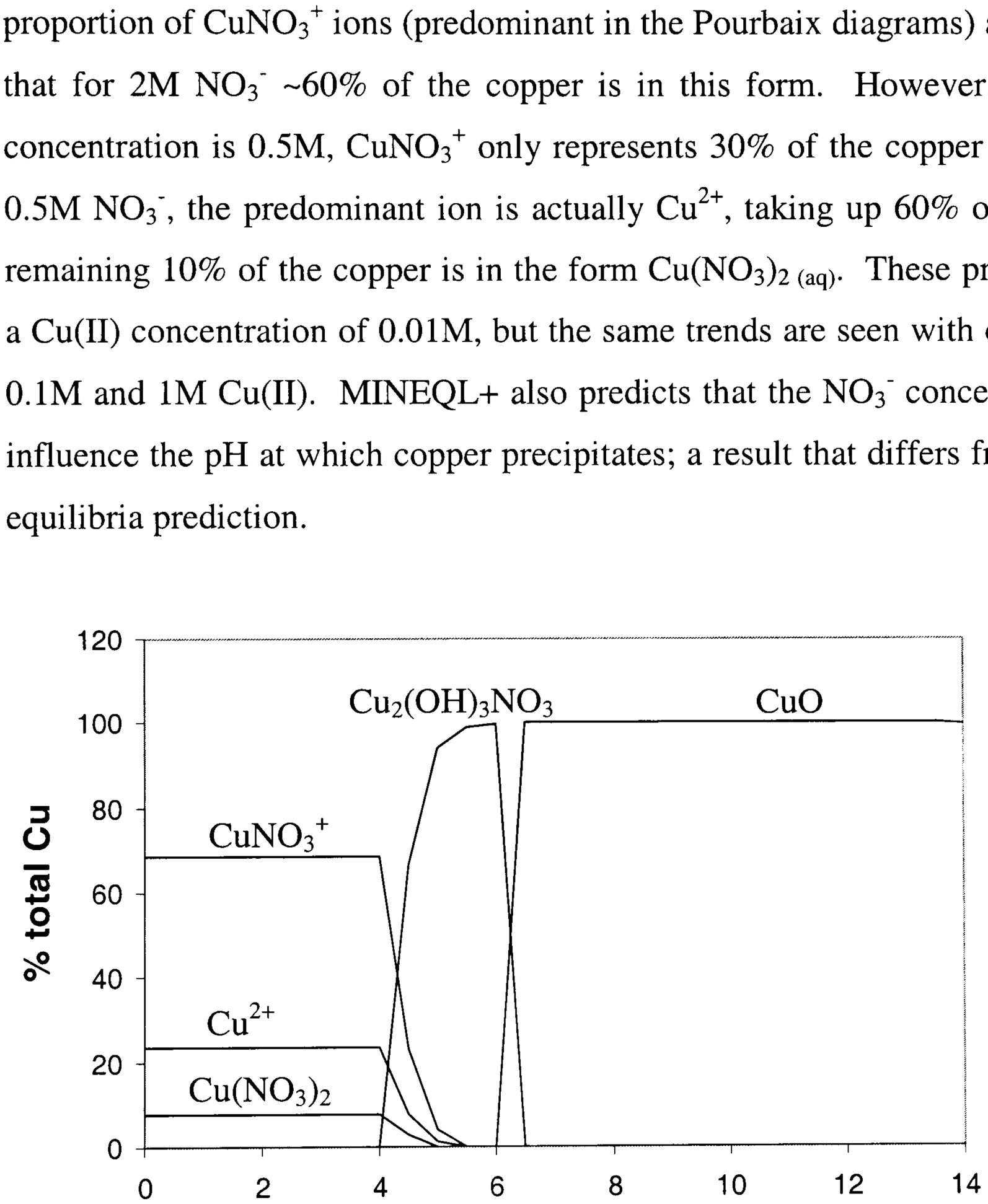

Figure 5-2 Cu(II) speciation; [Cu]=0.1M, [NO_3^-]=1M

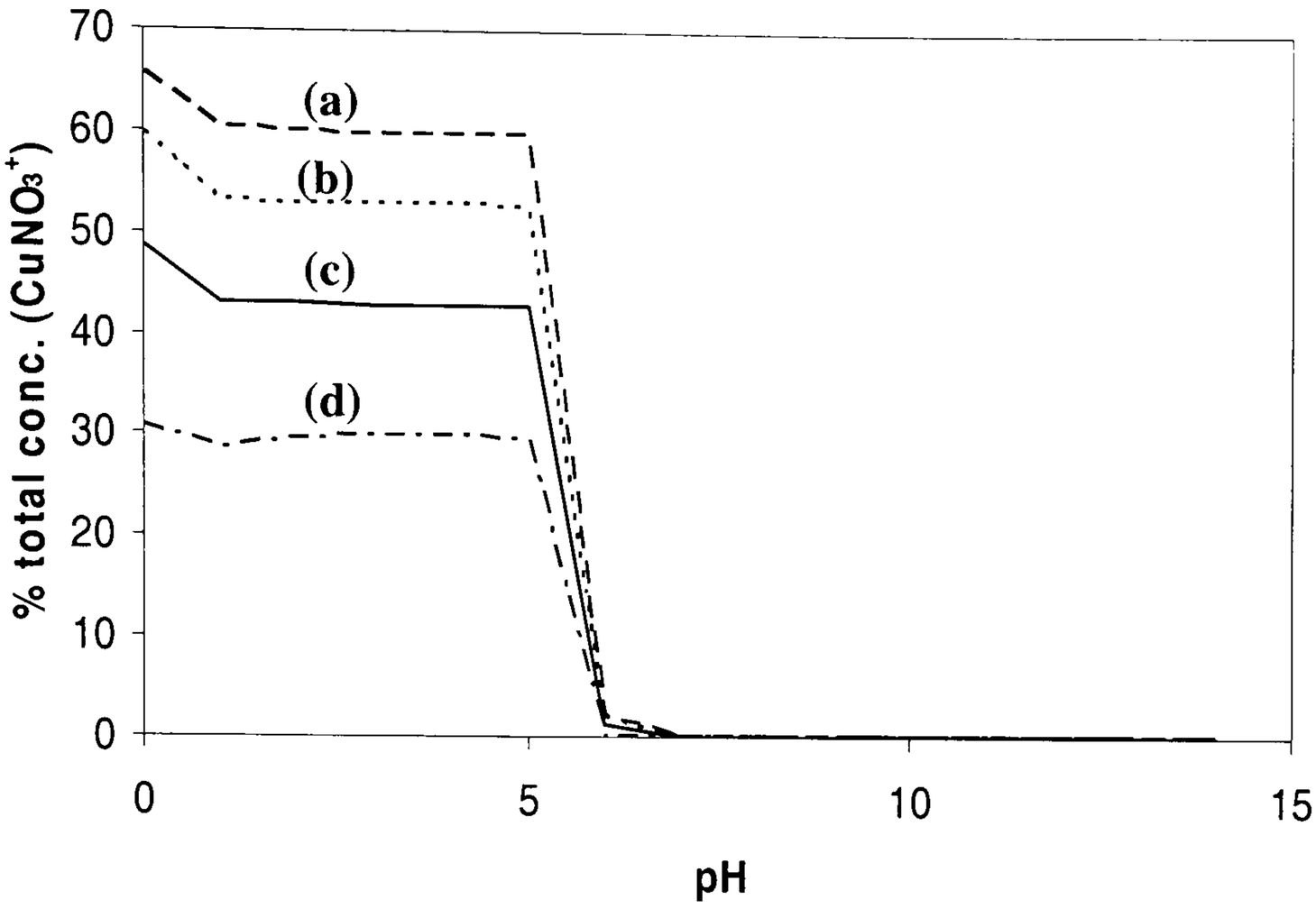

Figure 5-3 Variation in the proportion of $CuNO_3^+$ in a 0.01M Cu(II) solution with nitrate concentration (a) 2M (b) 1.5M (c) 1M (d) 0.5M NO_3^-

Apart from the differences in the dissolved ions, the solids that are predicted to precipitate differ between the two theoretical models. The reaction used for the Pourbaix plot is the precipitation of CuO from $CuNO_3^+$ ions; the MINEQL+ simulations show an extra solid phase, $Cu_2(OH)_3NO_3$, precipitating before CuO in the region 4<pH<6.5 (Figure 5-2). During the experiment it was observed that the precipitated solid was blue, most likely the hydrated $Cu(OH)_2$, rather than CuO. This agrees with the work of *Patterson et al* [5.3] who observed $Cu(OH)_2$ forming shortly after the addition of alkali. They found that the conversion of the $Cu(OH)_2$ to CuO by dehydration was complete after one month.

The MINEQL+ simulations were corrected for ionic strength, as well as taking into account the additional dissolved ions and solids, and thus extra reactions. The precipitation pH from MINEQL+ runs compares well with the experimental results (Figure 5-4), showing a better match than the predictions using the equilibrium shown in Eq (5.1). This result indicates that the additional species and correction for ionic strength are probably the main reasons for the discrepancy between the Pourbaix equilibria and the empirical results.

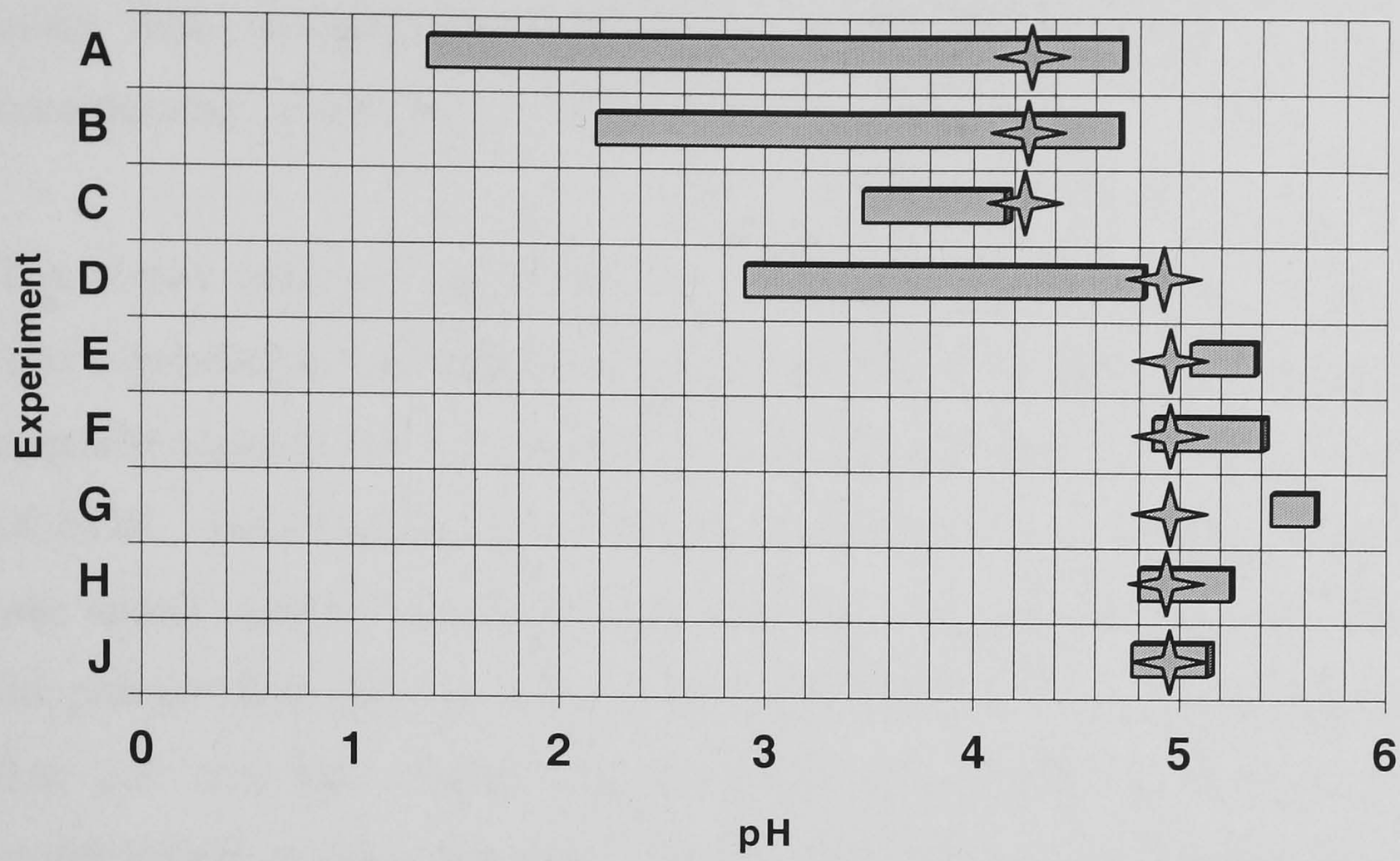

Figure 5-4 Graphical representation of copper/nitrate precipitation results compared to MINEQL+ runs (bars = experimental, stars = MINEQL+ prediction)

The other factors that may have caused discrepancies between the theoretical predictions and experimental results are the sample dilution, kinetics, errors in weighing and pH measurement. The addition of KOH to the metal salt sample increased the volume, thus leading to a decrease in the metal ion concentration. The equilibrium (Eq. 5.1) shows that this change will increase the precipitation pH of the solution. New values were calculated for each sample, but the changes were insignificant. Similarly, the effect of the possible errors in weighing the metal salts on the precipitation pH were compared to the accuracy of the pH probe and found to be insignificant. However, the slow kinetics of the precipitation reaction were found to be significant and the experimental method was therefore changed (Section 3.1.2).

5.2 Iron

Precipitation experiments were also carried out on the iron/nitrate system. The nitrate concentration in the waste was estimated as 1M (Appendix A). For comparison with the Pourbaix diagram, the iron concentration had to be less than 1M so the reaction products did not significantly alter the nitrate concentration. The iron concentrations used were therefore 0.1M and 0.01M; this was added as ferric ions. The sensitivity of the precipitation pH to the nitrate concentration was also tested by

using NO_3^- concentrations of 0.5M, 1M and 2M whilst keeping the Fe(III) concentration at 0.01M.

The results from the iron/nitrate precipitation experiments are shown in Table 5-2. The experimental precipitation pH is shown as a range. In this case, a rough approximation of the precipitation pH was initially found by the incremental addition of KOH. Four samples of the metal salt in solution were then prepared and KOH was added until the sample pH spanned that previously determined. For example, if the precipitation pH was found to be about 2, the samples would have values of 1.5, 2.0, 2.5, and 3.0. These samples were then left for a week to allow for the equilibration of slow reactions. At this point some of the samples had precipitated; the pH at which this happened was between that of the dissolved sample with the highest pH, and the precipitated sample with the lowest pH. The table also shows two theoretical predictions. Firstly, in order to verify the Pourbaix diagrams the precipitation pH was calculated using the appropriate reaction and its equilibrium expression:

$$2FeNO_3^{2+} + 3H_2O \rightarrow Fe_2O_3 + 2NO_3^- + 6H^+$$

$$\log[FeNO_3^{2+}] = -0.8470 + \log[NO_3^-] - 3pH \tag{5.2}$$

For the Pourbaix estimation, the activities of the metal and anion were assumed to be equal to their concentrations. The theoretical prediction from MINEQL+ is also shown in the table.

	[Fe] / M	[NO_3^-] / M	precipitation pH range	theoretical (Pourbaix)	theoretical (MINEQL+)
A	0.01	1	2.6 - 2.8	0.38	0.95
B	0.01	1	2.5 - 3.0	0.38	0.95
C	0.01	0.5	2.6 - 3.2	0.28	0.90
D	0.01	2	2.6 - 2.9	0.49	1.0
E	0.1	1	<1.8	0.051	0.60
F	0.1	1	1.7 - 1.8	0.051	0.60

Table 5-2 Iron/nitrate precipitation pH results

The results show that the precipitation pH increases as the metal ion concentration decreases, as predicted by the equilibrium expression shown as Eq (5.2). However, the ferric ions precipitate at much higher pH than was predicted by either the Pourbaix or MINEQL+ estimations. The differences between the experimental results and predictions based on the Pourbaix diagrams are shown graphically in Figure 5-5.

Figure 5-5 Graphical representation of iron/nitrate precipitation results compared to Pourbaix predictions (bars = experimental, stars = theory)

It is possible that these discrepancies are caused by extra solid or dissolved phases, or large differences between the concentration and activity, as they are thought to be for the copper. However, from experimental observation, the colour changes in the solution do not represent the changes predicted from the equilibrium reaction. This shows the precipitation of Fe_2O_3 (red/brown solid) directly from $FeNO_3^{2+}$ (presumably colourless[1]). However, during the addition of KOH, the solution turns from colourless to pale yellow and on to red/brown before precipitating the red/brown solid. *Dousma and de Bruyn* [5.4] have attributed this colouration to a multi-stage hydrolysis-precipitation process that involves the formation of polymers before the precipitation of a solid phase. The formation of large polymers is a slow

---

[1] The solution is colourless when freshly mixed; other Fe(III) ions are colourless in solution

process, which could explain the difference between the experimental and predicted precipitation pH.

The MINEQL+ predictions for iron precipitation do not match the iron/nitrate experimental results, although they are slightly closer than those predicted using the $FeNO_3^{2+}/Fe_2O_3$ equilibrium. The simulations showed that Fe^{3+}, as well as $FeNO_3^{2+}$, is in solution and precipitates as Fe_2O_3. Also, the ionic strength of these solutions is higher than the maximum value for which MINEQL+ can correct (I_c=0.5M). Differences between the predicted and experimental results could therefore arise because the ionic strength can affect the solubility products. A comparative graph showing the difference between the experiments and MINEQL+ predictions is shown in Figure 5-6.

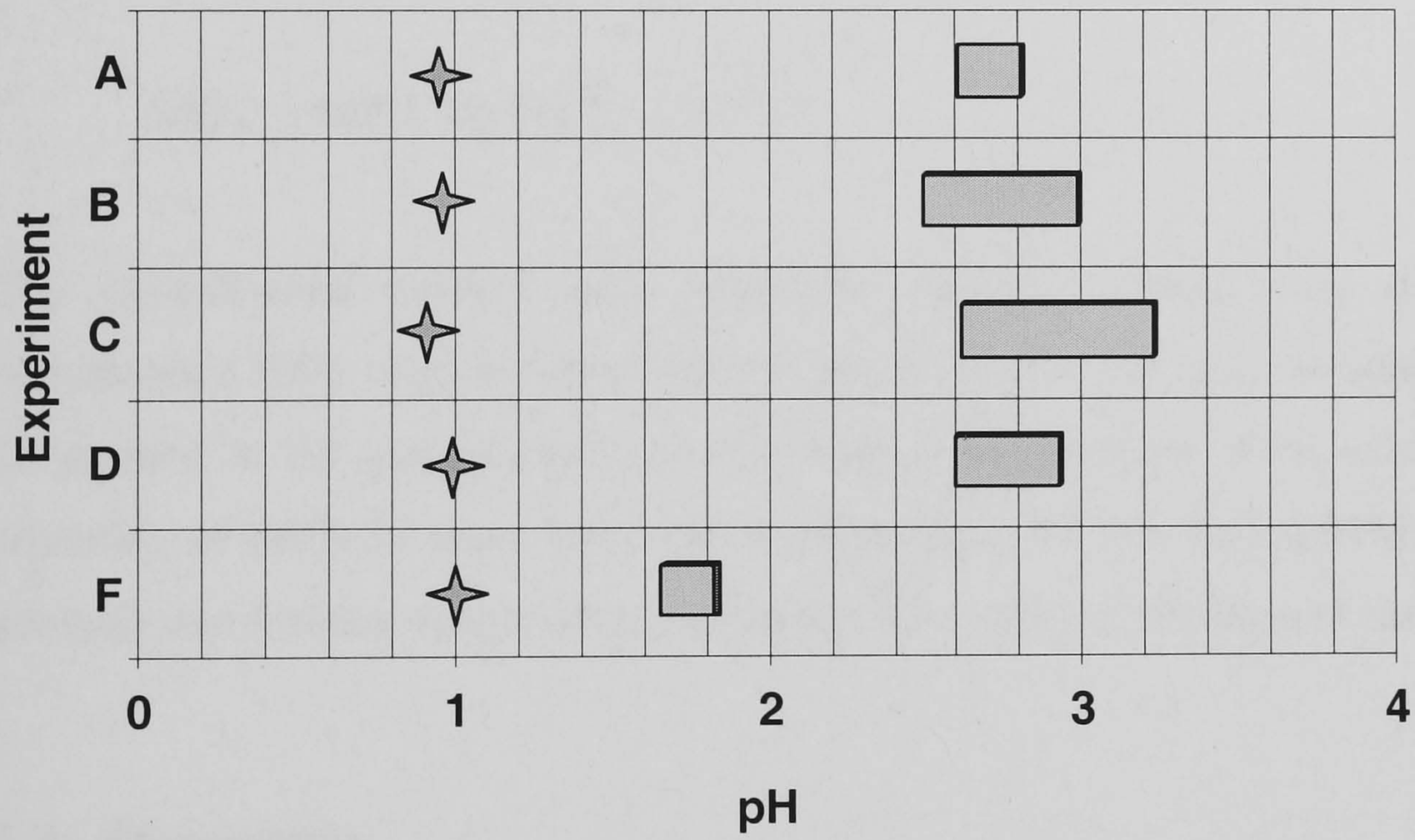

Figure 5-6 Graphical representation of iron/nitrate results compared to MINEQL+ runs (bars = experimental, stars = MINEQL+ prediction)

5.3 Tin

The verification of the Pourbaix plot for tin/chloride was attempted using the method for the copper and iron precipitation experiments. In this case the concentration of the anion (Cl^-) was 5M, as it was determined in Section 4.1.2 that a high concentration of chloride was required to dissolve tin. The metal concentration was

again kept low, so that the reaction products do not significantly alter the anion concentration.

The initial precipitation experiment was carried out on a sample of 0.01M $SnCl_4$ + 5M HCl. The theoretical precipitation pH of this sample, calculated using the appropriate reaction from the Pourbaix diagram was -0.024.

$$SnCl_6^{2-} + 2H_2O \rightarrow SnO_2 + 6Cl^- + 4H^+$$

The experiment was repeated twice, but no sustained precipitation was seen across a pH range of -0.28 to 13.18. A possible reason for the solubility is that SnO_2 may be formed when KOH first contacted the sample; but was then converted back to $SnCl_4$ due to the high concentration of chloride ions.

$$SnO_2 + 4HCl \Leftrightarrow SnCl_4 + 2H_2O$$

The experimental method was therefore changed. SnO_2 was dissolved in concentrated HCl, to give a maximum value of tin that can exist in solution, as the Cl^- content in the concentrated solution increases the region of tin solubility. The solubility of SnO_2 in conc. HCl was determined to be less than 0.01M. A yellow solution was formed, with a white precipitate that settled at the base of the beaker.

5.4 Discussion

The experimental precipitation results for copper show that the theoretical pH predictions, especially when all the species in solution are taken into account, model the actual behaviour well. In practical terms, this result means that copper will stay in solution and pass through the filtration stage to be electrodeposited, as long as the solution is maintained in the pH range determined in Chapter 4. The NO_3^- concentration does not appear to affect the solubility of Cu(II). Therefore, process variations that cause changes in the nitrate concentration are unlikely to disrupt the recovery scheme.

On examination of the Pourbaix diagram, the pH at which iron precipitates could be seen to be dependent on its concentration and the solution potential. These experimental results show that iron, in the form of ferric ions, precipitated at much higher pH than was predicted theoretically. In terms of the recovery process, this is an advantage because the iron is likely to stay in solution, passing through the filtration stage with the copper, rather then being distributed between the solid SnO_2 and dissolved Cu(II). However the ferric ions precipitate at a lower pH than copper, so the initial stage of acid recovery should be limited by the precipitation pH of Fe(III), rather than that of Cu(II).

The results from the tin dissolution experiments imply that the proposed stage of the recovery process, where SnO_2 is dissolved in HCl before electrodeposition, may not be practicable. Concentrated acid would be required to dissolve sufficient tin to ensure the deposition is efficient. Heating the acid will increase the tin solubility, but is not a realistic solution due to safety considerations. Tin(IV) oxide could be a product without further processing; it is used in the manufacture of lead crystal glass, as an opacifier in ceramic glaze and in gas sensors [5.5]. The possibility of this route would depend on the purity and particle size distribution of the recovered oxide and that required for a given application.

5.5 References

5.1 C. Kerr, *Transactions of the Institute of Metal Finishing*, **82**(B7-B12, Part1-2): (2004)

5.2 O. Sohnel and J. Garside, *Precipitation: Basic Principles and Industrial Applications*, Butterworth Heinemann, (1992)

5.3 J. W. Patterson, R. E. Bolce and D. Marani, *Environmental Science and Technology*, **25**(10): 1780-1787 (1991)

5.4 J. Dousma and P. L. De Bruyn, *Journal of Colloid and Interface Science*, **56**(3): 527-539 (1976)

5.5 N. N. Greenwood and A. Earnshaw, *Chemistry of the Elements*, Elsevier, (1997)

6 ELECTROCHEMICAL CHARACTERISATION

The feasibility of the recovery process proposed by *Kerr* [6.1] has been determined by the thermodynamic analysis (Chapter 4) and precipitation experiments (Chapter 5). The project now focussed on an individual stage in this process: copper electrodeposition. The aim of these experiments was to determine whether it is possible to deposit copper from an acidic nitrate solution with reasonable efficiency, and to find the effect of the stripping additives and iron/tin on the efficiency. The nitrate species in the stripping solution have been reported to reduce concurrently with copper deposition, decreasing the current efficiency [6.2].

In order to characterise the waste, two sets of experiments were performed: cyclic voltammograms and anodic stripping experiments. From these experiments, the deposition potential of the copper, the copper limiting current and the deposition efficiency were to be determined. The experiments were initially carried out with only copper and nitrate in solution. This indicated the feasibility of recovering copper ions from the additive free solution. Subsequent experiments with additives and other metals were carried out and compared with these results to evaluate their effect on the copper deposition.

6.1 Cyclic Voltammograms

Cyclic voltammograms were initially used to determine the deposition potential and limiting current of the copper in nitrate solutions, and the effect of metal and anion concentrations on these parameters. The experiments were carried out in solutions with and without the additives. These experiments were also used to estimate the current efficiency of deposition, and how this could be affected by nitrate and copper concentration.

The copper/nitrate solutions were made using $Cu(NO_3)_2$, acidified with HNO_3. To simulate some of the additives, $Fe(NO_3)_3$ and SnO_2 were added to the solutions. The concentrations are detailed in Section 3.2.1.

6.1.1 Copper / Nitrate i-E data

The cyclic voltammograms for Solution 1 (0.3M Cu^{2+}, 1M NO_3^-) at three rotational speeds are shown in Figure 6-1. The potential was initially scanned in the cathodic direction from 0 to -600mV; the current shows almost linear response to potential. The scan was then reversed; the response follows that from the cathodic scan until the potential is at -100mV, when the current becomes more negative. The current then rises gradually into the anodic section, reaches a maximum and falls suddenly to zero.

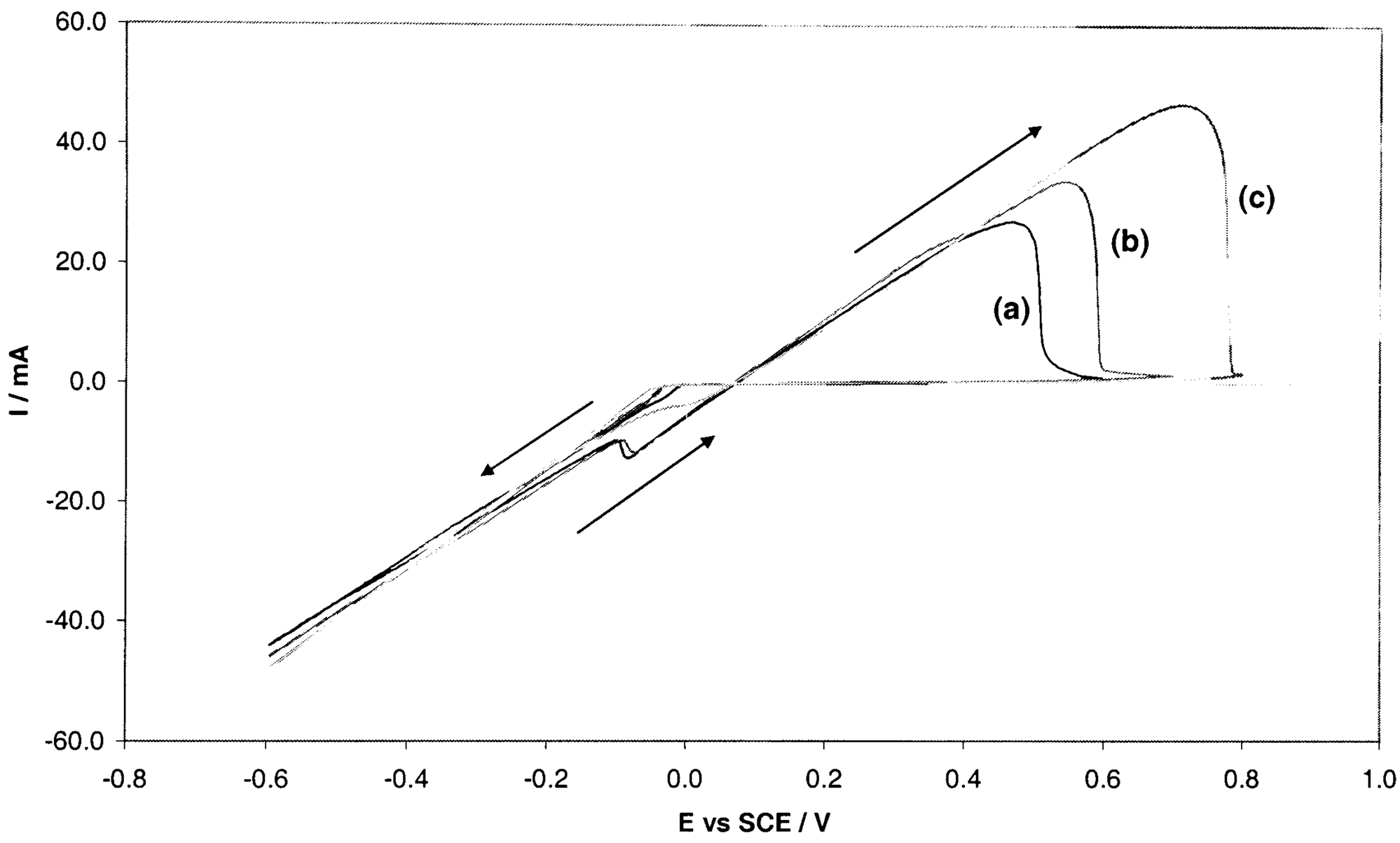

Figure 6-1 Cyclic voltammogram for 0.3M Cu^{2+} + 1M NO_3^- (Solution 1), scan rate 10mVs^{-1} (a) 200rpm (b) 600rpm (c) 800rpm

The traces for all rotational speeds overlie in the cathodic section. The i-E data are linear, rather than exponential in both the cathodic and anodic direction, indicating that the solution resistance is significant, or that multiple reactions are occurring on the electrode surface. No copper limiting currents are observed, possibly because they are masked by the reduction of NO_3^- and H^+, which is examined in more detail later.

The copper dissolution currents in the anodic section of the scan show a peak because the current decreases sharply when all the copper on the gold electrode has

been removed. Although no clear copper limiting current was observed during the cathodic scan, more copper is deposited at higher rotation speeds, as shown by the larger area under the anodic stripping curve. This clearly indicates that mass transfer affects the copper deposition rate. As the deposition current was independent of rotational speed, it can be said the deposition efficiency is greater at higher rotational speeds.

The voltammogram for Solution 4 (0.03M Cu^{2+}, 1M NO_3^-) is shown in Figure 6-2; the shape of the response is similar to that from Solution 1 for all rotational speeds. For example, the value of the deposition current at -600mV is -48mA for Solution 1 compared to -40mA for Solution 4. However, the maximum anodic stripping current is much lower, and the stripping is complete at lower anodic overpotentials. As a comparison it can be seen that at 800rpm the maximum anodic dissolution current is +45mA for Solution 1 versus +25mA for Solution 4. This decrease in anodic current indicates that the majority of the current during deposition is used for the reduction of other oxidised species, presumably NO_3^-, rather than copper deposition.

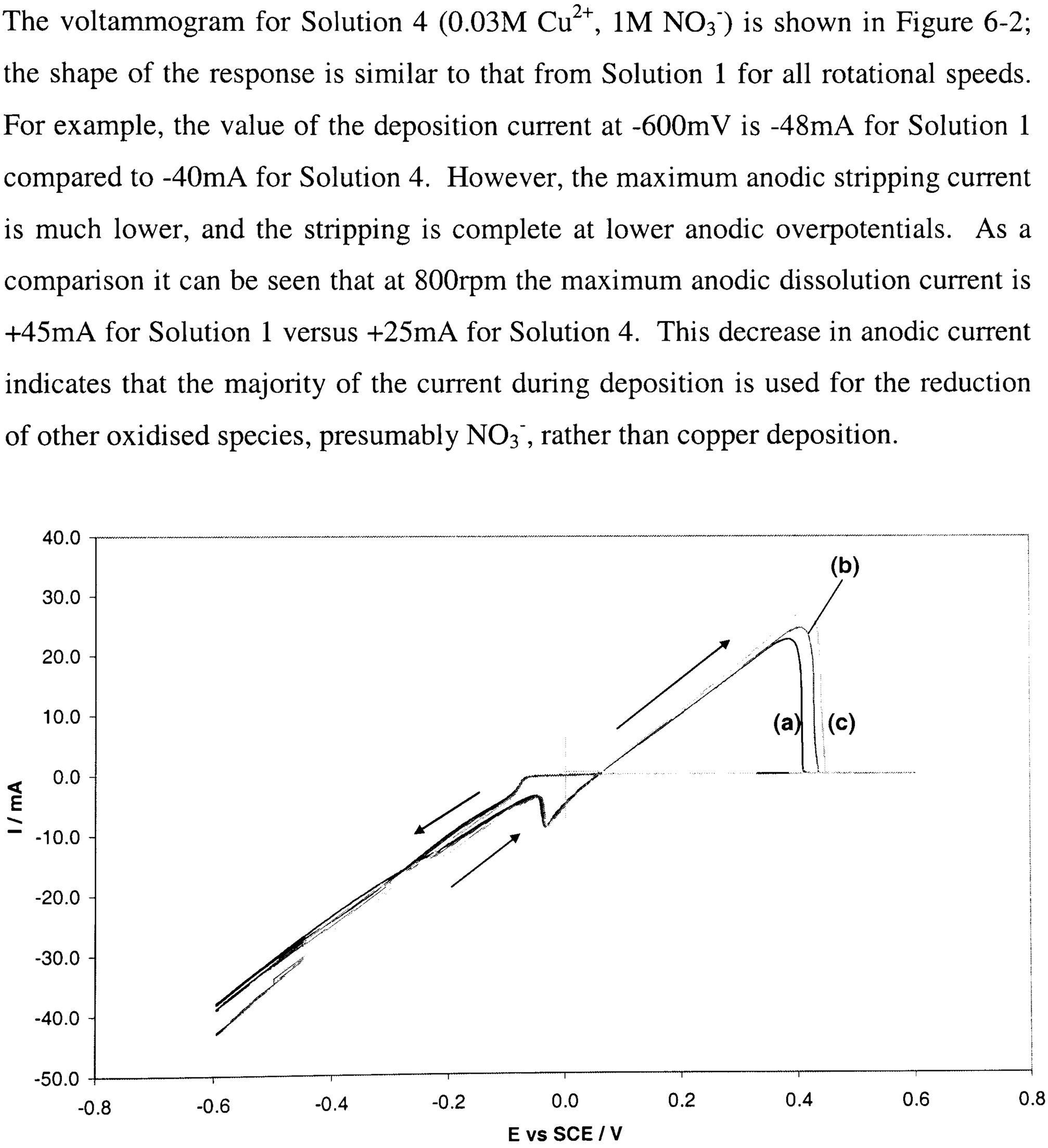

Figure 6-2 Cyclic voltammogram for 0.03M Cu^{2+} + 1M NO_3^- (Solution 4), scan rate 10mVs^{-1} (a) 600rpm (b) 800rpm (c) 1000rpm

Further cyclic voltammetry confirmed the dominance of the nitrate reduction current during cathodic polarisation. For example, scans with 0.1M NO_3^- and Cu(II) concentrations of 0.03M and 0.003M in Figure 6-3 and Figure 6-4 (corresponding to Solutions 5 and 8 from the matrix in Table 3.1) show similar currents. At -600mV, the cathodic currents are -14mA for Solution 5 compared to -15mA for Solution 8. Comparing the polarisation data for both solutions, we see that the raw i-E data arise mostly from NO_3^- and H^+ reduction and this reduction current masks the copper deposition current.

On further examination of the anodic stripping section of the i-E data it is clear that the amount of copper deposited from Solution 5 is greater for than for Solution 8. More copper was deposited from the solution with the higher copper concentration indicating the copper deposition may be mass transfer controlled, although this cannot be observed from the cathodic polarisation data.

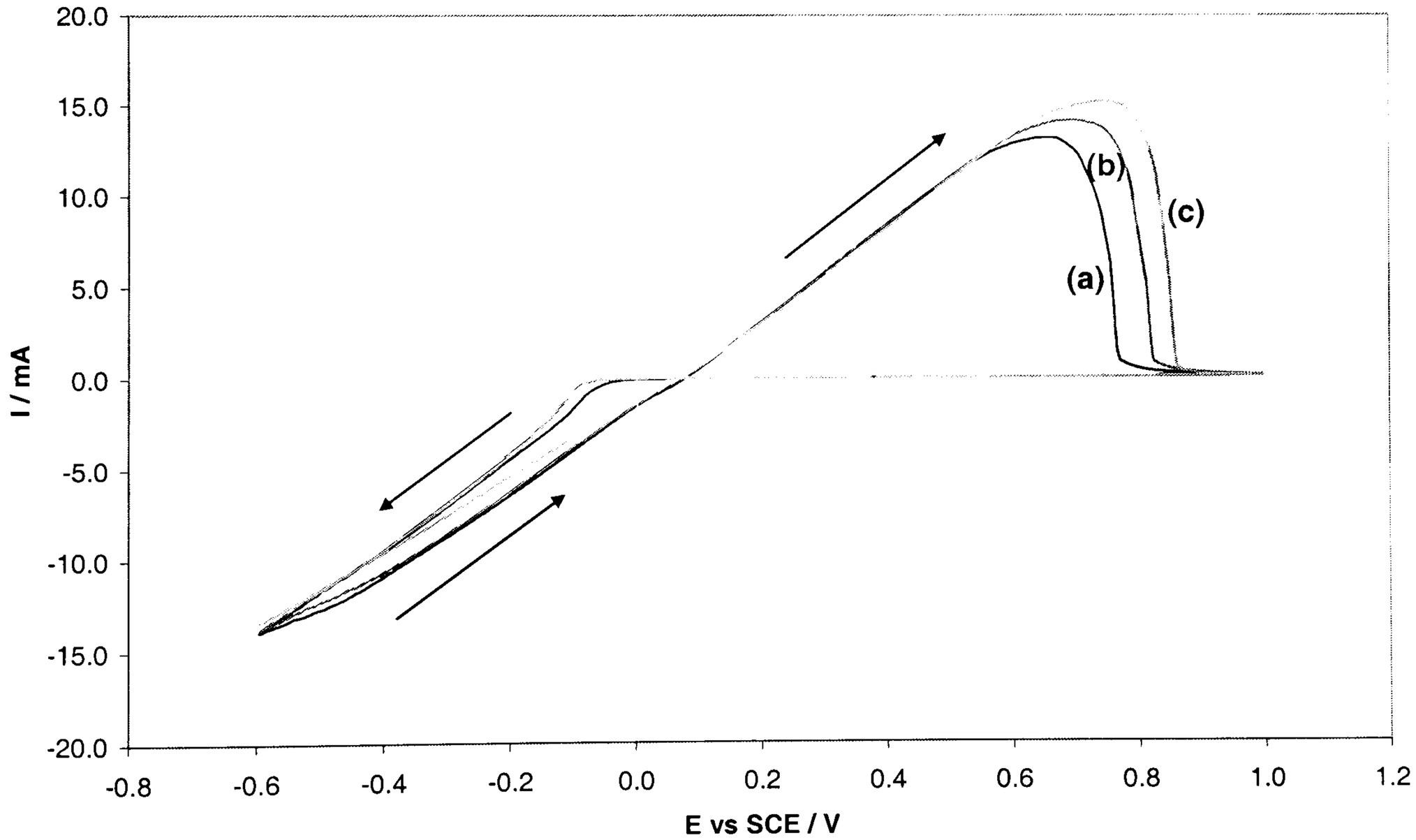

Figure 6-3 Cyclic voltammogram for 0.03M Cu^{2+} + 0.1M NO_3^- (Solution 5), scan rate 10mVs^{-1} (a) 600rpm (b) 800rpm (c) 1000rpm

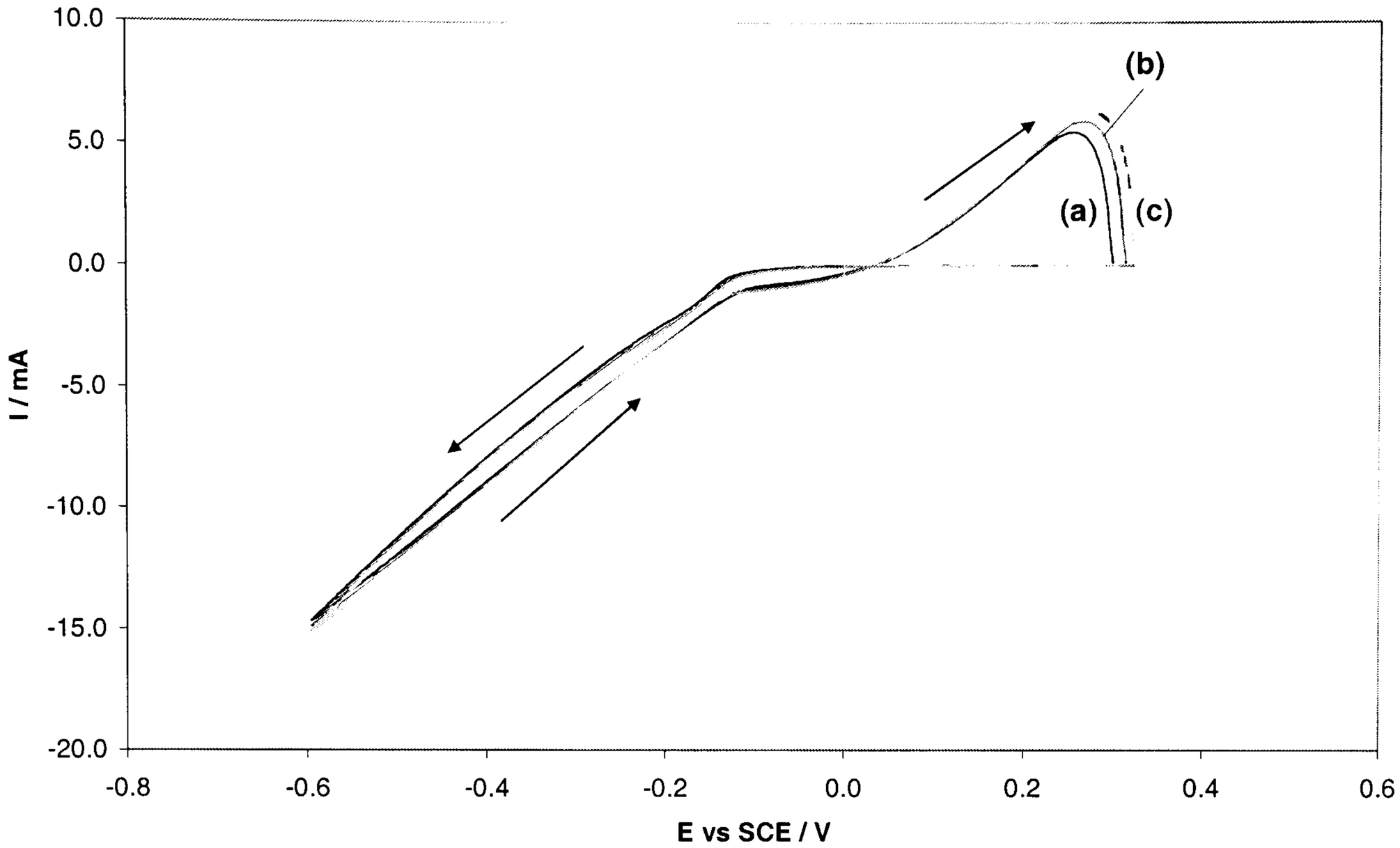

Figure 6-4 Cyclic voltammogram for 0.003M Cu^{2+} + 0.1M NO_3^- (Solution 8), scan rate 10mVs-1 (a) 600rpm (b) 800rpm (c) 1000rpm

As shown above, the reduction of nitrate contributes to the total current of the system. Since this masks the limiting current for copper and alters the deposition potential of the copper, an attempt was made to subtract the NO_3^- contribution from the total current. Therefore, cyclic voltammograms of solutions containing only nitrate electrolytes were obtained; these were then subtracted from the polarisation curves for copper/nitrate solutions to obtain the current for copper deposition.

Initially cyclic voltammograms were taken for nitric acid concentrations of 1M, 0.1M, and 0.01M. However, these solutions contain more hydrogen ions than the solutions for copper deposition, as part of the nitrate in the copper solution comes from $Cu(NO_3)_2$. To find if the additional H^+ ions affect the background electrolyte traces, a set of experiments using 1M KNO_3, instead of 1M HNO_3, was also carried out.

The polarisation curves for 1M HNO_3 and 1M KNO_3 can be seen in Figure 6-5 and Figure 6-6 respectively. The scans were carried out across negative potentials only, because nitrogen in the form of nitrate has a valency of +5; this is the highest state

that nitrogen can take, so it cannot be oxidised further and no current will be seen in the anodic region.

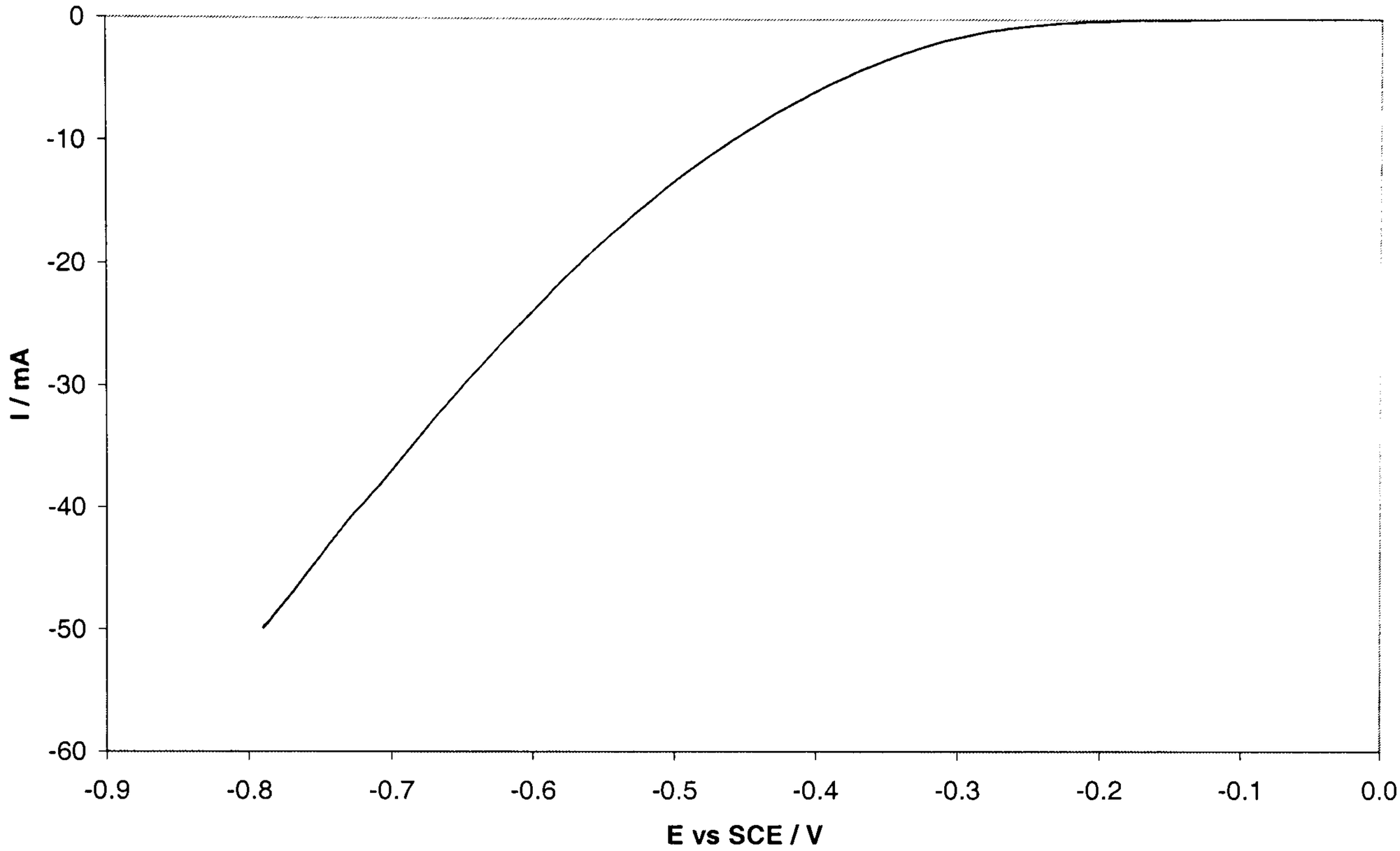

Figure 6-5 Linear sweep in 1M HNO_3, scan rate 10mVs^{-1}, 800rpm

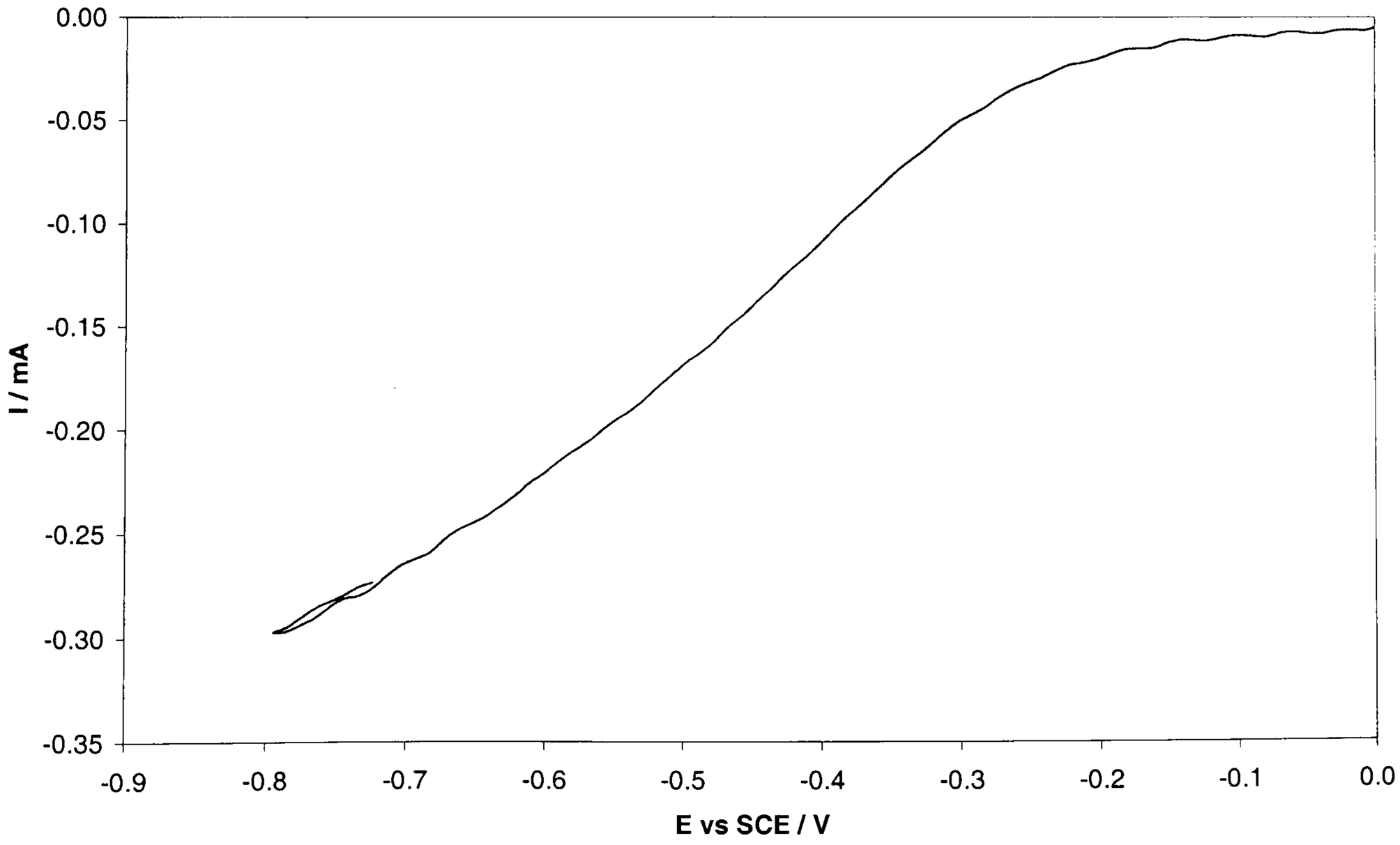

Figure 6-6 Linear sweep in 1M KNO_3, scan rate 10mVs^{-1}, 800rpm

From the comparison of the experiments on 1M HNO_3 and 1M KNO_3, it can be said the current due to the NO_3^- ion reduction is relatively small compared to the reduction current obtained when the NO_3^- ions are combined with H^+ ions. This agrees with the work of *Pletcher and Poorabedi* [6.3], who determined that nitric acid was the electroactive species in nitrate reduction. Therefore, to correctly determine the current due to the reduction of ionic species other than Cu(II), the scans were repeated with a mixture of HNO_3 and KNO_3 keeping the ratio H^+/NO_3^- the same as for the solutions detailed in Table 3.1. For example, Solution 1 contains 0.3M Cu^{2+} and 1M NO_3^-; it was made using $Cu(NO_3)_2$, with added HNO_3 to increase the nitrate concentration to 1M. The actual solution composition was therefore 0.3M $Cu(NO_3)_2$ and 0.4M HNO_3. To make up the background electrolyte the solution must contain 1M NO_3^- ions and 0.4M H^+ ions. The molar quantities required are therefore 0.6M KNO_3 + 0.4M HNO_3.

The scans for 1M NO_3^- (0.4M HNO_3 + 0.6M KNO_3) and 0.1M NO_3^- are shown in Figure 6-7 and Figure 6-8 respectively. It can be seen that the current due to the electrolyte increases sharply at potentials more negative than -0.6V for the lower nitrate concentration. If copper was to be deposited at potentials more negative than -0.6V, the current due to the electrolyte reduction would form a larger proportion of the overall deposition current. Since this was the lower potential limit for the cyclic voltammograms in copper solutions, the effect of 0.1M NO_3^- on copper deposition is small. However, for the larger NO_3^- concentration of 1M, the contribution of the nitrate on the total current during the deposition is significant.

The reduction potential of the nitrate was found from these figures to be -128mV and +32mV for solutions containing 1M and 0.1M NO_3^- respectively. As one of the aims of these experiments was to find the deposition potential of the copper, the current due to nitrate reduction at -200mV was found from the figures below (the cathodic current on all the copper voltammograms became significant below this potential). The currents from nitrate reduction at -200mV were found to be -0.143mA for 1M NO_3^- and -0.117mA for 0.1M NO_3^- solutions.

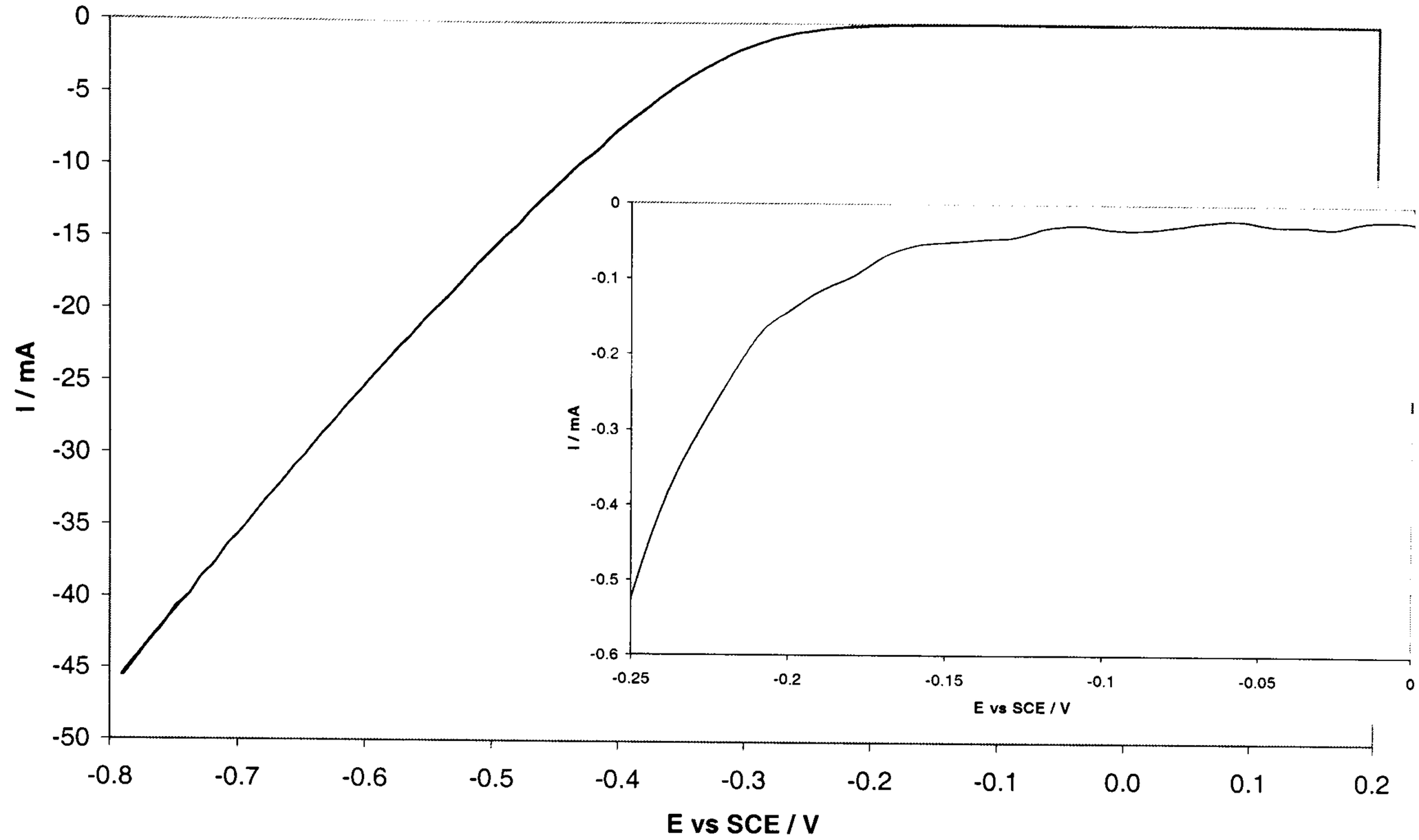

Figure 6-7 Linear sweep in 0.4M HNO_3 + 0.6M KNO_3, scan rate 10mVs^{-1}, 800rpm (inset, zoom in region 0 to -0.25V

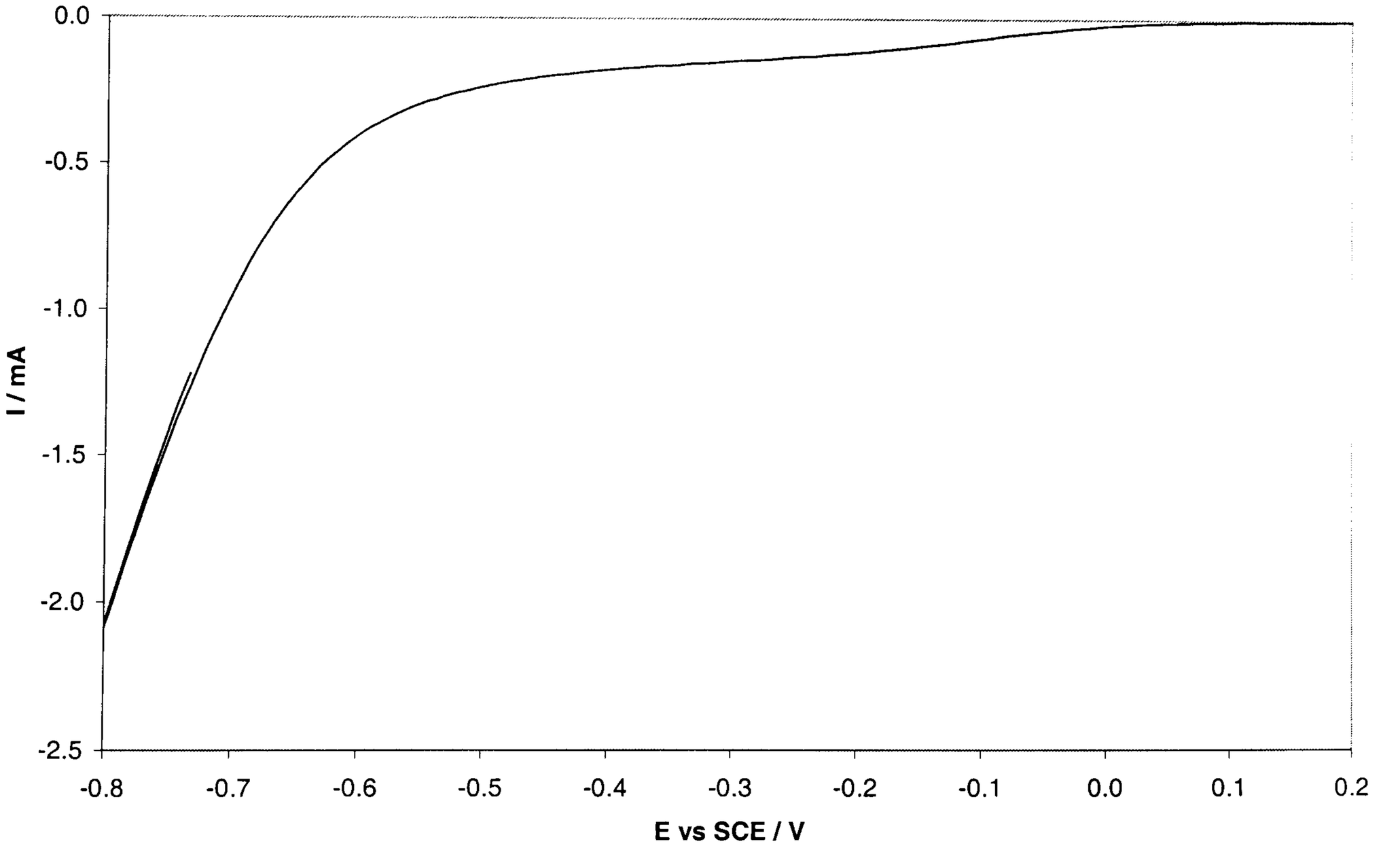

Figure 6-8 Linear sweep in 0.04M HNO_3 + 0.06M KNO_3, scan rate 10mVs^{-1}, 800 rpm

An attempt to subtract the current due to the background electrolyte, and thus find the copper limiting current, was made. The results from Solutions 1 and 4 are shown

in Figure 6-9. The deposition current apparently reaches a maximum and then decreases towards the end of the scan, the reason for which is unclear. The maximum current is -24mA for Solution 1 and -19mA for Solution 4. Since these solutions have the same NO_3^- concentration, but the Cu(II) concentration in Solution 4 is 0.03M and in Solution 1 is 0.3M, there is some dependence on material transfer, as was observed during the anodic stripping.

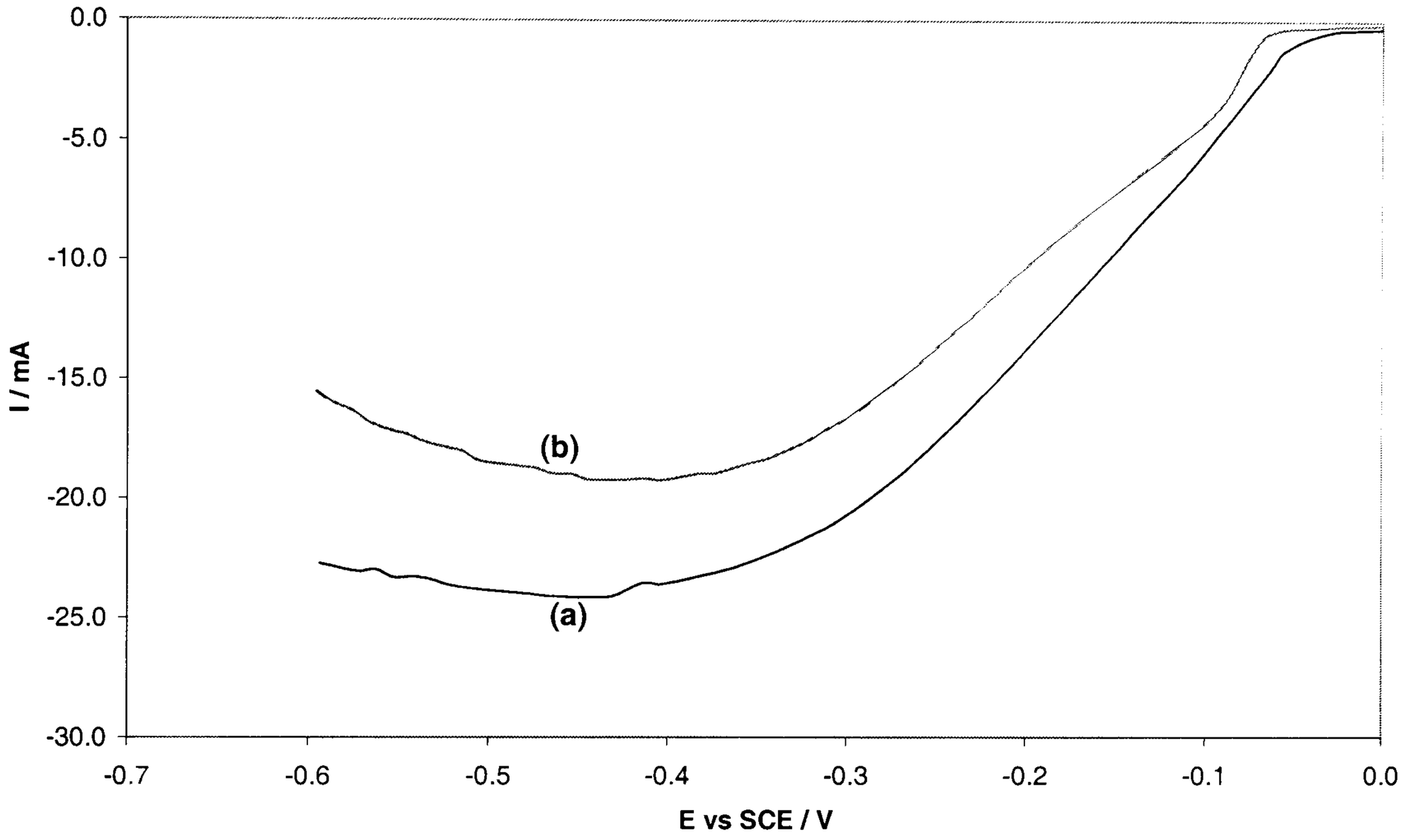

Figure 6-9 Total current obtained by subtraction of background current 0.4M HNO_3 + 0.6M KNO_3, scan rate 10mVs^{-1}, 800rpm (a) 0.3M Cu, 1M NO_3 (Sol 1) (b) 0.03M Cu, 1M NO_3 (Sol 4)

The extent to which material transfer governs copper deposition can be estimated by comparing the values of maximum current. If the Cu(II) was mass transfer limited, the maximum current should be proportional to the copper concentration. The maximum current for 0.03M (Solution 4), derived from the value for 0.3M (Solution 1), should therefore be -2.4mA. As this is not the case, the copper deposition and nitrate reduction reactions are thought to have some dependence on each other.

Figure 6-10 shows the typical result when the current due to nitrate reduction is subtracted from any of the other solutions (Solutions 5, 7, 8, 9). The current increases steadily across the potential range and does not reach a maximum. As

there has been no appearance of limiting currents for these solutions, the deposition appears to be at least partially kinetically controlled up to -600mV.

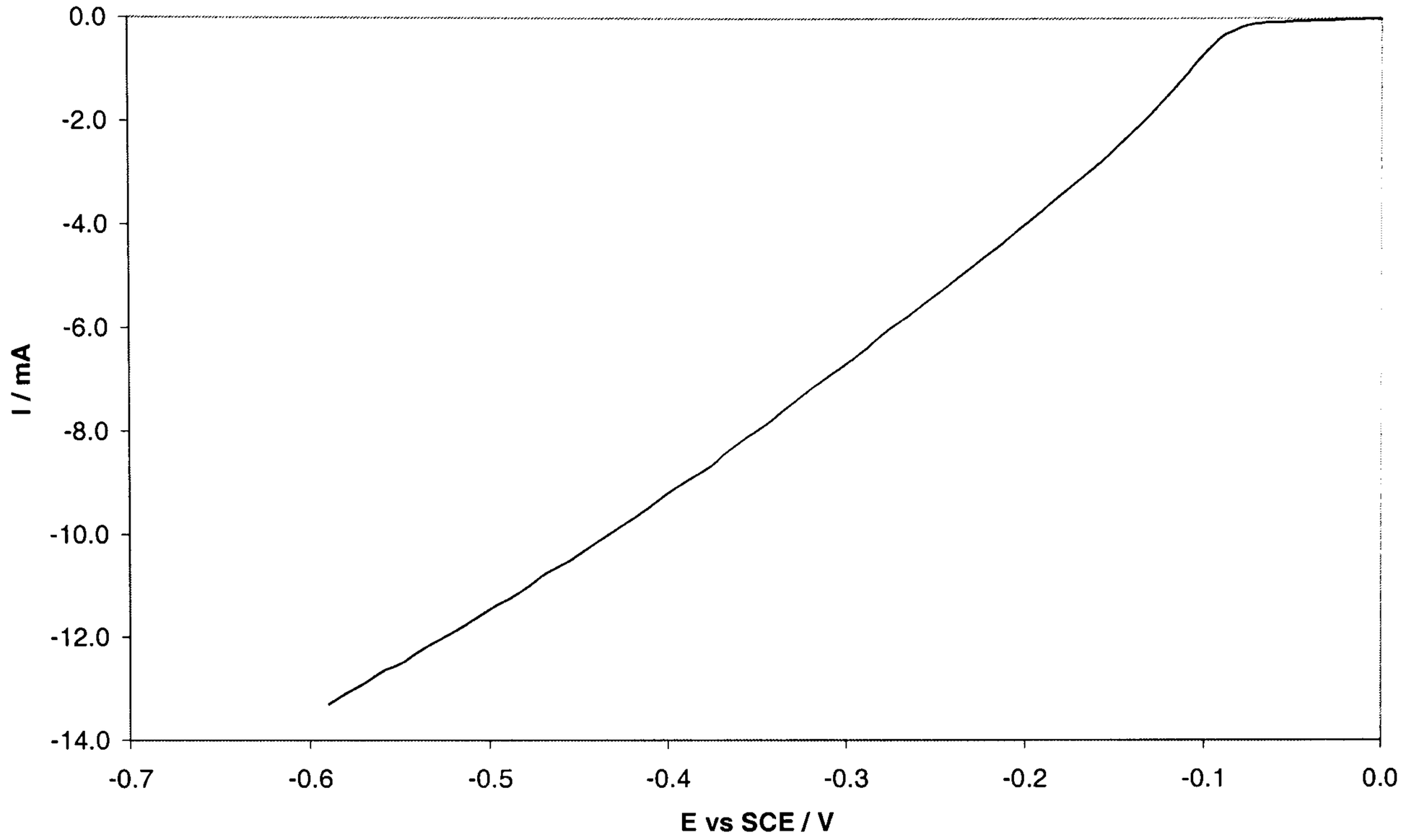

Figure 6-10 Total current obtained by subtraction of background current 0.04M HNO_3 + 0.06M KNO_3 from 0.03M Cu, 0.1M NO_3 (Sol 5), scan rate 10mVs^{-1}, 800rpm

The electrochemical reversible potential for copper deposition cannot be determined from cyclic voltammetry because this is a mixed potential system (cf. Section 2.2), with copper, nitrate and hydrogen reduction occurring concurrently. The electrode potentials where a substantial cathodic current was noted are shown in Table 6-1 for each solution. These mixed potentials correspond to a current of -2mA. This current was significantly larger than the current due to nitrate reduction up to -200mV, which ensured copper was being reduced. The potential for Solution 9 (0.003M Cu, 0.01M NO_3^-) is more negative then -200mV. Thus, the current due to nitrate reduction at -317mV was determined to be -0.105mA, a small fraction of -2mA.

[Cu] \ [NO_3^-]	1	0.1	0.01
0.3	-63mV		
0.03	-80mV	-132mV	
0.003	-163mV	-176mV	-317mV

Table 6-1 Deposition potentials for copper from nitrate solutions vs SCE (experimental)

It can be seen from Table 6-1 that the deposition potential becomes more negative as the Cu(II) and NO_3^- concentrations decrease. These trends can be compared to the Nernst equation (Eq. 6.1) for the relevant reaction (Figure 4-1). The equilibrium expression shows that the deposition potentials will become more negative as the copper concentration decreases, but become more positive with decreasing nitrate concentration.

$$E = 0.325 + 0.02955 \cdot \log \frac{[CuNO_3^+]}{[NO_3^-]} \qquad \text{(Eq. 6.1)}$$

The deposition potentials for each solution concentration, calculated as equilibrium potentials from Eq. (6.1), are shown in Table 6-2. These potentials are more positive than those found during the voltammetry. The differences between the theoretical and experimental potentials are probably due to the mixed potential system; the experimentally determined potentials have current contributions from nitrate and hydrogen reduction, as well as the copper reduction. Also, more than one copper species is expected to be in solution (Section 4.2.1), so the mixed potential will include the reduction of $CuNO_3^+$, Cu^{2+} and $Cu(NO_3)_{2\ (aq)}$. The experimentally determined values will be used as a comparison for solutions containing iron/tin ions and the industrial additives.

[Cu] \ $[NO_3^-]$	1	0.1	0.01
0.3	+68mV		
0.03	+38mV	+68mV	
0.003	+8mV	+38mV	+68mV

Table 6-2 Deposition potentials for copper vs SCE calculated from Eq. (6.1)

Estimation of Deposition Efficiency from i-E Data

The copper deposition efficiency, as a function of Cu(II) and NO_3^- concentration, was calculated by dividing the charge used for stripping the copper from the electrode, by the charge used during the deposition in the cyclic voltammetry experiments. The assumption that the charge used to strip the copper is equal to that

used to deposit it is valid because no other oxidation reactions can occur in these solutions at the potentials where copper is stripped. The results from this analysis, carried out on all solutions can be seen in Table 6-3.

[Cu] \ [NO_3]	1	0.1	0.01
0.3	69.6	-	-
0.03	22.3	71.8	-
0.003	1.7	12.2	32.0

Table 6-3 Copper deposition efficiencies from cyclic voltammetry data (%)

From these data it can be said that the efficiency of the copper deposition increases with increasing Cu(II) concentration and decreasing NO_3^- concentration, which is in agreement with previous results for copper deposition [6.4, 6.5]. Looking in more detail at the results for 1M nitrate, it can be seen that at the maximum copper concentration (0.3M), the current efficiency is ~70%. However, the efficiency decreases to 22% after the concentration of copper has been reduced to a tenth of its original value. If the concentration of copper is further reduced, the efficiency falls to 2% at 0.003M copper (~200ppm). The results indicate that for 1M NO_3^-, recovering copper to the discharge limit of 1.5ppm (10^{-5}M) is unlikely to be economical.

Correction of Cathodic Potential

As some of the solutions used in this set of experiments are fairly dilute, it is possible that there is uncompensated resistance between the working and reference electrodes. This resistance would cause a potential drop between the two electrodes.

In order to estimate the errors in the i-E data due to uncompensated ohmic drop through the solution, the conductivity of all the solutions was calculated using Kohlrausch's law of independent migration of ions. The ohmic drop ($I_{cell}R_s$) between the reference electrode and cathode at -600mV was then calculated (Section 3.2.4).

The results are shown in Table 6-4, where the final column shows the percentage of the applied potential that is used in passing current through the solution.

Solution	κ (calc) / S m^{-1}	R_s / Ω	$I_{cell}R_s$ / mV	$(I_{cell}R_s$ / -600)*100
1	24.35	0.435	-20.88	3.48
4	40.33	0.263	-10.52	1.75
5	2.44	4.34	-60.76	10.1
7	41.93	0.253	-9.62	1.60
8	4.03	2.63	-39.45	6.58
9	0.244	43.43	-217.15	36.2

Table 6-4 Solution conductivity, ohmic drop and percentage of potential used across solution resistance

The correction of the cathodic potential due to ohmic drop between the cathode and reference electrode is only necessary at high potentials and for solutions containing low ionic concentrations. The results from the above calculations show that resistance compensation is not required for Solutions 1, 4 and 7. However, the cyclic voltammograms for Solutions 5, 8 and 9 could have been significantly distorted at high cathodic overpotentials. The $I_{cell}R_s$ component was therefore subtracted from each potential step in the cyclic voltammogram for Solution 9 (the worst case). This is shown as Figure 6-11. Although the cathodic potentials have reduced, the overall shape of the voltammogram has not significantly changed; the cathodic portion is still almost linear, and the stripping peak is clearly seen at anodic potentials.

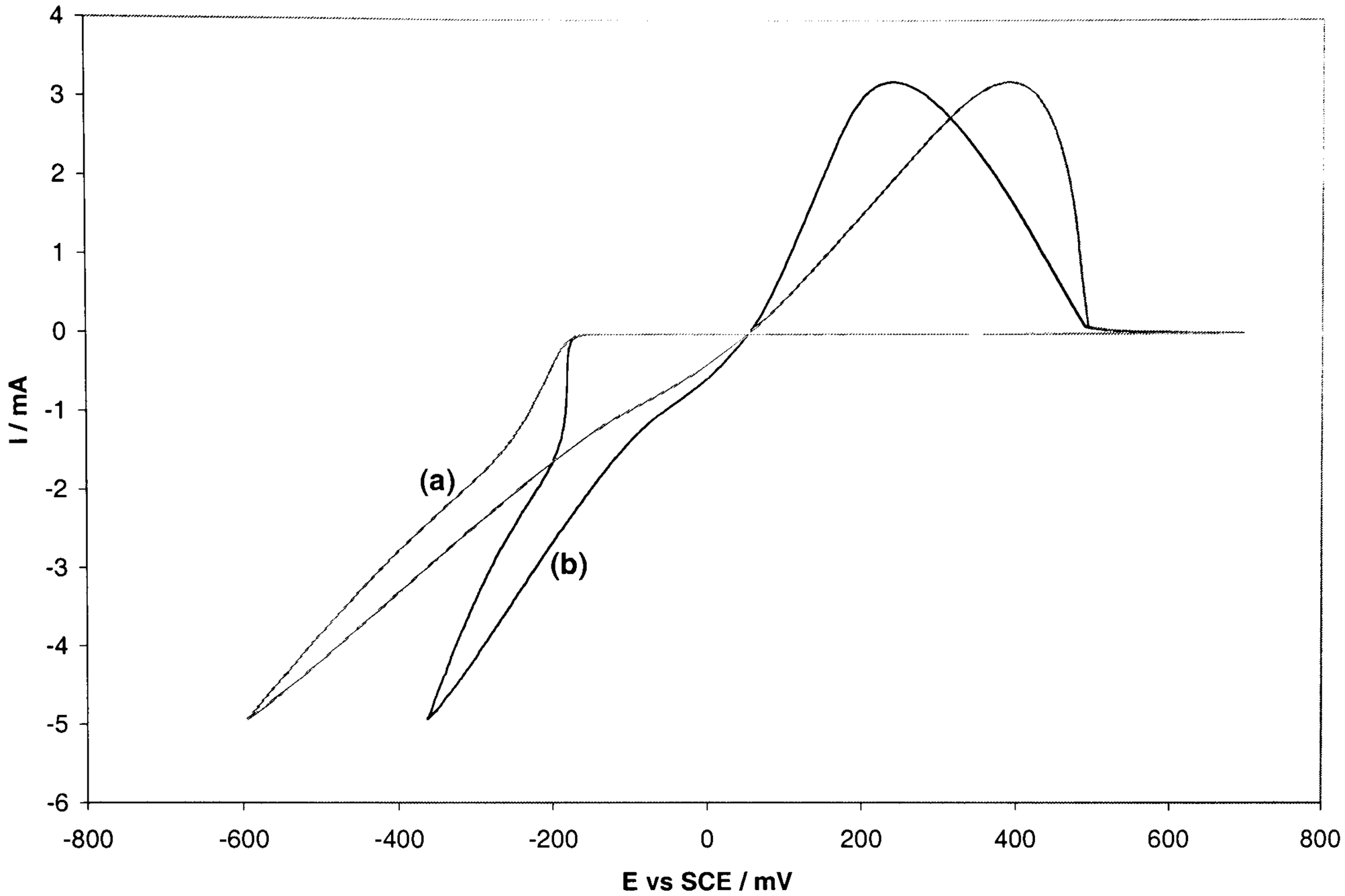

Figure 6-11 Cyclic voltammogram for 0.003M Cu, 0.01M NO_3^- (Solution 9), scan rate 10mVs^{-1}, 800rpm (a) without and (b) with solution resistance compensation

The calculated values of the solution conductivity were checked by measuring the conductivity of Solutions 1 and 9. These measured conductivities were 14.66 and 0.229 Sm^{-1} for Solution 1 and 9 respectively. The measured value for Solution 1 is lower than the calculated value of 24.35 Sm^{-1}; this was expected because the equation used for the calculations is only strictly valid for dilute solutions [6.6]. Solution 9 showed better agreement because the concentration of Cu(II) and NO_3^- ions are low. Using the measured value for Solution 1, the percentage of the applied potential used across the solution was 5.8%, still low enough to be disregarded.

The correction of the potential data does not affect the calculated efficiency values for copper deposition from these solutions. The only change is in the potential range over which the efficiency was calculated. Therefore, the decision on which solutions could be used for metal recovery was based on the values in Table 6-3.

6.1.2 Copper / Nitrate with the Addition of Iron / Tin: i-E Data

The cyclic voltammograms recorded for the copper/nitrate solutions were repeated with the addition of iron/tin, to determine the effect of these additional ions on the copper deposition efficiency. The amount of Fe(III) added to the solution was equal to the maximum concentration of Fe(III) detailed in the Tinsolv 2000 MSDS sheet [6.7]. This high concentration of Fe(III) was added in order to find the worst possible effect on the copper deposition efficiency. Tin oxide was added to produce a saturated solution. Details of the compositions are shown in Table 3.1.

The cyclic voltammogram for Solution 10 (0.3M Cu, 1M NO_3^-, 0.25M Fe(III), SnO_2) is shown in Figure 6-12. The shape of the voltammogram is similar to that for copper/nitrate solutions. The cathodic section of the curve shows linear response with no discernible copper limiting current. The anodic current rises as copper is dissolved from the electrode, falling suddenly when the copper has been removed.

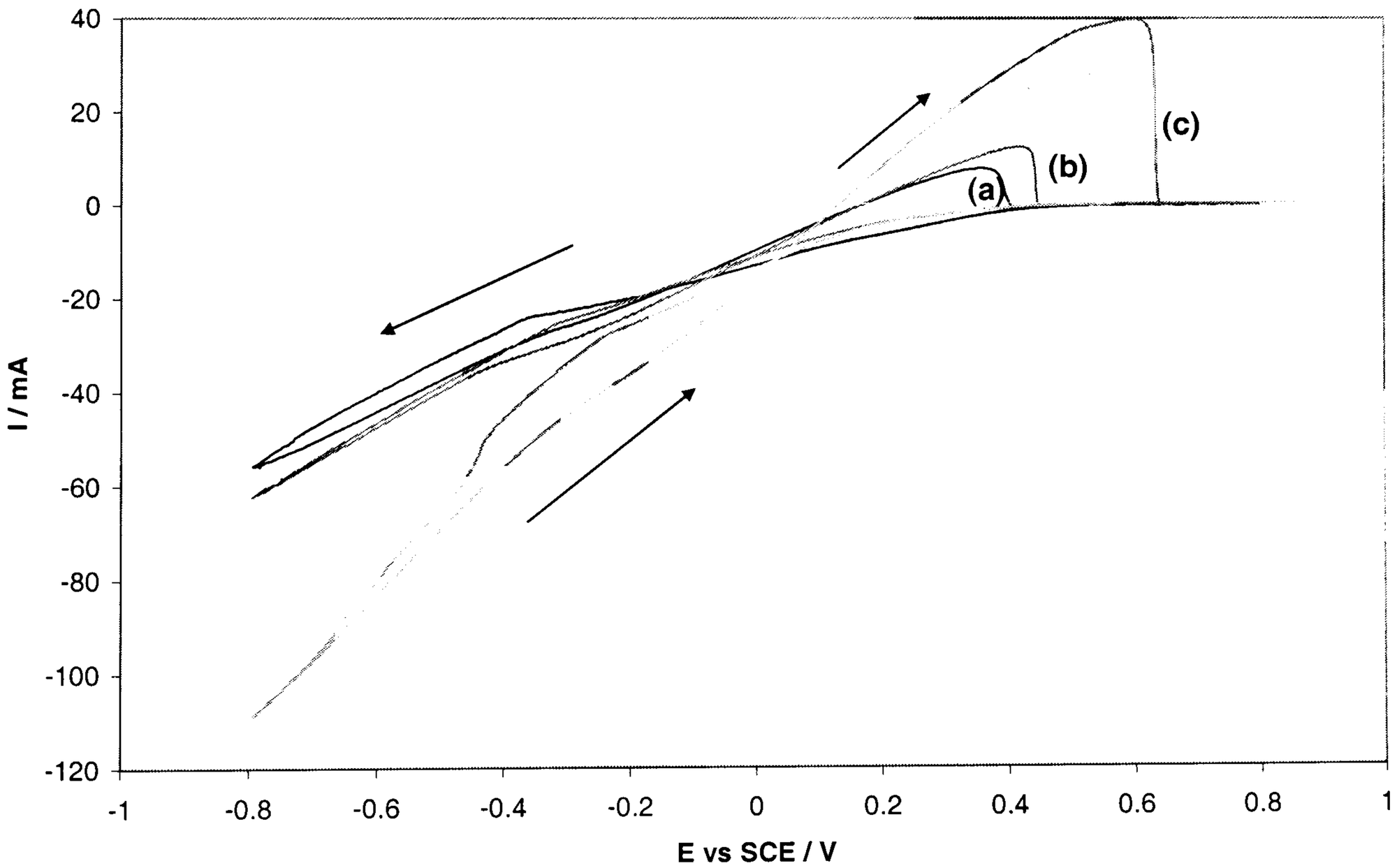

Figure 6-12 Cyclic voltammogram for 0.3M Cu^{2+} , 1M NO_3^-, 0.25M Fe^{3+}, Sn (Solution 10), scan rate 10mVs^{-1} (a) 600rpm (b) 800rpm (c) 1000rpm

Comparing the above voltammogram to the polarisation plot for the equivalent copper/nitrate solution without iron/tin (Solution 1, Figure 6-1), it can be seen that

when ferric ions are added to the solution the current becomes cathodic at more positive potentials. For example, at a rotation speed of 800 rpm, the current reaches -2mA at -63mV for Solution 1 and +303mV for Solution 10. The cathodic current at these positive potentials could be due to the reduction of Fe(III) to Fe(II).

$$Fe^{3+} + e^{-} \rightarrow Fe^{2+}$$

The ferric ion reduction should occur at a standard potential of +0.529mV vs SCE [6.8]. Therefore, it is expected that the reduction of Fe(III) occurs before Cu(II) and will mask the reduction potential for Cu(II), thus influencing the overall polarisation data. The flattening of the curves at -400mV is probably due to the appearance of an Fe(III) limiting current.

From Figure 6-12, the value of the current at -600mV for a rotation speed of 800rpm, is found to be -47mA. This current is very similar to that obtained from Solution 1 (-48mA), indicating that the reduction current at these cathodic potentials is still predominantly controlled by the nitrate/hydrogen content of the solution, rather than the reduction of copper, iron or tin. However, unlike the i-E data for solutions containing only copper/nitrate, the cathodic current increases with rotation speed.

After deposition from Solution 10 (Figure 6-12), the area under the anodic curve was found to be smaller than that from Solution 1 (Figure 6-1). This suppression of copper deposition is thought to be caused by the parasitic reduction of ferric ions; the concentration of tin is too low to produce a significant effect. This adverse effect of iron is in agreement with the work of *Das and Gopala Krishna* [6.9], who found that ferric ions reduced the efficiency of copper electrowinning in an open channel cell.

The effect of Fe(III) on Cu(II) reduction was confirmed for the other iron/tin containing solutions by carrying out polarisations. Figure 6-13 shows typical i-E data for the other solutions, in this case Solution 13 (0.03M Cu, 1M NO_3^-, 0.25M Fe(III), SnO_2). The cathodic section is still fairly linear, although the limiting currents for Fe(III) reduction start to appear at -350mV. The cathodic current increases as the rotational speed increases. However, during the anodic scan the

current only rises slightly above the current from the cathodic scan, showing that little copper had been deposited and then dissolved from the electrode.

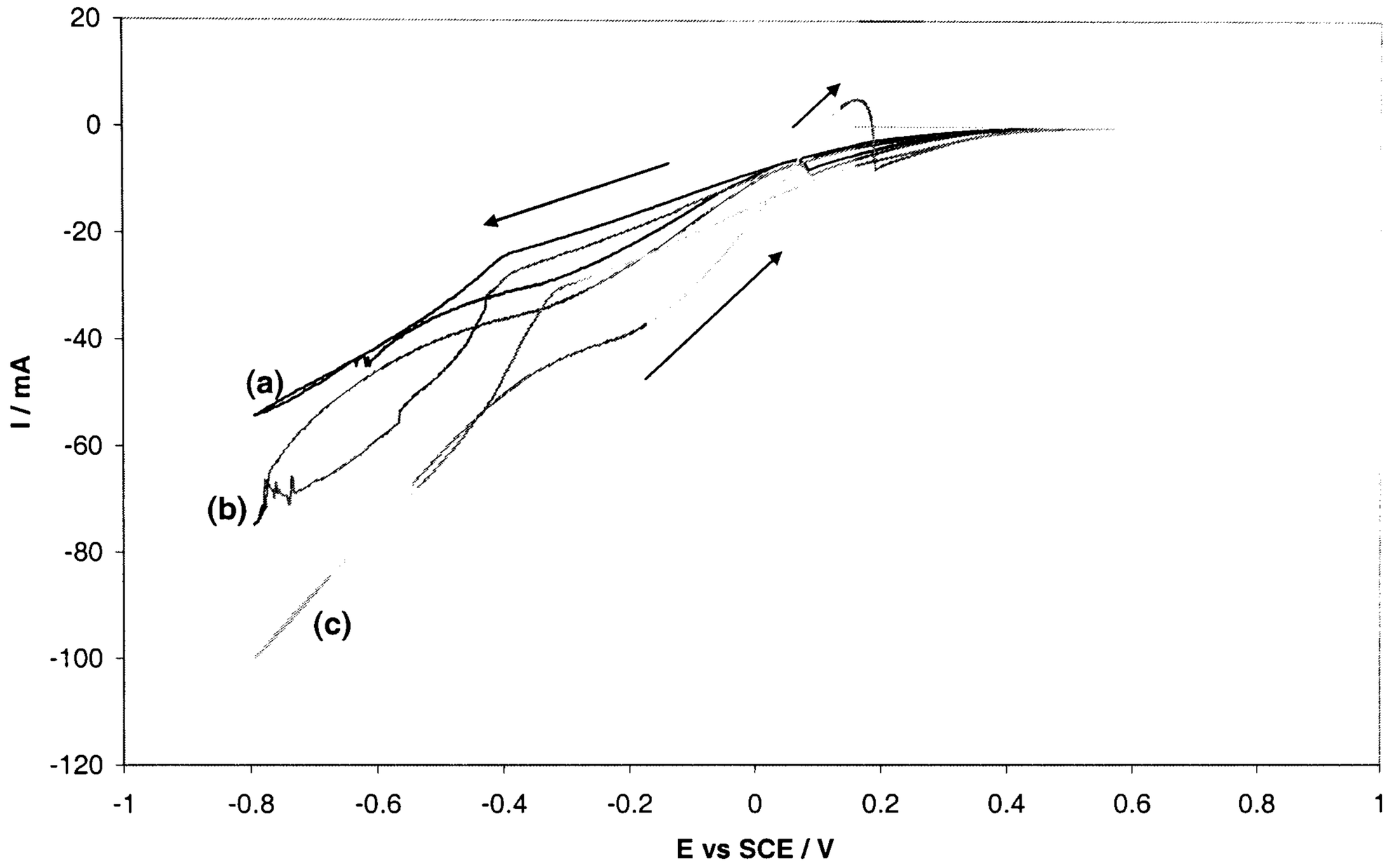

Figure 6-13 Cyclic voltammogram for 0.03M Cu, 1M NO_3^-, 0.25M Fe^{3+}, Sn (Solution 13), scan rate 10mVs^{-1} (a) 600rpm (b) 800rpm (c) 1000rpm

The deposition potential of copper from the iron/tin containing nitrate solutions has been shown to be masked by the Fe(III) reduction current. Therefore, an attempt was made to subtract the Fe(III) reduction current from the cyclic voltammograms to determine the Cu(II) reduction current.

Initially iron at a concentration of 1g/l (0.018M) was added to Solution 1. Figure 6-14 shows the polarisation curve for 0.018M Fe(III) in H_2SO_4. The iron reduction began at +500mV and attained a mass transport limited current of -2.5mA by -200mV. This curve was subtracted from that for 0.3M Cu + 1M NO_3^- + 0.018M Fe (Solution 1 + Fe). The results from this subtraction and a comparison with Solution 1 are shown in Figure 6-15.

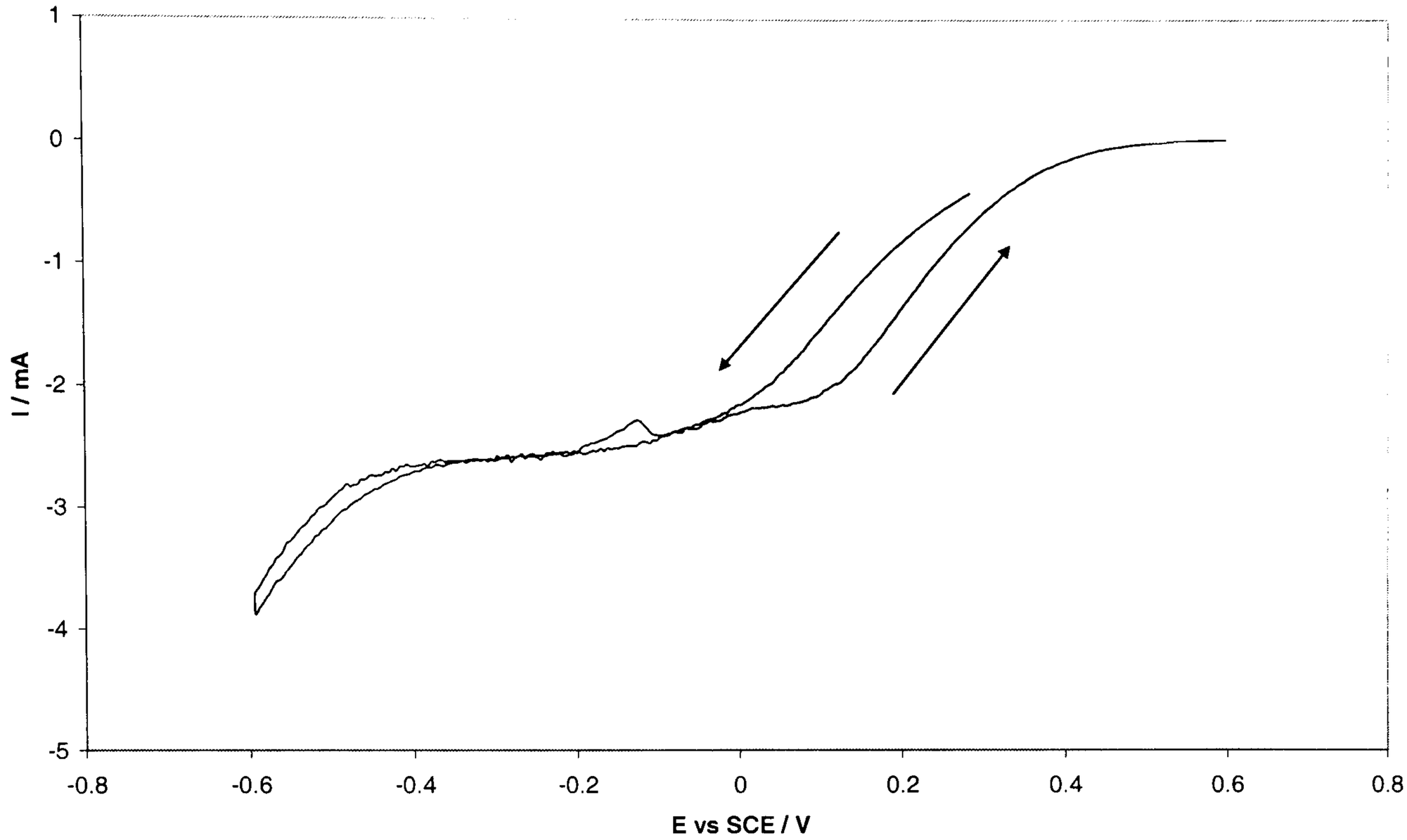

Figure 6-14 Cyclic voltammogram for 0.018M $Fe(NO_3)_3$ + 0.5M H_2SO_4, scan rate 10mVs^{-1}, 800rpm

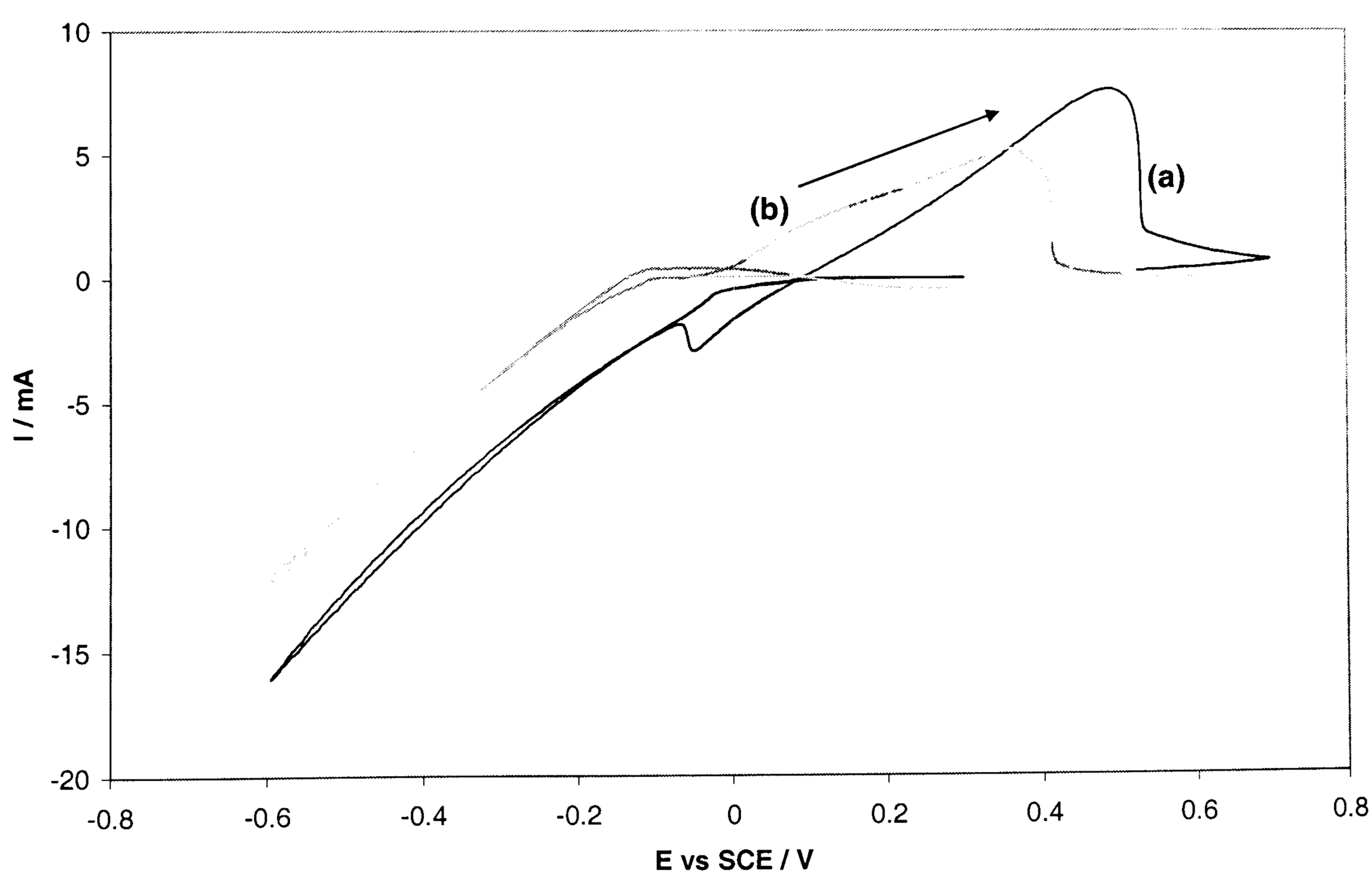

Figure 6-15 Cyclic voltammogram showing Fe data subtraction (a) 0.3M Cu + 1M NO_3^- (b) theoretical curve (0.3M Cu + 1M NO_3^- + 0.018M Fe) – (0.018M Fe + 0.5M H_2SO_4)

Figure 6-15 shows that the shape of the i-E data for 0.3M Cu(II), 1M NO_3^- (a) and the theoretical curve after ferric ion subtraction (b) are similar. However, both the reduction potential and the dissolution potential for the copper appear to be more negative on the theoretical curve. For Solution 1 (0.3M Cu, 1M NO_3^-), the Cu(II) reduction potential was estimated as -63mV, but for the subtracted curve the reduction occurs at -136mV. This potential shift implies that Fe(III) ions cause Cu(II) and NO_3^- to be reduced at more negative potentials.

In order to examine the effect of Fe(III) concentration on copper deposition, voltammograms of Solution 1 (0.3M Cu, 1M NO_3^-) with increasing quantities of Fe(III) were recorded. Figure 6-16 shows how the polarisation plots change with increasing concentration of $Fe(NO_3)_3$.

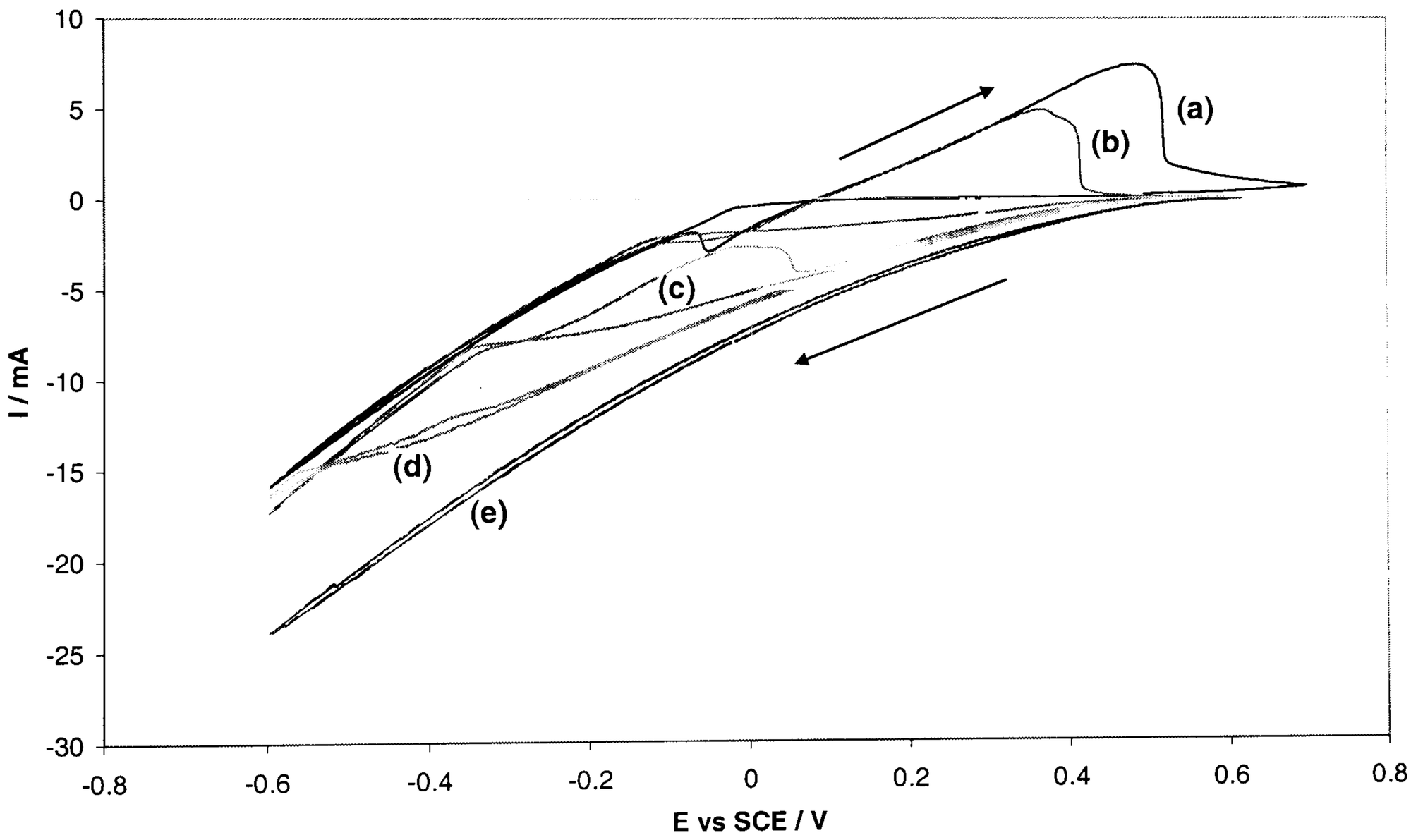

Figure 6-16 Cyclic voltammograms for 0.3M Cu, 1M NO_3^- + x g/l $Fe(NO_3)_3$, scan rate 10mVs^{-1}, 800rpm. Fe(III) conc. (a) 0 (b) 1 (c) 4 (d) 7 (e) 14g/l

As shown in Figure 6-16, the anodic currents associated with copper dissolution decrease as the Fe(III) concentration is increased, and disappear for Fe(III) concentrations of greater than 7g/l (0.125M). Therefore, at higher Fe(III) concentrations copper is not deposited from the solution. The Fe(III) limiting current is seen to increase, and appears at more negative potentials as the Fe(III)

concentration increases. For solutions containing less than 7g/l Fe(III), the i-E data for the Fe(III) containing solutions overlie the data for 0.3M Cu, 1M NO_3^- after a certain potential. This potential becomes more negative as the Fe(III) concentration is increased, for example at 1g/l Fe(III) (b) this potential is -100mV, and for 4g/l Fe(III) (c) it is -350mV. It is thought that copper is only deposited from the ferric containing copper/nitrate solutions at potentials more negative than this point, which could explain why no copper was deposited from the 14g/l Fe(III) solution. This shift in the Cu(II) reduction potential by ferric ions was also seen when the Fe(III) current was subtracted (Figure 6-15).

In addition to $Fe(NO_3)_3$, polarisation experiments were also carried out with $FeCl_3$ in the copper/nitrate solution, because the chloride is also used as a source of ferric ions in tin stripping solutions [6.10]. It can be seen from Figure 6-17, that the anodic currents for copper dissolution are absent for Fe(III) concentrations greater than 4g/l. Again, a limiting current plateau is observed for all ferric ion concentrations, which corresponds to the mass transfer limiting reduction current of ferric to ferrous ions. This is substantiated by the fact that the current plateau for 14g/l Fe (-35mA) is approximately double that for 7g/l Fe (-18mA).

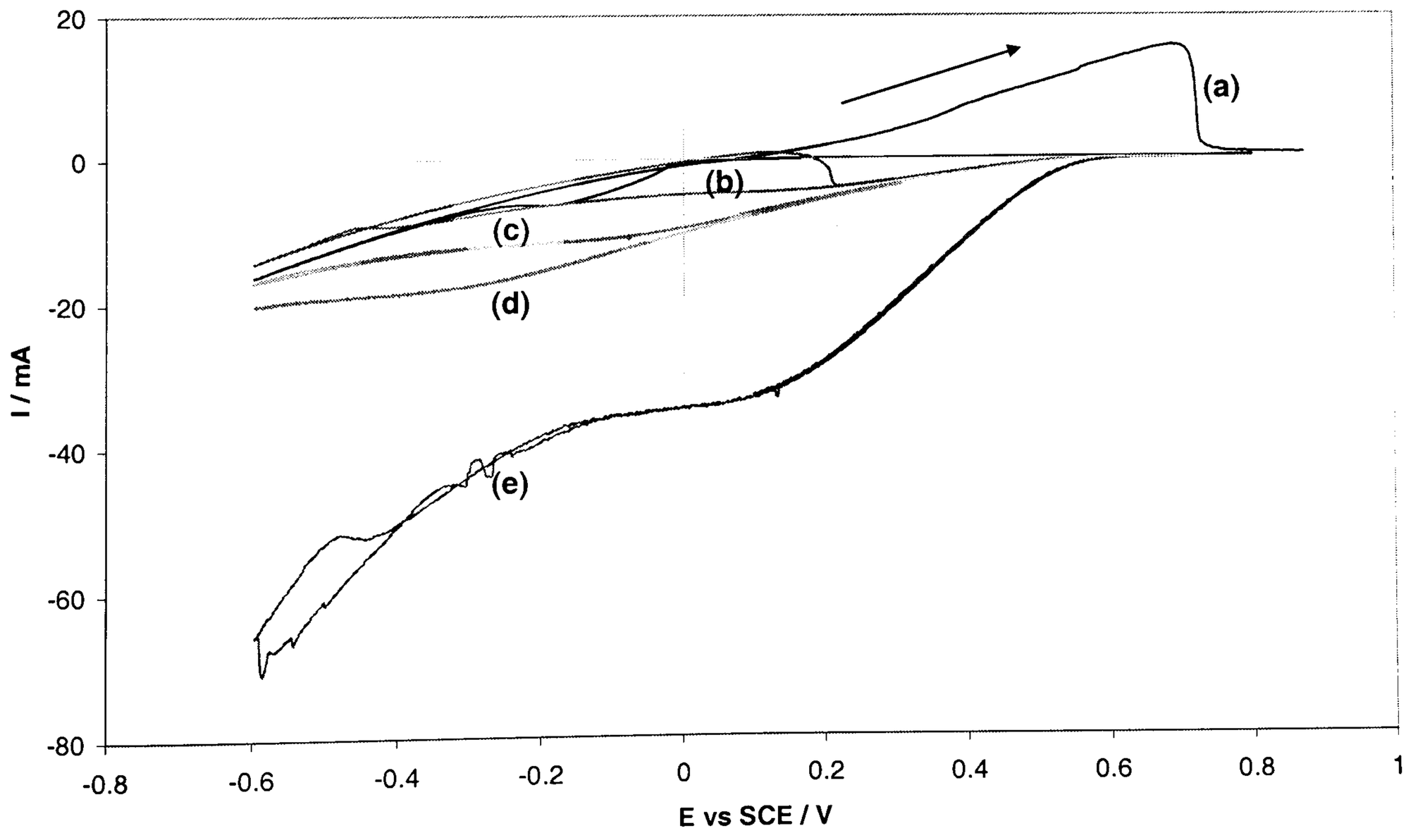

Figure 6-17 Cyclic voltammograms for 0.3M Cu, 1M NO_3^- + x g/l $FeCl_3$, scan rate 10mVs^{-1}, 800rpm. Fe(III) conc. (a) 0 (b) 1 (c) 4 (d) 7 (e) 14g/l

The above results show that although both ferric nitrate and ferric chloride shift the copper reduction potential to more cathodic values, $FeCl_3$ salts are more deleterious than those of $Fe(NO_3)_3$. Therefore, if copper recovery direct from the waste is desired, it is preferable to purchase a tin stripping solution that does not contain chloride.

The deposition efficiency of the copper from these iron/tin containing nitrate solutions could not be determined from the cyclic voltammograms, as it was for copper/nitrate solutions. These previous calculations assumed that no other reactions, apart from copper dissolution, occurred at positive potentials. This is not the case for these solutions containing Fe(III) in addition to Cu(II) and NO_3^-. Ferric ions are reduced at potentials more negative than +500mV, and therefore mask the Cu(II) stripping current.

6.1.3 Real Stripping Waste i-E Data

Cyclic voltammograms were recorded for samples of real waste tin stripping solution. The stripping solution was Tinsolv 2000 (Atotech), the second solution in a two stage process (Section 1.3), obtained from an industrial partner. The polarisation plot (Figure 6-18) shows a clear limiting current between +200 and -200mV. The cathodic region again shows linear response, which is similar to the voltammograms for the copper/nitrate and copper/iron/tin solutions. The anodic currents associated with copper dissolution are also clearly seen, unlike the polarisations for the copper/iron/tin solutions.

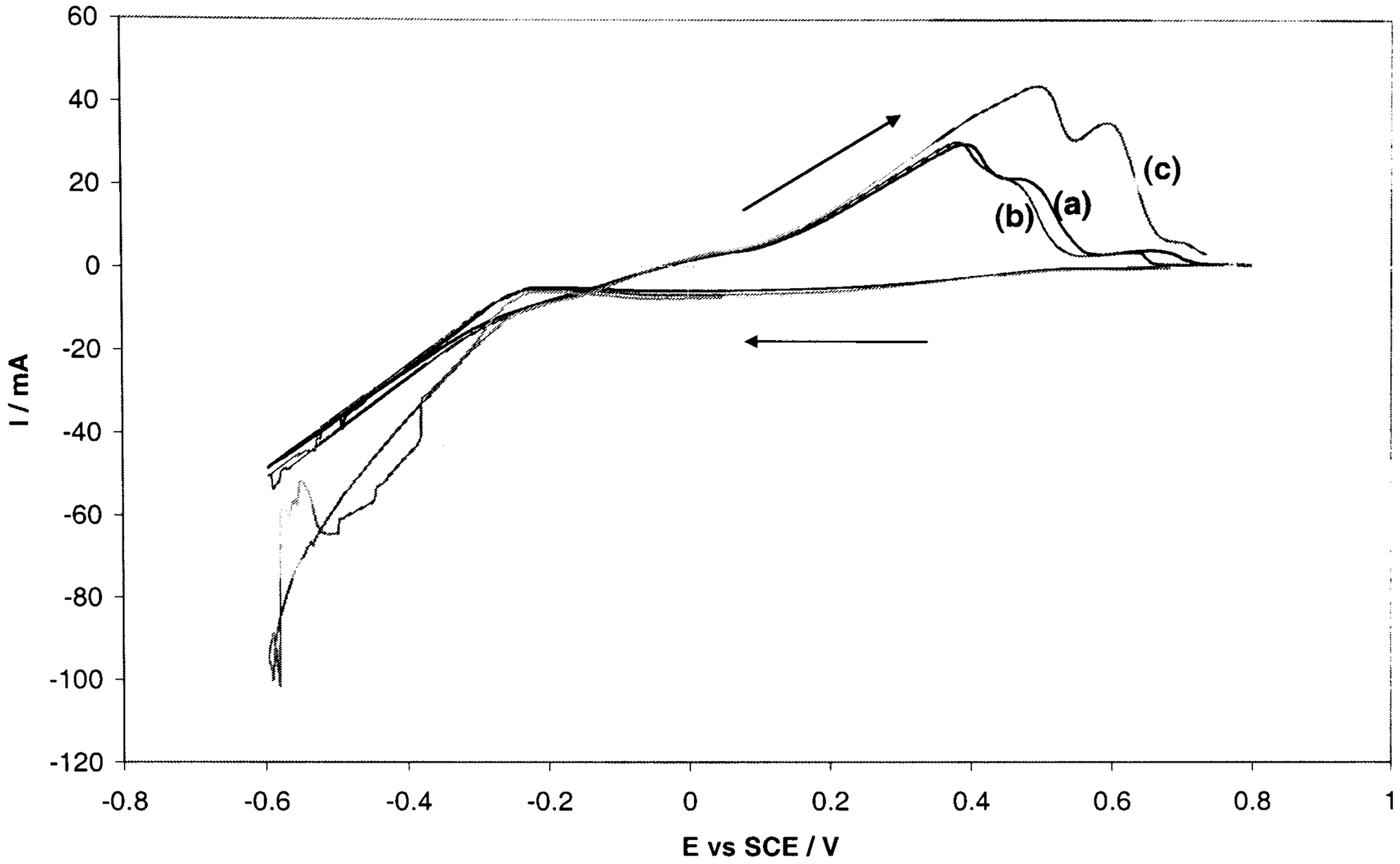

Figure 6-18 Cyclic voltammogram for waste Tinsolv 2000, scan rate 10mVs^{-1} (a) 600rpm (b) 800rpm (c) 1000rpm

From Figure 6-18, the current at -600mV for a rotation speed of 800rpm, was found to be -51mA. This current is similar to the values for the equivalent copper/nitrate solution with 0.3M Cu, 1M NO_3^- (Solution 1) and copper/iron/tin solution (Solution 10), which were -48mA and -47mA respectively. This again confirms the dominance of nitrate and hydrogen reduction on the polarisation data at these high cathodic potentials. The voltammograms also show that an increase in rotation speed from 600 to 800rpm has no effect on the i-E data.

The anodic currents associated with copper dissolution show that it is possible to deposit copper from the stripping waste. The maximum anodic current is 32mA above the baseline for a rotation speed of 800rpm (Figure 6-18). Comparing this current to the maximum anodic currents for Solution 1 (45mA) and Solution 10 (12mA), it can be said that the copper deposition is suppressed by the ferric ions and other additives in the real solution. However, the suppression not as severe as that seen from the copper/iron/tin solutions, probably because the Fe(III) concentration in the stripping waste is less than in the simulated copper/iron/tin solutions.

The limiting current plateau observed between potentials of +200 and -200mV is due to Fe(III) reduction. The other reduction reactions i.e. copper deposition, nitrate and hydrogen reduction, do not appear to start until -200mV; this is more negative than was expected by comparison with the copper/nitrate deposition potentials (-63mV for Solution 1). This substantiates the previously found result that ferric ions shift the copper reduction potentials to more negative values.

The limiting current for ferric ion reduction seen on Figure 6-18 can be used to estimate the Fe(III) concentration in the stripping waste. A calibration chart of Fe(III) concentration versus limiting current was therefore constructed. Figure 6-19 shows the voltammograms for a range of Fe(III) concentrations; the data show the increase in limiting reduction current with Fe(III) concentration.

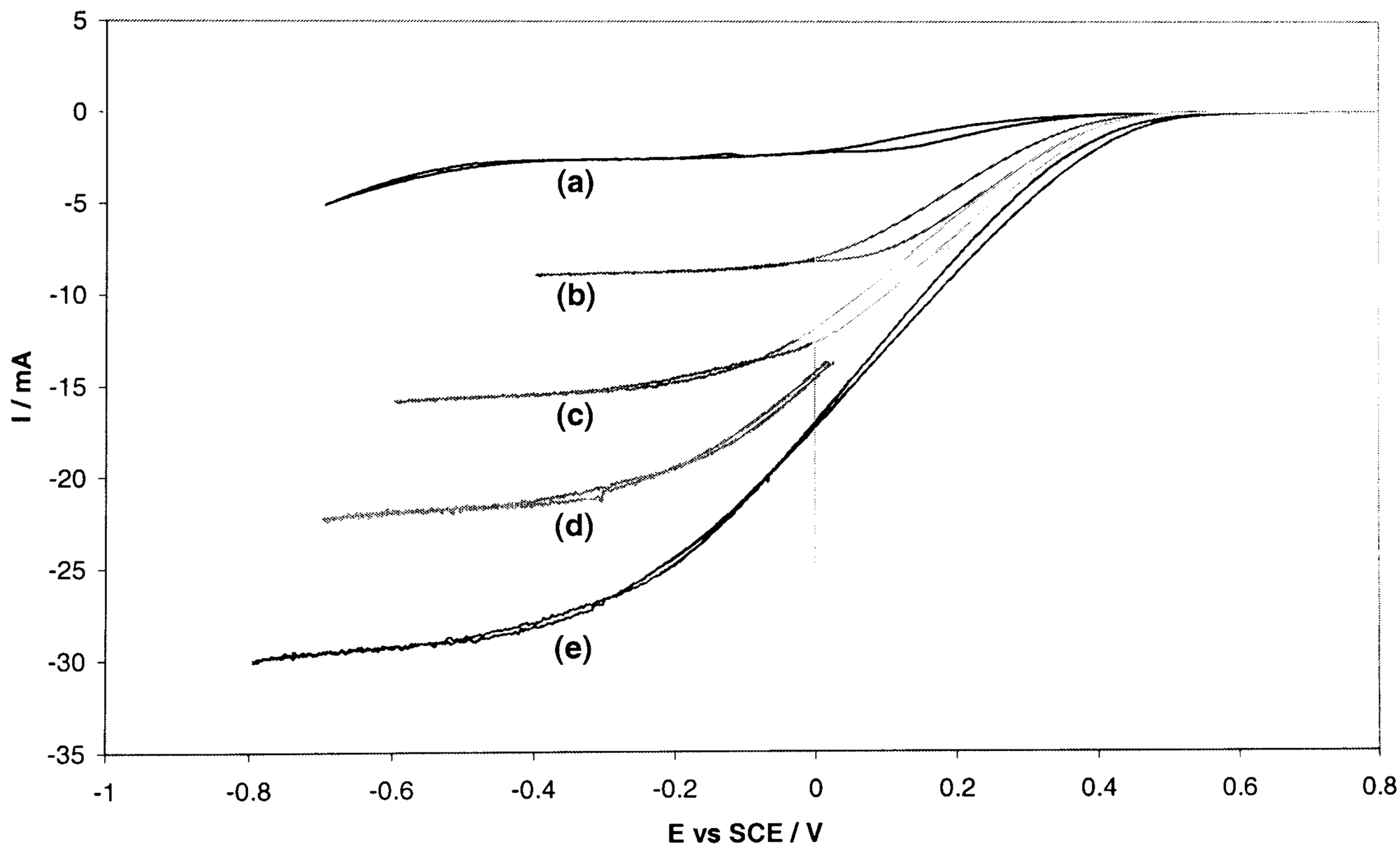

Figure 6-19 Limiting current of x g/l $Fe(NO_3)_3$ in 0.5M H_2SO_4, scan rate 10mVs^{-1}, 800rpm (a) 1 (b) 4 (c) 7 (d) 10 (e) 14g/l

If the limiting current is plotted against the Fe(III) concentration, a linear correlation is obtained (Figure 6-20), as predicted by the Nernst diffusion layer model (Section 2.2). The Fe(III) mass transfer limiting current, obtained from the cyclic voltammogram of the real waste solution (Figure 6-18), is -6.05mA measured at

-100mV. The concentration of ferric ions was therefore determined to be 2.62g/l (0.047M).

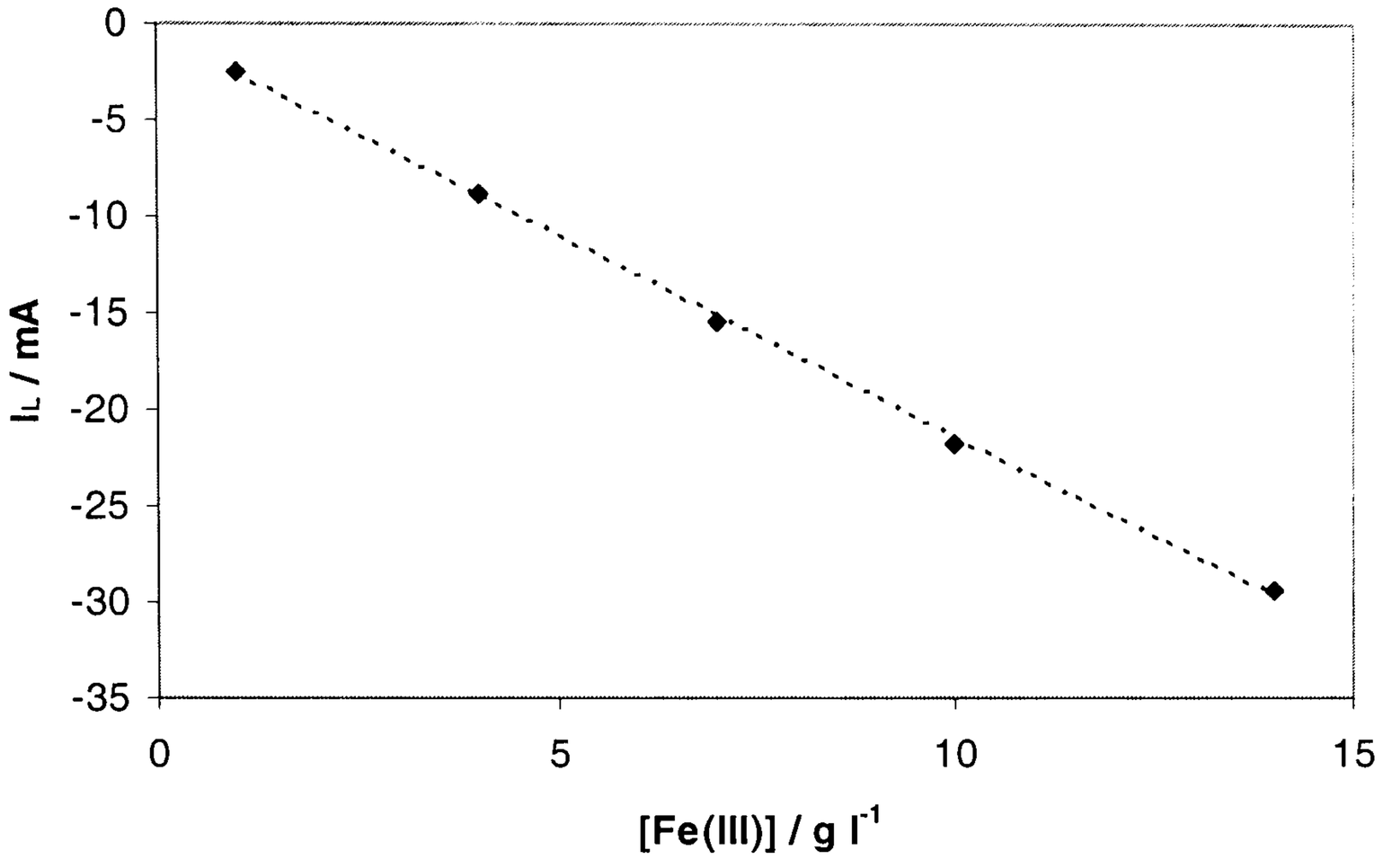

Figure 6-20 Calibration curve of limiting current against Fe(III) concentration

Due to the adverse effect of ferric ions on the deposition of copper, calculations were carried out to examine the feasibility of reducing the ferric ions to ferrous ions. This would allow the deposition of copper to be carried out at higher efficiency, as ferrous ions are not thought to affect the efficiency of copper deposition [6.11].

In the real waste stripping solution, the mass transfer limiting current for the Fe(III) reduction occurs at a potentials more negative than +200mV, and has the value of -6.05mA (Figure 6-18). Using Faraday's law (Eq. 6.2), the time required to reduce 2.62g/l Fe(III) (0.047M) in a volume of 50mls, was estimated to be 10.4hrs. The processing time could be decreased by increasing the area of the electrode.

$$t = \frac{mnF}{I} \qquad m = 0.047 \text{ x } 0.005 \text{ mol}, \quad n = 1, \quad I = 6.05mA \tag{6.2}$$

This process route is not thought to be feasible because if this stage was used, a membrane and separate anolyte would be required for the reactor, as the Fe(II) ions could be oxidised back to Fe(III) ions at the anode.

6.2 Anodic Stripping Studies to Determine Current Efficiency

In an industrial situation, a reactor would be expected to be operated under galvanostatic control. Therefore, it is necessary to determine the deposition efficiency of copper reduction at different applied cell currents. To find this relationship, copper was deposited at four different currents from each solution. The deposition efficiency determined from cyclic voltammetry was, however, very low for some of the solutions. Therefore, only solutions whose efficiencies, determined from the i-E data, were greater than 20% are investigated in these experiments. It is thought that recovery from solutions with efficiency lower than this will not be viable.

6.2.1 Copper / Nitrate Stripping Results

The deposition efficiency of copper from Solutions 1, 4, 5 and 9 was found for a range of deposition currents. These deposition currents spanned the full range of potentials used in the voltammetry. The chosen potentials and the corresponding currents taken from the copper/nitrate i-E data are shown in Table 6-5.

Potential / mV	Current / mA			
	Solution 1	Solution 4	Solution 5	Solution 9
-600	-48	-39	-14	-5
-450	-35	-28	-11	-3
-300	-22	-18	-7	-2
-150	-10	-7	-3	~0

Table 6-5 Deposition currents for copper/nitrate efficiency experiments

After deposition, the copper was stripped from the electrode at 0V vs SCE in 0.5M HCl, as it had been previously determined that copper was removed entirely into the Cu(I) oxidation state at this potential (c.f. Figure 3-6, p63). The current due to stripping copper, after deposition at -48mA from Solution 1, is shown in Figure 6-21. The two stripping curves correspond to two different times for copper deposition: 60 seconds and 20 seconds. The current rose steeply when the potential is switched to 0V vs SCE, and then remained constant until most of the copper had been removed.

The area under curve (a) is greater than that under curve (b), signifying that more copper was deposited during the longer deposition time.

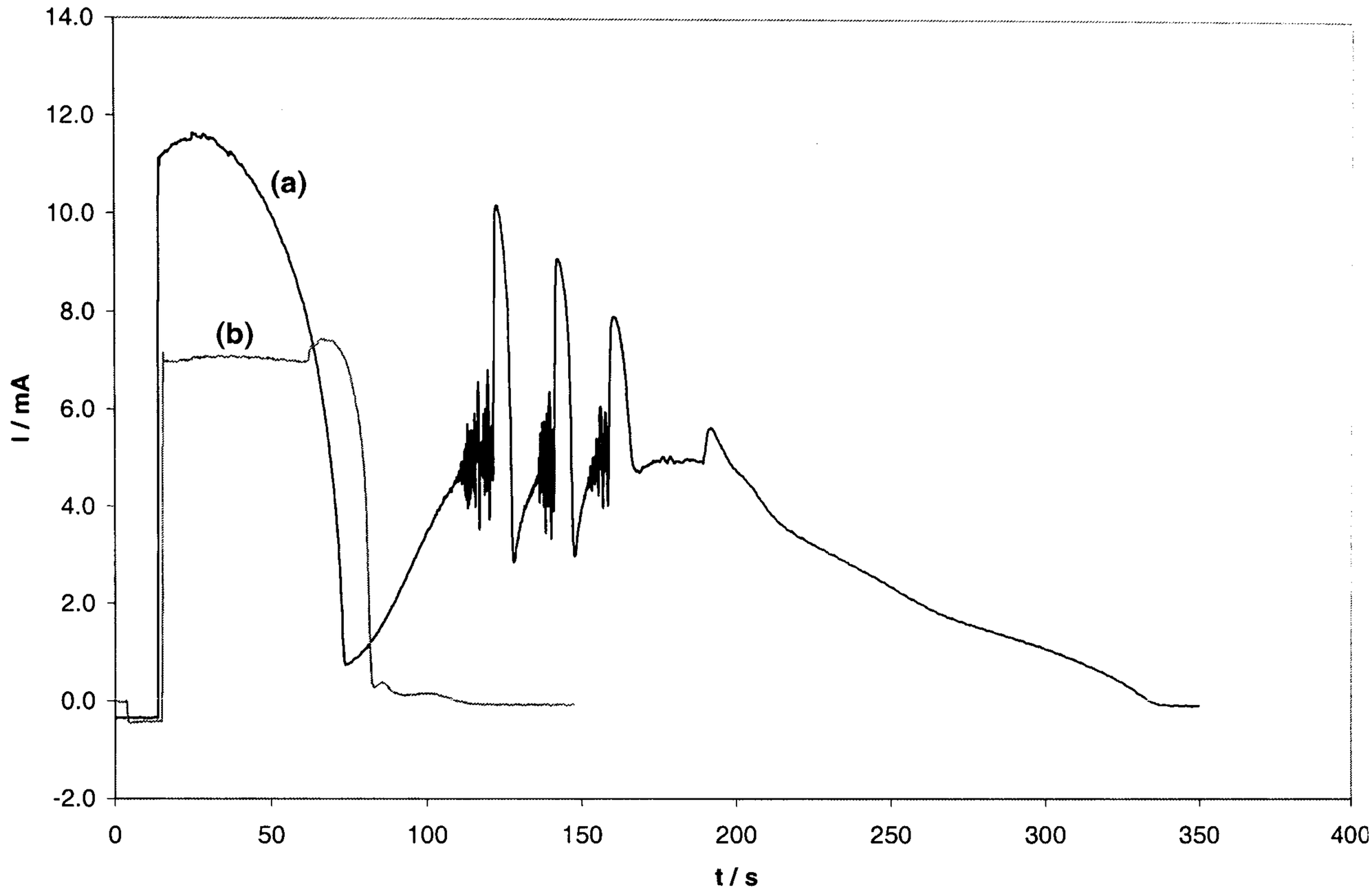

Figure 6-21 Stripping currents into 0.5M HCl after deposition at -48mA (Solution 1), scan rate 10mVs^{-1}, 800rpm. Deposition time (a) 60s (b) 20s

The current oscillations seen on curve (a) are the result of a thick film of CuCl forming on the electrode surface [6.12]. Copper is dissolved by Cl^- ions according to the following reactions:

$$Cu + Cl^- \rightarrow CuCl + e \qquad\qquad CuCl + Cl^- \rightarrow CuCl_2^-$$

When the film of CuCl on the copper surface exceeds a critical thickness, the rate limiting reaction periodically changes between film formation and film dissolution. When the film dissolution is fastest, the CuCl film thins, allowing Cl^- ions to reach the copper surface faster and therefore increasing the current temporarily.

The deposition time was decreased to 20 seconds to avoid this phenomenon. As shown in Figure 6-21, no current oscillations were observed during the stripping of copper deposited for 20s. This deposition time of 20 seconds was calculated to give

a copper film 0.9μm thick, whereas a layer 2.7μm thick would be deposited in 60 seconds.

For the deposition at -48mA, five runs were carried out to determine the experimental reproducibility. The results from these can be seen in Table 6-6. Although the deposition time varies from 60 to 15 seconds, the experimental uncertainty at 95% confidence interval was calculated to be ±2.6%. The reproducibility of these experiments is therefore good.

Experiment no.	Deposition time / secs	Current efficiency
1	60	97.8
2	60	97.7
3	20	96.6
4	15	94.3
5	15	93.2

Table 6-6 Current efficiencies for deposition at -48mA (Solution 1)

Figure 6-22 shows the current on stripping copper into 0.5M HCl after deposition at -35mA, from Solution 1 (0.3M Cu, 1M NO_3^-). These data again show the stripping current rising sharply after the potential was set to 0V vs SCE, and the region of constant current as copper is removed from the electrode. As for deposition at -48mA, more copper was deposited for a longer deposition time.

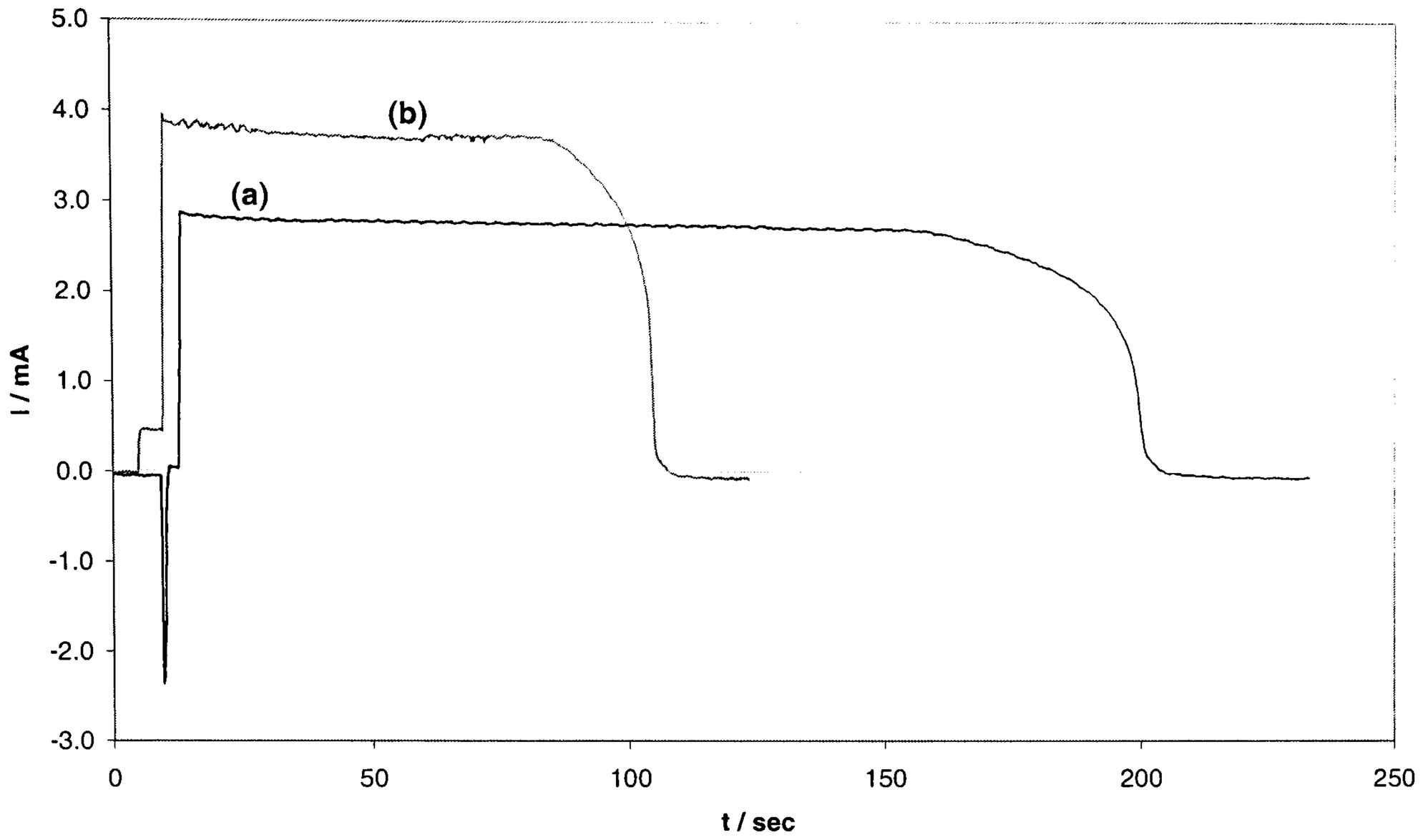

Figure 6-22 Stripping currents into 0.5M HCl after deposition at -35mA (Solution 1), scan rate 10mVs^{-1}, 800rpm. Deposition time (a) 30s (b) 20s

For copper deposition at -35mA from Solution 1, four experimental runs were completed. These multiple runs allow the experimental error at ±95% confidence interval to be calculated. The deposition time was also varied, because if insufficient copper is deposited, the current efficiency would relate to the nucleation of the copper on the gold electrode rather than bulk deposition. The current efficiency for each run is shown in Table 6-7. The error for these results is ±0.9%, once more demonstrating the reproducibility of these experiments.

Experiment no.	Deposition time / secs	Current efficiency
1	30	92.9
2	30	93.8
3	20	93.2
4	20	94.2

Table 6-7 Current efficiencies for deposition at -35mA (Solution 1)

Copper was also deposited at -22mA and -10mA from Solution 1; several experimental runs were carried out for each current. The efficiencies for these

depositions, calculated from the charge recorded whilst stripping the copper into the HCl, were 93.8 ± 1.8 % for -22mA, and 91.9 ± 3.5 % for -10mA. The efficiency of the deposition was high across the range of currents studied.

The stripping experiments were repeated for Solutions 4, 5 and 9. Copper was deposited at four currents from each solution, and then stripped into HCl. The deposition and stripping were repeated several times. The average efficiency (±95% confidence interval) for the copper deposition is shown in Table 6-8.

Solution 1		Solution 4		Solution 5		Solution 9	
I_{dep} / mA	Φ	I_{dep} / mA	Φ	I_{dep} / mA	Φ	I_{dep} / mA	Φ
-48	95.9 ± 2.6	-39	19.7 ± 2.5	-14	64.1 ± 7.4	-5	22.7 ± 0.7
-35	93.5 ± 0.9	-28	24.8 ± 5.6	-11	85.3 ± 5.9	-3	35.2 ± 4.5
-22	93.8 ± 1.8	-18	45.9 ± 2.6	-7	90.0 ± 7.5	-2	52.7 ± 4.4
-10	91.9 ± 3.5	-7	77.4 ± 6.5	-3	88.7 ± 1.8	-	-

Table 6-8 Current efficiencies for constant current deposition from copper/nitrate solutions

These results show that when deposition is performed from Solutions 4, 5 and 9 at lower currents, the efficiency is generally greater. This could be because the copper has reached its limiting deposition rate at the higher currents in these solutions. To confirm this theory, the amount of copper reduced during the depositions was calculated using Faraday's law. The calculated copper deposition rate from Solution 4 during the stripping experiments is shown in Table 6-9. The rate at which metal is deposited is roughly the same for the three highest currents. Using the average of these three deposition rates (4.02×10^{-8} mol s^{-1}), the limiting current was calculated to be 7.75mA.

I_{dep} / mA	Q_{Cu} (stripping) / mC	t_{dep} / s	deposition rate/ mol s^{-1}
-39	229	60	3.96×10^{-8}
-28	348	90	4.01×10^{-8}
-18	474	120	4.09×10^{-8}
-7	237	90	2.72×10^{-8}

Table 6-9 Copper deposition rates from Solution 4 calculated from the stripping experiments

Similar calculations were carried out for Solutions 1, 5 and 9; the deposition rates for each applied cell current are shown in Table 6-10. No limiting current could be found from the Solution 1 data, as the deposition rate was still increasing up to the maximum current of -48mA. However, Solutions 5 and 9 show similar behaviour to Solution 4, with the two largest currents giving roughly the same metal deposition rate.

Solution 1			
I_{dep} / mA	Q_{Cu} (stripping) / mC	t_{dep} / s	deposition rate/ mol s^{-1}
-48	1425	60	2.46×10^{-7}
-35	492	30	1.70×10^{-7}
-22	314	30	1.08×10^{-7}
-10	277	60	0.48×10^{-7}
Solution 5			
I_{dep} / mA	Q_{Cu} (stripping) / mC	t_{dep} / s	deposition rate/ mol s^{-1}
-14	290	60	5.00×10^{-8}
-11	476	90	5.48×10^{-8}
-7	387	120	3.34×10^{-8}
-3	242	180	1.39×10^{-8}
Solution 9			
I_{dep} / mA	Q_{Cu} (stripping) / mC	t_{dep} / s	deposition rate/ mol s^{-1}
-5	105	180	6.02×10^{-9}
-3	170	300	5.89×10^{-9}
-2	236	480	3.10×10^{-9}

Table 6-10 Copper deposition rates from Solutions 1, 5 and 9 calculated from the stripping experiments

The copper limiting currents for these copper/nitrate solutions, calculated from the stripping experiment data, are summarised in Table 6-11. These rate limiting currents show a dependence on the Cu(II) concentration, but are not proportional to the concentration. This dependence implies that the deposition is not fully limited by the mass transfer of copper to the electrode. The NO_3^- concentration also affects this limiting deposition rate, as shown by the difference in the limiting currents for Solutions 4 and 5.

	$-I_L$ (Cu) / mA
Solution 1 (0.3M Cu, 1M NO_3)	>47.5
Solution 4 (0.03M Cu, 1M NO_3)	7.75
Solution 5 (0.03M Cu, 0.1M NO_3)	10.11
Solution 9 (0.003M Cu, 0.01M NO_3)	1.2

Table 6-11 Calculated limiting currents of copper deposition from nitrate solutions

6.2.2 Copper / Nitrate with the Addition of Iron / Tin: Stripping Results

For the iron/tin containing solutions, the anodic stripping experiments were carried out after copper deposition from Solutions 10, 13, 14 and 18 (Table 3.1). These solutions correspond to those studied during the copper/nitrate stripping experiments, but with the addition of iron/tin. For example Solution 10 is equivalent to Solution 1 + 0.25M $Fe(NO_3)_3$ + SnO_2(sat). This allowed a direct comparison of how the iron/tin affected the deposition efficiency.

The copper deposition efficiency was found at four different currents for each solution. The deposition currents were chosen to span the potential range, 0 to -600mV, used during the voltammetry. The deposition currents are shown in Table 6-12 against the corresponding potentials from the i-E data (Section 6.1.2).

Potential / mV	Current / mA			
	Solution 10	Solution 13	Solution 14	Solution 18
-600	-47	-59	-35	-23
-450	-35	-39	-25	-19
-300	-25	-24	-19	-15
-150	-18	-17	-14	-11

Table 6-12 Deposition currents for copper/iron/tin efficiency experiments

After deposition from these iron/tin containing solutions at constant current, the copper was stripped into 0.5M HCl by holding the RDE potential at 0V vs SCE. As for the copper/nitrate experiments in Section 6.2.1, the deposition and stripping cycle was repeated several times. The stripping current, after deposition from Solution 10 at -47mA, is shown in Figure 6-23. The two traces correspond to deposition for 5 and 6 minutes.

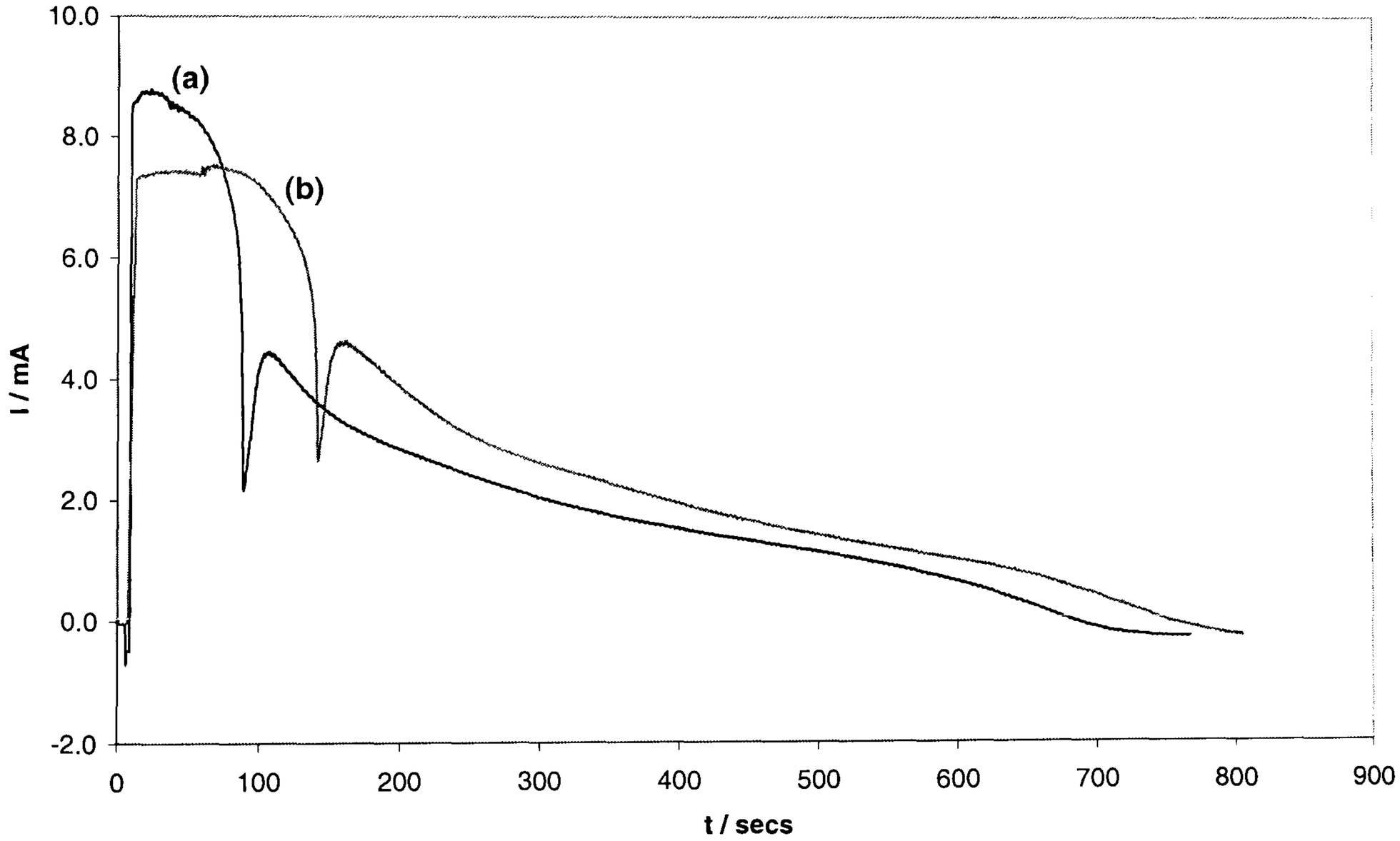

Figure 6-23 Stripping currents into 0.5M HCl after deposition at -47mA (Solution 10), scan rate $10mVs^{-1}$, 800rpm. Deposition time (a) 5mins (b) 6mins

The current efficiency calculated for deposition from Solution 10 at -47mA, is shown in Table 6-13 for each experiment. For this deposition current, six runs were carried

out because the deposited copper only formed a ring at the edge of the disc for the first three runs. These runs were repeated the next day and the disc was fully covered. However, the current efficiencies calculated from all experiments are similar, so the efficiency is thought to relate to bulk deposition, rather than nucleation. The average efficiency was calculated to be 23.8 ± 1.2 % (95% confidence interval). This copper deposition efficiency from Solution 10 (0.3M Cu, 1M NO_3^-, 0.25M Fe(III), SnO_2(sat)) was considerably lower than the deposition efficiency from Solution 1 (0.3M Cu, 1M NO_3^-), which had an efficiency of 95.9 ± 2.6 % for deposition at -48mA.

Experiment no.	Deposition time / mins	Current efficiency
1	4	24.5
2	4	23.2
3	6	21.9
4	4	24.7
5	5	23.9
6	6	24.8

Table 6-13 Current efficiencies for deposition at -47mA (Solution 10)

The anodic stripping current, after copper deposition from Solution 10 at -35mA, is shown in Figure 6-24, for two deposition times. Copper deposited slowly at -35mA, as seen by the small area under the curve (a) after deposition for 6 minutes. The experiment was repeated four times, and the average current efficiency was calculated to be 9.3 ± 3.6 %. The error on this efficiency is substantial; this method is therefore not reproducible for deposition at low current efficiency. To gain an improvement, the deposition should be carried out for longer times. The calculated efficiency is much lower than that for Solution 1, which was 93.5 ± 0.9% for deposition at -35mA.

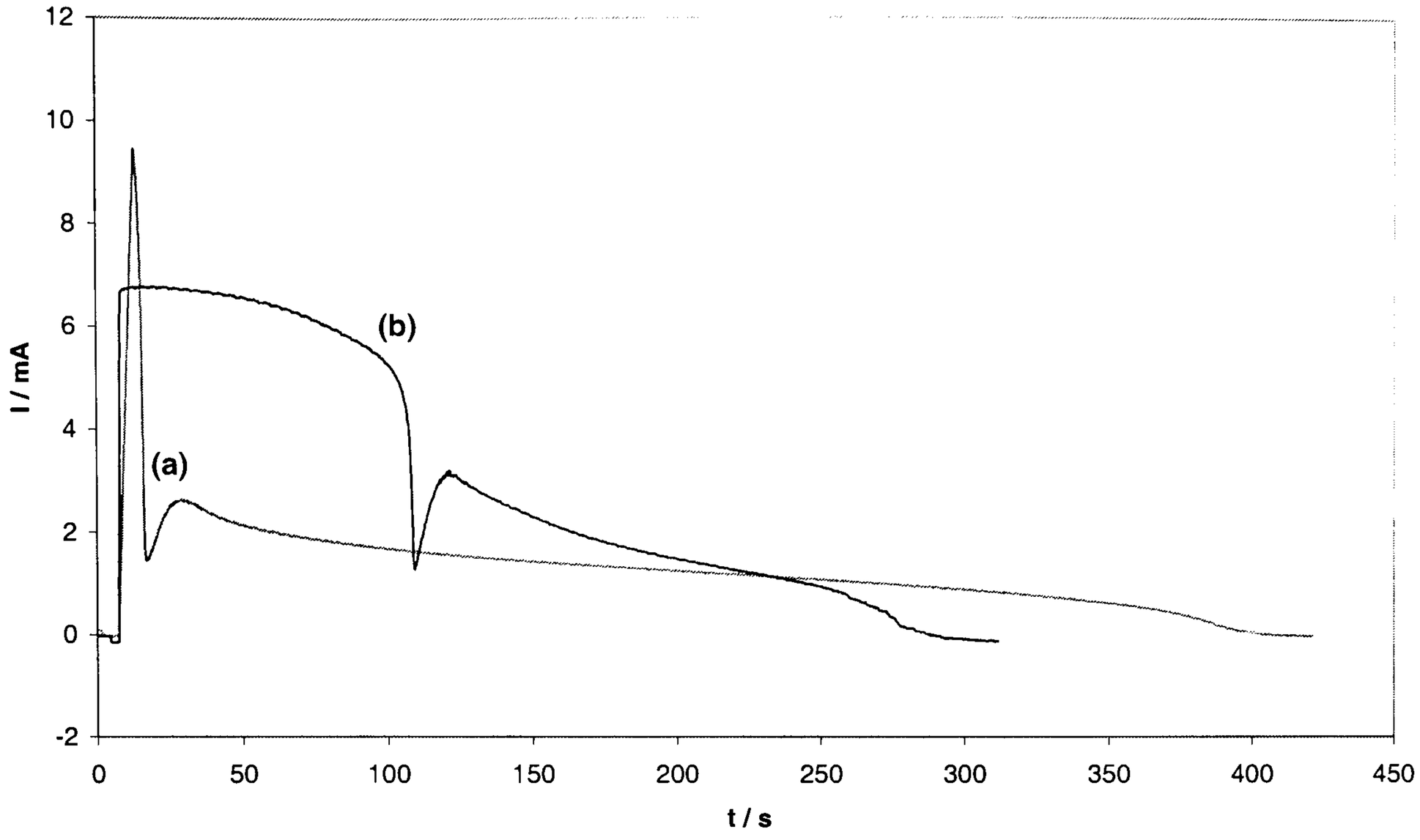

Figure 6-24 Stripping currents into 0.5M HCl after deposition at -35mA (Solution 10), scan rate 10mVs^{-1}, 800rpm. Deposition time (a) 6mins (b) 8mins

Deposition at -25mA and -18mA from Solution 10 was attempted, but no copper was deposited after 10 minutes. These experiments were stopped because the efficiency was so low that practical recovery would be unfeasible. The recorded efficiency of these depositions was therefore zero.

A comparison of the deposition efficiency between solutions containing 0.3M Cu(II) + 1M NO_3^-, with and without Fe(III), is shown graphically in Figure 6-25. The efficiency of copper deposition is significantly reduced by the addition of Fe(III) to the solution.

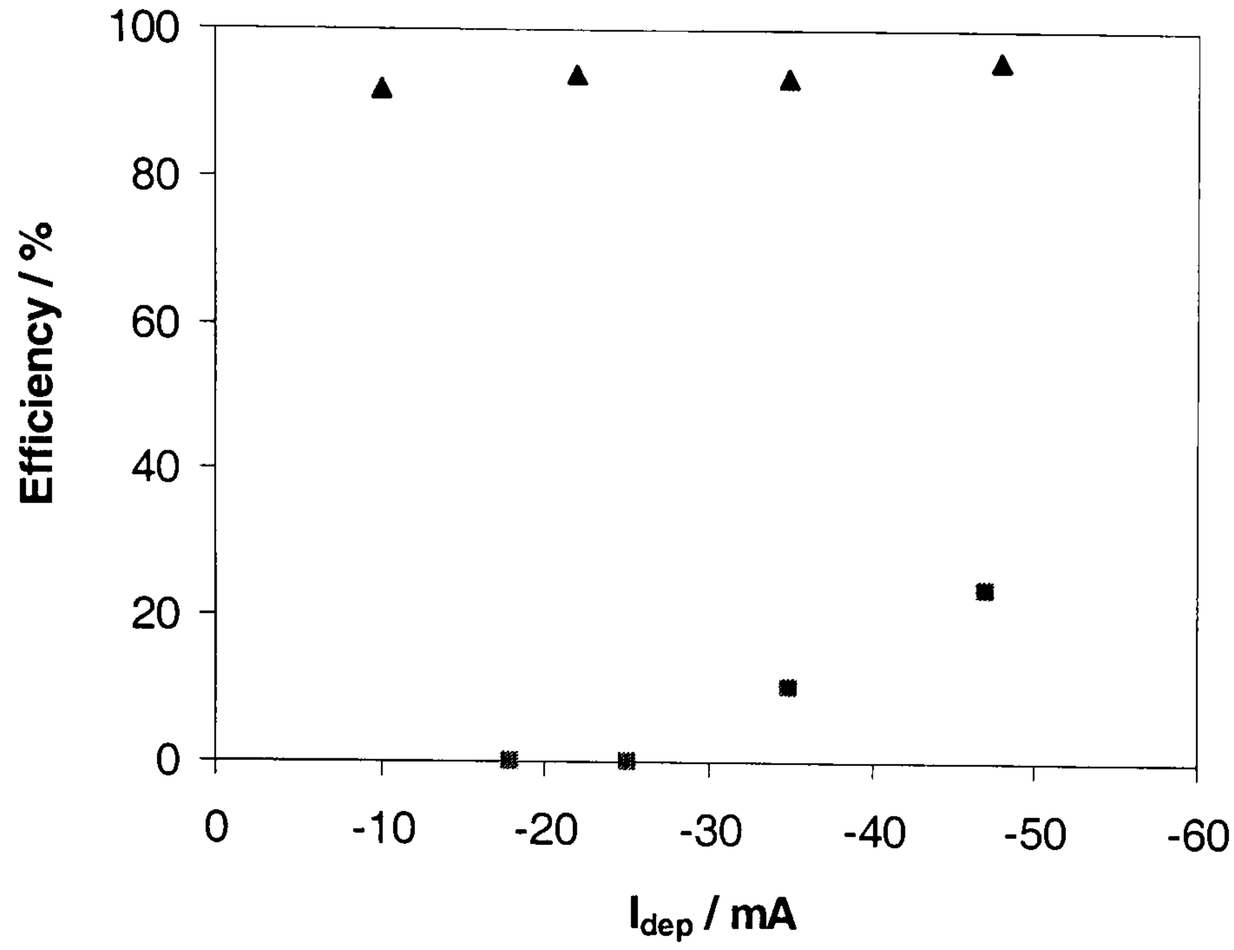

Figure 6-25 Efficiency comparison between (▲) Solution 1 (0.3M Cu, 1M NO_3^-) and (■) Solution 10 (0.3MCu, 1M NO_3^-, 0.25MFe, Sn)

These anodic stripping experiments were repeated for Solutions 13, 14 and 18. For each deposition current, several runs were carried out to find the experimental reproducibility. The average copper deposition efficiency (±95% confidence interval) from each solution is shown in Table 6-14. Copper was not deposited from any of the solutions at currents corresponding to -150 or -300mV, and for Solution 18 no copper could be deposited at any of the chosen currents.

Solution 10		Solution 13		Solution 14		Solution 18	
I_{dep} / mA	Φ	I_{dep} / mA	Φ	I_{dep} / mA	Φ	I_{dep} / mA	Φ
-47	23.8 ± 1.2	-59	12.8 ± 0.7	-35	4.9 ± 2.0	-23	0
-35	9.3 ± 3.6	-39	17.4 ± 2.1	-25	0	-19	0
-25	0	-24	0	-19	0	-15	0
-18	0	-17	0	-14	0	-11	0

Table 6-14 Current efficiencies for constant current deposition from copper/iron/tin solutions

The rate of copper deposition from Solutions 10, 13 and 14 was calculated for each deposition current, and is shown in Table 6-15. No limiting current could be estimated from the Solution 10 data, as the deposition rate was increasing up to the maximum current of -47mA. For Solution 13, ~ 3.8×10^{-8}mol s^{-1} may be the limiting

rate, but another data point at higher current would be required to confirm this. Similarly, more data would be required to find the limiting current for deposition from Solution 14.

Solution 10			
I_{dep} / mA	Q_{Cu} (stripping) / mC	t_{dep} / min	deposition rate/ mol s^{-1}
-47	1394	4	6.02×10^{-8}
-35	903	8	1.95×10^{-8}
Solution 13			
I_{dep} / mA	Q_{Cu} (stripping) / mC	t_{dep} / min	deposition rate/ mol s^{-1}
-59	1151	5	3.98×10^{-8}
-39	1054	5	3.64×10^{-8}
Solution 14			
I_{dep} / mA	Q_{Cu} (stripping) / mC	t_{dep} / min	deposition rate/ mol s^{-1}
-35	514	10	0.89×10^{-8}

Table 6-15 Copper deposition rates from Solutions 10, 13 and 14 calculated from the stripping experiments

6.2.3 Real Waste Stripping Results

The deposition efficiency of copper from the real waste stripping solution (Tinsolv 2000) was found for four deposition currents. These currents spanned the range of potentials used during the voltammetry (Section 6.1.3). The chosen potentials and the corresponding currents taken from the stripping waste i-E data are shown in Table 6-16.

Potential / mV	Current / mA
-600	-48
-450	-30
-300	-11
-150	-5

Table 6-16 Deposition currents for real waste efficiency experiments

Copper deposition from real stripping waste resulted in powdery deposits on the rotating electrode. These deposits could not be stripped electrochemically into the HCl. Although the stripping current fell to near zero, loose copper powder was observed on the surface when the electrode was removed. Therefore, instead of stripping the copper at 0V vs SCE, the deposited copper was left to dissolve into a known volume of 0.5M HNO_3. The copper concentration was then measured using an ion selective electrode (Section 3.4.2). From this measured copper concentration, the amount of copper that had been deposited onto the electrode, and thus the theoretical charge required for the deposition could be calculated using Faraday's law.

As an example, the total deposition time for copper deposition from real waste at -48mA was approximately 5 minutes. The measured Cu(II) concentration in 100mls of 0.5M HNO_3 was 1.72×10^{-4}M, therefore the amount of copper that had been deposited was 1.72×10^{-5}mol. Faraday's law (Eq 6.3) was used to calculate the theoretical charge to deposit this amount of copper ($m = 1.72 \times 10^{-5}$mol). The theoretical charge was 3.315C.

$$Q = mnF \qquad \text{where } n = 2 \tag{6.3}$$

The actual charge used in the copper deposition was calculated as the integral of the current-time data recorded during the deposition, and was 14.76C. The efficiency for copper deposition from the real waste at -48mA was therefore 22.5%.

The calculated efficiency for deposition at each current is shown in Table 6-17. The efficiency was highest for deposition at -11mA, and decreased as the deposition current increased. This trend of high efficiency at low current was also found for the copper/nitrate solutions, but not copper/iron/tin solutions.

Deposition Current / mA	Efficiency / %
-48	22.5
-30	20.7
-11	36.2
-5	0

Table 6-17 Current efficiencies for constant current deposition from real solutions

These deposition efficiencies can be compared to those from Solutions 1 and 10, as they have the same Cu(II) and NO_3^- concentration. Figure 6-26 shows that the efficiency of copper deposition from the real waste is lower than that from Solution 1 (0.3M Cu, 1M NO_3^-) across the full range of deposition currents. However, deposition from the real waste proceeds at greater efficiency than deposition from Solution 10 (0.3M Cu, 1M NO_3^-, 0.25M Fe(III), SnO_2(sat)), except at high current. This greater efficiency was expected because Solution 10 has a higher Fe(III) concentration than the real waste, and Fe(III) has been shown to suppress copper deposition.

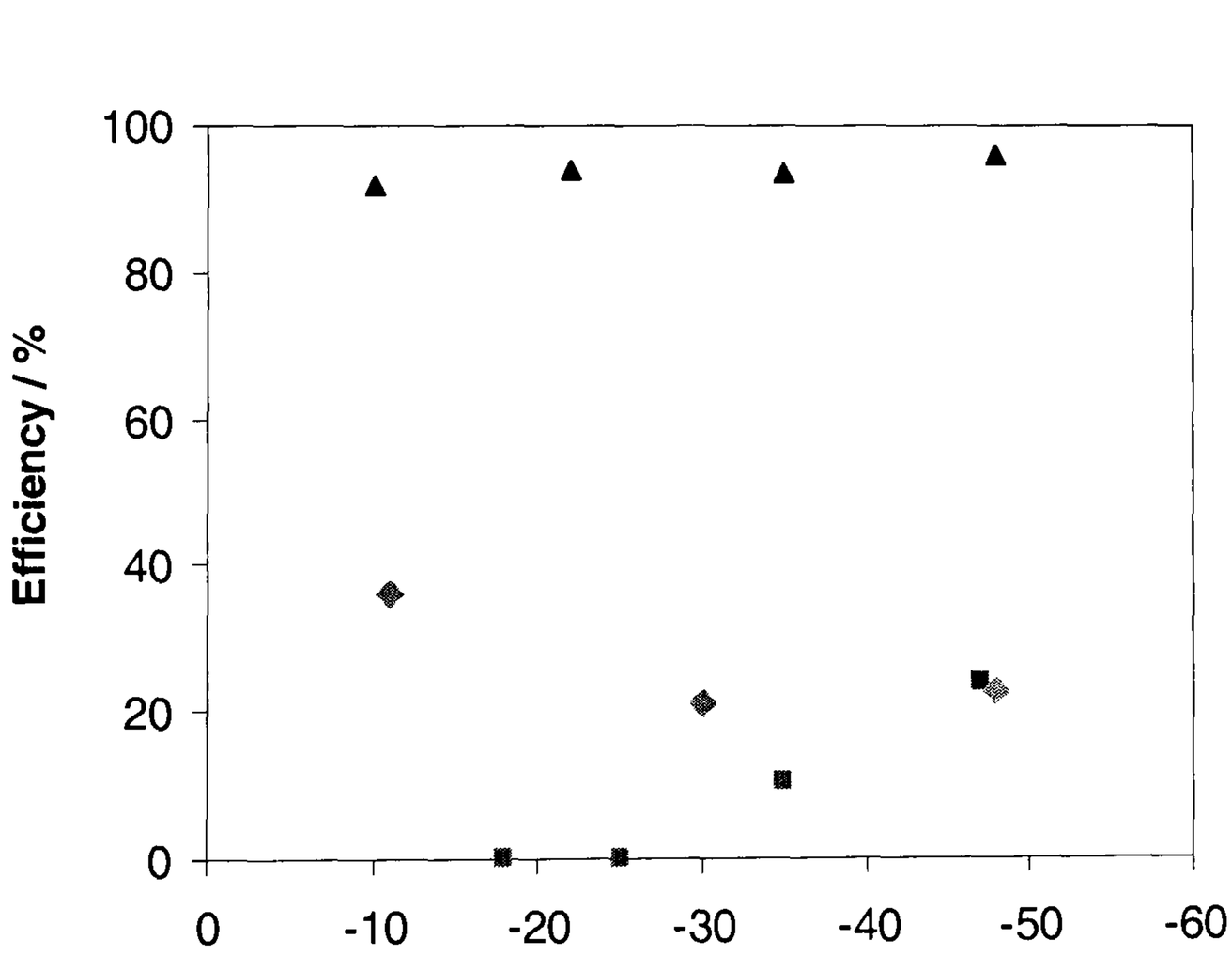

Figure 6-26 Comparison of deposition efficiencies between real waste (♦), Solution 1 (▲) and Solution 10 (■)

To obtain an estimate of the copper limiting current from the stripping waste, the molar deposition rate was calculated for each of the deposition currents (Table 6-18).

The deposition rate increased across the full current range; hence an estimate for the limiting current for copper deposition from this solution could not be made.

I_{dep} / mA	Q_{Cu} (stripping) / mC	t_{dep} / min	deposition rate/ mol s^{-1}
-48	1658	5	5.73×10^{-8}
-30	1081	7	2.67×10^{-8}
-11	3010	25	2.08×10^{-8}

Table 6-18 Copper deposition rates from real waste calculated from the stripping experiments

6.3 Discussion

The deposition of copper from acidic nitrate solutions occurs in a mixed potential system (Section 2.2). Cu(II), NO_3^- and H^+ are reduced concurrently; copper catalyses the nitrate reduction and the nitrate/hydrogen reaction is coupled [6.3]. From the i-E data for all solutions, it was observed that the cathodic current showed linear response to the applied potential. This indicated that the solution resistance was significant, or that multiple reactions occur on the electrode surface. The cathodic potential applied to Solution 9 was corrected to compensate for solution resistance, as this solution was the worst affected (Section 6.1.1). The shape of the polarisation did not change; the current was still linear in the cathodic region (Figure 6-11). Therefore, the linear data was attributed to the combined current from several reactions occurring concurrently. Figure 6-27 shows how currents from several reactions could add together (I_{TOTAL}) to give linear response. This diagram does not reflect the catalytic action of the Cu(II), NO_3^- and H^+ reactions, but suggests how a linear response was attained.

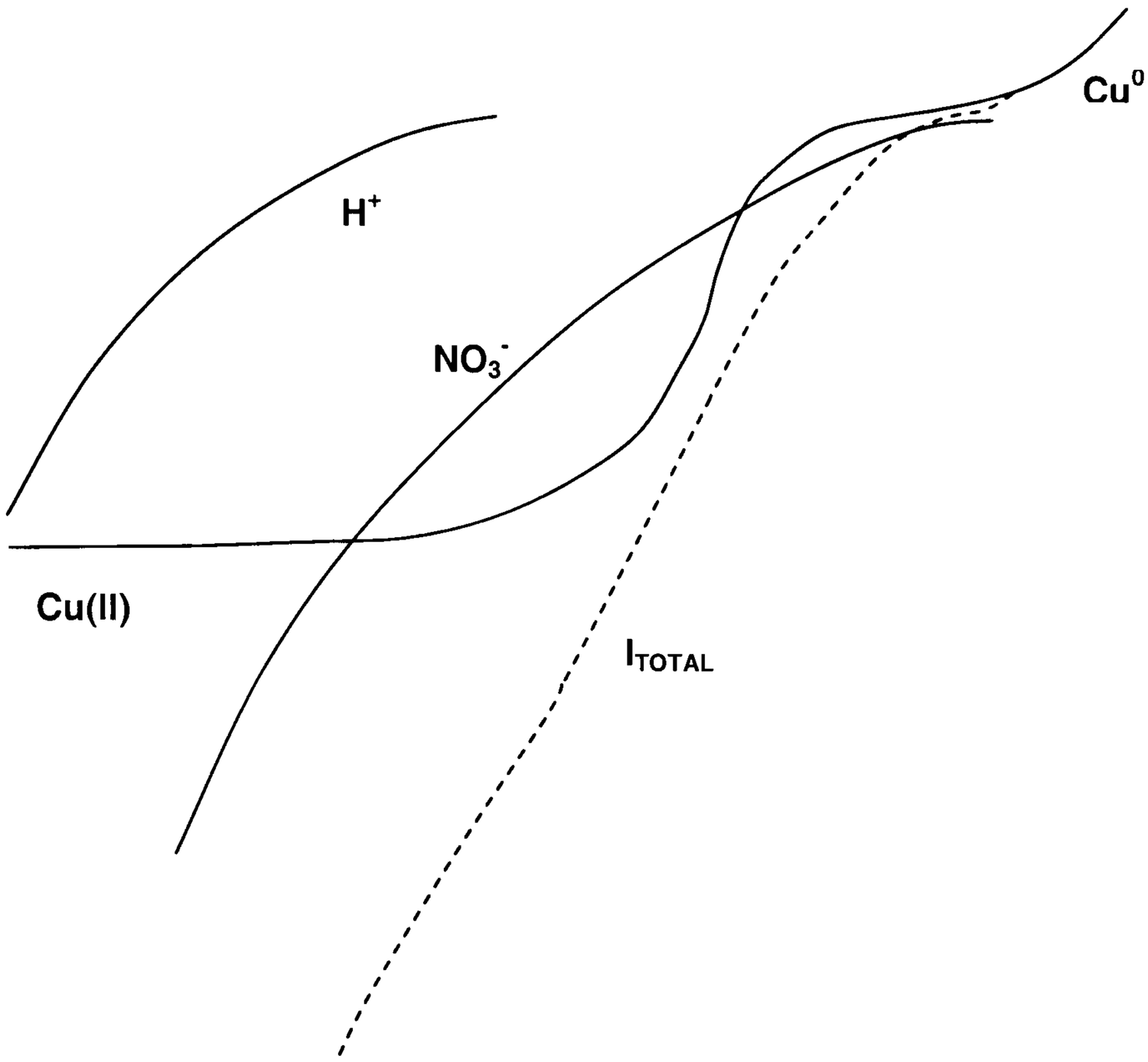

Figure 6-27 Diagram showing additive currents in the mixed potential Cu(II) / NO_3^- / H^+ system

The reversible potential for this mixed electrochemical system would not be the same as that for the Cu(II)/Cu^0 couple. The values quoted in Table 6-1 are the potential at which there is significant current. It is unknown whether copper was deposited at these potentials. The figure above demonstrates how a significant current could be generated by nitrate reduction before copper is deposited. However, this mixed potential was only used to compare solutions with and without Fe(III).

The mass transport limiting current for copper deposition could not be seen on the voltammograms because the cathodic current showed almost linear response to the applied potential. To determine the extent to which copper deposition from nitrate solutions is governed by mass transfer, the reduction current of NO_3^- and H^+ ions was subtracted from the copper/nitrate i-E data, and the copper deposition rate during the anodic stripping study was estimated. The results from both these analyses showed that the limiting rate of copper deposition increased with Cu(II) concentration. However, this rate was not proportional to the Cu(II) concentration, as is the case for a fully mass transport controlled reaction. The copper deposition rate also varied with NO_3^- concentration. As the limiting copper deposition rate varies with both

Cu(II) and NO_3^- concentration, the reactions are thought to be coupled. This is in agreement with *Antropov et al* [6.2] and *Carpenter and Pletcher* [6.13] who both found that copper ions catalyse nitrate reduction. *Dima et al* [6.14] found that copper is dissolved at more positive potentials in nitrate electrolytes, compared to sulphate electrolytes.

The i-E data for all the simulated solutions and the real waste show that at faster rotational speeds, there was an increase in area under the anodic dissolution current and thus an increase in the amount of copper deposited. For the copper/nitrate solutions the deposition current was independent of the rotational speed, and so the deposition efficiency was higher for higher rotational speeds. This increase in deposited copper with rotational speed has the implication that flow in the reactor should be high to ensure the maximum copper deposition rate, and possibly to maintain a high recovery efficiency.

Ferric ions were found to have a detrimental effect on copper deposition. The potential at which copper deposited from Fe(III) containing solutions appeared to be shifted towards more negative values (Figure 6-15). This shift in overpotential is thought to correspond to the point in the i-E data where the reduction of Fe(III) stops contributing to the total current. In Figure 6-28, curve (a) was recorded in a solution containing copper and nitrate only; curve (b) was recorded for the same solution, but with the addition of 4g/l Fe(III). The cathodic currents at positive potentials are due to the reduction of Fe(III). However, at potentials more negative than -0.35V, the data from both solutions overlie. It is thought that the Fe(III) reduction was suppressed in this range and copper was only deposited at these more negative potentials.

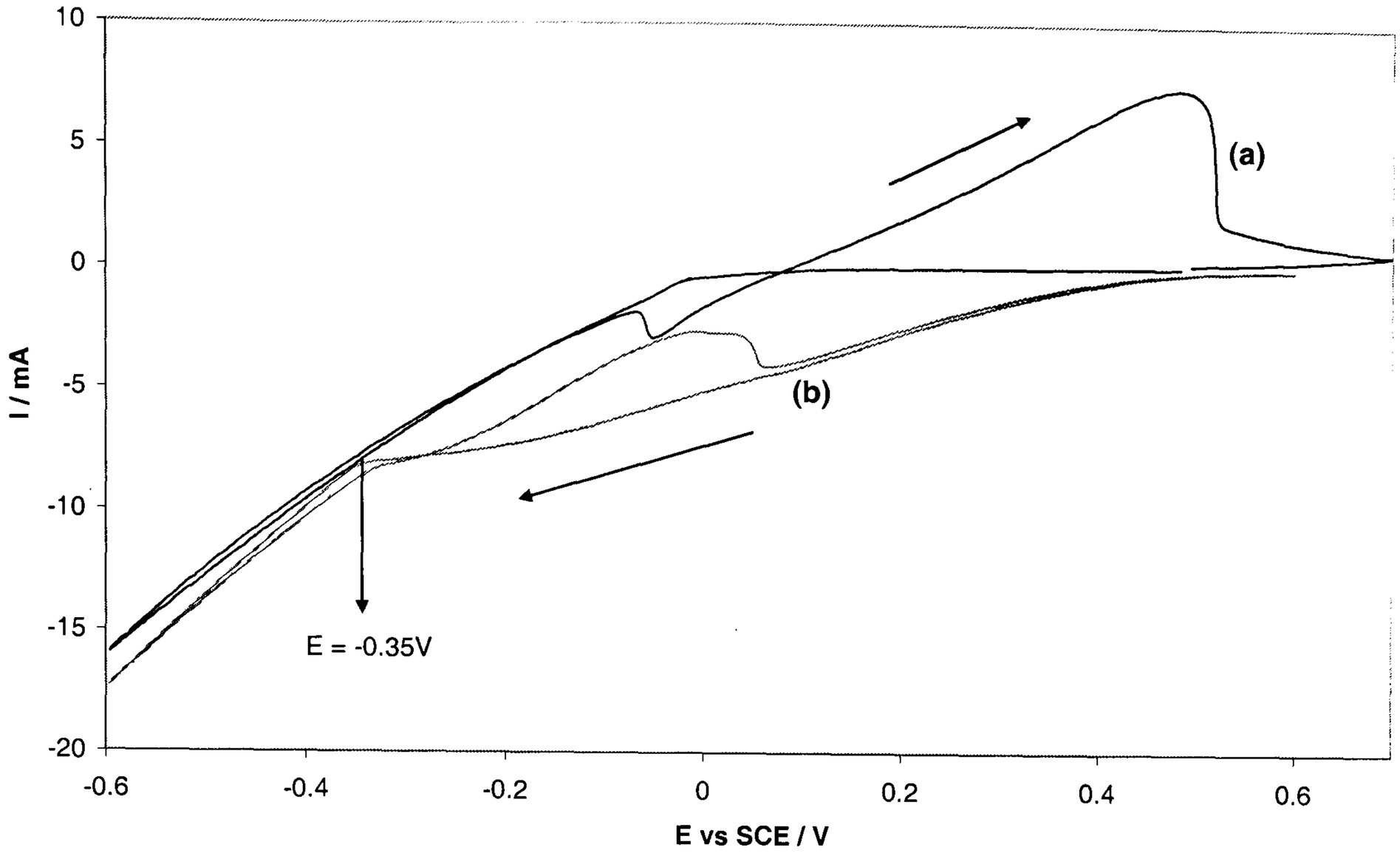

Figure 6-28 Polarisations for 0.3M Cu, 1M NO_3^- + x g/l $Fe(NO_3)_3$, scan rate 10mVs^{-1}, 800rpm. Fe(III) conc. (a) 0 (b) 4g/l

The potential at which the i-E data for copper/nitrate and copper/iron solutions starts to overlie became more negative as the concentration of Fe(III) was increased (Figure 6-16). As the amount of copper deposited decreased with increasing Fe(III) concentration during deposition between a fixed potential range, the fact that copper deposition is shifted to negative potentials was corroborated. The copper overpotential shift and Fe(III) suppression are thought to be due to the electrode surface. Initially the electrode was gold: *Barnartt* [6.15] found that the ferric/ferrous reaction is an order of magnitude faster on gold than on platinum. The reduction of the Fe(III) will proceed quickly, and appears to start near the standard reduction potential of +0.529V vs SCE [6.8]. At some potential, copper will start to deposit and cover the gold surface. It is thought that Fe(III) reduction may be suppressed on the copper surface, as *Bisang* [6.16] only observed a reduction current for ferric ions at a potential of -0.025V.

The anodic stripping studies show that the deposition of copper from nitrate electrolytes can be achieved with reasonable current efficiency. For example, copper can be recovered with 95% efficiency from a 0.3M Cu, 1M NO_3^- solution (Soln. 1). If the copper concentration was reduced by one tenth from this starting solution, the

efficiency would be reduced to a maximum of 77%, although the current density would have to be reduced. Although the deposition efficiency decreases as copper is recovered, the actual value is still high. The concentration of NO_3^- in the solution also affects the copper deposition efficiency. For example Solutions 4 and 5 contain the same Cu(II) concentration, but their NO_3^- concentrations differ by a factor of 10. The maximum deposition efficiency from both solutions is obtained at -7mA; however Solution 4 contains 1M NO_3^- and has a maximum efficiency of 77.4%, whilst Solution 5 has a tenth of the NO_3^- content and has a maximum efficiency of 90%. Thus, a higher degree of acid recovery in the initial process stage will maximise the efficiency of the copper electrodeposition.

Ferric ions reduce the efficiency of copper deposition; the severity of the reduction depends on the concentration of Fe(III). For example, copper was deposited with a maximum efficiency of 24% from a 0.3M Cu, 1M NO_3^-, 0.25M Fe(III) solution (Soln 10). The addition of 0.25M Fe(III) reduced the efficiency by 71%, compared to Solution 1. However, copper could be recovered from the real waste solution, which contained 0.047M Fe(III), at a maximum efficiency of 36%. This current efficiency for copper deposition shows that the recovery of copper from the real waste solution is feasible, and that the removal of stripping additives prior to the copper electrodeposition stage is not required.

6.4 References

6.1 C. Kerr, *Transactions of the Institute of Metal Finishing*, **82**(B7-B12, Part1-2): (2004)

6.2 L. I. Antropov, M. I. Donchenko and T. I. Motronyuk, *Protection of Metals*, **20**(1): 27-32 (1984)

6.3 D. Pletcher and Z. Poorabedi, *Electrochimica Acta*, **24**: 1253-1256 (1979)

6.4 A. Mecucci and K. Scott, *Journal of Chemical Technology and Biotechnology*, **77**(4): 449-457 (2002)

6.5 K. Scott, X. Chen, J. W. Atkinson, M. Todd and R. D. Armstrong, *Resources Conservation and Recycling*, **20**(1): 43-55 (1997)

6.6 J. H. Moore and N. D. Spencer, ed. *Encyclopedia of Chemical Physics and Physical Chemistry*, Vol. 1 (A2.4), Institute of Pysics, (2001)

6.7 Atotech UK Ltd, Material Safety Data Sheet, *Tinsolv 2000* (1999)

6.8 A. J. Bard, R. Parsons and J. Jordan, ed. *Standard Potentials in Aqueous Solution*, Dekker, New York (1985)

6.9 S. C. Das and P. Gopala Krishna, *International Journal of Mineral Processing*, **46**: 91-105 (1996)

6.10 C. Kerr and F. Coultard, *Sustainable Technologies for the Tin Stripping Process used in Printed Circuit Board Fabrication*, ITRI Ltd. & Intellect (2004)

6.11 D. W. Dew and C. V. Phillips, *Hydrometallurgy*, **14**: 351-367 (1985)

6.12 H. P. Lee and K. Nobe, *Journal of the Electrochemical Society*, **132**(5): 1031-1037 (1985)

6.13 N. G. Carpenter and D. Pletcher, *Analytica Chimica Acta*, **317**: 287-293 (1995)

6.14 G. E. Dima, A. C. A. de Vooys and M. T. M. Koper, *Journal of Electroanalytical Chemistry*, **554-555**: 15-23 (2003)

6.15 S. Barnartt, *Canadian Journal of Chemistry*, **47**(10): 1661-1666 (1969)

6.16 J. M. Bisang, *Journal of Applied Electrochemistry*, **26**: 135-142 (1996)

7 METAL RECOVERY

In this chapter the possibility of the copper recovery stage being performed using an electrochemical reactor, as would be utilised in an industrial situation, was examined. The ability to recover copper from the nitrate containing waste tin stripping solution was validated by the electrochemical characterisation study in Chapter 6. In this chapter, the efficiency of the copper recovery from waste stripping solution has been determined using a parallel plate reactor.

Initially, linear voltammograms in copper sulphate solution were recorded in the reactor. From these i-E data the limiting current for copper deposition in the reactor was determined for a range of flowrates. The reactor was then utilised to deposit copper from simulated stripping waste. The applied cell current was set equal to the copper limiting current, as calculated from the copper sulphate polarisations. As the concentration of copper in the reactor decreased, the cell current was reduced to keep the recovery efficiency high.

7.1 Mass Transfer Studies of Cu(II)

Linear voltammograms were recorded for solutions of $CuSO_4$ in H_2SO_4 to obtain the Cu(II) limiting current in the reactor. Sulphuric acid was used as the reference electrolyte because copper can be deposited with approximately 100% current efficiency from these solutions [7.1], unlike the nitrate electrolytes of interest [7.2]. Also, the reduction of nitrates has previously been shown to mask the Cu(II) limiting current. The Cu(II) concentration in the stripping waste is 0.3M [7.3], and after 90% Cu(II) recovery the concentration would reduce to 0.03M. Voltammograms were therefore recorded for 0.3M Cu(II) and 0.03M Cu(II) in solution to test if Cu(II) deposition was mass transport controlled in the reactor.

The voltammograms were recorded at several electrolyte flowrates in order to determine the effect of flowrate on the mass transport properties. The rotameters in-line with the reactor (Figure 3-9) could supply electrolyte in the range 600-1200 l/hr

($1.67 - 3.33 \times 10^{-4}$ $m^3 s^{-1}$). The flow area within the reactor was 2.688×10^{-3} m^2, with an equivalent diameter of 0.0517m calculated using Eq. (7.1). The Reynolds number was therefore determined from Eq. (7.2) to be 6410 at 1200l/hr and 3205 at 600l/hr. The flow regime was turbulent throughout these experiments.

$$d_e = \frac{4(\text{cross sectional area})}{\text{wetted perimeter}} \tag{7.1}$$

$$\text{Re} = \frac{\rho \cdot u \cdot d_e}{\mu} \tag{7.2}$$

The voltammograms recorded for 0.3M Cu(II) + 1M H_2SO_4, at three different flowrates, are shown in Figure 7-1. The polarisation data initially appear linear, with no distinct copper limiting current plateau. It can be seen that at currents below $-0.05 A cm^{-2}$ the data for all flowrates overlie; the flow through the reactor appears to have no effect on the i-E data. At higher currents the traces diverge; for an applied cell current of $-0.08 A cm^{-2}$, the cathodic potential is -0.94V for a flow of 1200l/hr, and -1.12V for the lowest flowrate of 600l/hr.

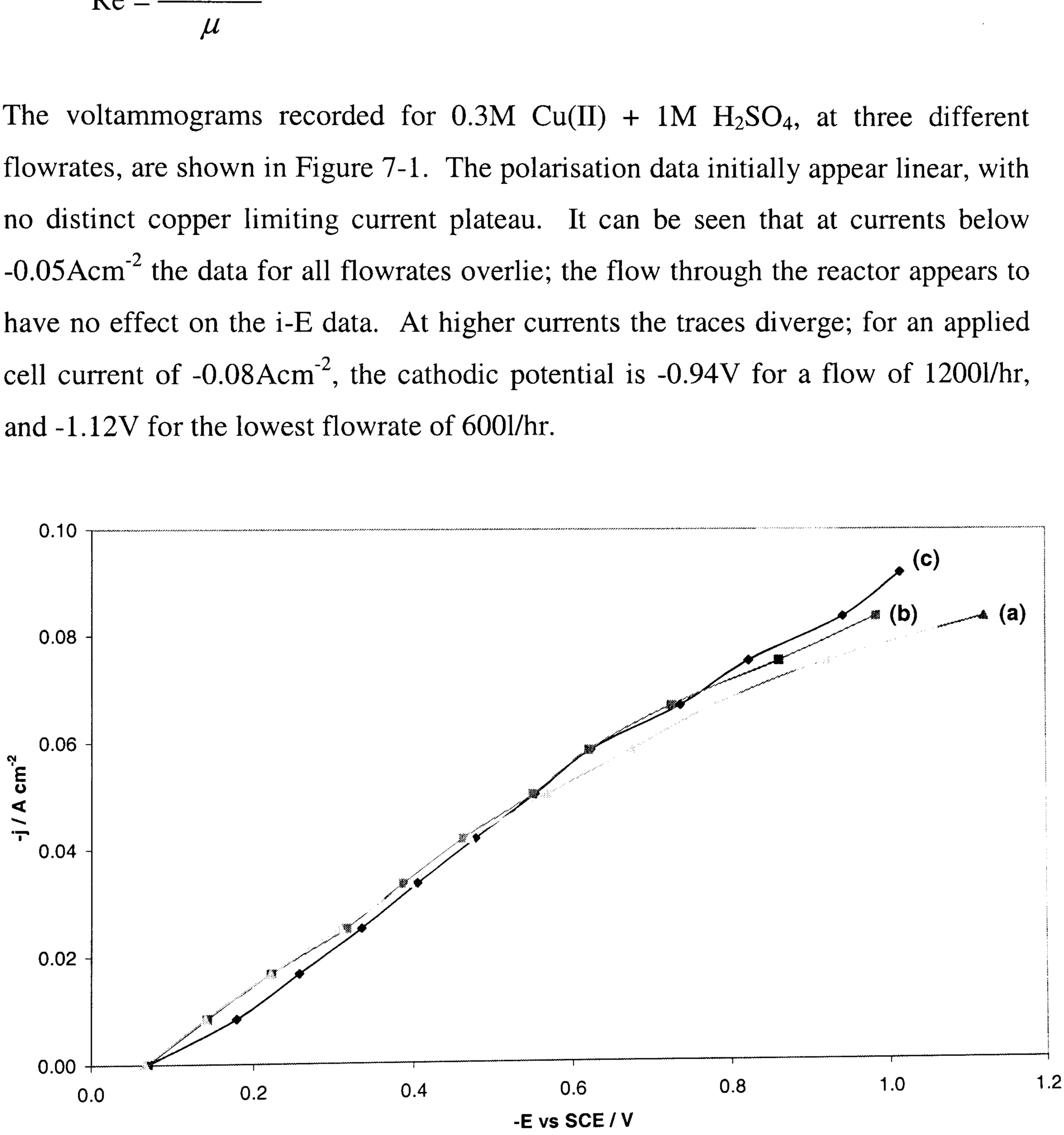

Figure 7-1 Polarisation data for 0.3M $CuSO_4$ + 1M H_2SO_4 at (a) 600l/hr (b) 800l/hr (c) 1200l/hr

Polarisation data for 0.03M Cu(II) are shown in Figure 7-2. The shape of the voltammograms are similar to the curves for 0.3M Cu(II). The voltammograms were only recorded for the lowest and highest flowrates, since the difference between the i-E data was found to be small in the 0.3M Cu(II) case. However, for the 0.03M Cu(II) solution, the data at the low and high flowrates diverge at much lower potentials, overlying below -0.0017 Acm^{-2} only.

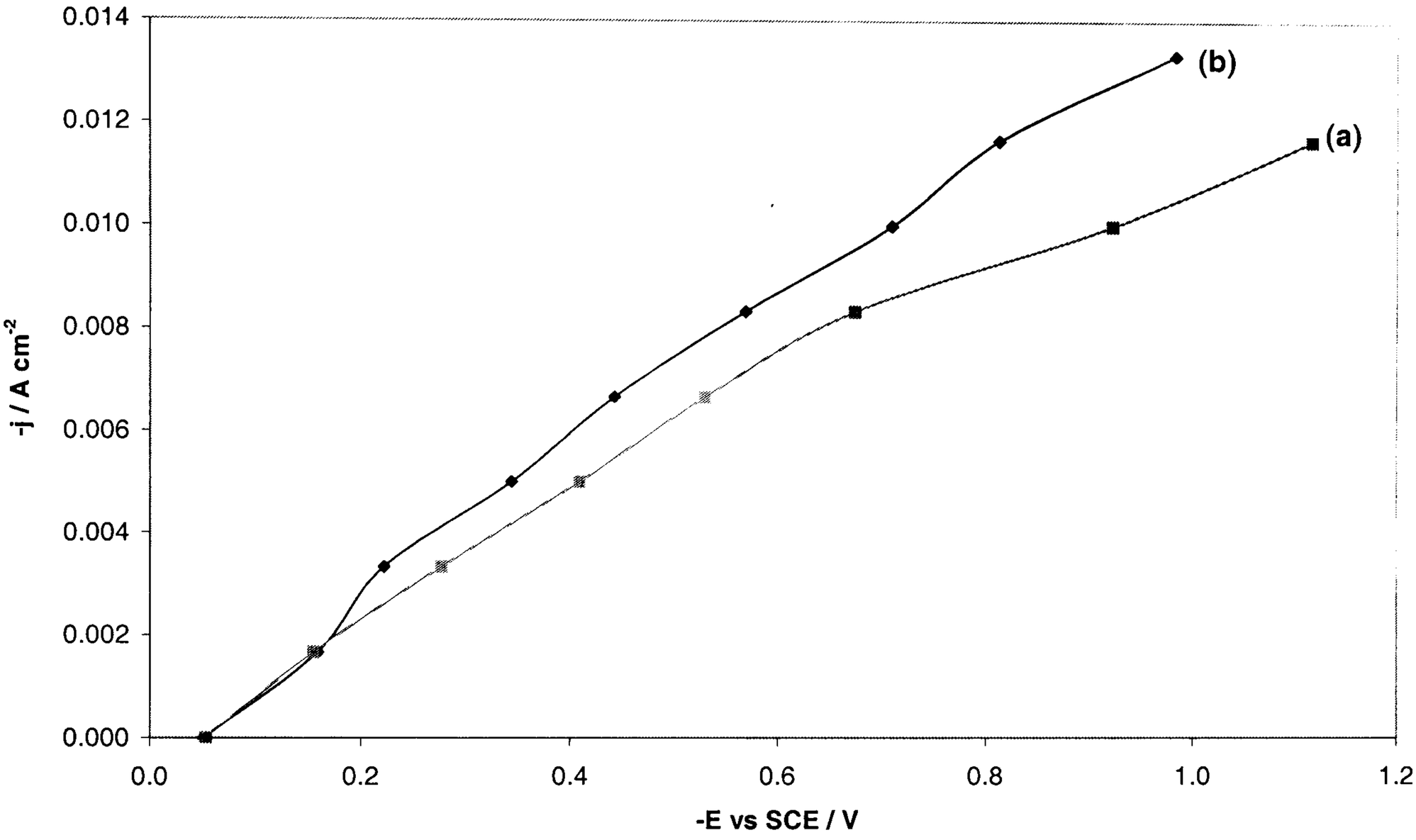

Figure 7-2 Polarisation data for 0.03M $CuSO_4$ + 0.1M H_2SO_4 at (a) 600l/hr (b) 1200l/hr

As seen in Figure 7-1 and Figure 7-2, no clear limiting current plateau for copper deposition can be discerned from these polarisation data. This may be due to the relatively high ohmic drop and large electrode surface area in these experiments. However, there is a decrease in the gradient of the voltammograms with increasing current and potential for all cases, denoting mass transfer limitations. The limiting current for copper deposition was estimated as the current at the point of gradient change (Figure 7-3); this occurs at approximately -0.6V for 0.3M Cu(II) and -0.45 for 0.03M Cu(II). This approach had been used earlier by *Denpo et al* [7.4].

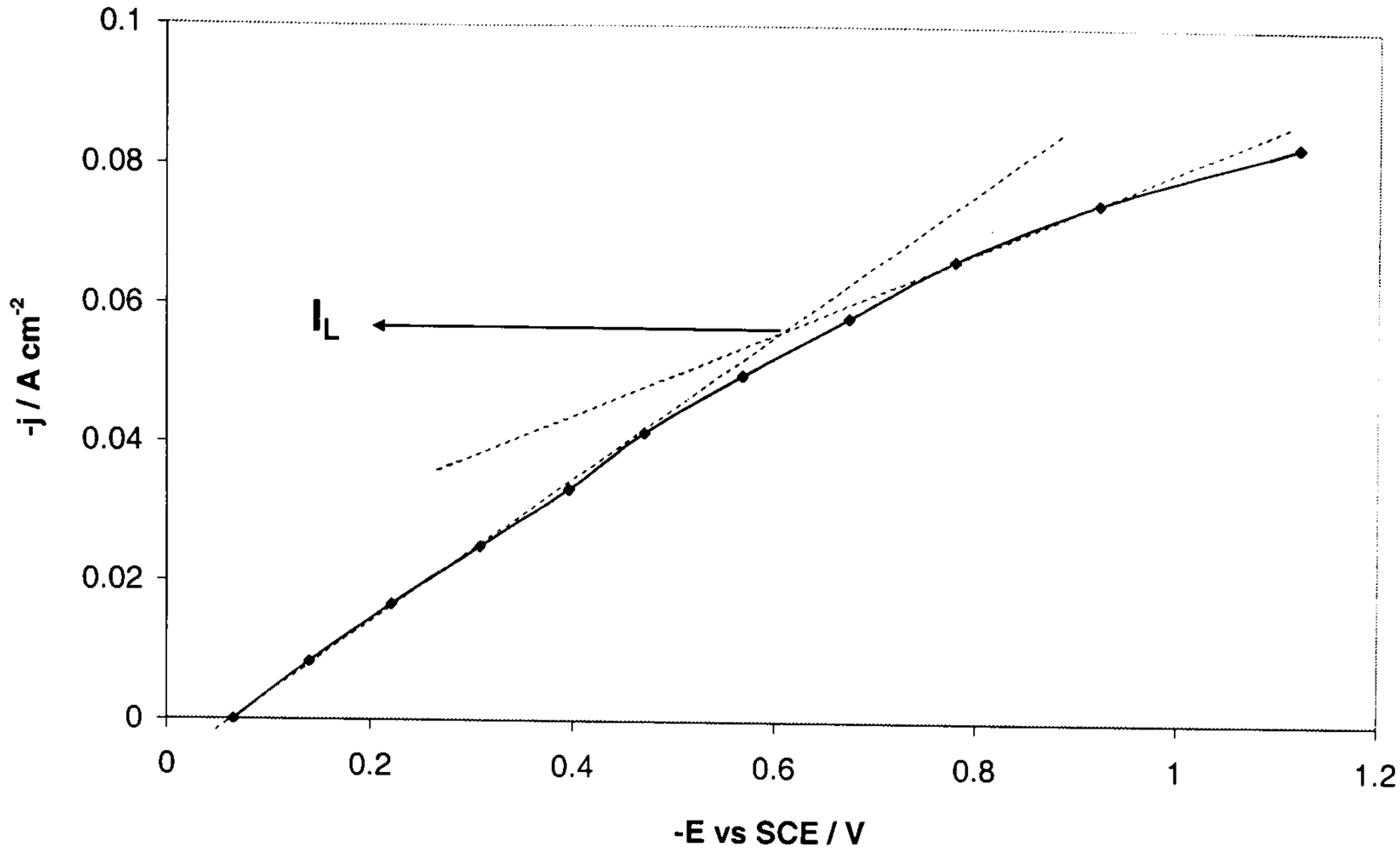

Figure 7-3 Estimation of limiting current from reactor i-E data

The results from this limiting current estimation are shown in Table 7-1. These calculations (Table 7-1) show that the limiting current is independent of the volumetric flow rate and thus Reynolds number. This has previously been reported to occur during copper electrowinning in tank cells [7.5]. The results also show that the limiting deposition current for 0.3M Cu(II) was approximately 8.4 times larger than the limiting current for 0.03M Cu(II), as determined from the i-E data. Any deviation from the proportionality predicted by the Nernst diffusion model could be due to the large inaccuracy in the limiting current estimation. As the gradient of the i-E data changes gradually, the choice of points through which to draw the tangents is not clear. To estimate the errors on the limiting currents obtained from this method, tangents corresponding to the maximum and minimum gradients of the data in the high and low potential regions were drawn; the highest and lowest values of I_L obtained then gave a range in which the true value of the limiting current for copper deposition is thought to lie.

As the solution is well aerated, parasitic oxygen reduction will also occur at the cathode. *Massé et al* [7.6] ascertained the oxygen reduction current at a rotating cylinder electrode in the turbulent regime to be 0.25-1.1mA cm^{-2}. As this oxygen reduction current is much smaller than the uncertainty in the copper limiting current estimation, it has been neglected.

[Cu] / M	I_L / mA cm^{-2}	
	600l/hr	1200l/hr
0.3	61 ± 6	58 ± 2
0.03	7.3 ± 0.7	7.6 ± 2.3
$I_L(0.3M)/I_L(0.03M)$	8.4	7.6

Table 7-1 Limiting currents for copper deposition from sulphate electrolytes using a parallel plate reactor

The mass transfer coefficients for copper were then calculated from these limiting current values using Eq. (7.3), and are shown in Table 7-2.

$$I_L = AnFk_m c_0 \tag{7.3}$$

[Cu] / M	k_m / 10^{-5} m s^{-1}	
	600l/hr	1200l/hr
0.3	1.105 ± 0.105	1.002 ± 0.035
0.03	1.261 ± 0.121	1.313 ± 0.397

Table 7-2 Mass transport coefficients for copper deposition from sulphate electrolytes using a parallel plate reactor

Theoretically, the correlation between the mass transfer coefficient and Reynolds number is of the form:

$$k_m \propto \mathrm{Re}^m \tag{7.4}$$

The experimental results above imply that m is near zero. For fully developed turbulent flow in a parallel plate reactor, *Pickett* [7.7] determined the value of the constant m to be 0.8, which is contrary to the current findings. The full correlation is shown in Eq. (7.5).

$$Sh = 0.023\,\mathrm{Re}^{0.8}\,Sc^{1/3} \qquad for\ L/d_e \geq 12 \tag{7.5}$$

$$\text{where } Sh = \frac{k_m d_e}{D} \qquad \text{and } Sc = \frac{\mu}{\rho D}$$

In order to examine why the experimental mass transfer coefficients do not follow Eq. (7.5), theoretical values for the mass transfer coefficient of copper in acid sulphate media were calculated using the above correlation. For a volumetric flowrate of 1200l/hr, the values of k_m from Eq. (7.5) for 0.3M Cu(II) and 0.03M Cu(II) were $0.318\text{x}10^{-5}\text{ms}^{-1}$ and $0.183\text{x}10^{-5}\text{ms}^{-1}$ respectively. These calculated values for the mass transfer coefficient are at least a third lower than the values estimated from the polarisation data. This indicates that the mechanism for ionic transfer in the reactor is not governed by bulk electrolyte convection.

7.2 Ideal Copper Recovery Profile

The maximum rate of copper deposition from the simulated waste solution will occur when the current through the reactor is equal to the copper limiting current. At higher currents the excess charge would be wasted on side reactions, such as nitrate and hydrogen reduction. The Cu(II) limiting current is proportional to the Cu(II) concentration (Eq 7.3). Therefore, as the concentration of copper decreases, the limiting current for deposition will also decrease. To minimise the charge used in side reactions, the reactor current should be periodically reduced in line with the copper concentration.

In order to reduce the reactor current in line with the Cu(II) concentration, the variation of Cu(II) concentration with processing time in the simulated waste solution needs to be estimated. A theoretical plot of the normalised Cu(II) concentration was constructed using Eq. (7.6); the derivation of this equation is shown in Section 2.4. The equation assumes that the copper is recovered at the mass transfer limiting rate.

$$c(t) = c(0) \cdot \exp\left(-\frac{k_m A}{V_T} t \right) \tag{7.6}$$

For Eq. (7.6) to model the behaviour of the stripping solution, the mass transport coefficient should be based on a nitrate electrolyte. However, the mass transfer coefficients determined in Section 7.1 are based on a sulphate electrolyte. Diffusion coefficients were used to derive a relationship between the mass transfer coefficients

for copper in sulphate and nitrate electrolytes, as described in Section 3.3.3. This relationship is given by Eq. (7.7), and the mass transfer coefficients for copper in nitrate solutions are shown in Table 7-3.

$$k_m(Cu, NO_3) = 1.68 \cdot k_m(Cu, SO_4) \tag{7.7}$$

[Cu] / M	k_m / m s^{-1}
0.3M	1.87×10^{-5}
0.03M	2.14×10^{-5}

Table 7-3 Mass transfer coefficients of copper in nitrate electrolytes

The Cu(II) concentration of the waste tin stripping solution (0.3M) was used as the starting concentration *c(0)* to calculate the recovery plot. The volume of the tank V_T was 0.01m^3, and the electrode area *A* 6×10^{-3} m^2.

Figure 7-4 shows the theoretical depletion plot for the copper. The required processing time to recover 90% of the copper was calculated to be about 57 hours. To reach the discharge limit of 1.5mg/l (2×10^{-5}M) [7.3] a reduction of 99.993% is needed; this would take approximately 239 hours.

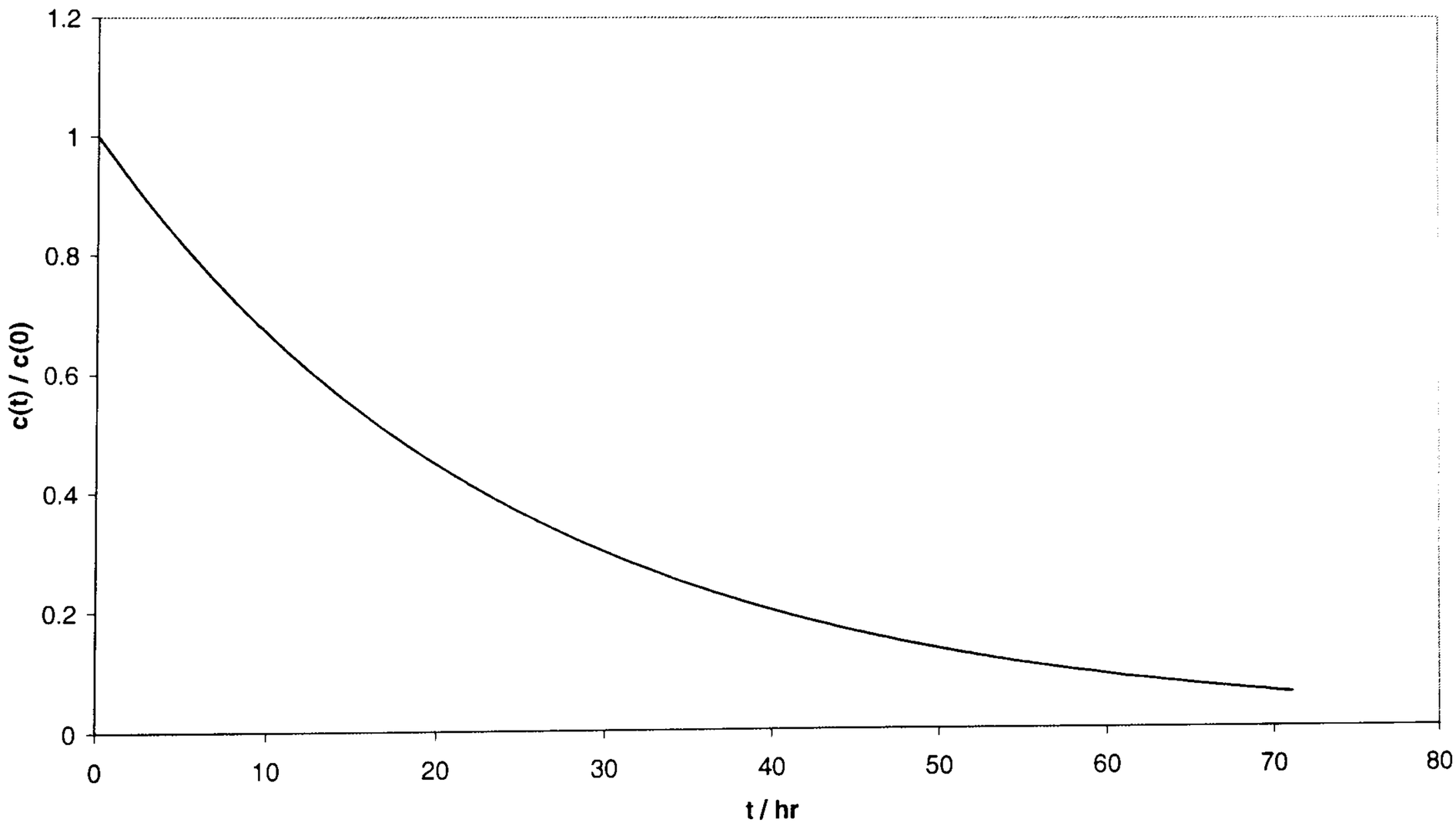

Figure 7-4 Theoretical plot of normalised Cu(II) concentration against time for c(0)=0.3M

The theoretical times for copper recovery shown in Figure 7-4 are based on the assumption of 100% current efficiency. In practice this is not the case, and the experimental recovery time may be longer. However, the efficiency of the recovery is to be determined and cannot be assessed without experiments. To obtain a meaningful result, the copper concentration must decrease significantly during the experiment. A copper depletion of 50% was chosen; according to Figure 7-4, a minimum processing time of 16 hours would be required.

The copper depletion curve (Figure 7-4) was used to predict the Cu(II) concentration of the waste stripping solution after each hour of processing. From these theoretical concentrations, the limiting current for copper deposition was calculated using Eq. (7.3). For the first hour in the reactor, the cell current was set to the limiting current for 0.3M Cu(II), the initial concentration. After this hour, the cell current was reduced to the estimated Cu(II) limiting current, calculated from the theoretical Cu(II) concentration (this is shown graphically in Section 3.3.3). This periodic reduction in cell current minimised parasitic reactions e.g. NO_3^-, H^+ reduction, and maximised the deposition efficiency. Table 7-4 shows the current profile used in the copper recovery experiments, with the predicted Cu(II) concentrations. This is illustrated graphically by Figure 7-5.

time / hr	[Cu] / M	Current / A	time / hr	[Cu] / M	Current / A
0	0.300	6.5	8	0.217	4.7
1	0.288	6.2	9	0.209	4.5
2	0.277	6.0	10	0.201	4.3
3	0.266	5.7	11	0.193	4.2
4	0.255	5.5	12	0.185	4.0
5	0.245	5.3	13	0.178	3.8
6	0.236	5.1	14	0.171	3.7
7	0.226	4.9	15	0.164	3.5

Table 7-4 Predicted copper concentration and corresponding limiting currents after 15hrs of processing using the parallel plate reactor

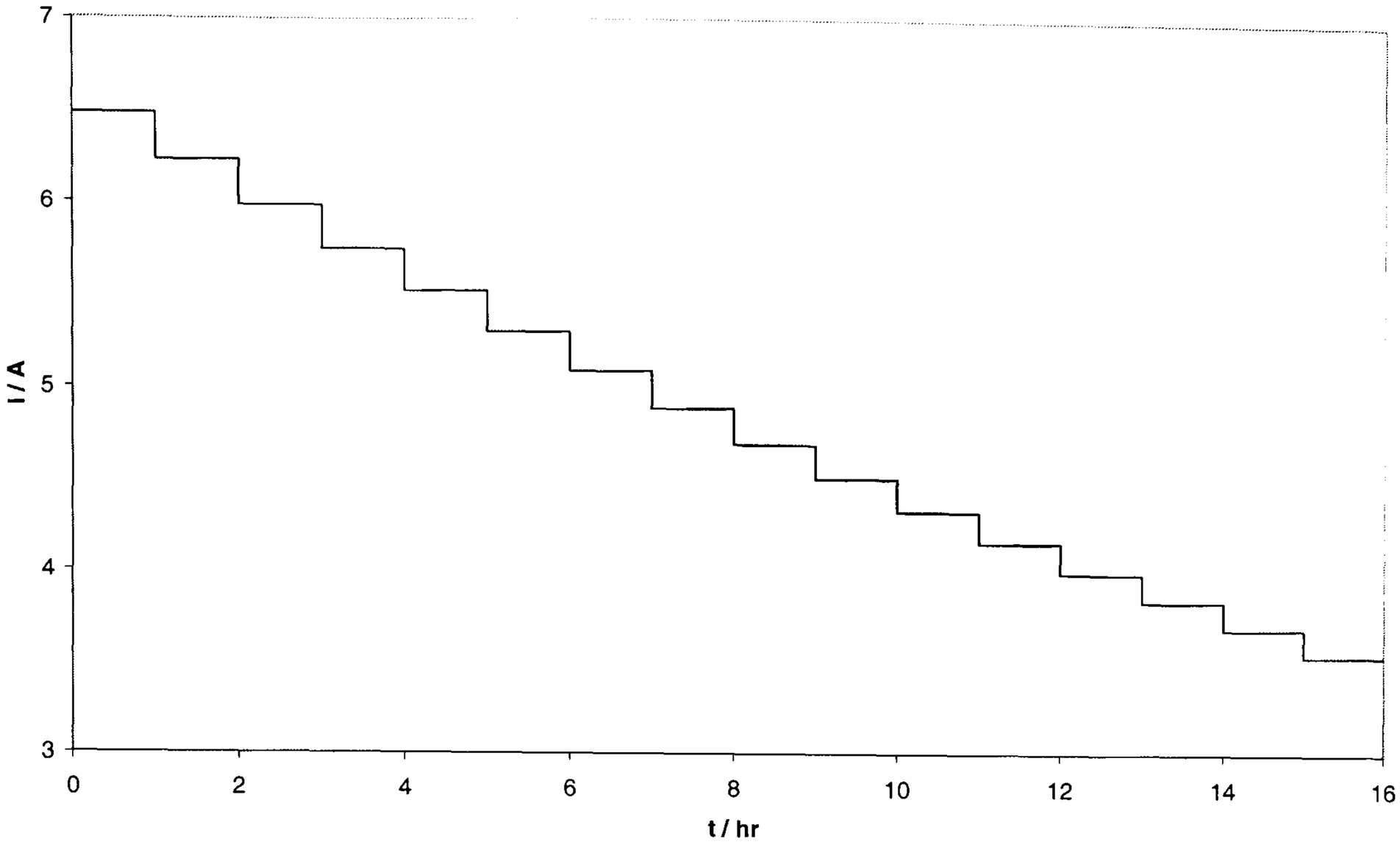

Figure 7-5 Current profile used to recover copper from simulated waste using a parallel plate reactor

7.3 Copper Recovery from Stripping Waste

Ideally, waste solution from a tin stripping process would be used as the electrolyte for these recovery experiments, as it was for the electrochemical characterisation. However, sufficient waste was not available to fill the 10 litre tank associated with the reactor. Therefore, a simulated solution was prepared using concentrations from the Tinsolv 2000 MSDS sheet [7.8], and the ratio of Fe(III)/Fe(II) previously determined (Section 6.1.3). The solution composition is shown in Table 7-5, with the description of the concentration calculations in Appendix A.

HNO_3	1M
$Cu(NO_3)_2$	0.3M
$FeSO_4$	0.2M
$Fe(NO_3)_3$	0.05M
NH_4NO_3	0.375M
glycolic acid	0.131M

Table 7-5 Composition of simulated stripping solution for reactor experiments

The reactor was run for 8 hours a day over two days, to complete the 16 hours of processing required for the idealised copper depletion of 50%. A 50ml sample was taken every hour and analysed for Cu(II) concentration using ICP (Section 3.4.2). The Cu(II) concentration in each sample was measured three times to allow the error at 95% confidence interval to be calculated.

Figure 7-6 shows the decrease in Cu(II) concentration with time. The bold solid line is the previously calculated theoretical curve, the dashed line shows the trend of the experimental data, and the points represent the experimental data. The error bars on the experimental data correspond to the uncertainty in the concentration measurement (± 95% confidence interval), but do not include any indication of other experimental errors e.g. the preparation of samples for ICP analysis. An indication of the uncertainty in the copper recovery profile due to the limiting current estimation has also been included on this figure.

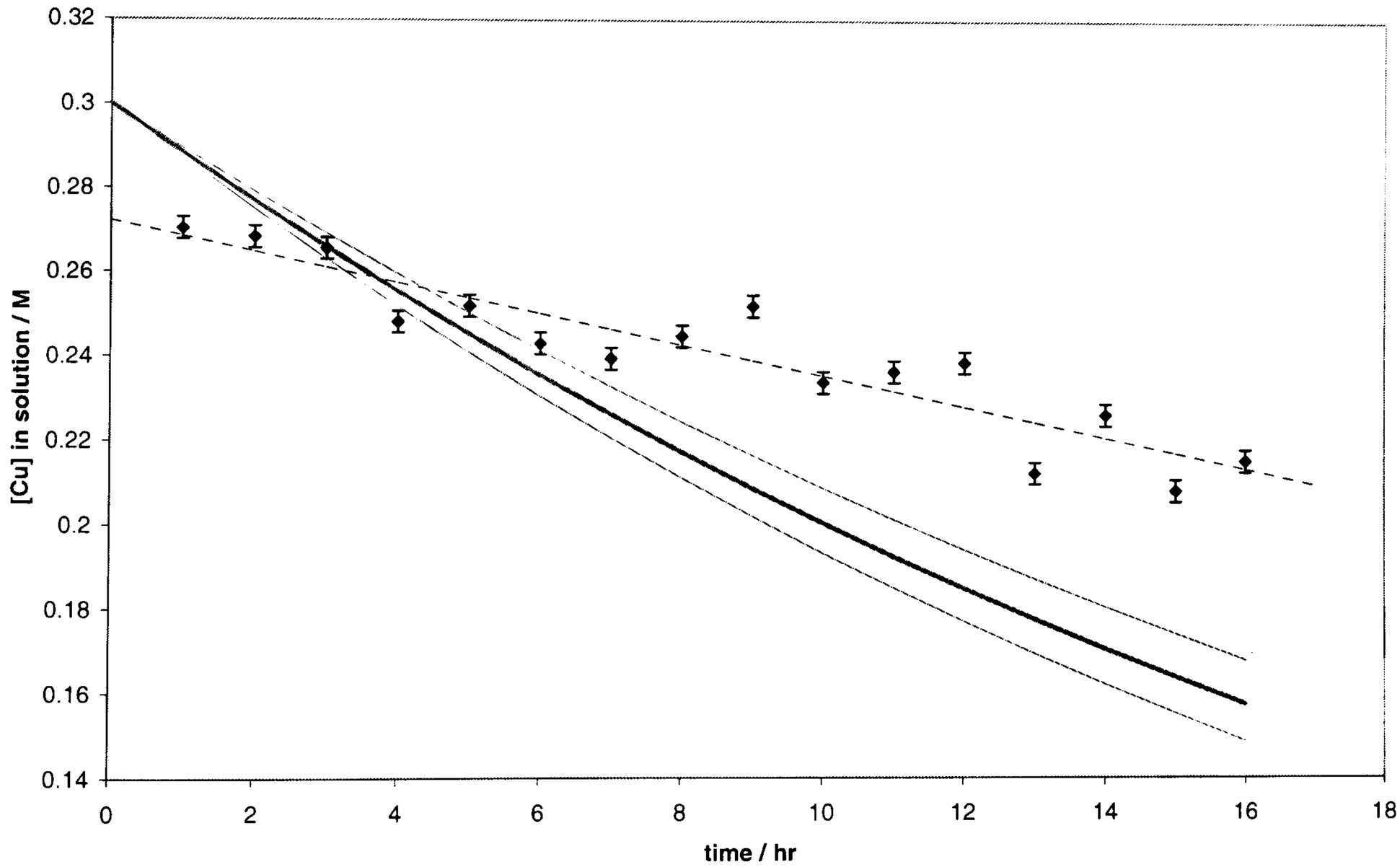

Figure 7-6 Comparison between experimental results and theoretical curve for copper recovery using a parallel plate reactor (bold solid line: theory, faint solid lines: uncertainty bounds, points: experimental data, dashed line: experimental data trend)

As shown in Figure 7-6, the Cu(II) concentration in the simulated waste solution decreased more slowly than predicted for Cu(II) reduction at 100% current

efficiency. During the first four hours of processing the measured Cu(II) concentration in the system was found to be lower than theoretical prediction. These lower values of Cu(II) concentration could be due to: (i) inaccuracies in the value of k_mA that were used to calculate the depletion curve via Eq. (7.6); (ii) the initial Cu(II) concentration being less than 0.3M; (iii) or errors in the ICP analysis. After 5 hours, the measured Cu(II) concentration was greater than the theoretical prediction, indicating that the current efficiency for copper deposition was less than 100%. This result was expected, because the efficiency of the deposition, found from the stripping experiments in the previous chapter (Section 6.2.3), ranged between 20-36%. If the theoretical curve for Cu(II) depletion with 40% current efficiency is calculated, we can see from Figure 7-7 that the Cu(II) reduction in the reactor lies between 40% and 100% The final concentration of copper after 16 hours was 0.2M, a reduction of 33%.

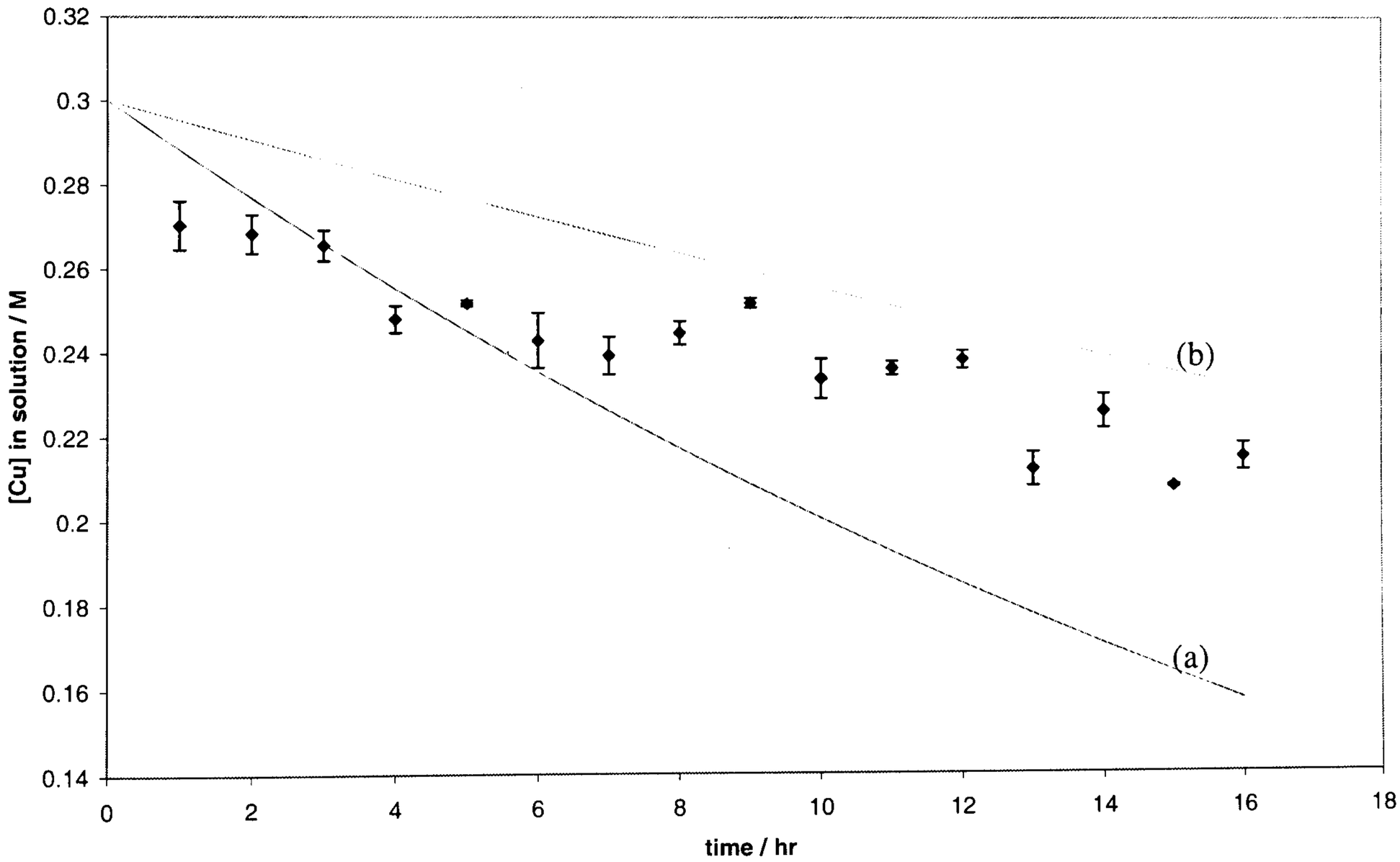

Figure 7-7 Comparison between experimental recovery (data points) of Cu(II) from simulated stripping solution and theoretical curves with efficiency (a) 100% (b) 40%

Another notable point in the Cu(II) experiments is that the Cu(II) concentration did not decrease smoothly. At several points, the Cu(II) concentration appeared to increase (e.g. between 7 and 8 hours). This could be due to the redissolution of copper into the stripping solution. Loose, powdery copper deposits were observed on the cathode during the stripping experiments from real waste (Section 6.2.3).

This loose copper could be detached by the flow and redissolved into the stripping solution. The increase in copper concentration between 8 and 9 hours supports this theory; before this hour of processing, the electrolyte was left in the tank overnight, providing adequate time for copper dissolution. The copper dissolution could also be caused by adsorbed oxygen on the cathode surface [7.9].

The detachment and dissolution of copper from the cathode was confirmed by leaving the processed solution in clean plastic containers for three days after the electrolysis. It was postulated that this solution contained copper particles detached from the electrode. There was a significant increase in the Cu(II) concentration of the remaining solution, assumed to be from the dissolution of these copper powders.

The overall current efficiency for copper deposition was calculated at the end of each hour. The variation of the efficiency with time is shown in Figure 7-8. Initially the copper recovery proceeds with an apparent current efficiency of 100% (in the first four hours the efficiency ranged between 255-110%, so was set equal to 100%). After 6 hours the efficiency falls to ~70% and is approximately constant for the remainder of the experiment. This current efficiency of 70%, at which most of the deposition was carried out in the reactor, was more than double the values obtained during the stripping experiments (20-36%).

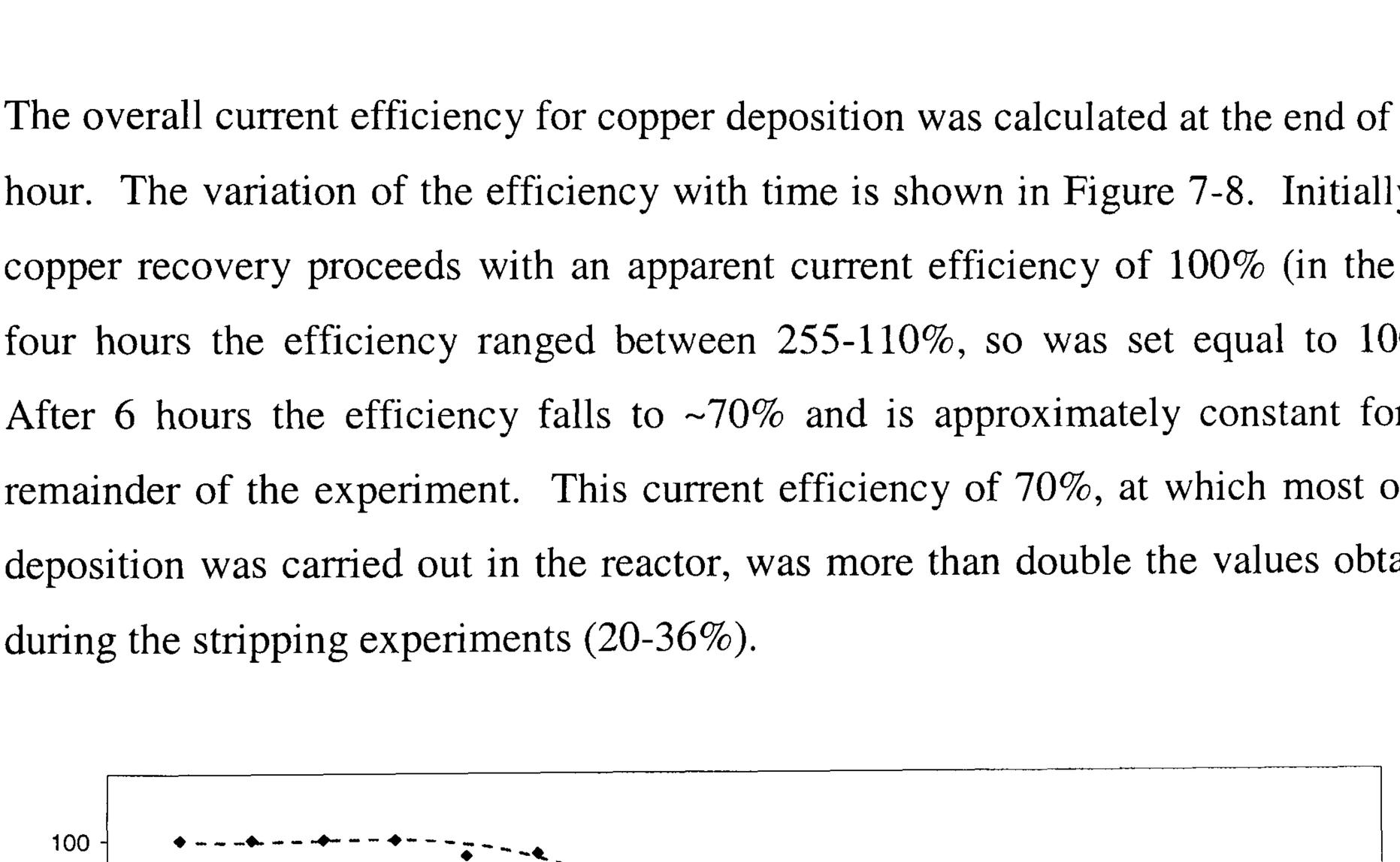

Figure 7-8 Variation of overall current efficiency of copper deposition with processing time

7.4 Discussion

The polarisation data for acidified copper sulphate in the parallel plate reactor show no dependence on the flow, nor any clear limiting current plateau for copper deposition. Both these characteristics are thought to be due to flow patterns induced by entry into the reactor. The reactor used in this work had two inlets at right angles to the reactor flow (c.f. Figure 3-8); the diameter of these inlets was less than that of the reactor. Therefore, as the fluid entered, it was subjected to a sudden change of direction and expansion; this expansion can cause a recirculation bubble to form close to the walls that moves backwards against the main flow [7.10]. Downstream of this recirculating zone, the main flow becomes reattached to the walls and subsequently develops into turbulent or laminar flow. This flow pattern is thought to exist in the parallel plate reactor because bubbles released from the anode were moving against the bulk flow, indicating the presence of a recirculation zone.

The lack of a limiting current plateau could be explained if the local limiting current for copper deposition varied along the electrode. This can be caused by the flow patterns described above [7.10]. The electrode could span three flow regimes: the slow recirculation bubble, developing flow and fully turbulent flow. The thickness of the Nernst diffusion layer depends on the velocity and flow regime of the fluid. Thus in the slow recirculation bubble, the diffusion layer is likely to be thicker than in the faster downstream section, giving rise to a lower limiting current for copper deposition. As the reaction kinetics are unchanged by flow velocity, the lower limiting current in the recirculation bubble would be attained at smaller overpotentials than the higher limiting current in the fast downstream region. Therefore, areas of the electrode could then obtain limiting current for copper deposition at different applied potentials. The voltammograms would not exhibit a current plateau until mass transfer was limiting at all areas, which may occur at the potentials for H^+ reduction. In order to observe a limiting current, the flowrate through the reactor would need to be reduced to minimise the entrance effects.

The lack of correlation between the polarisation data (and thus mass transfer coefficient) and the flow can also be explained by the fluid entry. The theoretical correlations between the Reynolds and Sherwood numbers only apply to fully

developed flow, usually achieved by including a calming section before the electrodes [7.11], this is not the case for the reactor in this study. It is usual for industrial reactors to operate with developing flow, because their inlet configuration subjects the fluid to a sudden expansion [7.12]. Operating with developing flow is beneficial, as it can increase the mass transfer coefficient considerably [7.13] and therefore the rate of metal recovery. This enhancement was observed in this study, as the experimentally determined mass transfer coefficients (Table 7-1) were at least three times higher than the values calculated using Eq. (7.5). Also, flow entrance effects have previously been found to produce regions of Reynolds number where the mass transfer coefficient appears constant [7.10, 7.13]. The range of Reynolds number for which this holds true is dependent on the system geometry. If the flow regime in the parallel plate reactor was dominated by a recirculation bubble due to the inlet configuration, this could explain why the mass transfer coefficient is unchanged over the range of Reynolds number in this study. It is thought that if the flowrate was reduced sufficiently, changes in the i-E data, and thus the mass transfer coefficient would be seen.

In order to calculate the ideal copper depletion profile, the value of k_m was based on the mass transfer limiting current for copper deposition, derived from the copper sulphate polarisation data. However, there were large inaccuracies associated with the limiting current estimation, and the electrochemical characterisation study in Chapter 6 found that although the rate of copper deposition from the nitrate solutions was constrained, this was not necessarily by the mass transfer of copper to the surface. The theoretical depletion profile was used to calculate the Cu(II) concentration and thus limiting current that was applied across the electrodes. The applied cell current may therefore be larger than required, enabling more charge to be available for side reactions, and lowering the possible efficiency. It is difficult to say whether this is the case, as a large source of inefficiency in this reactor is the redissolution of deposited copper. The current efficiency was therefore a measure of the relative deposition and dissolution of the copper, not just the deposition.

The efficiency of copper deposition in the parallel plate reactor was, at 70%, higher than the efficiency found from the stripping experiments. However, the reactor

efficiency is not directly comparable to efficiency obtained during the stripping experiments, as the efficiency from the stripping experiments included the nucleation of copper on the gold disc. Also, in Section 6.3, the change in reduction products with cathode surface was discussed; a copper cathode, as used in the reactor, appeared to promote Cu(II) reduction over Fe(III) reduction. The efficiency of the copper recovery in the reactor is expected to decrease as the Cu(II) concentration is reduced further. As copper is recovered, the limiting current for copper reduction, and thus the cell current is reduced. The Fe(III) concentration, and therefore its limiting current, is assumed to be constant because the reduced Fe(II) ions could be oxidised at the reactor anode. The limiting current for Fe(III) reduction would therefore become a larger fraction of the applied cell current as the copper recovery progresses.

In both the electrochemical characterisation study, and these reactor experiments, the copper deposited from the real (or simulated) waste tin stripping solutions was powdery. Roughened or powdery deposits are a common consequence of metal deposition at or near the mass transfer limiting current [7.14]. The copper deposit is thought to become detached from the cathode and redissolve into the waste, decreasing the efficiency of the recovery. To avoid this problem, the reactor design or operation could be modified. For example, copper could be deposited at a lower current, although this would increase the recovery time, or the deposited copper could be removed from the cathode frequently.

7.5 Cost Effectiveness of Copper Recovery

The economic viability of metal recovery from tin stripping solution is obviously dependent on each stage in the proposed recovery process. The operating and capital costs for the process as a whole should be considered, as well as other factors such as the cost of non-compliance with environmental legislation. These costs should be offset against the costs of disposal and the possible resale value of the recovered metals, in order to determine the process feasibility. For the copper recovery stage, the major factors that are thought to influence the feasibility are:

- Capital costs: reactor, pump, electrodes
- Operating costs: electrolytic power, electrolyte pumping

As yet, there is no fixed design for the electrochemical reactor that would be used for copper recovery from waste stripping solution. The size of the reactor, electrodes and pump will be dependent on the batch size. As the volume of tin stripping waste produced can range from $10m^3$ per annum for a small facility to $40m^3$ per annum for a large facility [7.15], the batch size would vary between plants. A series of reactor sizes may therefore be required.

The estimate for the capital cost was based on the parallel plate reactor used during these experiments. It is assumed that as the batch takes 16 hours over two days, the reactor will process two batches per week, for 50 weeks per year (i.e. 100 batches / year). The cost of our reactor, including the pump, piping, rotameters and electrodes was £5000. If this is depreciated over 5 years, the capital cost per batch would be:

$$C_C = \frac{5000}{(5\times100)} = £10$$

The operating costs, as well as the capital costs, depend on the design of the reactor. To gain an estimate of the costs involved, the electrolytic power and pumping costs were determined per batch for the copper recovery achieved during these experiments with a parallel plate reactor. During this batch, 1mol of copper was recovered.

The electrolytic power cost for copper recovery will be influenced by the deposition efficiency, the electrolyte and the available price of electricity. Faraday's law (Eq. 7.8) was used to calculate the theoretical amount of charge needed to recover the copper. This calculation was based on the recovery at 70% efficiency in the parallel plate reactor. The charge required to was $2.76x10^5$ C per mol Cu.

$$Q = \frac{mnF}{\Phi} \qquad m = 1 \text{ mol, n} = 2, \text{F} = 96485 \text{ C/mol}, \Phi = 0.7 \tag{7.8}$$

The energy required for this deposition was then found by multiplying the charge by the cell potential (Eq. 7.9). The cell potential, measured during the reactor recovery experiments, was 3.5V. The cell potential is dependent on the equilibrium potentials, overpotentials and electrolyte ohmic drop. The energy requirement to decrease the Cu(II) concentration by 0.3-0.2M in $0.01m^3$ of stripping solution was therefore 965kJ.

$$W = Q \cdot E_{cell} \tag{7.9}$$

The median cost of electricity purchased by manufacturing industry in the UK in the third quarter of 2006 was 6.653pence per kWh [7.16]. Therefore the electrolytic power cost for the above recovery, using the parallel plate reactor, would be 1.78p (£0.018) per mol Cu.

The power of the pump used in our experiments was 60W. The major factors likely to affect this pumping power requirement are the flow rate and inter-electrode gap. The pump was run for 16 hours, at a cost of 6.653p/kWh. The pumping costs were therefore 0.06kW x 16h x £0.0653/kWh = £0.063 per mol Cu.

The total costs calculated for the parallel plate reactor, to reduce the Cu(II) concentration in $0.01m^3$ of solution from 0.3M to 0.2M, were:

$$C_R = 10 + 0.018 + 0.063 = £\ 10.081 \text{ per mole}$$

This estimate is dominated by the reactor cost. The reactor used in these experiments was a one-off, therefore the manufacturing costs associated with it would be much higher than for an off-the-shelf item. The depreciation time of 5 years also has a large influence on the capital cost per batch. It is probable that the whole reactor system would not need to be replaced every 5 years, just components such as pumps and electrodes.

The above cost estimate also contains no disposal element. The cost of disposal will be dependent on whether the waste solution can go directly for sewage treatment or

whether the waste must be sent for further processing. The copper discharge limit for our industrial partner was 1.5ppm (10^{-5}M); the final copper concentration that was achieved during the reactor recovery experiments was 0.2M. Therefore, longer term reactor experiments combined with other separation stages e.g. ion exchange, would be required to determine the minimum Cu(II) concentration that could be achieved economically, and thus the disposal route and costs. The removal of SnO_2 would also have a significant affect on this disposal cost by reducing the volume of waste and metal loading. If, after the recovery process, the remaining solution could go directly down the drain, the costs for additional treatment would be saved. The disposal of mixed aqueous wastes costs the university approximately £1/litre, and the disposal of tin stripping solution costs about £0.50/litre in the USA [7.17]. Therefore, for comparison with the recovery costs, the disposal per mole of copper was estimated to be £2.50/mole, assuming a copper concentration of 0.3M in the untreated waste.

The cost of copper recovery would be offset by the purchase price of copper, as well as the saving on disposal costs. The price of copper, which almost doubled in 2006, is £3.03/kg, or £0.19/mol. The total cost benefits of recovering the copper are therefore:

$$C_B = £2.50 + £0.19 = £2.69/\text{mol}$$

By comparing the recovery costs of the copper (£10.08/mol) with the cost benefits (£2.69/mol) it can be seen that copper recovery is currently not economically feasible. The capital cost of the reactor, and its useful life, and the disposal costs have the largest influence on the economic feasibility. As these costs are estimates the feasibility of the process may change if the costs change e.g. higher disposal costs, copper price rising. If the cost benefits increase, and the recovery costs decrease by 20%, the new cost estimates would be C_R = 8.06 and C_B = 3.11; the process is still not economically feasible. However, the cost associated with not complying with the environmental legislation is high.

References

7.1 D. Barker and F. C. Walsh, *Transactions of the Institute of Metal Finishing*, **69**(4): 158-162 (1991)

7.2 A. Mecucci and K. Scott, *Journal of Chemical Technology and Biotechnology*, **77**(4): 449-457 (2002)

7.3 R. Massey, Personal Communication, (2005) [e-mail, 27/04/05]

7.4 K. Denpo, T. Okumura, Y. Fukunaka and Y. Kondo, *Journal of the Electrochemical Society*, **132**: 1145-1150 (1985)

7.5 L. Cifuentes, M. Grageda and G. Crisostomo, *Chemical Engineering Science*, **61**: 3623-3631 (2006)

7.6 N. Massé, J. St-Pierre and M. Bergeron, *Journal of Applied Electrochemistry*, **25**: 340-346 (1995)

7.7 D. J. Pickett, *Electrochemical Reactor Design*, Elsevier, Amsterdam (1979)

7.8 Atotech UK Ltd, Material Safety Data Sheet, *Tinsolv 2000* (1999)

7.9 I. V. Kreizer, I. K. Marshakov, N. M. Tutukina and I. D. Zartsyn, *Protection of Metals*, **40**: 23-25 (2003)

7.10 D. J. Pickett and C. J. Wilson, *Electrochimica Acta*, **27**: 591-594 (1982)

7.11 F. C. Walsh, *A First Course in Electrochemical Engineering*, The Electrochemical Consultancy, (1993)

7.12 J. Legrand, P. Legentilhomme, S. Farias Neto and H. Aouabed, *Electrochimica Acta*, **42**: 805-811 (1997)

7.13 A. Djati, M. Brahimi, J. Legrand and B. Saidani, *Journal of Applied Electrochemistry*, **31**: 833-837 (2001)

7.14 D. Pletcher and F. C. Walsh, *Industrial Electrochemistry*, Chapman and Hall, (1990)

7.15 C. Kerr and F. Coultard, *Sustainable Technologies for the Tin Stripping Process used in Printed Circuit Board Fabrication*, ITRI Ltd. & Intellect (2004)

7.16 Department of Trade and Industry, *Quarterly Energy Prices Tables*, http://www.dti.gov.uk/energy/statistics/publications/prices/tables/page18125.html, accessed on 22/01/07

7.17 CAI Resources Inc, *Printed Wiring Board Pollution Prevention and Control Technology: Analysis of Updated Survey Results*, (1998)

8 CONCLUSIONS AND FURTHER WORK

8.1 Conclusions

The electronic component market in the UK and Ireland grew by €1bn in 2004. This growth has lead to an increased build up of waste hardware in the environment, and liquid discharges for disposal. The liquid wastes contain dissolved metals, as well as substances which could potentially harm the environment. A process that could reclaim the metals for reuse would be desirable because of raw material and disposal costs, and the increasing amount of environmental legislation. The aim of this project was to develop a systematic method to determine the feasibility of metal recovery from such solutions.

This work focussed on waste from the tin stripping stage of printed circuit board manufacture. This waste is a nitric acid based solution containing dissolved copper and iron, and a suspension of tin oxide. Currently the metals are precipitated and sent to landfill despite several studies into the recovery of copper and tin from tin stripping solution. None of the proposed processes are used industrially, and there were questions remaining about the thermodynamic feasibility of the recovery processes, and the effect of the constituent ions on copper electrodeposition. The method developed for this waste stream was used to form a systematic approach to metal recovery from aqueous wastes.

Previous research into separation schemes for the tin and copper have established a recovery method; in general this involves filtration to remove tin oxide, followed by copper electrodeposition. The recovery scheme that was thought to be the most feasible contained an initial diffusion dialysis stage to recover nitric acid. The solution was then aerated and passed to a filtration stage to remove tin(IV) oxide, which could then be dissolved and electrowon, or sold as the oxide. The filtrate would pass through to another electrodeposition stage to recover copper. After deposition, the water could be cleaned using ion exchange before being returned to the manufacturing process.

To determine the feasibility of copper and tin recovery from the waste tin stripping solution, the thermodynamics of the system were studied to ascertain if the metals were in the solid or liquid phase, depending on the concentration of metal and anions, the pH and the system potential. This information was then compared to the proposed separation scheme. The feasibility and operating conditions for each stage are described below:

- Acid recovery. The theoretical analysis showed that the HNO_3 recovery was limited by the precipitation of copper. A 0.3M Cu(II) solution precipitated at a pH of 2.4, corresponding to a HNO_3 concentration of 0.6M.
- Aeration. This will increase the system pH, ensuring tin exists as the oxide. However, this stage could be omitted as MINEQL+ analysis showed tin was in the form SnO_2 in the pH range 0 to 13.
- Filtration. This stage would be used to separate the solid tin and dissolved copper. With a Cu(II) concentration of 0.3M, the pH should be maintained between -0.4 and 3.8 to ensure separation. As the acid recovery scheme is limited to pH less than 2.4, the filtration stage should operate in the range -0.4 to 2.4.
- Ferric ions. These exist in solution as an additive; ideally they should all stay in solution with the copper or all precipitate to be removed with the tin. The distribution of Fe(III) between the streams could not be resolved by the theoretical analysis.
- Copper electrodeposition. Copper could theoretically be removed to an activity of 10^{-6} if a potential of +0.15V is applied. If Fe(III) is in solution, the metals can be separated as their deposition potentials are sufficiently different.
- Tin electrodeposition. To dissolve the SnO_2 concentrated HCl and/or elevated temperatures would be required; this may not be practicable.

Experiments to verify these theoretical conclusions were then undertaken. It was determined that the predictions for copper precipitation from nitrate solutions model the actual behaviour well. Ferric ions were found to precipitate at much higher pH

than predicted, meaning they are likely to stay in solution and pass through to the electrodeposition stage with the copper. Results from the SnO_2 dissolution implied that the recovery of SnO_2 as the product is the more feasible process route. Overall, the proposed recovery process was ascertained to be theoretically feasible.

The project then focussed on an individual stage in the proposed recovery scheme: copper electrodeposition. Electrochemical characterisation experiments were carried out to determine the possibility of depositing copper from a nitrate electrolyte with reasonable efficiency. The effect of copper and nitrate concentration and the stripping additives on this deposition efficiency were also determined. The study showed that copper could be recovered at an efficiency of 95% from a 0.3M Cu(II), 1M NO_3^- solution. The deposition efficiency fell as the copper concentration decreased, reducing to a maximum efficiency of 77% from a 0.03M Cu(II), 1M NO_3^- solution. As Cu(II) was further recovered the efficiency fell to around 2% from a 0.003M Cu(II), 1M NO_3^- solution, hence a reduction in Cu(II) to meet discharge limits is unlikely to be economical. A high concentration of nitrate ions was also found to reduce the deposition efficiency, thus a higher degree of acid removal in the first recovery stage will maximise the efficiency of the copper electrodeposition. Ferric ions, existing in solution as an additive, were found to severely suppress copper deposition. However, copper was recovered from real stripping wastes with an efficiency of 36%. Therefore, the recovery of copper from nitrate electrolytes is feasible, and the removal of stripping additives prior to copper electrodeposition is considered unnecessary.

In industry, the recovery of copper would be carried out using an electrochemical reactor. A parallel plate reactor was successfully used to recover copper from a simulated solution containing the industrial additives. After 16 hours of processing, 33% of the Cu(II) had been removed, at an efficiency of 70%. The deposited copper was powdery and was thought to become detached from the cathode, lowering the current efficiency for the deposition. This could be resolved by removing the copper frequently.

In conclusion, the results of the thermodynamic analysis and subsequent experiments to verify the feasibility of the copper deposition show that the proposed recovery scheme is feasible. The systematic method that was used to establish the feasibility of copper and tin recovery from the stripping solution is completely general and could be applied to any aqueous metal baring solution. This method initially involves reviewing the literature to determine suitable technologies for separation, and their possible combinations. The thermodynamics of the waste are then investigated to ascertain the regions where the metals are in the solid or dissolved forms. This theoretical information can then be compared to the modus operandi of the identified separation stages to determine their feasibility and the possible operating ranges. The outline of a recovery process can therefore be established. Individual stages in this recovery process can then be studied in more detail to determine their efficiency, and resolve any practical issues.

8.2 Further Work

Although the theoretical feasibility of the proposed process to recover copper and tin from waste stripping solution has been determined, only the copper electrodeposition stage was examined in detail. Therefore, the diffusion dialysis stage for acid recovery, and the filtration stage to remove SnO_2 could be investigated further.

The value of the SnO_2 recovered from this solution could also warrant further investigation. The particle size distribution and precipitate purity could be compared with possible uses for this oxide. The SnO_2 may need further processing to meet the requirements, and the process to do this, and the costs involved may affect the viability of the overall recovery from the stripping solution.

The removal of metals from aqueous waste streams, down to levels that would enable the water to be reused in the manufacturing process, was only mentioned in this work. The separation stages required and the integration of the water into the manufacturing process could be examined.

APPENDIX A: CALCULATION OF THE SIMULATED WASTE SOLUTION COMPOSITION

The recovery of copper using a parallel plate reactor would ideally be performed using waste tin stripping solution as the electrolyte. However, insufficient process waste solution was available to fill the $0.01m^3$ tank associated with the reactor. A simulated solution was therefore prepared. The calculations below describe how the concentrations of Cu, Sn, Fe, and NO_3^- in the waste solution were determined.

Copper

The concentration of copper in the waste stripping solution was known from the tin stripping process control information supplied by our industrial partner. The maximum concentration allowed in the waste before the solution is sent to disposal is 0.3M Cu. The copper was added to the simulated solution as $Cu(NO_3)_2$ because it would be dissolved during the stripping process according to the reaction A1.

$$Cu + 8HNO_3 \rightarrow Cu(NO_3)_2 + 2NO + 4H_2O \qquad \text{A1}$$

Tin

Tin exists in the waste stripping solution as a suspension of SnO_2. It can be reasonably assumed that the SnO_2 is in equilibrium with the waste, thus forming a saturated solution of Sn(IV) ions. Thus, to make the simulated solution, SnO_2 powder was added to the solution and then left several days to allow for equilibration.

Iron

Iron initially exists in the fresh tin stripping solution as ferric ions. The MSDS for Tinsolv 2000 (the second stripping solution used in a two stage process) shows that the concentration in the fresh solution is 0.25M Fe(III). During the tin stripping process, these ferric ions are reduced as tin and copper are dissolved from the PCB.

The concentration of ferric ions remaining in the waste stripping solution was estimated during the electrochemical characterisation of the real waste, as 0.047M (Section 6.1.3). Ferric ions were added to the simulated solution as $Fe(NO_3)_3$ because this salt is specified on the MSDS.

If it is assumed that the ferric ions are reduced to ferrous ions, a concentration of 0.25-0.047 = 0.203M Fe(II) will exist in the waste solution. Ferrous ions were added to the simulated solution as $FeSO_4$ because the nitrate was not easily available and sulphates are not reduced in the potential range of these experiments.

Nitrate

According to the MSDS, the concentration of HNO_3 in the fresh Tinsolv 2000 is <15%, which is equivalent to 2.58M. The HNO_3 will be consumed during the dissolution of copper and tin from the circuit board. For this calculation it is assumed that the tin is all dissolved during the first stage in the stripping process. Copper is therefore dissolved by the reduction of ferric and nitrate ions. As the proportion of ferric ions that were reduced has previously been estimated, the proportion of the copper that was dissolved via Fe(III) reduction can be estimated from reaction A2.

$$Cu + 2Fe^{3+} \rightarrow Cu^{2+} + 2Fe^{2+} \qquad \text{A2}$$

0.203M ferric ions were reduced to ferrous ions; from reaction A2, 0.203M Fe^{3+} would oxidise 0.102M Cu. As the waste contains 0.3M Cu(II), and the amount of copper dissolved via the reduction of Fe(III) is 0.102M Cu(II), the remaining 0.218M Cu must have been dissolved via the reduction of nitrate. According to reaction A1, for every mole of copper dissolved, 8 moles of HNO_3 will be consumed. Therefore, to dissolve 0.218M Cu, 1.74M of HNO_3 would be reduced. The initial HNO_3 concentration in the Tinsolv 2000 was 2.58M, therefore after the stripping stage 2.58-1.74 = 0.84M HNO_3 would remain; this has been approximated to 1M. As the HNO_3 used for tin stripping has been neglected, the estimated HNO_3 concentration used in these experiments will be higher than in reality, which is a conservative estimate.